UNIVERSITY OF SOUTHAMPTON

SYNTHESIS AND CHARACTERISATION OF ALUMINOSILICATE AND FRAMEWORK MODIFIED SODALITES

A thesis submitted for the Degree of Doctor of Philosophy

Geoffrey Mark Johnson

DEPARTMENT OF CHEMISTRY

FACULTY OF SCIENCE

DECEMBER 1996

UNIVERSITY OF SOUTHAMPTON

ABSTRACT

FACULTY OF SCIENCE
DEPARTMENT OF CHEMISTRY

Doctor of Philosophy

SYNTHESIS AND CHARACTERISATION OF ALUMINOSILICATE AND FRAMEWORK MODIFIED SODALITES

By Geoffrey Mark Johnson

The synthesis and characterisation of a wide range of sodalites has been achieved via ionic substitution of both framework and non-framework species. These materials conform to the general formula $M_8[ABO_4]_6.X_2$, where M = Na, Li, K, Ag, A = Al and Ga, B = Si and Ge, and X includes Cl, Br, I, ClO_4, MnO_4 and SCN. Aluminosilicates were generally prepared by structure conversion of zeolite 4A at 800 °C, or from condensation reactions in basic solution at 120 °C. Gallium and germanium substituted sodalites have been synthesised using hydrothermal reaction between 90 and 180 °C, for which the type of framework precursor has been shown to significantly affect the product purity and crystallinity. Experiment has shown that gallogermanates are the most difficult of the framework substituted sodalites to prepare, with only the halides producing phase pure products. Post synthetic exchange of sodium by lithium and potassium was achieved via nitrate melt reactions in the temperature range 270-370 °C for 3-16 hours; silver was introduced by reflux with concentrated silver nitrate solution at 100 °C for 16 hours.

All of the sodalites adopt the space group $P\bar{4}3n$ indicating a perfectly ordered alternating array of framework tetrahedra, thus showing that Loewenstein's rule of aluminium avoidance within zeolites can be extended to include framework linkages such as Ga-O-Ga. Rietveld profile refinement of powder x-ray and neutron diffraction data has been undertaken and yields structural parameters which have been used to investigate structure-property relationships revealing how the introduction of gallium and germanium produces subtle changes in bond lengths and angles. For a particular entrapped anion, the larger frameworks undergo greater relative cell collapse which is principally accommodated by co-operative rotations of the TO_4 tetrahedra manifested by variation in tetrahedral tilt angles and framework T-O-T bond angles.

^{27}Al, ^{29}Si and ^{71}Ga MASNMR spectroscopy has been used to confirm the framework ordering via observation of a single resonance when applied to either of the framework constituents. The effect of framework substitution has been monitored by MASNMR and FT-IR spectroscopy, both of which allow the correlation of spectroscopic band position with structural parameters such as cell parameter and framework bond angle. It is envisaged that the resultant linear relationships may be able to be extrapolated to aid characterisation of more complex gallium and germanium doped zeolites.

Extension of the hydrothermal method to solution has been successfully achieved for gallosilicates and aluminogermanates, and allows the entrapment of relatively sensitive anions such as permanganate which cannot be enclathrated using hydrothermal means. Divalent anions such as $(SO_4)^{2-}$, $(MoO_4)^{2-}$, $(WO_4)^{2-}$ and $(S_2O_3)^{2-}$ can also be incorporated within gallosilicate or aluminogermanate frameworks and, in an analogous manner to aluminosilicates, form materials with the cancrinite structure. The formation of ultramarine from this latter anion is observed upon thermal treatment in a similar fashion to thiocyanate. The increased size of the aluminogermanate cage has been utilised to entrap the $(S_2O_5)^{2-}$ and $(SeCN)^-$ anions; selenium ultramarine is the thermolysis product of selenocyanate sodalite.

"In the field of observations, chance favours the mind that is prepared"

Louis Pasteur

TABLE OF CONTENTS

DECLARATION

The material contained herein has not been submitted by the author for a degree at any other institution. The work was performed exclusively by the author excepting selected MASNMR spectra which were run by Dr S.E. Dann (University of Southampton).

ACKNOWLEDGEMENTS

I should like to thank first and foremost my supervisor Professor Mark T. Weller for all of his help and guidance over the past three years, in addition to his generosity in giving me the opportunity to attend several conferences both at home and abroad. I also extend my appreciation to my industrial supervisor Dr. Desmond Eadon and all at Johnson Matthey, particularly Helen Hatcher, for their input into the project and for their help and friendliness during my visits to Sonning. Dr. Philip Mead, with whom I have been priveleged to work in close cooperation for the last two and a half years, for many fruitful (and many not so fruitful) discussions on a wide range of topics. Dr Sandra Dann for her help collecting MASNMR spectra, Mr Dave Johnson for his assistance in the teaching laboratory, and to my project students for helping with the synthetic work. I am also extremely grateful to the EPSRC and Johnson Matthey for funding this work.

Thanks to the seventh level members and the Weller group past and present for their good nature and general banter, especially the following. Richard "Tommy" Needs for his finesse and positional awareness in 11-a-side football and for sensible reasoning in all walks of life. Phil "Billy Bandwagon" Mead for never showing the slightest inclination to mirror my work and for being the heavyweight of the Stanley midfield. Adam "If life were basketball.." Healey for unbiased judgements on Spurs players and for making those long winter nights simply fly by with many a captivating tale. Chris "Ken" Knee for rivalling Phil for that Mr Universe title. Annie "Jeans" Gormezano for her excellent taste in music and her shy and retiring manner. Richard "Radar" Crooks for his frighteningly efficient production line of novel compounds. Maria "Dewberry" Pack for her loud and vociferous nature. Darren "Youngster" Ogborne for his high spirited enthusiasm and punctuality to the pub. Jon "Nipper" Fitzmaurice for those quick singles and constant yip-yapping. Matt "Billiard Ball" Brenchley for extreme joviality. Eric "Ginger" Hughes for bringing a ray of sunshine to the lab. Zobir Hussein for his inimitable telephone answering service. Sandra "Fantasy Football Expert" Dann for constantly asking me whether or not I'd made red. Dave "Penalty King" Currie for quiet sufferance of cold and flu symptoms.

Thanks to all of the people I've lived with in Southampton and not mentioned above, namely Alex "Sav" Gibson, Dale "Niles" Atkin, Mark "Mr Motivator" Davis, Jon "Jay Leno" Amphlett and Tony "Alistair" Genge. A big thank you to Daf and Bev for their friendship and support over the last three years and those occassional nights in The Richmond, and of course to all involved with making Stanley such a pleasure to play for and such a highly skilled and attractive footballing outfit!!!

Finally, and most importantly, I thank all of my family for their unfailing love and support in all I have done, without which none of this could have been achieved.

NOMENCLATURE

Common abbreviations used throughout this thesis are listed below:

XRD	X-Ray Diffraction
PXD	Powder X-ray Diffraction
PND	Powder Neutron Diffraction
MASNMR	Magic Angle Spinning Nuclear Magnetic Resonance
FT	Fourier Transform
IR	Infra-Red
TGA	Thermo-Gravimetric Analysis
UV/VIS	Ultraviolet/Visible

Sodalite formulae are commonly abbreviated as follows:

$M_8[ABO_4]_6.X_2$	M[AB]X	e.g. $Na_8[AlGeO_4]_6.(MnO_4)_2$	$Na[AlGe]MnO_4$

For sodalites exchanged with cation N:

$M_{8-n}N_n[ABO_4]_6.X_2$	N[AB]X	e.g. $Na_5K_3[AlSiO_4]_6.(MnO_4)_2$	$K[AlSi]MnO_4$

Chapter One

INTRODUCTION

1.1 INTRODUCTION

This thesis describes an investigation of the sodalite system, in which the effect of framework substitution is reported. Following the study of structure-property relationships, it is the aim of this project to investigate the potential of the sodalite framework to entrap a variety of coloured anions in an attempt to provide suitable alternatives to pigments currently used in industry.

1.1.1 Silicate Structures

The fundamental unit in silicates is a tetrahedral complex consisting of Si^{4+} in tetrahedral coordination with four oxygen atoms [1]. The complexity of silicates derives from the various ways tetrahedral groups can be linked via common oxygen atoms yielding polynuclear complexes. The composition and structure of silicate species is further diversified by cationic substitution in which elements such as B, Be, P, Al, Ge, Ga and Mg replace Si in the framework [2]. The most common of these substitutions is that of Al, which can coordinate both tetrahedrally and octahedrally; this has a profound effect on the structure and composition of aluminosilicate materials. The introduction of aluminium results in a deficiency in electrical charge on the framework that must be locally neutralised by the presence of an additional positive ion within the interstices of the structure, typically an alkali metal, R^{+}, or alkaline earth, R^{2+}. Different aluminosilicates arise from the various ways tetrahedra are linked in one, two and three dimensional space, in addition to the incorporation of different ions substituted within the interstices. Framework structures are formed when SiO_4 and AlO_4 tetrahedra are linked three dimensionally via mutual sharing of oxygen alone.

1.1.2 Types of silicate and aluminosilicate structures

In nesosilicates such as olivine, Mg_2SiO_4, SiO_4 tetrahedra are discrete with Mg^{2+} cations associated with each unit for charge balance. More common is linkage between adjacent SiO_4 tetrahedra via oxygen bridges [1]. There are several mineral groups in which SiO_4 tetrahedra are linked in chains; single chains are present in the pyroxenes and double chains in amphiboles. In pyroxenes, each SiO_4 group shares two oxygens with adjacent tetrahedra, and the Si:O ratio is 1:3 with two extra positive charges supplied by cations.

There are two structural groups of pyroxenes, the first an orthorhombic system such as $MgSiO_3$, and the second monoclinic system in which two cationic sites are present, such as $CaMg(SiO_3)$. Amphiboles are chemically similar to pyroxenes but have a Si:O ratio of 4:11 and include hydroxyl groups in addition to metallic cations.

Linkage of three corners of each tetrahedron to neighbouring tetrahedra gives rise to sheet structures or phyllosilicates. Many silicates display two dimensional planar networks of tetrahedra linked to from infinite anions of composition $(Si_2O_5)_\infty^{2-}$. The largest family of layer structures are composed of one or two Si-O sheets. These have a Si:O ratio of 1:5, and the cations and water molecules present within the structure reside between the sheets. Examples include micas and clays, which have prominent cleavage directions parallel to the sheets. Kaolinite, $Al_4(Si_4O_{10})(OH)_8$, consists of Si_2O_5 sheets joined with Al^{3+} ions in octahedral coordination.

Three dimensional continuous framework structures, termed tectosilicates, are formed when all four oxygens of the tetrahedron are mutually shared between the tetrahedral silicon or aluminium. When Al^{3+} tetrahedrally substitutes for Si^{4+} in 3D frameworks, the framework adopts the stoichiometry $[(Al_xSi_{1-x})O_2]^{x-}$ for which positive ions must be present to balance the electrostatic charge held by the framework. In aluminosilicate framework materials, since every aluminium and silicon is tetrahedrally coordinated to four bridging oxygens, the ratio of oxygen to framework cation, i.e. O/(Al + Si), always equals two [3]. The three main groups of aluminosilicate framework structures are feldspars, feldspathoids and zeolites.

Feldspars are the most abundant rock forming minerals and comprise approximately two-thirds of all igneous rocks [4]. There are two main types of feldspars each containing two end members with a solid solution in between. The orthoclase feldspars possess the end members orthoclase, $KAlSi_3O_8$, and celsian, $BaAl_2Si_2O_8$, and the plagioclase feldspars the end members albite, $NaAlSi_3O_8$, and anorthite, $CaAl_2Si_2O_8$. All possess compact structures composed of corner sharing TO_4 tetrahedra with metal cations entrapped in the cavities created by the framework oxygens.

Feldspathoids are more open in structure than feldspars, and possess larger cavities; they contain additional cations, and in some cases, anions in their channels. Water molecules are present in some synthetic varieties, which then fall within the classification of a zeolite, since they may display ion exchange properties and limited adsorption towards water/water vapour. Examples of feldspathoids include sodalite, cancrinite, scapolite and nepheline. Scapolite is a seldomly occurring member of tectosilicates, and contains only two end

members, marialite, $Na_4Al_3Si_9O_{24}Cl$, and meionite, $Ca_4Al_6Si_6O_{24}CO_3$, with a solid solution between the two. They possess a tetragonal cell composed of TO_4 tetrahedra in four, six or eight membered rings. The eight rings give rise to channels in the a and b direction, containing anions as well as cations in square planar coordination around the anion. Nepheline, $NaAlSiO_4$, has a distorted tridymite-type structure, with the distorted six rings forming channels which run parallel to the c-axis. The structure contains sixteen tetrahedra per unit cell. Sodalites and cancrinites are of greater relevance to this work, and will be discussed in more detail below.

1.2 ZEOLITES

Zeolites were discovered in 1756 by Axel Cronstedt [5], a Swedish mineralogist, who noticing that a new type of crystal boiled when heated using a blowpipe flame, named them "zeolites" or "stones which boil", from the greek "zeo" to boil, and "lithos", stone.

Until the early 1960's, zeolite minerals were thought to occur mainly in cavities of basaltic and volcanic rocks. Since then, several zeolite minerals have been shown to have formed by the natural alteration of volcanic ash in alkaline environments over long periods of time, for example in the Cenozoic lakes, such as the alkaline lake beds of the western United States, where they have been identified by x-ray diffraction techniques [6]. The more common topological types identified include analcime (ANA), clinoptilolite (HEU), mordenite (MOR), chabazite (CHA), erionite (ERI) and phillipsite (PHI). Due to the hydrolysis of the alkaline constituents of the volcanic ash, the water in these lakes became salty and alkaline with pH up to 9.5, resulting in the crystallisation of zeolites from this deposit. Of the fifty or so known zeolite minerals chabazite, erionite, mordenite and clinoptilolite exist in sufficient quantity and purity for use as commercial products. Generally, high grade zeolite ore is mined, then processed by crushing, drying, powdering and screening. Depending on its use, it may then be chemically modified by ion exchange, acid extraction, and then calcined at 350-550 °C [6]. In addition to mineral zeolites, many synthetic varieties exist, for example zeolite beta, which was prepared for the first time in 1967 [7].

Despite having been known for a considerable time, zeolites did not become of great industrial importance until the 1960's, when they began to be used as catalysts in the petroleum industry. They are also used as adsorbents in the drying of industrial gases [2].

1.2.1 General structure of zeolites

A zeolite can be defined as an aluminosilicate with a framework comprising SiO_4 and $(AlO_4)^-$ tetrahedra linked by the mutual sharing of an oxygen atom [3]. This framework gives rise to cavities, cages and channels of dimensions dependent on the stoichiometry of the zeolite. The aperture dimensions which control entry into the internal pore volume are determined by the number of framework cations and oxygen atoms in the rings that define them. According to Loewenstein's rule [8] two aluminium atoms cannot be joined to the same oxygen, and hence, the ratio of aluminium to silicon in the zeolite framework must be

less than or equal to unity. The cavities of a zeolite are occupied by cations or water molecules which can easily be replaced to allow facile ion exchange or reversible dehydration [9].

The general formula of a zeolite can be expressed as:

$$M_{(x/n)}{}^{n+}(AlO_2)_x(SiO_2)_y.mH_2O$$

where M^{n+} is a cation compensating for the negative charge generated by the $(AlO_4)^-$ tetrahedron. Generally, the cations are those of the alkali metals or alkaline earths which can be easily replaced by protons, ammonium ions, and rare earth and transition metal cations [3].

The introduction of various cations leads to different catalytic properties, and the abundance of cations is dependent on the number of $(AlO_4)^-$ tetrahedra in the framework. The water molecules which can be readily adsorbed and eliminated explain the desiccant nature of zeolites [9].

1.2.2 Zeolite Compositions

The composition of zeolite frameworks directly affects their characteristics. As the silicon to aluminium ratio is increased, the level of non-framework cations is reduced and the system favours the formation of five membered rings. Silicon rich materials have increased stabilities and the acid site density is decreased, although the individual acid sites are stronger. Sorbed phases tend therefore to be hydrophobic or organophilic rather than hydrophilic [2].

1.2.3 Framework Substitution

Although zeolites are strictly defined as materials containing silica and alumina tetrahedra interconnected by oxygen atoms [3], many framework substitutions for silicon and aluminium have been achieved. The replacement of aluminium by gallium is well known, with the resultant structures having similar properties to their aluminosilicate analogues [10, 11]. Germanium substitution is also known, although the aluminogermanates and gallogermanates have been much less well explored [3]. No naturally occurring gallium or germanium zeolite types have yet been uncovered. Other cationic species successfully

incorporated on the aluminium site include Zn, Be, Co, B, Ti, Fe, Ni, Sn, V and Cr [2]. However, the doping level of these species, particularly the transition metal cations, is often low and definitive evidence that they are present only as framework species is often difficult to obtain. Replacement of Si by As and P has also been reported [12].

The replacement of Si by P gives rise to the important aluminophosphate (AlPO) series developed by Union Carbide [13]. These have several structure types in common with aluminosilicates, in addition to novel structures, and consist of alternating $[AlO_2]^-$ and $[PO_2]^+$ units. Since the framework is neutral there are no non-framework cations, resulting in their organophilic and non acidic properties. Partial replacement of silicon for phosphorus gives silicoaluminophosphates (SAPOs) [14]. MeAPO or MeAPSO species are created by the inclusion of other metal species such as Li, Be, Mg, Co, Fe, Mn, Zn, B, Ga, Fe and As [15]. All these systems show the same tendency as aluminosilicates to avoid direct linkages of the tetrahedra on the aluminium sites [16].

1.2.4 Zeolite Structural Types

In general, zeolites are classed in three groups as a function of their structure:

- cubic system: zeolite A, Faujasite (X, Y)
- hexagonal system: Erionite, Offretite, Omega
- orthorhombic system: Mordenite, ZSM-5

Only the cubic system will be discussed in detail here, since it is the most relevant to the research undertaken in this work. In the cubic system, the base unit is the "sodalite unit",. a cubo-octahedron possessing eight hexagonal and six square faces, as shown in Figure 1.1(a). The sodalite cage is 6.5 Å in diameter accessible by apertures of diameter 2.2 Å. Sodalite units are linked either by the square faces, yielding zeolite A as shown in Figure 1.1(b), or by hexagonal faces giving rise to large cavities of 13 Å called supercages, accessible by apertures of diameter 7.4 Å in the case of zeolites X and Y [17]. The internal surface of these zeolites is vastly more important than the external surface which explains the catalytic activity observed inside the supercages.

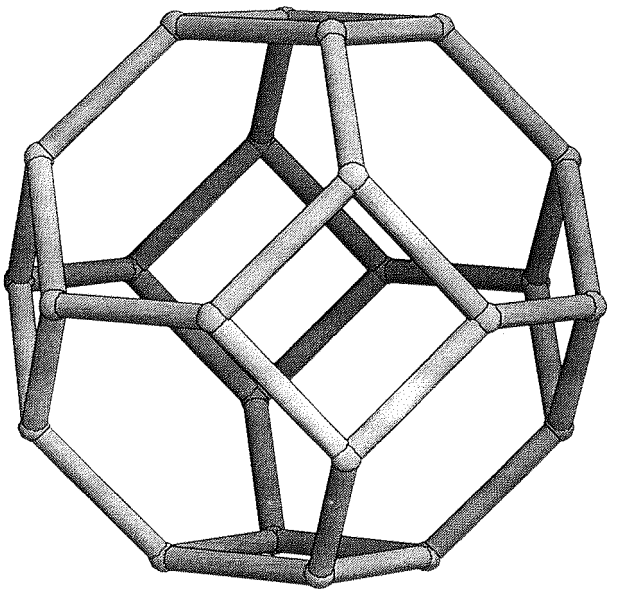

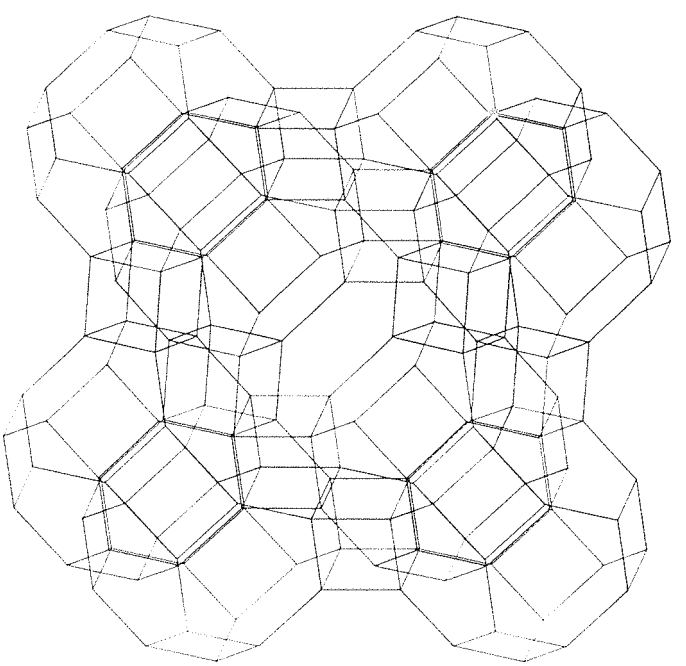

Figure 1.1(a) Sodalite cage, top **(b)** Zeolite A, bottom

1.2.5 Properties of Zeolites

Zeolites possess three essential characteristics which are the origin of their numerous applications: acidity, selectivity and ion exchange capacity [6].

The catalytic activity of zeolites is caused by the presence of acidic sites in the framework, and this acidity is determined by the number of acid sites, their nature and their strength. These sites vary according to the zeolite in question. Two types of acidity are observed in zeolites: Bronsted and Lewis acidity. Bronsted sites are due to hydroxyl groups, created in the framework either by exchange of a cation by protons of an acid, or by exchange by ammonium ions followed by thermal treatment to expel NH_3. Lewis sites are obtained by partial dehydration at the surface of the zeolite at temperatures in excess of 400 °C [18].

Due to their varied pore structure, zeolites are susceptible to the adsorption of organic molecules, resulting in their molecular sieving properties which permits the separation of molecules as a function of the dimensions of both the zeolite and the molecules in contact with it. At temperatures in excess of 350 °C *in vacuo*, water is expelled from the zeolite, resulting in empty cages and cavities within the structure; molecules of appropriate dimensions can then be incorporated into the zeolite, where they are held by Van der Waals and electrostatic forces.

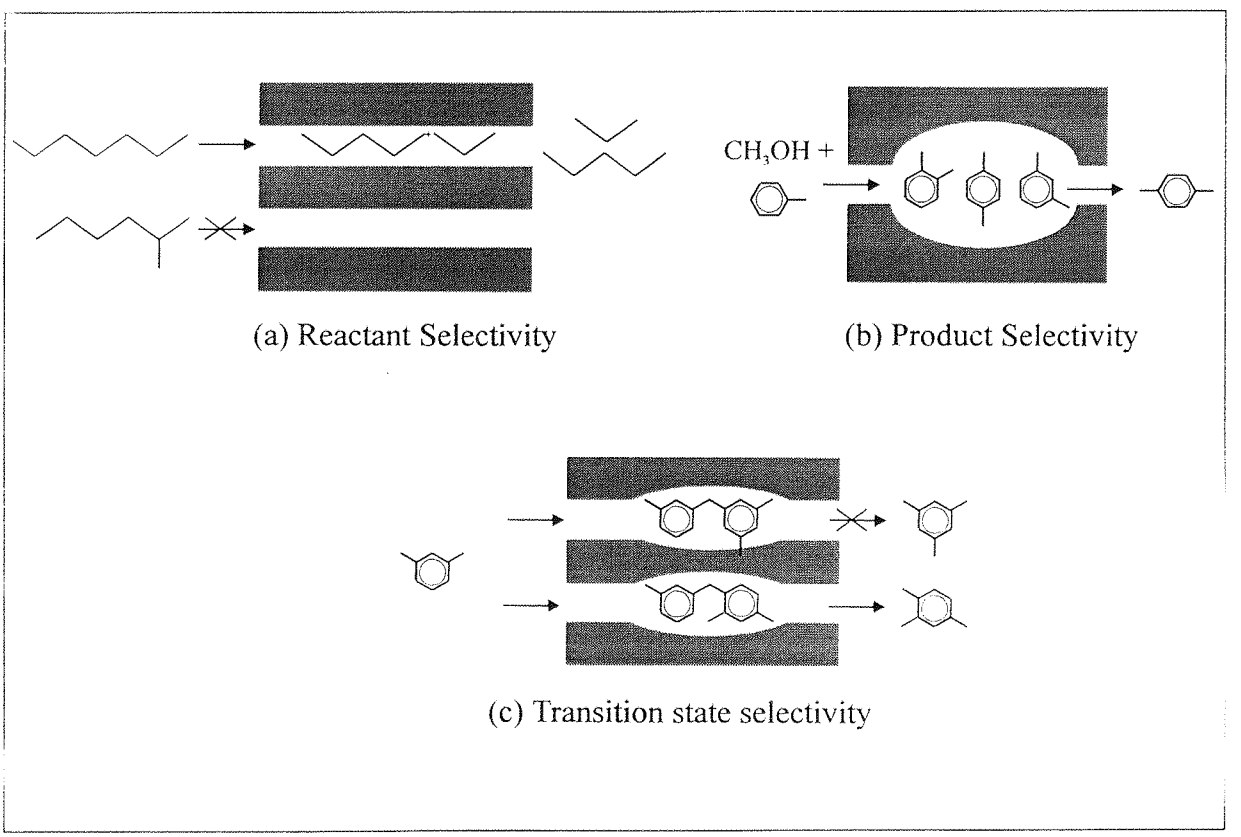

Figure 1.2(a)-(c) Shape selectivity of zeolites.

For a given reaction, this selectivity can be represented in three distinct stages, as shown in Figure 1.2: certain reagents are denied access to the active sites of the zeolite on account of their size; formation of bulky intermediates or transition states is hindered; particular products cannot diffuse towards the cavity exterior, or out of the pores.

Such a property is utilised for the separation of fractions in gas-liquid chromatography as a function of their size and shape: straight chain hydrocarbons can be admitted into the zeolitic network, whereas branched forms are excluded, allowing the facile separation of such entities [19].

The vast range of zeolite species can be further diversified by partial or full exchange of the non-framework cations. Thompson [20] first recognised the capacity of ion exchange in zeolites, and this can be achieved via solution and/or melt reactions [6]. Many of the earliest applications of zeolites centred on their ion exchange ability, although these were superseded by the extensive use of ion exchange resins. However, in recent times, environmental issues have come to the fore, and since zeolites degrade to soil like materials, they have once again adopted the mantle of the most important industrial ion exchangers; the extensive use of zeolite A as water softeners in washing powders provides a case in point [21]. Further uses include the removal of ammonia from waste water and treatment of radioactive waste [2].

1.3 SODALITES

The name sodalite is derived from the high sodium content of the mineral, $Na_8[AlSiO_4]_6.Cl_2$; it was subsequently proposed by Henderson and Taylor [22] that the name be used to describe the family of compounds possessing the same structure as the mineral itself. The sodalite unit is the building block of many important zeolites, as described previously, and has the ability to entrap a wide range of anionic species, affording them improved thermal and chemical stability. Since they are highly symmetrical, they are provide an ideal model for the study of host-guest interactions. The simplicity of sodalites allows the facile elucidation of structural parameters, which can then be correlated with spectroscopic data from UV/VIS, IR, Raman and MASNMR experiments; such information may then be used to obtain information regarding more complex framework materials.

1.3.1 Sodalite Compositions

Sodalites can be described by the general formula $M_8[ABO_4]_6.X_2$, where M is a monovalent such as Na^+, Li^+ and Ag^+ [23-25], A and B are tetrahedral forming species such as Al and Si [2], and X can be a variety of mono or divalent anions, including Cl, Br, I [26, 27], $(ClO_4)^-$ [28], $(SO_4)^{2-}$ [29] and $(MoO_4)^{2-}$ [30]. The structure is based upon a truncated octahedral cage linked in three dimensions [31], yielding four and six membered rings which are directly linked to form the overall structure. Aluminosilicates are by far the most well known and characterised sodalites, in which a monovalent anion typically resides at every cage centre and is coordinated to sodiums resulting in the formation of M_4X clusters in each beta cage [32]. Sodalites are synthesised with Na^+ as the non-framework cation, which can then be exchanged by a range of other monovalents such as Li^+, K^+, Rb^+ and Ag^+ [23-25]. Direct synthesis using these other cations results in various zeolite frameworks [32].

Several sodalite sub-groups exist, and these include hydrosodalites [12, 34], noselites [26, 35], hauynes [36] and perhaps the most important of all sodalite species, the ultramarines [37-39]. Whereas aluminosilicate sodalites have monovalent anions in every cage, hydrosodalites, for example $Na_6[AlSiO_4]_6.8H_2O$, contain water molecules instead of anions in the beta cages, and as such only require six monovalent cations to charge balance the negative framework [12, 34]. Noselites have divalent anions in alternate cages [35]. In the hauyne sub-group, two sodium cations are replaced by divalents, with the extra positive

charge compensated by the existence in each cage of divalent anions. The general formula for a hauyne is thus written $M^{2+}{}_2M^{+}{}_6[ABO_4]_6(XO_4)_2$, where M includes Ca [36], Sr, Cd, Mn and Pb [40], and X includes S, Mo, W and Cr [36, 40].

A variety of framework substitutions have also been reported, similar to those found for zeolites [2]. The most common trivalent species incorporated into the framework is gallium, which can totally replace aluminium; similarly germanium can supplant silicon, and together these give rise to frameworks of formulae $(GaSiO_4)_6^{6-}$ [12, 41, 42], $(AlGeO_4)_6^{6-}$ [12, 40, 43, 44] and $(GaGeO_4)_6^{6-}$ [12], with properties similar to their aluminosilicate analogues. Incorporation of divalent species such as Be^{2+} or Zn^{2+} [12, 45] instead of Al^{3+} leads to an increased negative charge on the framework which is compensated by the inclusion of divalent non-framework cations such as Ca^{2+}, giving rise to stoichiometries such as $Ca_8[BeSiO_4]_6(SO_4)_2$ [45]. Similar stoichiometries arise from frameworks in which there is only one trivalent framework species, for example $Ca_8[AlO_2]_{12}S_2$ [46]. Such moieties disobey Loewenstein's rule [8] of aluminium avoidance, since they must necessarily contain direct Al-O-Al linkages.

1.3.2 Ultramarine

Ultramarine has been known since ancient Babylonian times, and is the species responsible for the colour in the semi-precious mineral lapis lazuli. This occurs naturally in China, Persia and Tibet, and was brought into Europe through the port of Venice, Italy hence the name ultramarine which is derived from the term "azurro ultramarino", the blue from beyond the seas [47]. The extraction of ultramarine from the mineral was first described in 1271 by Marco Polo, and there were many subsequent attempts at its synthesis, but the first proven route was not until 1828 by Guimet [48] and Gmelin [49]. Ultramarine is used extensively as a pigment in eye make up, food dyes, paint, ceramics and plastics. It is also responsible for the "bluey-whiteness" of washing powder under ultraviolet light [50]. There are several forms of ultramarine, containing sulphur in various ionic forms. In an analogous manner to sodalites its structure is comprised of the truncated octahedron, although it has been reported that the framework aluminium and silicon cations are often disordered, thus disobeying Loewenstein's rule of aluminium avoidance [8].

The green, blue, pink, red and violet forms of ultramarine have all been reported as being caused by polysulphide radical species S_n^- entrapped in the sodalite cages [51-55]. Since framework disorder is present, these compounds adopt the space group $I\bar{4}3m$ rather

than that of the ordered sodalites $P\bar{4}3n$. In the 1960 s and 1970 s, extensive spectroscopic characterisation was performed on the ultramarine system, and it was proposed that the S_2^-, S^{2-}, S_3^- and S_4 as the cavity species present in various ratios in the different forms [51-53]. Diffuse reflectance spectra for ultramarine green and red show common bands at approximately 400 and 600 nm assignable to S_2^- ($^2\Pi_{1/2u} \leftarrow {}^2\Pi_{3/2g}$) and S_3^- ($^2B_1 \leftarrow {}^2A_1$) respectively. For ultramarine red the additional band at 520 nm has been assigned to a non-ring form of S_4, possibly the D_{3h} form having no unpaired electrons . The chain form which would be a diradical is thought unlikely due to the large number of S atoms (75) per unpaired electron reported for ultramarine reds [55, 56]. Ultramarine blue contains the S_3^- chromophore shown by a single band at 600 nm. The incorporation of the S_3^- ion provides an excellent example of the stabilising effect of the sodalite cage, since no simple salts of S_3^- exist due to rapid dimerisation upon addition of counterions to its solutions [57].

1.3.3 The Structure of Sodalites

The structure was first determined by Linus Pauling [58] in 1930 using a sample of the mineral, $Na_8[AlSiO_4]_6.Cl_2$, from Bancroft, Ontario. His single crystal study yielded a cubic cell of cell parameter 8.870 Å, and examination of the systematic absences indicated the space group $P\bar{4}3n$. Aluminium, silicon and chlorine were on fixed sites, with the framework oxygens between the aluminium and silicon, and closer to silicon than aluminium as would be expected from the ionic radii. The aluminium and silicon tetrahedral sites are located on the faces of a cube, giving rise to four rings on the faces and six rings on the cube vertices providing the basic beta cage unit. Loewenstein's rule of aluminium avoidance is obeyed, and hence there is strict ordering of the framework aluminium and silicon, with silicon to oxygen distances approximately 1.65 Å and aluminium to oxygen 1.73 Å. These distances do not vary significantly as the composition is changed, whereas the Al-O-Si framework bond angle can vary in the range 120 - 160 ° depending on the cell parameter [59]. The oxygen geometry forces them out of the plane defined by the aluminium and silicon, leading to four and six ring puckering, in which the individual oxygens alternate in and out from the plane. The metal ions, situated in or near the six rings, coordinate to the framework oxygens with the degree of bonding dependent on the level of puckering in the system. A low degree of ring puckering, and hence an open framework, results in strong coordination of the metal to six framework oxygens, whereas a high level of puckering leads

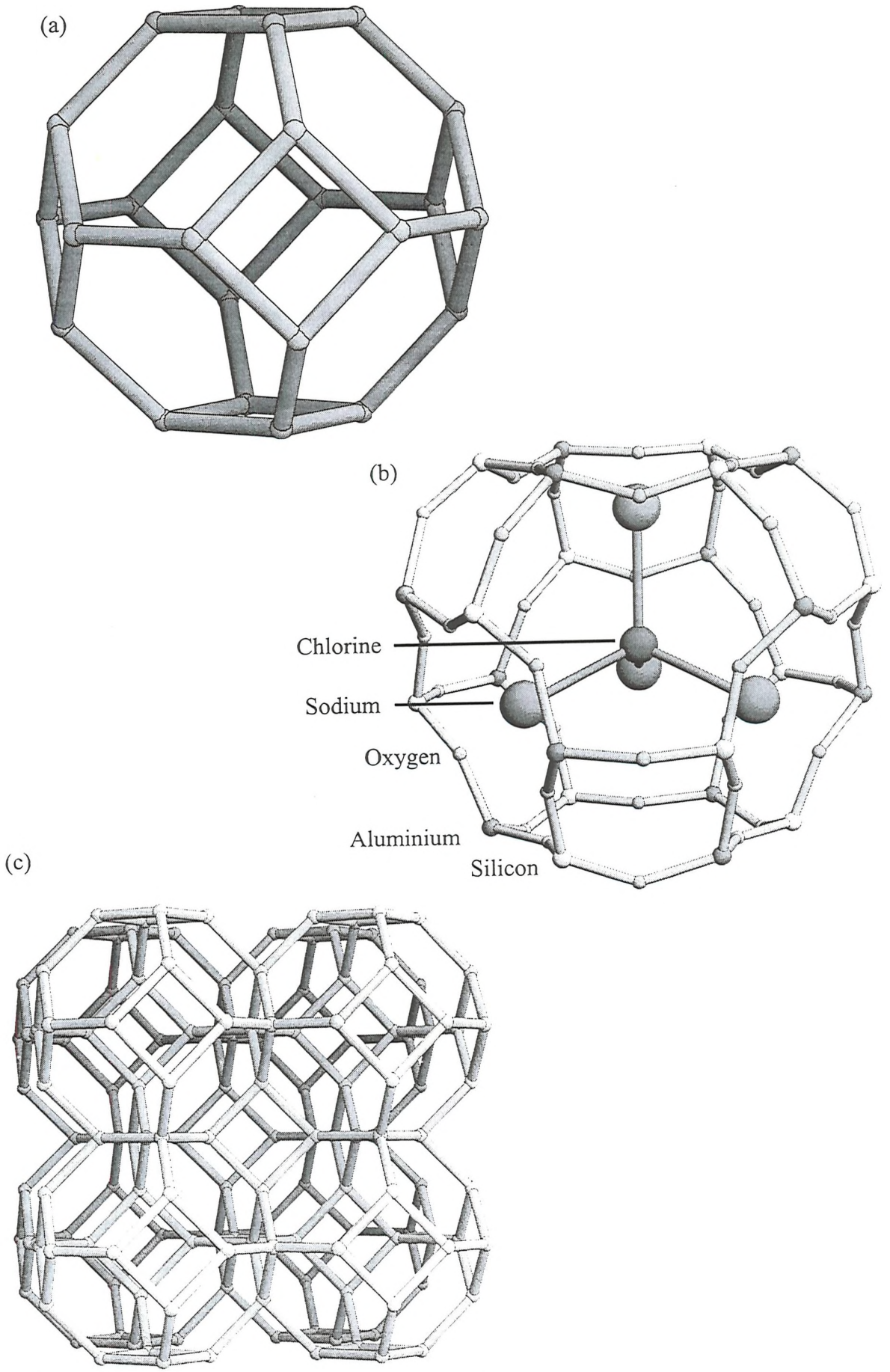

Figure 1.3(a) Truncated octahedron **(b)** Sodalite structure **(c)** Linkage of cages via the four rings

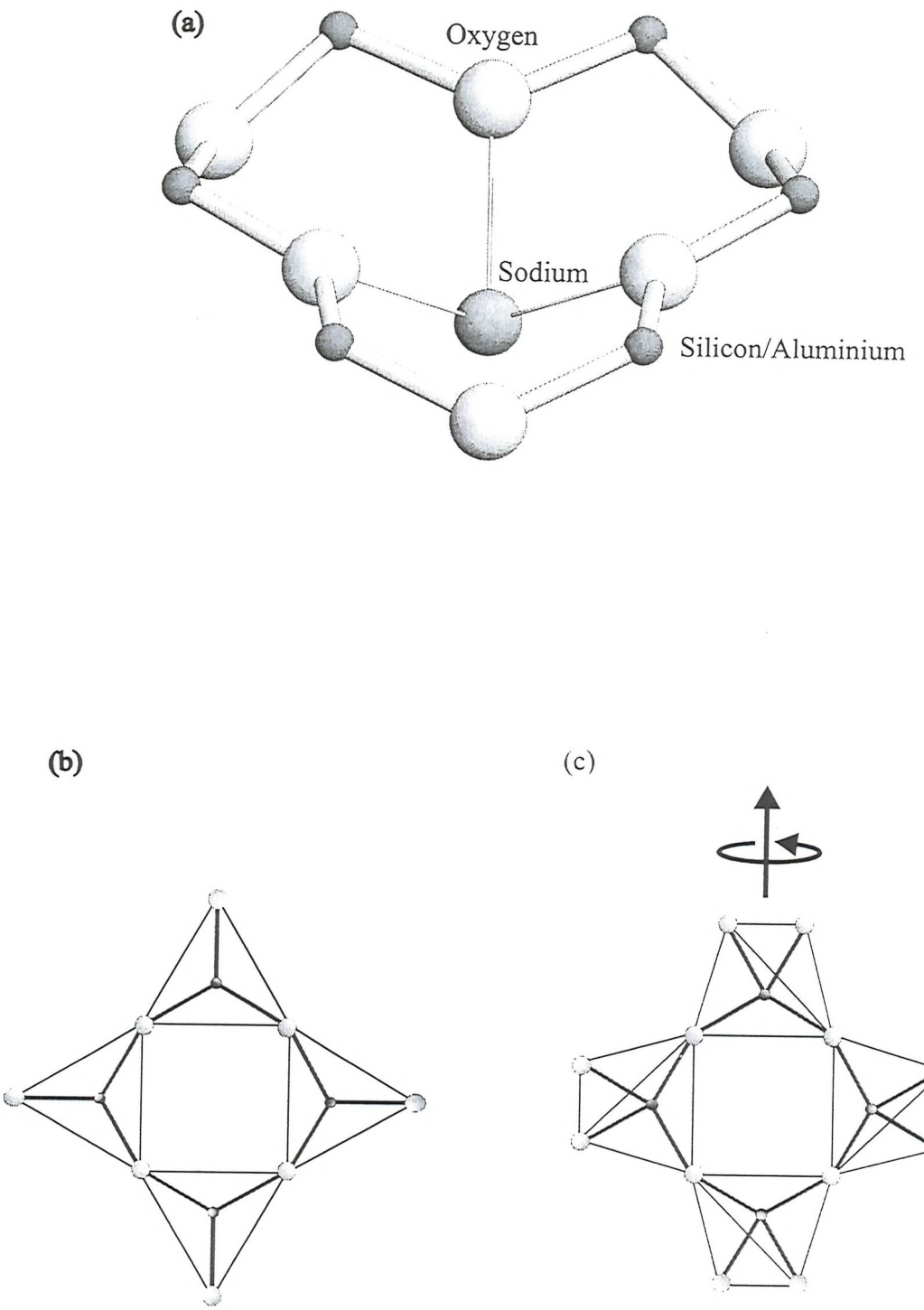

Figure 1.4(a) Sodium coordination to the framework oxygens, **(b)** Fully expanded four ring tetrahedral positions, and **(c)** collapsed structure showing tetrahedral tilting.

to strong coordination to three oxygens and weak coordination to three others. The metal is also bonded to the anion, which is located at the origin and the centre of the unit cell, corresponding to the centre of the beta cage. Thus the metal species has a coordination which can be viewed as either four or seven.

Sodalites can accommodate a large range of anions and cations due to the flexibility of the framework, which is manifested in two ways. Cooperative rotations of TO_4 tetrahedra about the 4 axis can occur, where the tilt angle, Ø, takes values between 0 and 30 °, and is greater for Si than Al due to the shorter T-O distance. Tetrahedral tilting leads to a decrease in the Al-O-Si angle and hence a smaller cell. Fully expanded sodalites, of space group Im3m, have a zero tilt angle, whereas for partially collapsed sodalites, the tetrahedra tilt and the symmetry is lowered to $I\bar{4}3m$. It has been argued that for aluminosilicate sodalites, only those rich in aluminium can take low Ø values [60]. The second mechanism is TO_4 deformation, although in sodalites significant deviation from the ideal tetrahedral angle is not generally observed, with angles typically in the range 105 ° ≤ O-T-O ≤ 114 °. Such framework collapse allows cell parameters to take values in the range 8.45 - 9.4 Å.

1.3.4 Properties of Sodalites

The most important property of sodalites is the improved chemical and thermal stability afforded to the entrapped anions, and this property is exploited in their use as pigments. Ultramarine has already been discussed in some detail, and provides the classic example of a sodalite pigment. However, there are several other important properties of sodalite compounds. Sodalites display both photochromic and cathodochromic effects [61-65], which has led to their use in graphic and digital information storage systems [66]. Sodalite excitation results in the expulsion of the halogen from the cage centre creating a negative ion vacancy, called an F centre impurity, and an associated characteristic absorption band in the visible region [67]. Photochromism involves excitation via red light, and the sodalite may be bleached by green light in the presence of an electric field. When the excitation occurs using an electron beam, the effect is called cathodochromism, and the system can be bleached by a laser [65, 66]. Such behaviour under the influence of an electron beam has been shown to be preferable to that of the simple alkali halides: the sodalites are more stable, and there is greater colouration and bleaching. This has led to their use in storage cathode ray tubes [68].

1.3.5 Cancrinite

Cancrinite is a naturally occurring mineral, $Ca_2Na_6(AlSiO_4)_6(CO_3)_2$ which belongs to the chabazite zeolite sub-group which also contains sodalite, and is based on the stacking of six rings. Sodalite is comprised of the six ring stacking sequence ABCABC, whereas cancrinite is represented as ABAB shown in Figure 1.5. The cancrinite structure is a common intergrowth in sodalite products, and can adopt the same general formula as a sodalite. In low temperature solution synthesis, it commonly arises when the anion is divalent. The structure, shown in Figure 1.6, is built up from 11-hedral cages and channels both surrounded by puckered twelve membered rings [69, 70]. Water molecules reside in the cages, anions in the channel centres, and, as in sodalites, the metal cations are located in the six ring windows.

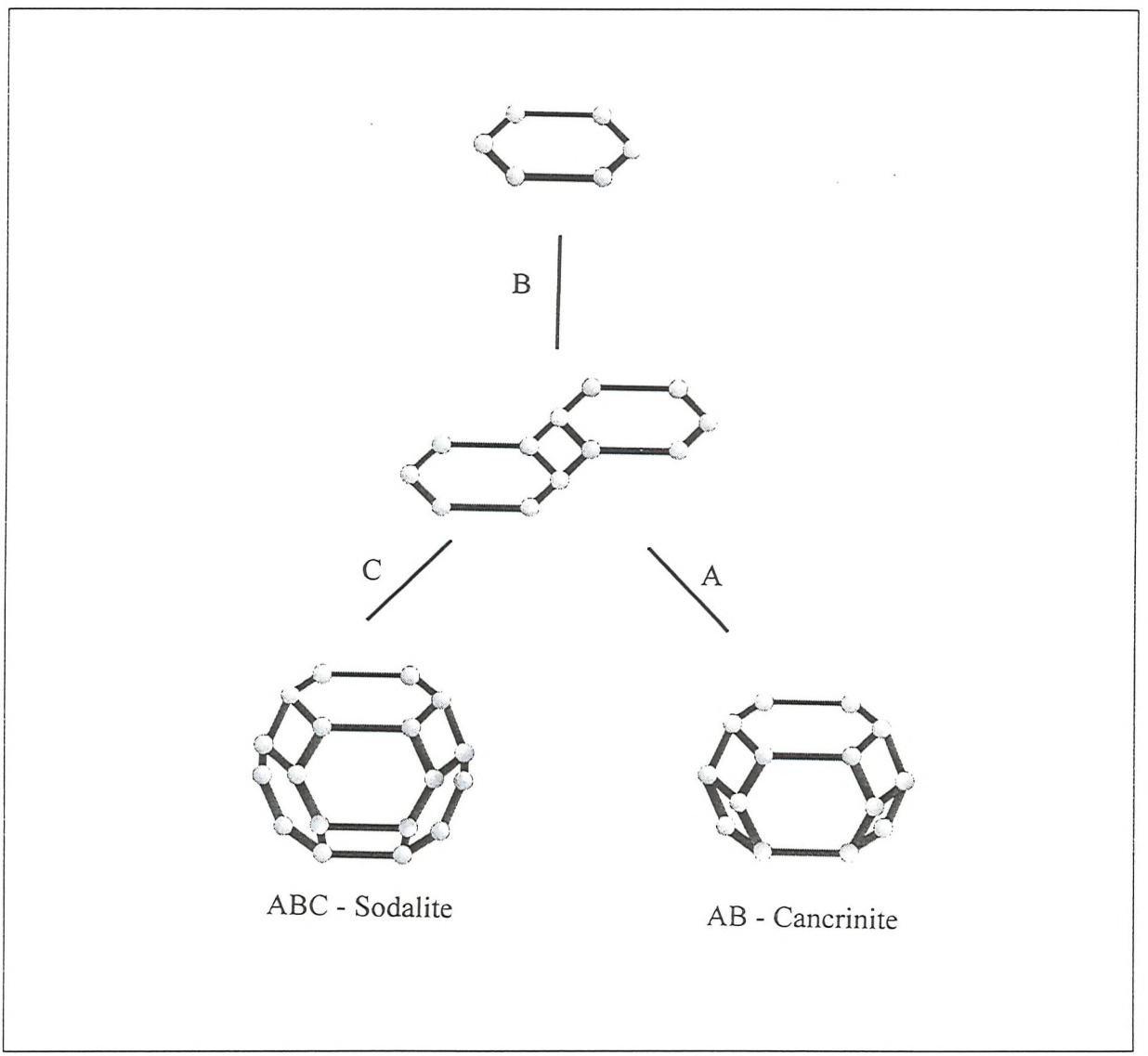

Figure 1.5 Six ring stacking to yield cancrinite and sodalite.

Ion exchange of the non-framework cations can take place in the same way as sodalites, as can intra-cage modification of the anions [71]. The structure can be converted to sodalite in some cases [72] by heating to approximately 800 °C, if the anion displays sufficient thermal stability. Since the structure is rather more open than that of sodalites, cancrinites are hygroscopic and are less thermally stable, thus limiting their industrial use.

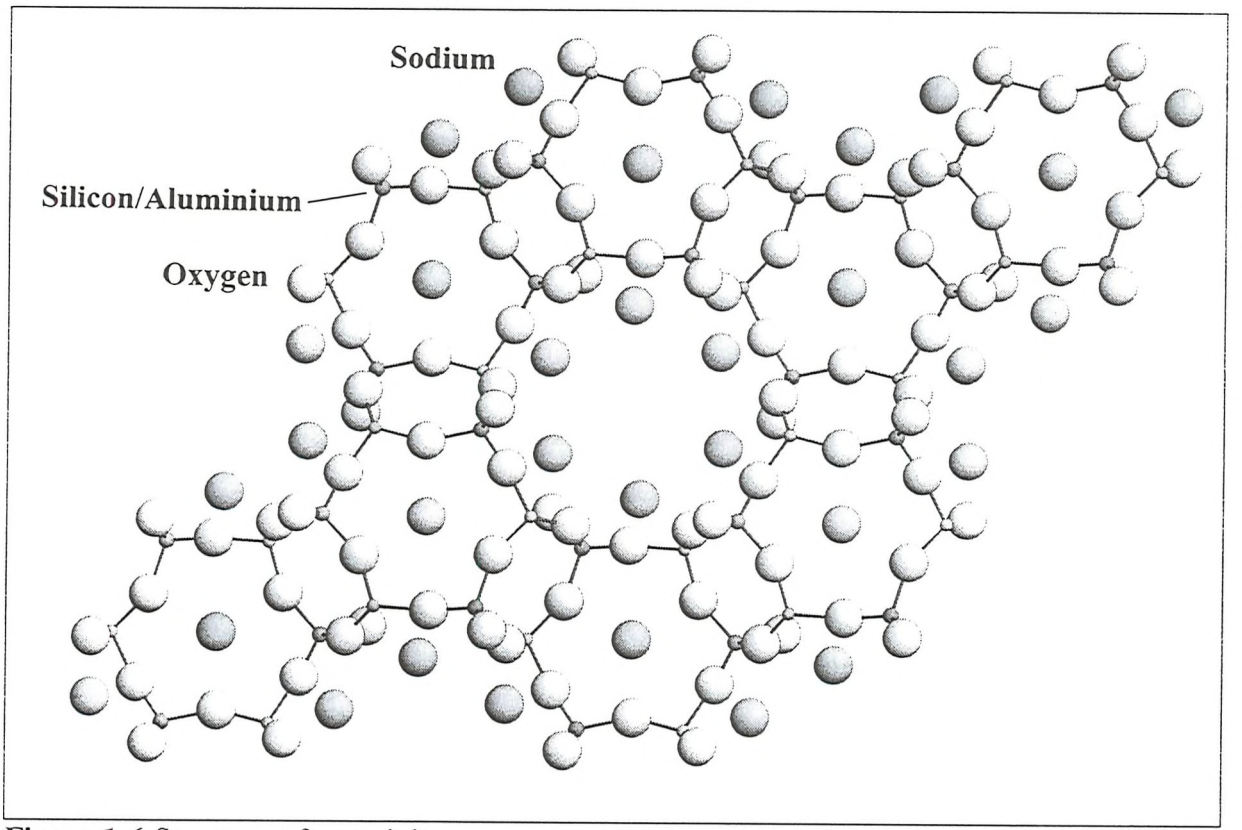

Figure 1.6 Structure of cancrinite.

1.4 PIGMENTS

The Dry Colour Manufacturers Association (DCMA) [73] provides a legally accepted definition of a pigment: "A pigment is a coloured, black, white or fluorescent particulate organic or inorganic solid which is usually insoluble in, and essentially physically and chemically unaffected by, the vehicle or substrate into which it is incorporated. A pigment will alter appearance by selective absorption and/or scattering of light. The pigment is usually dispersed in a vehicle or substrate for application as, for example, in the manufacture of paints, plastics, or other polymeric materials and inks. The pigment will retain its own unique crystalline or particulate structure throughout the incorporation period."

Economic aspects of industrial pigments illustrate the important role which inorganic species play. In 1989, the world production of pigments was (4-5) x 10^6 tonnes, with inorganic pigments accounting for approximately 96 %. The United States supplied about a third, The European Community a third, and the final third by all the remaining countries. The German pigment industry supplied more that 40 % of the world consumption of inorganic coloured pigments, including over 50 % of the iron oxides. The sales of inorganic pigments in 1989 was in the region of US \$13 x 10^9 [73].

Inorganic pigments can be classified [47] as shown in Table 1.1 below.

Pigment Term	Definition
White	Optical effect caused by non- selective light scattering (e.g. ZnS, TiO_2)
Coloured	Optical effect caused by selective light absorption and selective light scattering (e.g. Cd, Cr and Co pigments)
Luminescent	Optical effect caused by capacity to absorb radiation and emit it as light of longer wavelength
Fluorescent	Light of longer wavelength emitted after excitation without a delay (e.g. Ag doped ZnS)
Phosphorescent	Light of longer wavelength emitted several hours after excitation (e.g. Cu doped ZnS)

It is coloured pigments which are of relevance to this work, and those currently widely used in industry are detailed below. The properties which make them suitable as pigments, as well as the drawbacks of each are highlighted.

1.4.1 Iron oxide pigments

The yellow, brown and red natural iron oxides are all based on the chemical formula Fe_2O_3 with varying degrees of hydration, amounts of FeO and clay depending on the grade and pigment type [47]. Yellow iron oxide, limonite, is represented as $Fe_2O_3.xH_2O$, and is found in the common yellow grades from South Africa and India; light to dark yellow ochres originate from France, Georgia and Virginia, and medium to dark yellow siennas from Italy and America: the darker shades tend to be richer in iron content. Hematite, Fe_2O_3, a light to medium red sourced from Spain and New York, and the red/orange burnt siennas which are calcined limonites from Italy or USA, together comprise the red iron oxides. Iron browns consist of limonite, carbon and manganese dioxide known as the green/brown raw umber or the deep brown burnt umber, both from Cyprus. Historically, these iron oxides have been used as primary colour pigments in paint, plastics, paper, woodstains and ceramics, and are second only to TiO_2 in volume consumed. They are insoluble in almost everything except very strong acids.

Synthetic coloured iron oxide pigments provide a wide colour range and are cheap to synthesise, display high stability and are non-toxic [47]. Reds, Fe_2O_3, are synthesised by four routes, each producing a typical particle size, and depending on the thermal history or precipitation cycle, it is possible to produce a family of products with hues ranging from light to main red. High temperature calcination of either iron sulphate, black iron oxide, $Fe_2O_3.FeO$, or yellow iron oxide, $Fe_2O_3.H_2O$, yields red iron oxide, as does precipitation via oxygen from an aqueous medium containing scrap steel. Applications involve coatings, plastics, rubber and ceramics due to their acid and alkali resistance, purity and thermal stability. They have little or no reflectance below 400 nm, and thus are strong UV absorbers helping to protect the binders in paint, plastic and paper from sunlight degradation. Industrial synthetic reds tend to be 10 -25 % the cost of organics, and are of higher chemical purity than their natural equivalents.

Synthetic yellow iron oxides, $Fe_2O_3.xH_2O$, where x is 11-14 % by weight, have narrow particle size distributions which enhance colour purity. Since they contain chemically combined water, they are subject to temperature limitations, and lose H_2O at 177 °C. They

are synthesised in three main ways: in the Penniman-Zoph process [74] scrap steel and a ferrous salt are used to grow the seed particle to the finished particle; by direct precipitation from alkali and a ferrous salt; via the aniline process reacting nitrobenzene and metallic iron to yield iron yellow and aniline. They possess the unique acicular (needlelike) shape required for magnetic tapes, and as such are used worldwide as the major raw material for magnetic particles, from which water is removed and subsequent reduction and oxidation produce acicular magnetic iron oxide.

Synthetic brown oxides, $(FeO)_x.(Fe_2O_3)_y.(H_2O)_z$, are permanent, non toxic pigments with good chemical resistance. They are ideal for floor stains, house paints, furniture stains, leather finishes and concrete colouring. They are manufactured mainly by physically blending red, yellow and black iron oxides.

Zinc and magnesium ferrite tans, $ZnO.Fe_2O_3$ and $MgO.Fe_2O_3$, are not technically iron oxide, but are similar in composition and characteristics. Prepared by calcining iron oxides with elemental zinc or magnesium [75, 76], they are highly pure and exhibit good heat resistance, but are approximately 50 % more expensive than other synthetic iron oxides and thus are only used when their inert, non reactive, non toxic and temperature resistant properties are required.

1.4.2 Lead chrome pigments

Lead chromate occurs naturally as the orange-red mineral crocoite, whose chemical composition was identified in 1797 by L.N. Vauquellin, who subsequently carried out the first synthetic preparation in 1809 [47]. Its desirable colour, wide ranging applications and low cost make it appealing, but since the mid 1970s the concern regarding lead toxicity has restricted its use. The major component in these pigments is lead chromate itself, with other lead compounds present as solid solutions.

Medium chrome yellow closely approaches pure lead chromate, and is represented as $PbCrO_4$. Lemon and primrose yellows, $PbCrO_4.xPbSO_4$, are coprecipitates of lead chromate and lead sulphate. Molybdate oranges are coprecipitates of lead chromate with lead molybdate and lead sulphate, $PbCrO_4.xPbMoO_4.yPbSO_4$, and chrome orange is the basic lead chromate, $PbCrO_4.xPbO$.

Medium chrome yellow is prepared by reacting a soluble lead salt such as lead nitrate with a soluble chromate salt such as dichromate. Orthorhombic lead chromate crystals precipitate out, but these are thermodynamically unstable, so conversion to other crystal

forms is possible. Since the different crystal forms different colour properties, control of the crystallisation process is critical. Medium chrome yellow is monoclinic, and conversion from orthorhombic is achieved using high temperature and an excess of $(CrO_4)^{2-}$ salt, then stabilised by precipitating metal hydroxides such as Ti, Si and Al onto the surface. Light chrome yellow is attained by forming monoclinic crystals in which 20-40 % soluble sulphate is substituted for chromate to yield a solid solution of lead chromate-lead sulphate. As the level of sulphate is augmented the pigment becomes lighter, greener and weaker. An excess of Pb^{2+} leads to orthorhombic primrose chrome yellow, stabilised by precipitation in the presence of certain additives.

The range of lead chromes is diversified by forming solid solutions with lead molybdate [77]. Whilst monoclinic or orthorhombic lead chromate is yellow and lead molybdate is white, coprecipitation of the two yields a tetragonal solid solution which is a brilliant orange/red shade. Most commercial grades of molybdate orange also contain lead sulphate to help stabilise the structure, which thus can be written $PbCrO_4.PbMoO_4.PbSO_4$. The redder shades are lower in molybdenum content.

The main applications of lead based pigments are in paints, plastics and printing inks, with smaller outlets in paper and fabrics. They are not, however, recommended for foodstuff packaging due to the lead content, and display insufficient chemical resistance as inks for certain products such as soaps and fertilisers.

1.4.3 Cadmium pigments

Cadmium pigments typically involve the use of five basic elements: Cd, S, Se, Hg and Zn. They provide infinite shades of light yellow through to orange, red and deep maroon, and this array of brilliant shades show stability to high temperature, fade resistance to UV light, good durability, resistance to alkalis and dilute acids and good dispersibility. The development of cadmium sulphide, which exists as the natural mineral greenockite, in 1918 was recorded by Gay Lussac. Friedrich Strohmeyer is credited with first isolating metallic cadmium from the mineral sphalerite in 1817 [47]. Cadmium pigments are the only class which can provide bright reds at the usual ceramic glaze temperatures of 1010-1040 °C; and their encapsulation in zirconium silicates further extends their thermal stability to 1230 °C. The molybdate oranges and chrome yellows provide alternatives to Cd colorants, although these are limited in the heat-light area, and are difficult to apply to nylon, polyethene, acrylic and polycarbonates [73].

The commercial preparation of CdS is achieved using highly pure Cd metal, CdO or $CdCO_3$, which is dissolved in mineral acid, yielding $CdSO_4$. This is then reacted with sodium sulphide to give a finely divided precipitate of the concentrated pigment:

$$CdSO_4 + Na_2S \rightarrow CdS + Na_2SO_4$$

CdSe is produced in an analogous manner, whereby an appropriate amount of selenium is dissolved in the sodium sulphide solution. Calcination at 600 °C follows the precipitation stage.

Cadmium mercury sulphides, CdS.xHgS, are of variable composition, the redder shades being richer in mercury. They are described as a series of mixed crystals with CdS as the host lattice in which Hg displaces a portion of Cd, or alternatively as a solid solution of HgS in CdS. In the early 1950s, the two general classes of cadmium pigments in use were the yellows and reds. The Cd reds were solid solutions of CdSe in CdS, and although more expensive than other inorganics, they were vastly superior in quality and properties. In 1948, a selenium shortage affected the pigment industry with the vast majority of the available selenium going to the electronics industry. This led to the Imperial Paper and Colour Corporation developing Mercadmium® (now licensed to The Ciba-Geigy Corporation) alternatives to Se reds in 1955 [78]. Being very similar to cadmium sulphoselenides, these quickly filled the void left by the Se shortage, and due to their more economical production the Cd-Hg sulphides have held many of their original applications since. Precipitation of cadmium and mercury sulphides from solutions of their salts is followed by calcination in non-oxidising atmospheres to convert the cubic to the hexagonal form of the species. The resultant pigments have excellent heat stability, extreme insolubility in organic solvents, good chemical resistance to alkalis and weak acids, excellent lightfastness and easy dispersion. The obvious drawback is the toxicity of the Hg and Cd components: the use of cadmium is already restricted by EC law, and further stringent regulations soon to be introduced will further limit its use.

1.4.4 Titanium based pigments

Nickel antimony titanate yellow, $NiO.Sb_2O_5.20TiO_2$, and chrome antimony buffs, $CrO_3.Sb_2O_5.31TiO_2$, were developed approximately fifty years ago. They are manufactured by calcining oxides of the components at *circa* 1000 °C. They are chemically inert, insoluble

in most solvents, display high thermal stability, are resistant to alkali and acid, but are not bright, having weak tints which require a high pigment loading in coatings and paints, the main market for these colorants. Antimony can be replaced by niobium in both of these systems to give the same colour and properties, whilst removing the problem of the toxicity associated with Sb. The manganese antimony titanate browns, $(Mn,Sb,Ti)O_2$ were developed about twenty years ago and have both similar properties and preparations as the other titanates [47].

1.4.5 Iron Blue

$M^{I}Fe^{II}Fe^{III}(CN)_6.H_2O$, where M = NH_4^+ or an alkali metal cation, is also known as Milori Blue or Prussian Blue. The potassium version is generally preferred due to its excellent hues in industrial manufacture. It was the earliest synthetic pigment, discovered in 1704 in Berlin by Diesbach, and possesses a very hard texture. The Frenchman Milori developed a version with improved texture, hence the name Milori Blue [47]. Iron blue pigments are produced by the precipitation of complex iron(II) cyanides by iron(II) salts in aqueous solution. The product is Berlin white, a precipitate of iron(II) hexacyanoferrate (II), $M^{I}_2Fe^{II}[Fe^{II}(CN)_6]$ or $M^{II}Fe^{II}[Fe^{II}(CN)_6]$, which is then digested in H_2SO_4 and oxidised using $Na_2Cr_2O_7$ or $NaClO_3$ to yield the blue pigment. Properties include good permanency, excellent light fastness and brilliant shades, but they are alkali sensitive and thermally stable to only 120 °C.

1.4.6 Bismuth Vanadate/Molybdate yellow

This two phase pigment, $4BiVO_4.3Bi_2MoO_6$, consists of tetragonal $BiVO_4$ of scheelite structure, and the metastable, orthorhombic perovskite Bi_2MoO_6. The hue is controlled by the $BiVO_4/Bi_2MoO_6$ ratio, for which $BiVO_4$ is the colour carrier. Increasing the level of molybdate makes the pigment greener. Bismuth vanadate is primrose yellow and is found in the mineral pucherite. Pure $BiVO_4$ was first synthesised in 1924 by Zintl [79] and was used initially for pharmaceutical purposes. It came to prominence as a pigment in 1976 when it was developed by DuPont [80-82]. Its manufacture is a two stage process [83] in which an amorphous oxide precipitates from an aqueous solution of Bi, V and Mo salts in nitric acid. These small amorphous gel particles do not have any pigment properties, but are subsequently reacted at 600 °C to simultaneously form crystalline $BiVO_4$ and Bi_2MoO_6.

This non-toxic green/yellow inorganic species is used widely in industrial paints and automotive finishes, and has excellent weathering properties.

1.4.7 Cobalt Blue

Cobalt chemistry is said to date from the sixteenth century, but Co has been found in ancient glazes and glasses from Persia as early as 2250 BC [84]. In China, cobalt colorants were used as early as the T'ang Dynasty, dating from 618-906 AD Smalt, a potassium silicate glass coloured with cobalt was used in the mid 1550s, but it was not until 1777 that the effect of alumina on cobalt was described by Wenzel, who detailed a more neutral blue [84]. This cobalt aluminate blue, $CoO.Al_2O_3$, is generally attributed to Thénard, who produced it some thirty years later, and who is credited with beginning the proper study of cobalt chemistry in 1802 [84]. Calcination of $CoCO_3$ and alumina trihydrate at temperatures up to 1300 °C gives the cubic spinel of composition $CoO.Al_2O_3$. Chromium can be introduced into the system to yield the blue, green or turquoise cobalt chrome aluminate, $2CoO.Cr_2O_3.Al_2O_3$.

These cobalt pigments are relatively inert, resistant to acids, alkalis, oxidation and reduction, have high thermal stability, and are extremely lightfast and weather resistant. Their main applications are in the plastics and coatings industry. The dramatic increase in the price of elemental cobalt in recent years has made cobalt pigments very expensive.

1.4.8 Ultramarine

As described previously, ultramarine is the pigment present in the mineral lapis lazuli, found in ancient times in abundance in China, Persia and Tibet. Industrially ultramarine is synthesised from calcined kaolin, soda ash, sulphur, silica, coal or pitch and sodium sulphate [47]. The materials are dry ground to a mean particle size of 15 μm, and heated to 750 °C under reducing conditions. The sodium carbonate reacts with sulphur and the reductant at 300 °C to form sodium polysulphide. At higher temperature, the kaolin is restructured to form a 3D network, which at 700 °C is transformed to the sodalite structure with the associated entrapped sodium and polysulphide ions. In order to oxidise the polysulphide anions, the furnace is allowed to cool to 500 °C, at which point air is admitted: the excess sulphur reacts to form SO_2 which exothermically oxidises the di- and tri-polysulphide ions to S_2^- and S_3^- free radicals, leaving sodium sulphoxides and sulphur as by

products. The sulphoxides are washed out, and sulphur removed by slurrying and wet grinding, leaving the raw blue compound. This blue can be reacted at 240 °C with NH_4Cl in air to yield violet, which in turn can be treated with HCl gas at 140 °C to give the pink derivative. The shade obtained from the furnace is varied by altering the ratio of starting components: the green and blue ultramarines contain more Al and less S than the red shades, which incorporate extra silica in the reagent mixture.

Ultramarines display hydrophilic surface characteristics, excellent lightfastness, high thermal stability, solvent resistance, are alkali stable, but sensitive to acids. Their low toxicity makes them ideal for many applications which include eye make-up, food dyes, paint, ceramics and plastics, as well as being responsible for the "bluey whiteness" of washing powders under ultraviolet light.

1.4.9 The requirement for new pigments

The main problem associated with present inorganic pigments is one of toxicity and therefore a move towards organic based pigments cannot be discounted. In general, however, organic pigments are 25-30 % more expensive than inorganics; most inorganic pigments are prepared in high yields (> 90 %) by solid state reactions, whereas for the organics, yields of less than 80 % are not uncommon [85]. Inorganic pigments also display the higher thermal stability than organics which is required for their use in ceramics and plastics. New inorganic pigments are thus required which do not result in toxic species during preparation, use or disposal.

The properties of an ideal inorganic pigment include low toxicity, light and heat fastness, high thermal stability, resistance to acids and alkalis, good weathering, uniformity of colour, insolubility in solvents, with an easy and cheap synthetic route. Ultramarine possesses many of these qualities, and hence sodalites have been selected as potential alternatives for some of the pigments in current use.

1.5 SCOPE OF THE CURRENT WORK

The sodalite family has been the subject of a vast amount of research, concerning all aspects such as synthesis, modification, characterisation and computer modelling. The vast majority of this research has targeted aluminosilicate framework materials. It is the intention of this work to use the aluminosilicate framework as a basis for an investigation of the sodalite series, which will then be extended to other framework compositions, allowing a study of dependence of sodalite properties on composition.

1.5.1 Investigation of aluminosilicate sodalites

Aluminosilicate sodalites containing a wide range of anions will be synthesised by solution, hydrothermal or solid state techniques. Subsequent analysis by powder diffraction will permit the accurate determination of structural parameters such as cell parameter, atomic positions and bond lengths and angles. The effect of non framework cations and anions on these variables can be resolved using powder x-ray and neutron diffraction, and the resultant structural parameters can be related to spectroscopic parameters such as MASNMR chemical shift and infra-red band positions.

1.5.2 Effect of sodalite framework compositions

The introduction of gallium and germanium in zeolite frameworks has been shown to affect properties such as redox activity and acidity. Hence, there has recently been increased interest concerning these substitutions in zeolites and their rather simpler sodalite analogues. It is one aim of this work to investigate various synthetic routes to gallium and germanium substituted sodalites, and to establish preparative conditions rather less drastic than those previously reported. The influence on structural and spectroscopic properties will be investigated, and compared with their aluminosilicate counterparts.

1.5.3 Sodalites as potential pigments

Nature provides us with a classical example of a sodalite pigment in ultramarine. It is the intention of this project to emulate nature and incorporate coloured anions within the sodalite ß-cage, or anions which once entrapped can be modified to yield coloured species. It

is hoped that the increased cage size associated with gallium and germanium framework substitution can be used to enclathrate anions normally too large to be entrapped by aluminosilicates, thus increasing the scope of sodalite based pigments. Those anions so entrapped will be afforded much improved chemical and thermal stability compared with the free sodium salts.

1.6 REFERENCES

[1] W.A. Deer, R.A. Howie and J. Zussman, 'An Introduction to The Rock Forming Minerals', Longmans, London (1966).

[2] J.M. Newsam, 'Solid State Chemistry: Compounds', Chapter 7, A.K. Cheetham and P. Day (eds.), Oxford University Press (1992).

[3] R.M. Barrer, 'Hydrothermal Chemistry of Zeolites', Academic Press, London (1982).

[4] W.L. Brown (ed.), 'Feldspar and Feldspathoids', (NATO ASI Series No. C137), D. Riedel, Dordrecht (1984).

[5] A.F. Cronstedt, *Akad. Handl. Stockholm*, **17**, 120 (1756).

[6] D.W. Breck, 'Zeolite Molecular Sieves, Structure, Chemistry and Uses', Wiley-Interscience, New York (1974).

[7] R.L. Wadlinger, G.T. Kerr and E.J. Rosinski, *US Patent* 3, 308, 069 (1967).

[8] W. Löwenstein, *Am. Miner.*, **39**, 92 (1954).

[9] R.M. Barrer, 'Zeolites and Clay Minerals as Sorbents and Molecular Sieves', Chapter 2, Academic Press, London and New York (1978).

[10] J.M. Newsam and D.E.W. Vaughan, 'New Developments in Zeolite Science and Technology', 457-464, Tokyo and Elsevier, Amsterdam (1986).

[11] R. Szostak, 'Molecular Sieves: Principles of Synthesis and Identification', Van Nostrand Rheinhold, New York (1988).

[12] T.M. Nenoff, W.T.A. Harrison, T.E. Gier, N.L. Keder, C.M. Zaremba, V.I. Srdanov, J.M. Nicol and G.D. Stucky, *Inorg. Chem.*, **33**, 2472 (1994).

[13] S.T. Wilson, B.M. Lok, C.A. Messina, T.R. Cannan and E.M. Flanigen, *J. Am. Chem. Soc.*, **104**, 1146 (1982).

[14] B.M. Lok, C.A. Messina, R.L. Patton, R.T. Gajek, T.R. Cannan and E.M. Flanigen, *J. Am. Chem. Soc.*, **106**, 6092 (1984).

[15] E.M. Flanigen, B.M. Lok, R.L. Patton and S.T. Wilson, 'New Developments in Zeolite Science and Technology', 103-112, Kodansha, Toyko and Elsevier, Amsterdam (1986).

[16] E.M. Flanigen, R.L. Patton and S.T. Wilson, *Stud. Surf. Sci. Catal.*, **37**, 13, Elsevier, Amsterdam (1988).

[17] J.V. Smith, *Adv. Chem. Ser.*, **101**, 171 (1971).

[18] J.B. Uytterhoeven, L. Christner and W.K. Hall, *J. Phys. Chem.*, **69**, 2117 (1965).

[19] J.A. Rabo, 'Zeolite Chemistry and Catalysis', *ACS Mon.*, **171** (1976).

[20] J.W. Mellor, 'A Comprehensive Treatise on Inorganic and Theoretical Chemistry Volume VI', Longmans, London (1981).

[21] G. Gottardi and E. Galli, 'Natural Zeolites', Springer-Verlag, New York (1985).

[22] C.M.B. Henderson and D.Taylor, *Spectrochim. Acta*, **35**A, 929 (1979).

[23] D. Taylor, *Contrib. Mineral. Petrol.*, **51**, 39 (1975).

[24] C.M.B. Henderson and D. Taylor, *Spectrochim. Acta*, **33**A, 283 (1977).

[25] J. Godber and G.A. Ozin, *J. Phys. Chem.*, **92**, 4980 (1988).

[26] M.T. Weller and G. Wong, *Solid State Ionics*, **33**, 430 (1989).

[27] B. Beagley, C.M.B. Henderson and D. Taylor, *Mineral. Mag.*, **46**, 459 (1982).

[28] M.T. Weller and K.E. Haworth, *J. Chem. Soc., Chem. Commun.*, **10**, 373 (1991).

[29] T. Tomisaka and H.P. Eügster, *Miner. J.*, **5**(4), 249 (1968).

[30] G. Wong, *Ph.D. Thesis*, Unversity of Southampton (1990).

[31] I. Hassan and H.D. Grundy, *Acta Cryst.*, B**40**, 6 (1984).

[32] M.T. Weller and G. Wong, *Solid State Ionics*, **33**, 430 (1989).

[33] R.M. Barrer, J.F. Cole, and H. Sticher, *J. Chem. Soc.*, A**10**, 2475 (1968).

[34] G. Engelhardt, J. Felsche and P. Sieger, *J. Am. Chem. Soc.*, **114**, 1173 (1992).

[35] H. Schulz and H. Saalfeld, *Tschermaks Miner. Petrogr. Mitt.*, **115**, 460 (1961).

[36] J. Löhn and H. Schulz, *N. Jb. Miner. Abh.*, **109**(3), 201 (1968).

[37] F.M. Jaeger, *Trans. Faraday Soc.*, **25**, 320 (1929).

[38] S.D. McLaughlan and D.J. Marshall, *J. Phys. Chem.*, **74**(6), 1359 (1970).

[39] S.E. Tarling and P. Barnes, *Acta Cryst.*, B**44**, 128 (1988).

[40] R.R. Neurgaonkar and F.A. Hummel, *Mat. Res. Bull.*, **11**, 61 (1976).

[41] J.M. Newsam and J.D. Jorgensen, *Zeolites*, **7**, 569 (1987).

[42] L.B. McCusker, W.M. Meier, K. Suzuki and S. Shin, *Zeolites*, **6**, 388 (1986).

[43] M.E. Fleet, *Acta Cryst.*, C**45**, 843 (1989).

[44] M. Wiebcke, P. Sieger, J. Felsche, G. Engelhardt, P. Behrens and J. Schefer, *Z. Anorg. Allg. Chem.*, **619**, 1321 (1993).

[45] S.E. Dann and M.T. Weller,

[46] M.E. Brenchley and M.T. Weller, *J. Mater. Chem.*, **2**(10), 1003 (1992).

[47] G. Buxbaum (ed.), "Industrial Inorganic Pigments", VCH, Weinheim, Federal Republic of Germany (1993).

[48] J.B. Guimet, *Bull. Soc. Enc. Ind. Nat.*, **27**, 346 (1828).

[49] C.G. Gmelin, *Bull. Soc. Enc. Ind. Nat.*, **27**, 216 (1828).

[50] R.C. Brasted, 'Comprehensive Inorganic Chemistry Vol. VIII', 1st Edition, London (1961).

[51] R.J.H. Clark and M.L. Franks, *Chem. Phys. Lett.*, **34(1)**, 69 (1971).

[52] F.A. Cotton, J.B. Harmon and R.M. Hedges, *J. Am. Chem. Soc.*, **98(6)**, 1417 (1975).

[53] R.J.H. Clark and D.G. Cobbold, *Inorg. Chem.*, **17(11)**, 3169 (1978).

[54] E. Podschus, U. Hofmann and K. Leschewski, *Z. Anorg. Allg. Chem.*, **228**, 305 (1936).

[55] U. Hofmann, E. Herzensteil, E. Schoneman and K.-H. Schwarz, *Z. Anorg. Allg. Chem.*, **367**, 119 (1969).

[56] K.-H. Schwarz and U. Hofmann, *Z. Anorg. Allg. Chem.*, **378**, 152 (1970).

[57] R.J.H. Clark, T. Dines and M. Kurmoo, *Inorg. Chem.*, **22**, 2766 (1983).

[58] L. Pauling, *Z. Kristallogr.*, **74**, 213 (1930).

[59] B. Beagley and J.O. Titiloye, *Structural Chemistry*, **3**(6), 429 (1992).

[60] W. Depmeier, *Acta Cryst.*, B**40**, 185 (1984).

[61] I.F. Chang, *J. Electrochem. Soc.*, **121**(6), 815 (1974).

[62] I.F. Chang and O. Onton, *J. Electron. Materials*, **2**, 1 (1973)

[63] G.H. Brown, 'Photochromism', 1st Edition, John Wiley and Sons Inc., New York (1971).

[64] M.J. Taylor, D.J. Marshall and H. Evans, *J. Phys. Chem. Solids*, **32**, 2021 (1971).

[65] P.T. Bolwijn, D.J. Schipper and C.Z. van Doorn, *J. Appl. Phys.*, **43**(1), 132 (1972).

[66] M.R. Tubbs and D.K. Wright, *Phys. Stat. Sol. (A)*, **7**, 155 (1971).

[67] M.F. Miller, E.B. Bradley and L.T. Todd, *Infra-Red Phys.*, **25**(3), 531 (1985).

[68] A. Stein, G.A. Ozin and G.D. Stucky, *J. Soc. Photogr. Sci. Technol. Japan*, **53**(4), 322 (1990).

[69] H.D. Grundy and I. Hassan, *Can. Mineral.*, **20**, 239 (1982).

[70] H.D. Grundy and I. Hassan, *Can. Mineral.*, **29**, 377 (1991).

[71] G.G. Linder, W. Massa and D. Reinen, *J. Sol. State Chem.*, **117**, 386 (1995).

[72] S.E. Dann, *Personal Communication*, University of Southampton (1995).

[73] P.A. Lewis (ed.), "Pigment Handbook, Volume I: Properties and Economics",2nd Edition, Wiley-Interscience, New York (1990).

[74] R. Penniman and N. Zoph, US Patent 1, 268, 748 (1921).

[75] C.D. Downs and J. Martin, US Patent 2, 502, 130 (1950).

[76] C.D. Downs and J. Martin, US Patent 2, 904, 395 (1959).

[77] E. Lederle and H.G. Grimm, German Patent 574, 379 (1933).

[78] Ciba-Geigy Corporation, US Patent 2, 878, 134 (1955).

[79] V. Zintl, German Patent 4, 22, 947 (1924).

[80] Du Pont, US Patent 40, 26, 722 (1976).

[81] Du Pont, US Patent 40, 63, 956 (1976).

[82] Du Pont, US Patent 41, 15, 141/2 (1976).

[83] BASF, European Patent 74, 049 (1982).

[84] R.S. Young (ed.), "Cobalt: Its Chemistry, Metallurgy and Uses", Reinhold, New York (1960).

[85] J. Novotny, *RSC Inorganic Pigments Conference*, London (1994).

Chapter Two

EXPERIMENTAL TECHNIQUES

2.1 INTRODUCTION

Characterisation of materials prepared in this work was achieved using several techniques. The main method used was powder x-ray diffraction (PXD) which allowed rapid analysis of sample purity, cell parameter and phase identification using data collected over 20 minutes. Samples were subsequently characterised more fully using the Rietveld method [1, 2] from data acquired over a longer timescale, approximately 900 minutes, and selected materials were examined by powder neutron diffraction (PND). This allowed more accurate determination of lighter atoms, especially oxygen and lithium. This facilitated relationships between structural information and other spectroscopic data to be examined.

Fourier transform infra-red (FT-IR) and Raman (FT-Raman) spectroscopy were principally used in order to confirm the presence of anionic species within the sodalite cages. The former was also used to examine the effect of framework substitution on position and number of framework absorptions. Magic angle spinning nuclear magnetic resonance (MASNMR) spectroscopy was primarily employed to investigate framework ordering, but similarly to FT-IR spectroscopy, was also used to study the effect of sodalite composition on band positions. Coloured species were also characterised using ultraviolet-visible (UV/VIS) spectroscopy allowing the species responsible for the colouration to be identified.

Thermogravimetric analysis (TGA) permitted the stability of synthesised materials to be determined, in addition to providing information regarding the extent of surface adsorbed and entrapped water molecules. The thermal stability of anions could also be examined as a test for their suitability for entrapment within sodalite materials. Chemical analysis was used in conjunction with TGA results to confirm anion entrapment levels, and flame photometry yielded information regarding non-framework cations.

2.2 DIFFRACTION METHODS

Diffraction is conventionally explained using the Bragg Law [3]. A crystal is perceived as being comprised of planes acting as semi-transparent mirrors in which some rays are reflected whilst others pass through to be reflected by neighbouring planes. A typical situation is shown in Figure 2.1 Two parallel x-ray beams with an angle of incidence θ are diffracted by adjacent planes of separation d. For constructive interference to occur the path difference must correspond to an integral number of wavelengths. Simple trigonometry yields the Bragg equation:

$$n\lambda = 2d\sin\theta \qquad \textbf{2.1}$$

The angle of incidence, θ, is known as the Bragg angle. At angles of incidence other than the Bragg angle, diffracted beams are out of phase and thus destructive interference or cancellation occurs. The interplanar separations in the crystal are calculated by measuring the diffraction maxima and generally first order diffraction only is considered. The crystal system is derived from these d values by identification of the planes involved. Planes are defined by their Miller indices, hkl, the reciprocal values of the positions where the plane cuts the a, b and c axes respectively.

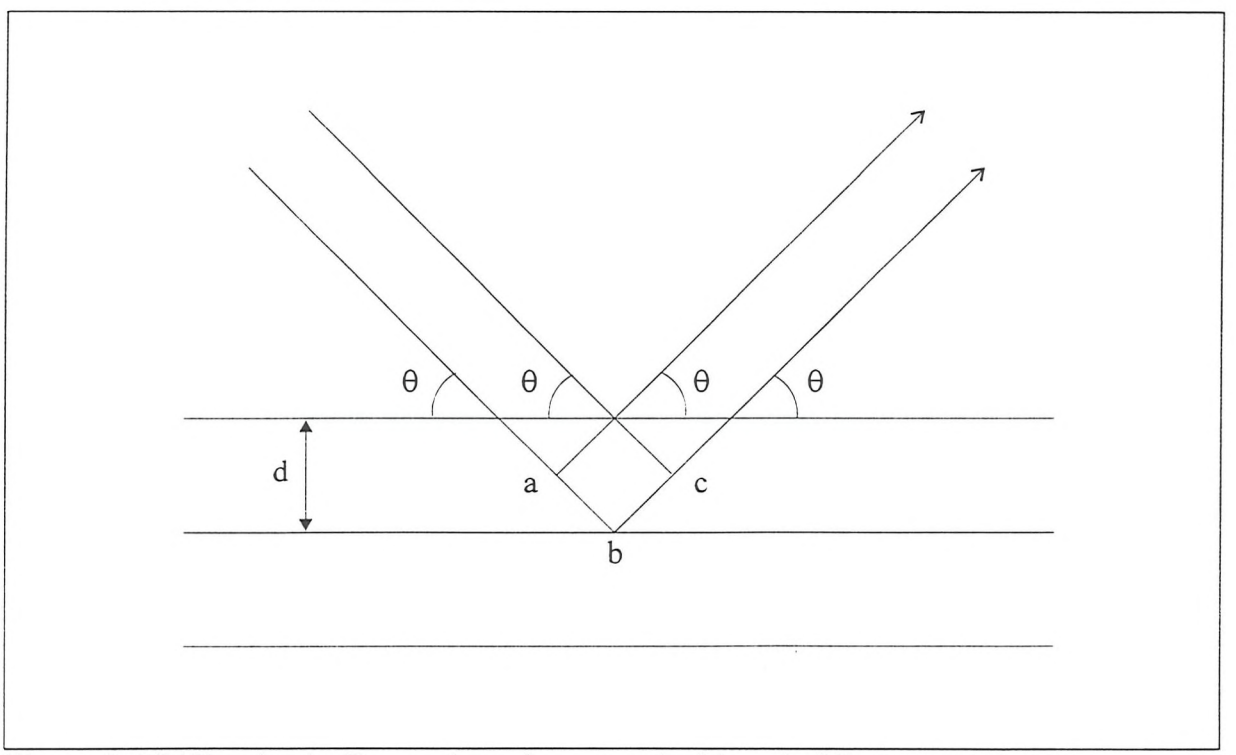

Figure 2.1 Diffraction by Bragg planes in a crystal with path difference = ab +bc.

For orthorhombic systems the relationship between the Miller indices and planar separation is thus given by:

$$\frac{1}{d^2_{hkl}} = \frac{h^2}{a^2} + \frac{k^2}{b^2} + \frac{l^2}{c^2} \qquad 2.2$$

For cubic systems in which a=b=c, this equation simplifies to:

$$d = \frac{a}{(h^2 + k^2 + l^2)^{1/2}} \qquad 2.3$$

The diffraction maxima are measured and, from the d values obtained, Miller indices are assigned allowing the determination of cell type and size. The crystal symmetry can be found from the systematic absences from the diffraction pattern. In theory a crystal should display diffraction for each of its lattice planes giving rise to an observed intensity in the resultant trace at 2θ values corresponding to all the planes. Intensity is not always observed at all possible positions however and this arises from the existence of reflection conditions or systematic absences which result from symmetry elements of the structure.

In addition to absences arising from a non-primitive lattice type, a number of space symmetry elements may also cause systematic absences, such as screw axes and glide planes [4, 5].

2.3 POWDER X-RAY DIFFRACTION (PXD)

The realisation that diffraction of x-rays by crystalline materials could occur as a result of the similarity between x-ray wavelength and interatomic separation has led to the routine application of x-ray diffraction as a characterisation tool in materials chemistry. The pioneering work of Bragg [3] demonstrated the applicability of diffraction to the determination of cell type and size, and the subsequent development of experimental and computational techniques has permitted the elucidation of a far wider range of structural parameters. It was understood at an early stage that powder data could provide more information than just cell type and size such as atomic arrangements within the material, but the extraction of this information due to overlap or coincidence of diffraction maxima was the overriding problem. Early work was therefore restricted to trial and error structural characterisation or simple phase identification by comparison with other diffraction patterns. The situation was dramatically improved by H.M. Rietveld [1, 2] who developed his widely acclaimed structure refinement technique which permitted the determination of detailed structural information from powdered samples. Initial applications to PXD data were limited by the fact that it was developed principally for neutron data, combined with the fact that the computing facilities generally available were relatively poor. Since these problems have been overcome, PXD has evolved into an extremely powerful tool for structure solution in materials chemistry. It permits the determination of crystal structure, particle size, detection of crystal defects and disorder, and may allow the resolution of phase transitions. In the current work, PXD was principally used to determine phase identification and purity; all samples studied were in powdered form, and no attempt was made to synthesise single crystals. Short run times of 20 minutes over the 2θ range 20-60 ° with a step size of 0.02 ° were employed for initial characterisation, and longer runs of 900 minutes over the 2θ range 20-60 ° with a step size of 0.02 ° were used to allow Rietveld refinement [1, 2] for samples of suitably high quality.

2.3.1 The Powder X-ray Experiment

All PXD data used in this work were acquired using a Siemens D5000 diffractometer, shown schematically in Figure 2.2. X-rays are generated by accelerating an electron beam through 40 keV onto a copper target providing copper K_α radiation which passes through a single crystal monochromator leaving only K_{α_1}, $\lambda = 1.5406$ Å. An aperture

diaphragm collimates the radiation which is subsequently directed on to the sample mounted in a recessed plastic or aluminium holder and the emergent X-rays are detected by a conventional scintillation counter. The incident beam, sample and detector are arranged according to the Bragg Brentano parafocusing geometry in which the incident beam and take off geometry is fixed at a $\theta/2\theta$ relationship by rotating the sample plate at precisely half the rate of the detector through the angular range to be studied. The instrument is calibrated mechanically and this calibration periodically checked using α-SiO_2.

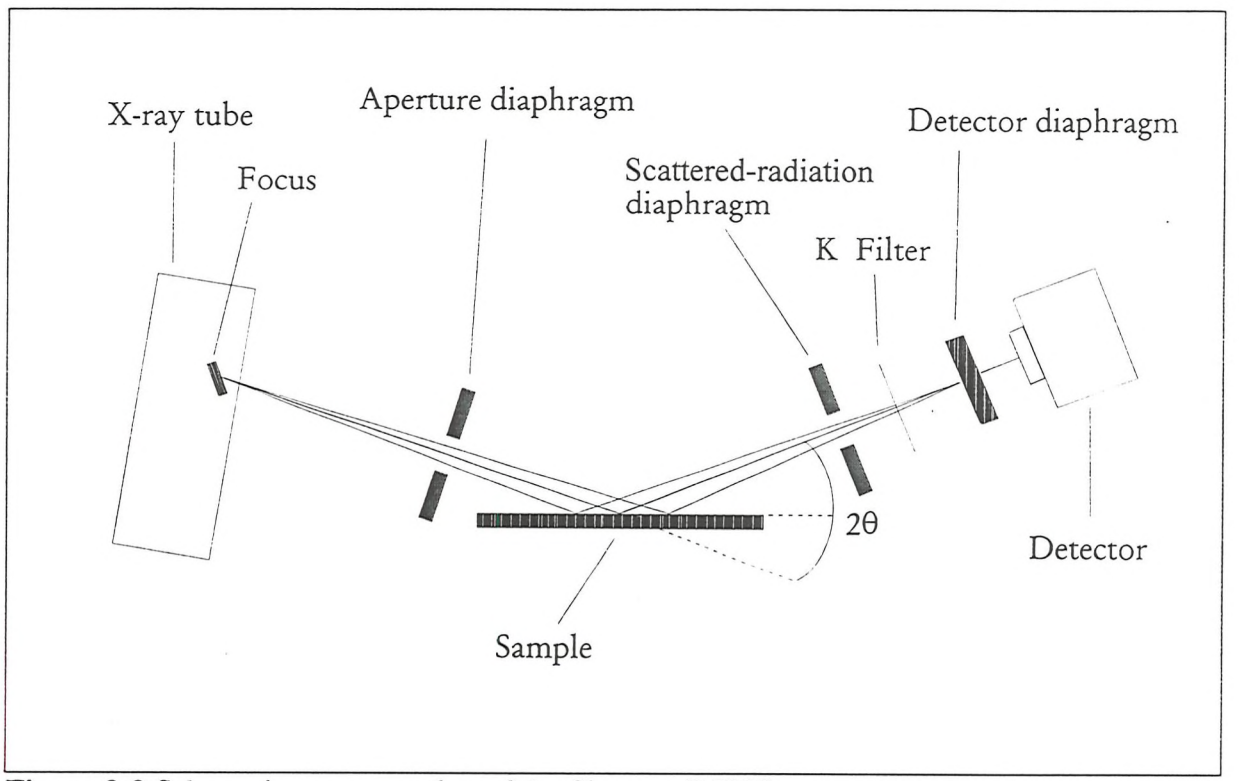

Figure 2.2 Schematic representation of the Siemens D5000.

2.3.2 Powder X-ray Data Analysis

The data are transferred automatically to a Digital MicroVAX 2000 computer allowing a real time visual display of the data to be viewed. The SIEMENS DIFFRAC D500 version 2.0 software package allows the acquired data to be analysed, and fingerprinting of the pattern achieved via the JCPDS Powder Diffraction File [6]. This permits the target species to be compared with similar structures previously determined as well as determination of impurity phases. The program "CELL" was used to obtain refined cell parameters via minimisation of the expression:

$$M = \sum_{n} W_n \left(\sin^2\theta_n^{obs} - \sin^2\theta_n^{calc} \right)^2 \qquad 2.4$$

using an iterative least squares procedure. W_n is a weighting factor, proportional to $tan\theta$. The cell parameters so produced are attributed estimated standard deviations (ESDs), although these reflect only the goodness of fit between the observed and calculated 2θ positions, and provide no indication of systematic experimental errors.

2.3.3 Generation of Intensities

In addition to yielding information regarding the structure type and cell size, x-ray diffraction permits the resolution of atoms within the structure via consideration of peak intensities. Since x-rays are scattered by electron clouds surrounding atoms, those atoms with high atomic number tend to dominate the diffraction profile. The scatter of x-rays by the electron cloud is dependent on the term $\sin\theta$, where is the angle of diffraction, and decreases as $\sin\theta$ increases. This results in weak scattering at high angle (back scatter) and strong scattering at low angle [4]. As the angle is increased therefore, the signal to noise ratio drops off until the diffraction pattern becomes indistinguishable from the background.

The intensity of each diffraction maximum is related to the structure factor, F. It can be shown that, for any regular arrangement of stationary atoms, F is the sum of the contributions of the scattering amplitudes, f, and the phases, δ, of each atom [7] giving the expression:

$$F = \sum_{j=1}^{N} f_j \exp\left[i\delta \right] \qquad \textbf{2.5}$$

In a unit cell, the total phase shift of an atom j at a point (x_j, y_j, z_j) from the origin is the sum of the phase shifts in each direction. When the phase shift is evaluated, the structure factor for one unit cell becomes:

$$F_{hkl} = \sum_{j=1}^{N} f_j \exp\left[2\pi i \left(hx_j + ky_j + lz_j \right) \right] \qquad \textbf{2.6}$$

where h, k and l are the Miller indices defining the plane from which the reflection occurs. For very small crystals, it may be shown that the intensity of the scattered beam is proportional to the square of the structure factor:

$$I_{hkl} = k L^2 \mid F_{hkl} \mid^2 \qquad \textbf{2.7}$$

where k is a scaling constant and L is the Lorentz factor, a geometric function of the method of data collection and hence the instrument used [7].

In real crystals, the scattered intensity is modified by imperfections in the lattice structure. Defects and substitutional disorder cause local structural irregularities, particularly in non stoichiometric materials. In addition, thermal motion causes a reduction in scattered intensity as a result of time dependent vibrations of the atoms about their mean positions: the atoms in a plane hkl are displaced randomly from their ideal in-plane positions, disrupting the in-phase behaviour of their combined scattering. The correction to a structure factor reflected by a plane hkl takes the form [7]:

$$T_{h\,k\,l} = \exp\left[-B_{h\,k\,l} \frac{\sin^2\theta}{\lambda^2} \right] \qquad \textbf{2.8}$$

so that for a unit cell, the structure factor becomes:

$$F_{h\,k\,l} = \sum_{j=1}^{N} f_j\, n_j \exp\left[-B_j \frac{\sin^2\theta_j}{\lambda^2} \right] . \exp\left[2\pi i \left(hx_j + ky_j + lz_j \right) \right] \qquad \textbf{2.9}$$

where n_j is the occupation factor of the *jth* atom, equal to one in a structure free from defects. However, this assumes that the displacements due to thermal motion are isotropic, which is seldom the case, except in some highly symmetric special positions of cubic space groups [8]. A more rigorous analysis [7, 9] describes the anisotropy of thermal motion in the form of an ellipsoid, replacing equation (2.8) above with:

$$T_{hkl} = \exp\left[-\tfrac{1}{4} \left(B_{11} h^2 a^{*}2 + B_{22} k^2 b^{*}2 + B_{33} l^2 c^{*}2 + 2 B_{12} hka^{*}b^{*} + 2 B_{23} klb^{*}c^{*} + 2 B_{13} hla^{*}c^{*} \right) \right]$$

There are a number of other expressions for T_{hkl} [7] but the form given here is used to describe the anisotropic temperature factors used throughout this work.

The intensities of the diffracted beams are also governed by the multiplicity of an hkl reflection; that is, for a particular hkl reflection in a given crystal symmetry class, there are a number of equivalent planes diffracting at the same angle to give an enhanced intensity.

2.4 POWDER NEUTRON DIFFRACTION (PND)

The realisation in 1936 that neutron motion was governed by wave mechanics was followed in the same year by the first diffraction experiments involving neutrons [10]. This led to a relationship proposed by de Broglie between mass, velocity and associated wavelength of any particle:

$$\lambda = \frac{h}{p_n} \qquad 2.11$$

$$= \frac{h}{m_n v_n} \qquad 2.12$$

where h is Planck's constant. At a particular temperature, a Boltzmann distribution of neutron velocities will be found assuming that neutrons behave as a gas; at 273 K this corresponds to a root mean square velocity of 2200 ms^{-1}, or a wavelength of $\approx$ 1.55 Å. This wavelength is of comparable size to atomic separations in crystals, and therefore at moderate velocities neutrons may be utilised to perform diffraction experiments. Although the experimental set-up is far more complex than the x-ray counterpart, this is more than compensated by the advantages of neutron diffraction over x-rays.

X-rays are diffracted by electrons with a characteristic X-ray form factor which results in the problem of low scattering from light elements and the inability to distinguish adjacent elements in the periodic table. Neutrons, however, are scattered by nuclei which due to their small size compared to the neutron wavelength eliminate the scattering power drop off at higher angles observed in X-ray diffraction [4]. This results in the observation of reflections at high angle with neutron diffraction which would simply not be detected using x-rays; many more reflections can thus be measured giving a more complete data set which allows the more accurate determination of atomic positions and thermal parameters.

For neutron diffraction the scattering power of a nucleus is dependant on both resonant scattering and neutron absorption which increase or decrease the scattering to sometimes give adjacent elements in the periodic table vastly different scattering powers. Light elements have increased relative scattering ability compared with X-ray diffraction which permits the determination of atomic parameters for light species such as Be which are commonly masked in x-ray diffraction experiments by the presence of heavier atoms in the material. Neutron diffraction experiments also offers the possibility of differentiating elements adjacent to one another in the periodic table such as Al and Si: these have virtually

identical x-ray scattering abilities, but their neutron scattering lengths differ by more than 10%. This is important for zeolite materials in which the level of framework order is of prime importance in structural studies. PND has therefore assumed great importance in the structural characterisation of framework materials, and has been employed in the current work using both time-of-flight and constant wavelength experimental procedures.

2.4.1 Time-of-flight (t.o.f.) PND

T.o.f. PND data were collected on the POLARIS high flux, medium resolution diffractometer [11] on the ISIS facility at the Rutherford Appleton Laboratory (RAL), Oxon. ISIS is a synchrotron spallation source which provides pulsed variable wavelength neutrons which cover the entire neutron spectrum. Using fixed angle detectors diffracted radiation is separated according to its t.o.f. and hence over a fixed detection distance its wavelength. By considering Bragg's Law, $n\lambda = 2dsin\theta$, in the t.o.f. method, λ and d are the variables at fixed θ. This contrasts with conventional diffraction methods where d and θ are the variables at fixed λ.

Thus diffractometers such as POLARIS at pulsed neutron sources operate in a fundamentally different manner from their conventional reactor-based counterparts. Instead of measuring Bragg reflections by scanning a detector from low to high 2θ scattering angles, POLARIS uses the pulsed white beam and measures the Bragg reflections at fixed scattering angles, monitoring the time of arrival of the neutron after the initial neutron burst produced in the target. The relationship between t.o.f. and d-spacing is linear and thus can be derived by combining the de Broglie equations above (2.11 and 2.12) with Bragg's Law (2.1 above).

Given a primary flight path (moderator to sample) of L_1, a secondary flight path (sample to detector) of L_2 and corresponding times of flight t_1 and t_2 we have:

$$\frac{h}{m_n} \cdot \left[\frac{t_1}{L_1} + \frac{t_2}{L_2} \right] = 2d\sin\theta \qquad \textbf{2.13}$$

Hence with an overall flight path L and time of flight t such that:

$$L = L_1 + L_2 \quad , \quad t = t_1 + t_2 \qquad \textbf{2.14}$$

this gives:

$$t = 2dL(m_n / h)\sin\theta \qquad \textbf{2.15}$$

$$\therefore \quad t \propto d$$

Thus for a 12 m instrument such as POLARIS a 1 Å d-spacing refection will be detected in the backscattering bank at a t.o.f. of $\sim$5000 μs.

2.4.2 T.o.f. PND: POLARIS instrumentation

On the POLARIS t.o.f. neutron source short pulses (<90 μs), suitable for diffraction work at wavelengths down to 0.2 Å, are attained from proton spallation of an tantalum target. Pulsed neutrons are produced in the first case by an electron Bremsstrahlung-photoneutron reaction, and in the second case by the spallation process (spalling, or chipping, of the target nucleus). These bursts of fast neutrons must then be slowed down in a moderator to provide a pulsed beam. The 295 K gadolinium poisoned

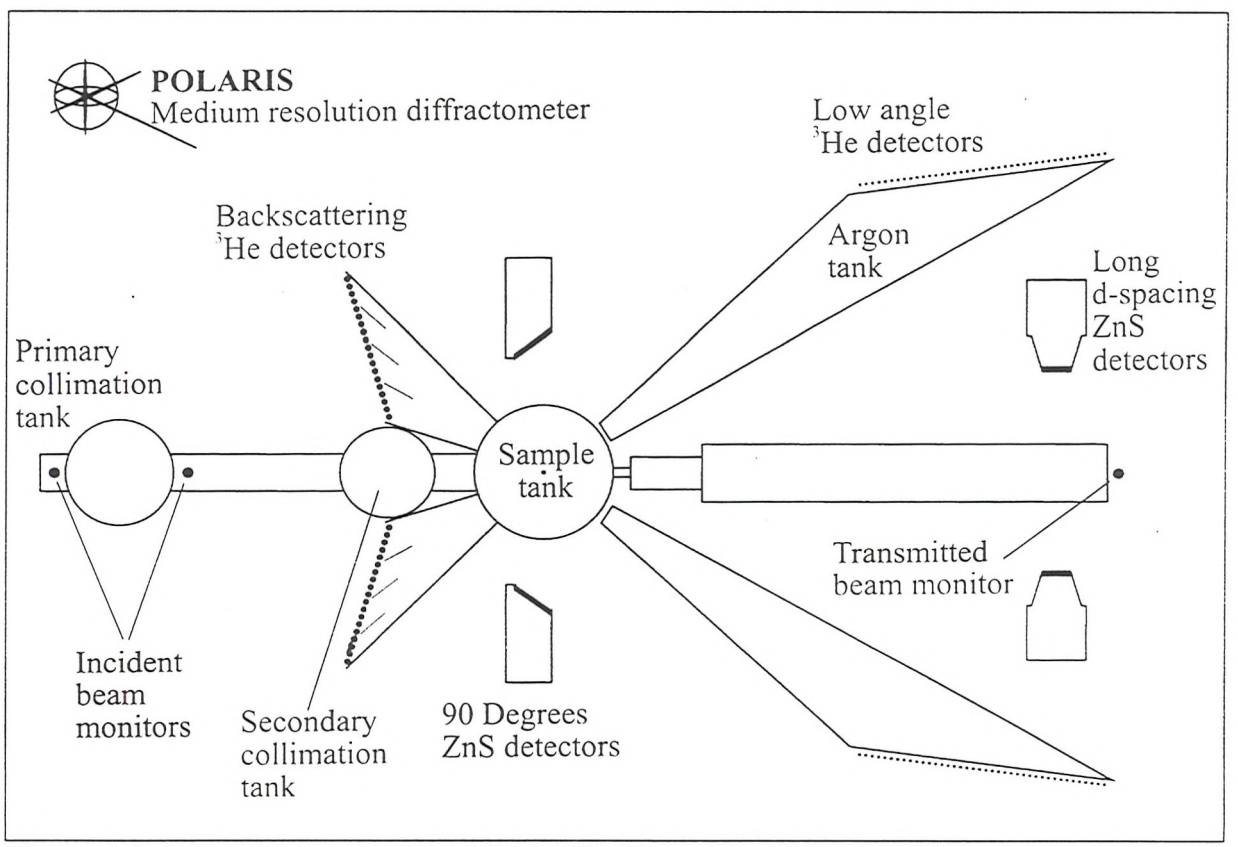

Figure 2.3 Schematic layout of the POLARIS diffractometer (June 1994).

water moderator gives the required 'tight' neutron pulse time structure over a wide range of wavelengths.

Samples are loaded into vanadium cans within an evacuated sample chamber and the backscattered neutrons detected by 38 ^{3}He gas filled detectors ($135\ ° < 2\theta < 160\ °$) giving a resolution $\Delta d/d$ of $\sim 5 \times 10^{-3}$ and a d-spacing range of 0.2-3.2 Å. A schematic representation of the POLARIS diffractometer is shown in figure 2.3.

A variety of cryostats and furnaces enable samples to be studied at temperatures between 4 and 973 K. Typical data collection times range between 1½ and 4 hours for reasonably large samples (2-4 g) and measurement of samples down to 0.1 g is also feasible.

2.4.3 Liquid and Amorphous Materials Diffractometer (LAD) Instrumentation

LAD is a total scattering instrument which has been optimised for the study of liquid and amorphous materials, and can be used as a moderate resolution diffractometer. It incorporates helium detectors at 5, 10 and 150 °, and scintillation counters at 25, 35, 58 and 90 °. Its use as a medium resolution diffractometer is primarily focused towards the study of magnetic ordering and the solution of simple structures.

2.4.4 Constant wavelength PND

The fixed wavelength PND experiment is fundamentally identical to the PXD experiment shown previously with θ and d variables in the Bragg equation. Data were collected on the D2B high resolution instrument [12] on the high flux reactor at the Institut Laue Langevin (ILL) in Grenoble, France. The instrument has a near perfect gaussian peak-shape in the 2θ range 30-160 ° permitting Rietveld refinement of monoclinic cell volumes up to 2000 Å^3 and 250 structural parameters.

2.4.5 Constant wavelength PND: D2B instrumentation

The incident white neutron radiation is monochromated by an anisotropically squashed germanium monochromator focusing a 300 mm beam down to 50 mm with a take off angle of 135 ° producing a backscattering resolution of $\Delta d/d$ of $\sim 5 \times 10^{-4}$. Samples are mounted in vanadium cans and the scattered neutrons detected by a bank of 128, 3 inch collimators and ^{3}He counters at intervals of 2.5 ° which sweep through 0-160 ° in 0.025 °

steps. A range of wavelengths can be used from 1.05 to 1.59 Å and variable temperature studies achieved between 1.5 and 1273 K. Typical data collection times range between 4 and 12 hours for sample sizes of 0.5 to 3 g.

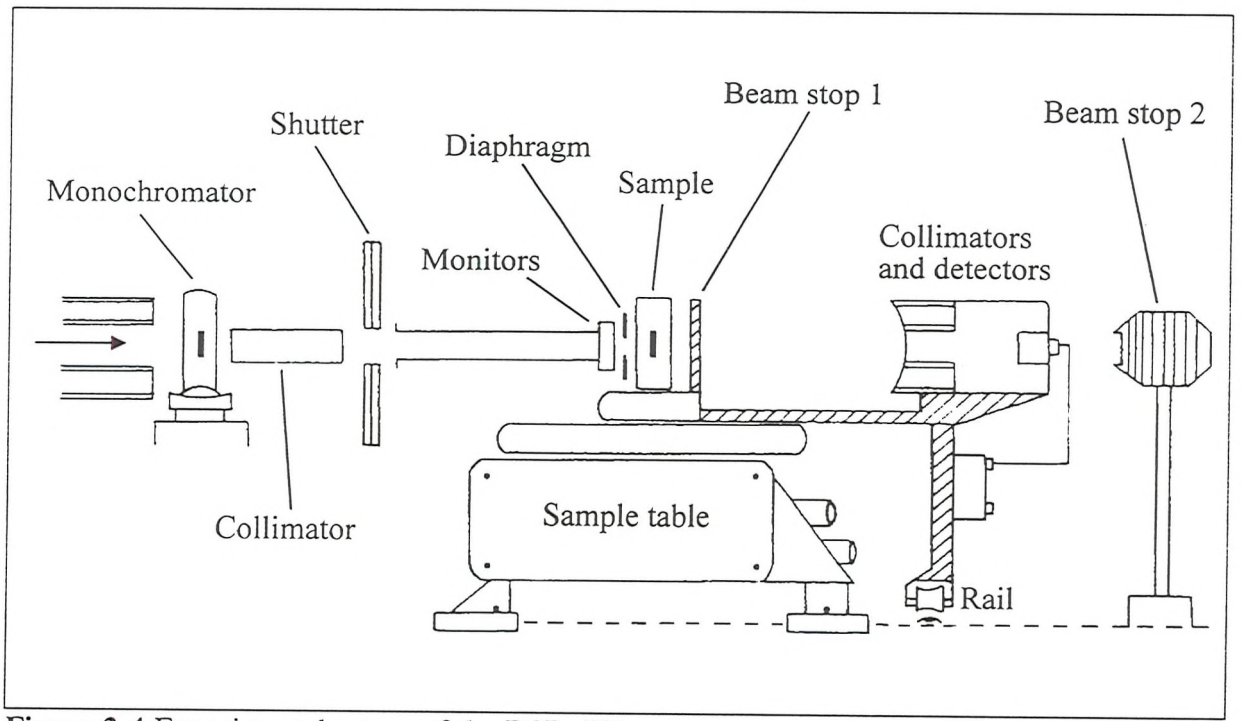

Figure 2.4 Experimental set up of the D2B diffractometer.

2.6 THE RIETVELD METHOD

In 1967 H.M. Rietveld [1] introduced a method for least squares refinement using an entire powder neutron diffraction pattern. This was a revolutionary process which has subsequently attained great importance in the extraction of detailed structural information from both powder neutron and x-ray diffraction data. Until the evolution of this procedure, refinement of powder data was carried out using least squares refinement using structure factors extracted from the profile; in the case of overlapping or partial coincidence of diffraction maxima the obtention of structure factors is particularly problematic and as such severely limited the information which could be deduced. Rietveld realised that although many individual reflections did overlap and thus could not be modelled as single entities, they could be fitted using simple peak shape parameters in order to determine the total intensity and peak shape of a cluster of reflections. Although initially applicable to only simple crystal systems, the advent of computers permitted the consideration of a vast amount of information and hence far more complex structural problems were able to be solved.

The general refinement process begins with the input of a suitable starting model. This can be obtained from a similar crystal system, and a good initial model is important to the success of the Rietveld method: not only does it greatly speed up structure solution, but will help to prevent the assignation of incorrect structure to the material under investigation. Scale factor and background parameters are next introduced, and because refinement of these parameters involves only coefficients of ordinary or orthogonal polynomials the problem is linear and should immediately converge irrespective of the starting values. Positions of Bragg reflections are then deduced from lattice parameters, zero-point correction and sample displacement, followed by refinement of atomic positions within the structure which directly affects peak intensities. Atomic vibrations are modelled using isotropic temperature factors, and peak shape parameters allow sample broadening effects to be taken into account. If the data are of sufficiently high quality, anisotropic temperature factors may also be refined. From the parameters entered into the refinement package, a computer generated pattern is compared with the observed data set, and adjustments made to the model in order to minimise the difference between these two patterns. In an ideal situation refinement will terminate when the generated pattern exactly matches that of the experiment, at which point the model structure will reflect the structural features of the sample.

In the constant wavelength PND Rietveld method with a Gaussian shape assumed the background-corrected observed counts are compared with the calculated counts, y_i, for a trial structure at each point $2\theta_i$ on the profile, and the parameters which define $y_i(calc)$ are adjusted to minimise the function:

$$M_i = \Sigma\ W_i \left[Y_i^{obs} - Y_i^{calc} \right]^2 \qquad \textbf{2.16}$$

where W_i is a weighting factor given by $1/Y_i(obs)$. The background intensity of the recorded diagram is fitted by a polynomial background. The measured profile of a single diffraction peak depends upon many factors such as sample shape and crystallinity, and the neutron spectral distribution. The summation for Y_i^{calc} is over all reflections contributing to point i on the diffraction pattern. For other applications of the Rietveld method, such as t.o.f. PND or PXD the details of the calculation of Y_i^{calc} will differ from the above, but the principle is the same as for the original formulation.

Time of flight neutron sources tend to produce gaussian peak shapes with exponential components characteristic of the moderator observed by the instrument. Such peaks are relatively simple to model, whereas those from an x-ray diffractometer tend to be more complex and are fitted using pseudo-Voigt functions allowing the contributions from both Gaussian and Lorentzian peak shapes to be modelled. All peak shapes are corrected for breadth dependence on angle using the expression:

$$H_k^2 = U\tan^2\theta_k + V\tan\theta_k + W \qquad \textbf{2.17}$$

where H_k is the full peak width at half maximum peak intensity, U,V,and W are refinement parameters. This formula takes account of the peak broadening resulting from the particle-size effect.

In the Rietveld method the difference between the observed diffraction profile and that calculated for a trial structure is minimised by an iterative least squares procedure. These least squares parameters can be considered as two distinct groups. The first group defines the position and shape of the peaks and consists of the unit cell parameters, the counter zero offset, and the asymmetry factor. The second group, the structural and thermal parameters, defines the contents of the unit cell. These consist of the profile scale factor, and the co-ordinates, occupation and temperature factor of each atom. In addition to graphically representing the calculated and observed profiles in a Rietveld plot, it is usual to reflect how well the two match using statistical goodness of fit functions. These reliability indices are defined as follows:

$$R_{profile} = R_p = \left[\frac{\sum_i \left| Y_i^{obs} - Y_i^{calc} \right|^2}{\sum_i \left(Y_i^{obs} \right)^2} \right]^{1/2} \times 100\ \% \qquad \textbf{2.18}$$

This may be compared with the reliability index $R_{expected}$ derived purely from statistical considerations:

$$R_{expected} = R_e = \left[\frac{(N - P + C)}{\sum_i W_i \left(Y_i^{obs} \right)^2} \right]^{1/2} \qquad \textbf{2.19}$$

where N = number of observables, P = number of refinable parameters and C = number of constraints.

In addition, R_{wp} and R_I may be defined as:

$$R_{weighted\ profile} = R_{wp} = \left[\frac{\sum_i W_i \left| Y_i^{obs} - Y_i^{calc} \right|^2}{\sum_i W_i \left(Y_i^{obs} \right)^2} \right]^{1/2} \qquad \textbf{2.20}$$

$$R_{integrated\ intensities} = R_i = \left[\frac{\sum_k \left| I_k^{obs} - I_k^{calc} \right|}{\sum_k I_k^{obs}} \right] \qquad \textbf{2.21}$$

Finally the chi-squared parameter may be defined as:

$$\chi^2 = \left[\frac{1}{(N + P + C)} \right] \cdot \sum_i W_i \left(Y_i^{obs} - Y_i^{calc} \right)^2 \qquad \textbf{2.22}$$

$$= \left[\frac{R_{wp}}{R_e} \right]^2 \qquad \textbf{2.23}$$

which is the natural measure of the fit, and is normally minimised in the refinement. Thus for a good fit, the weighted profile R-factor should approach the statistically expected R-factor value. PXD data were refined using the PC based GSAS package of Larsen and Von Dreele [13], and PND data were refined using GSAS on an HP Apollo workstation.

2.6 MAGIC ANGLE SPINNING NUCLEAR MAGNETIC RESONANCE (MASNMR) SPECTROSCOPY

The application of NMR to solution systems is well documented and has yielded a wealth of structural information derived from chemical shifts, couplings and integrated intensities of spectral resonances. However, until relatively recently, the application of this technique to solid samples has proven particularly problematic. [14,15]. In the liquid state, molecular tumbling is rapid and random and the direct nuclear fields fluctuate significantly in both intensity and direction, conveniently averaging to exactly zero. In the solid state these magnetic dipole-dipole interactions are not averaged to zero: this results in considerable spectral broadening to yield broad featureless bands using standard NMR methods.

In general, the nuclear spin in the solid state may interact in a number of ways dependent on the orientation of the nuclear spin vector to the magnetic field. These interactions can be separated into five distinct components [4]: the Zeeman interaction, the chemical shift interaction, the dipolar interaction, electron spin interaction and the quadrupolar interaction. In general it is these second and third interactions which give rise to severe spectral broadening. The chemical shift interaction adjusts the resonance position due to the magnetic field modification by surrounding electrons which in solids can be anisotropic leading to broad peaks. Dipolar interactions between equal or unequal nuclear spins, only significant between adjacent nuclei since it is inversely proportional to distance cubed, splits the resonance by an amount dependant on the two spins orientation with respect to the magnetic field. It is therefore an immense problem for solids since all orientations are present. The quadrupolar interaction occurs for nuclei with non integral spin above ½, which experience non spherically symmetric electric fields proportional to the field strength and the quadrupolar coupling constant. It is thus not manifested for silicon which explains the multitude of research undertaken on that particular nucleus. Electron spin interaction is very small and can often thus be neglected. Finally, the Zeeman interaction is that which determines the observational frequency, and aligns the nucleus to the applied field.

The technique of "magic angle spinning" (MAS) has been developed for use in solid state NMR spectroscopy in order to reduce the problem of spectral line broadening. In this experiment, the sample is spun mechanically around an axis inclined at an angle θ to the magnetic field axis at a frequency comparable with the frequency spread of the chemical shift anisotropy. Both the dipolar interaction and chemical shift anisotropy are dependant on

an orientation term proportional to $(3cos^2\theta-1)$, and thus both can be reduced to zero by setting the value of θ to the magic angle, θ = 54.73 °. Spinning rates used are in the order of several kHz, with slower rates leading to non-averaging of the dipolar interactions resulting in spinning side bands separated by the spinning frequency and central peak broadening.

In non integral spin nuclei the Zeeman splitting is modified to allow transitions other than -½ to ½. These transitions are usually too broad and shift too far to be observed but asymmetric peaks are observed for the basic transition due to second order quadrupolar interaction. This broadening is proportional to the electric field gradient which is determined by the symmetry of the environment around the nucleus. The interaction contains an angular term, which analogous to dipolar interactions can be summed to zero by spinning at 30.56 ° to the magnetic field. This is accomplished by simultaneously spinning at the magic angle yielding the double rotation or dynamic angle spinning experiments [16]. Only the technique of MASNMR was used to study the materials prepared in the current work.

2.6.1 The MASNMR Experiment

Powdered samples were run on a Bruker AM300 spectrometer at Southampton. The Bruker machine consisted of a 7 Tesla superconducting magnet with a multinuclear probe

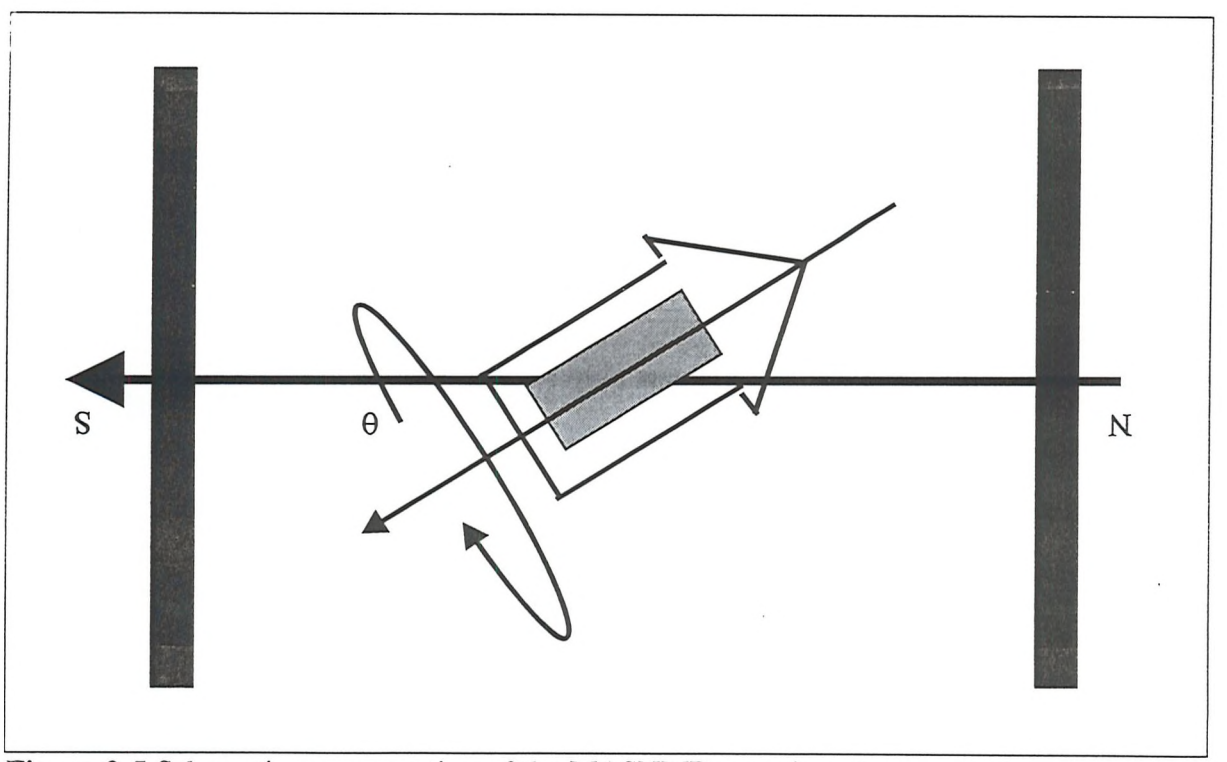

Figure 2.5 Schematic representation of the MASNMR experiment.

ranging between ^{31}P at 121 MHz to ^{2}H at 46 MHz. The spinning rates used were between 2.5 and 6 kHz. The magic angle was set using the ^{79}Br resonance in solid KBr and the pulse length calibrated using a secondary reference sample of 3-(trimethyl silyl)-1-propane sulphonic acid. ^{29}Si, ^{27}Al and ^{71}Ga spectra were obtained at a field of 59.584 MHz relative to TMS, saturated Al(acac) in benzene and 1 M $Ga(NO_3)_3$ using a 4 μS 90 ° pulse with the decay acquired for 49.0 μS (200-300 transients).

2.7 FOURIER TRANSFORM INFRA-RED (FT-IR) SPECTROSCOPY

All FT-IR spectra were recorded using a Perkin Elmer FT-IR 1710 spectrometer equipped with a Perkin Elmer 3600 data station which was employed to perform peak location on all bands observed. Materials to be analysed (1-5 % w/w) were intimately ground with spectroscopic KBr and pressed into a disc using a pressure of 10 tonnes, and spectra acquired over the range 4000-400 cm^{-1} with a resolution of 2 cm^{-1}. The spectra were used essentially to investigate the presence and nature of the species entrapped within the sodalite cages.

2.8 ULTRAVIOLET/VISIBLE (UV/VIS) SPECTROSCOPY

UV/VIS spectra were acquired using a Perkin Elmer Lambda 19 spectrometer set up for diffuse reflectance spectroscopy with tungsten and deuterium lamps. Diffraction gratings allow the selection of the required wavelengths. Spectra were recorded using the Kubelka Munk function, which attempts to compensate for the effect of sample particle size on the scattering as the wavelength is shortened. It should be noted that reliable intensity data is not obtainable using solid state spectra, and only relative intensities of the bands within spectra can be viably extracted. Samples in powder form were loaded into a glass fronted aluminium holder, and spectra recorded over the range 1000-200 nm using $BaSO_4$ as a reference sample. The sample was intimately ground with $BaSO_4$ when a diluant was necessary. The species responsible for colouration of the materials analysed were determined.

2.9 FLAME PHOTOMETRY

Lithium and potassium containing samples were investigated for the degree of exchange using a Corning 400 flame photometer. Solutions containing the target cation were passed through a gas flame from which their characteristic emission spectra were exhibited. This passed through an elemental filter and the absolute intensity was measured by a photodetector.

The photometer was calibrated using standard solutions in 2 M nitric acid in the range 0 to 10 ppm and the target solution was prepared by dissolution of ~0.1 g of sample in conc. nitric acid followed by dilution to 2 M (~500 ml). This stock solution was then

further diluted to give a cation level between 1 and 10 ppm which was measured, standardised and hence the extent of ion exchange calculated.

2.10 THERMOGRAVIMETRIC ANALYSIS (TGA)

Thermogravimetric analysis was performed using a water cooled Polymer Laboratories PL STA 1500 instrument. Approximately 20 mg of sample was heated from ambient temperature to 1000 °C at a heating rate of 25 °C/minute, held for 15 minutes, and cooled back to room temperature at a rate of 40 °C/minute. Various atmospheres could be used for the analysis, including air, oxygen, hydrogen , nitrogen and argon. The results allowed the water content of the material, both surface adsorbed and enclathrated, to be resolved. The temperature at which intra-cage modification of entrapped anions occurred, as well as thermal stability of potential enclathrates could also be determined.

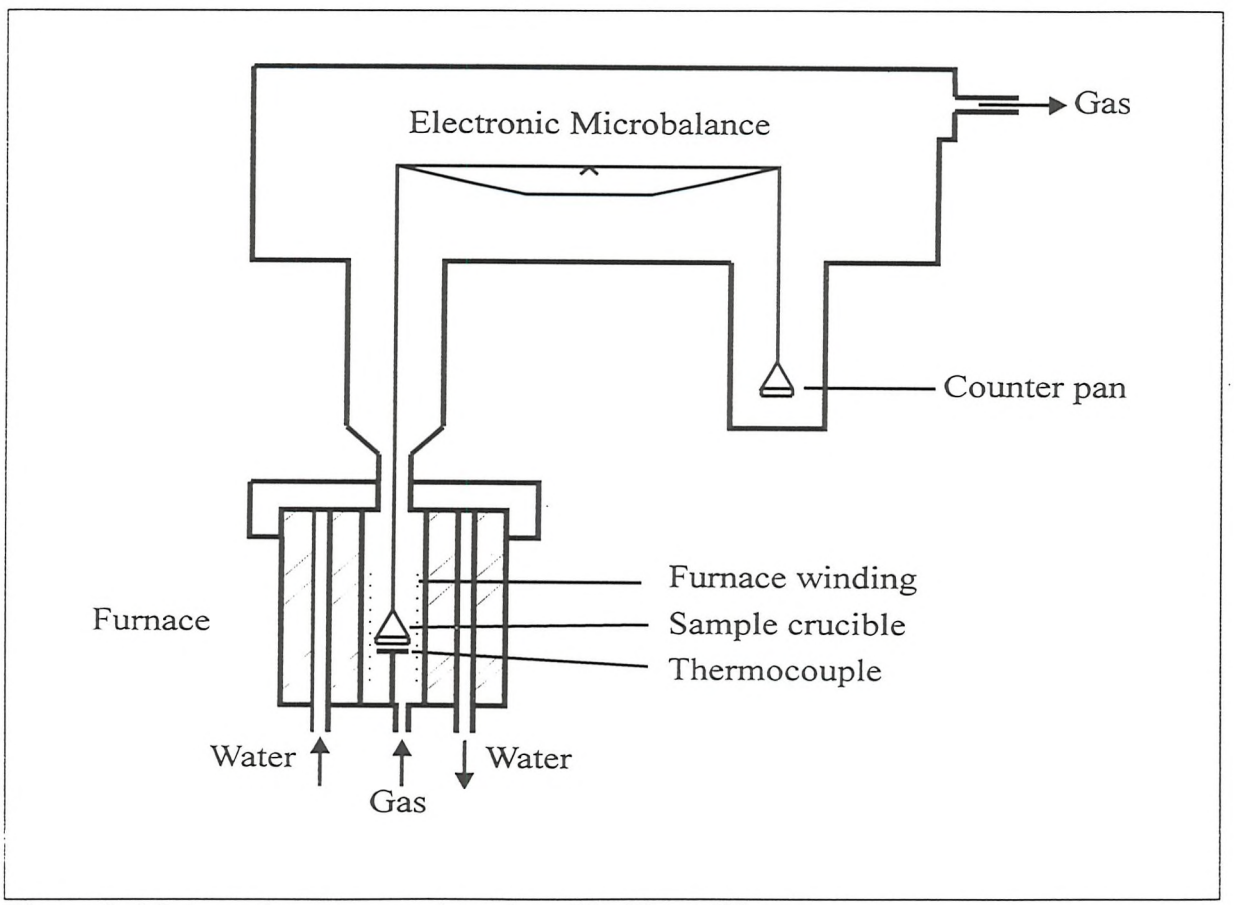

Figure 2.6 Schematic representation of the PL-STA 1500.

2.11 REFERENCES

[1] H.M. Rietveld, *Acta Cryst.*, **22**, 151 (1967).

[2] H.M. Rietveld, *J. Appl. Cryst.*, **2**, 65 (1969).

[3] W.L. Bragg, *Proc. Camb. Phil. Soc.*, **17**, 43 (1913).

[4] A.K. Cheetham and P. Day, 'Solid State Chemistry: Techniques', Oxford Science Publications, Clarendon Press, Oxford (1988).

[5] T. Hahn, 'International Tables For Crystallography Vol. A', D. Reidel, Dordrecht (1983).

[6] International Centre for Diffraction Data, 12 Campus Boulevard, Newton Square, Pennsylvania 19073-3273, U.S.A (1995).

[7] M.J. Buerger, 'Contemporary Crystallography', Chapter 11, McGraw-Hill (1970).

[8] B.T.M. Willis and A.W. Pryor, 'Thermal Vibrations in Crystallography', Chapter 4, Cambridge University Press (1975).

[9] H.A. Levy, *Acta Cryst.*, **9**, 679 (1956).

[10] D.P. Mitchell and P.N. Powers, *Phys. Rev.*, **50**, 486 (1936).

[11] S. Hull and R.I. Smith, 'User Guide for the Polaris Powder Diffractometer at ISIS', Version 2 (1993).

[12] H. Blank and B. Maier, 'Guide To Neutron Research Facilities at the ILL' (1988).

[13] A.C. Larson and R.B. Von Dreele, Generalized Structure Analysis System, MS-H805, Los Alamos, NM 87545 (1990).

[14] E.R. Andrew, *Prog. NMR Spectroscopy*, **8**, 1 (1971).

[15] E.R. Andrew, *Int. Rev. Sci. Phys. Chem.*, **2**(4), 173 (1975).

[16] A. Samoson, E. Lippmaa and A. Pines, *Mol. Phys.*, **65**, 1013 (1988).

Chapter Three

SYNTHETIC METHODS

3.1 INTRODUCTION

The range of preparative conditions applicable to sodalites demonstrates the stability of the system, and offers the possiblilty of enclathrating a wide variety of anions. The aluminosilicate sodalite family has been extensively studied, and the synthetic methods used can be divided into three categories: solid sate, hydrothermal and lower temperature solution methods. Solid state techniques typically involve temperatures between 800 and 1200 °C, and yield products of high crystallinity from either a mixture of the component oxides or a zeolite with the appropriate framework composition which is subsequently restructured *in situ*. The main disadvantage is the high temperature involved, which precludes the entrapment of anions of limited thermal stability. In such cases, hydrothermal or solution reactions are usually employed. These generally involve a basic solution containing the silicon and aluminium sources in addition to an excess of the salt to be entrapped. It is imperitive that the anions are thus base stable, and show no tendancy to hydrolyse. The main problem encountered with this type of reaction is the entrapment of water molecules and/or hydroxide anions; a large excess of the required salt is hence usually present in the reaction medium, although this not necessarily give phase pure products, especially if the anion in question is one which does not promote sodalite formation to any great degree.

Although sodalites can only be synthesised directly with sodium as the non-framework cation, post synthetic treatment allows the introduction of other cations. This can be achieved via low temperature solution reactions between room temperature and 120 °C, nitrate melt reactions in the range 240-370 °C, or higher temperature solid state reactions at approximately 800 °C. The method chosen depends on the stability of the anion entrapped within the sodalite cage, with the higher temperature reactions tending to yield the most highly crystalline products.

Post synthetic modification is not limited to non-framework cation exchange. The framework composition can also be altered and dealumination is common. This can be achieved in several ways. For example, when an ammonium exchanged zeolite Y (Faujasite) with a Si:Al ratio of 3:1 is subjected to repeated steaming, acid extraction and ammonium exchange treatment it is converted to a highly crystalline material which has a framework composition close to SiO_2 and which shows only a small number of point defects [1]. The zeolite framework has in effect been completely annealed and recrystallised without at any stage destruction of the basic FAU framework structure. Dealumination increases the Si:Al ratio which in turn improves the hydrothermal stability and alters the chemical characteristics

of the zeolite. Aluminium extraction can also be achieved via mild acids, or other agents such as EDTA, $SiCl_4$ or $(NH_4)_2SiF_6$ [1]. The latter two permit direct silicon insertion without the necessity of silicon transport from other regions of the crystallite. In general, however, isomorphous framework substitution is generally achieved by altering the composition of the starting solution or gel. More common is the intra cage modification of the entrapped anion. An example of this is the transformation of the thiocyanate ion to yield ultramarine [2], producing S_2^- and S_3^- polysulphide species, the exact ratio of which is dependent on the particular thermal treatment employed. Intra cage reductions are also possible, such as reduction of $(SO_4)^{2-}$ to S^{2-} [3].

In this chapter the preparation of a wide range of sodalites by solution, hydrothermal and solid state reactions will be described, and will be dealt with according to framework composition. The exact synthetic conditions employed depend on both the nature of the cavity anion and the framework composition.

3.2 SYNTHETIC BACKGROUND

A review of the methods outlined in the literature for the synthesis of sodalites of varying composition will be given, and dealt with according to framework composition. As indicated previously, the majority of the research performed has been on the aluminosilicates but in recent years the interest in frameworks of differing composition has increased, and this will also be discussed prior to detailing the synthetic methods used in the current work.

3.2.1 Aluminosilicate Sodalites

The solid state reactions generally applied to sodalite synthesis are direct solid state sintering and the structure conversion method (SCM). The former involves intimate mixing of stoichiometric quantities of Na_2CO_3, SiO_2, Al_2O_3 and NaX, where X is the anion to be encapsulated, and firing at temperatures between 800 and 1200 °C for 24-48 hours [4]. A prerequisite of this method is high thermal stability of the anion to be entrapped, thus precluding a large number of thermally unstable anions from use in this way. This particular technique of anion entrapment was therefore not used widely in the present work. The latter is that outlined by Chang [5] which uses commercially available molecular sieves with the appropriate ratio of framework components as the starting reagent; these are restructured between 400 and 800 °C with the anion acting as a template for sodalite formation. It has been proposed [2] that the reaction proceeds via nepheline, $NaAlSiO_4$, as an intermediate which subsequently reacts with the sodium salt to form the sodalite. This method avoids the higher temperatures and longer reaction times required for solid state sintering.

Solution reactions allow a far wider range of anions to be entrapped than solid state reactions due to the far lower temperatures involved, typically between 80 and 120 °C. Thus anions such as $(MnO_4)^-$ and $(SCN)^-$ can be incorporated into sodalites using these methods. The main disadvantages of the solution methods are the entrapment of water and hydroxide anions, coupled with a product lower crystallinity, both of which make structural refinement problematic [6].

The two methods reported by Hund [7, 8] and Barrer [9] are the basis for much of the work on aluminosilicates, with modifications made as necessary. In the Hund method, a highly basic solution of sodium aluminate is mixed with a large excess of the appropriate sodium salt and heated under reflux to 120 °C. Sodium silicate solution is added slowly to this solution, and the product crystallises out over the reaction time of 24 hours with the

anion acting as the synthetic template. Monovalent anions generally tend to form sodalites, although planar anions such as $(NO_3)^-$ yield cancrinites; all divalent anions give cancrinitic products [7, 9, 10].

The Barrer method uses kaolinite, $Al_4(Si_4O_{10})(OH)_8$, as the starting reagent which dissolves in basic solution and subsequently recrystallises in the presence of an excess of the desired sodium salt to form the product. It has been shown that at 80 °C the reaction proceeds via zeolite A as an intermediate [11], and therefore reaction directly from zeolite A instead of kaolin may speed up sodalite formation. Reaction temperatures are between 50 and 150 °C, with pressures of up to 15 kbar employed to aid the crystallisation process. This method yields products of sodalitic or cancrinitic nature depending on the particular sodium salt present. The results published by Barrer show that certain divalent anions such as SO_3^{2-}, WO_4^{2-} and S^{2-} give sodalites at 80 °C after 120 hours whereas others such as SO_4^{2-}, MoO_4^{2-} and CrO_4^{2-} give cancrinites. This is of particular interest since the Hund method always yields a cancrinite whatever the divalent sodium salt used. It is therefore a possible low temperature route for the synthesis of sodalitic materials which would be cancrinitic if synthesised by other methods. The lower temperature involved may prove useful for the encapsulation of thermally unstable anions, although this advantage is tempered by the longer reaction time: 120 hours as opposed to 24 hours for the Hund method.

The problem of water entrapment may be circumvented by the use of alternative solvents. Van Erp *et al.* [12] have reported the synthesis of sodalites using hexanol, glycol, glycerol and pyridine, for which crystalline aluminosilicates could be produced when the molar ratio of base to silica was greater than 0.5. The larger solvents such as hexanol are simply too large to be accommodated by the sodalite structure, but reaction times are usually extended to 2-3 weeks. Another method of avoiding water entrapment in sodalites has been outlined by Todd and Stroud [13]. In their study of bromide sodalite, low solvent concentration led to the formation of a second phase, $Na_6Al_6Si_6O_{24}.2NaOH.nH_2O$. A Low Temperature Reaction (LTR) process in which the solid is treated with 10 M NaOH at 130 °C for 3.5 hours allows the removal of water molecules, with hydroxide replacing the missing Br^- anions. However, rather than use post synthetic procedures, it is preferable to avoid water entrapment by use of low water content in the starting mixture or by employing a different solvent altogether which cannot get enclathrated within the beta cages.

3.2.2 Framework Substituted Sodalites

Much of the work regarding isomorphous substitution in the sodalite structure has centred on gallium and germanium, and it is these replacements which will be detailed here since they are the most relevant to the current work. Solid state substitutions of Ga and Ge into sodalites are rare, but have been reported by Neurgaonkar and Hummel [14] for the parent aluminosilicate hauyne $Ca_2Na_6[AlSiO_4]_6(XO_4)_2$. Replacement of four aluminiums by gallium was achieved for X = S, Cr, Mo and W, and full replacement of silicon by germanium was successful for X = Mo and W.

Schipper *et al.* [11] reported the low temperature synthesis of Ga and Ge sodalites in which appropriate mixtures of Al_2O_3, Ga_2O_3, SiO_2 and GeO_2 were mixed with 4 M NaOH and an excess of NaX, where X is the anion to be entrapped, sealed in glass bottles and heated at 80 °C for a minimum of 5 days. The series of halide sodalites thus synthesised showed cell parameters only marginally larger than their aluminosilicate equivalents consistent with only partial framework substitution. It is believed that leaching of the borosilicate glass vessel due to the basic medium used was the cause of the problem. Similar difficulties were encountered by Barrer *et al.* [15] in their synthesis of gallium and germanium containing hydroxide sodalies.

Suzuki *et al.* [16] reported the synthesis of a new gallosilicate hydroxide sodalite with a Ga:Si ratio of 5:1 in 1985, which would thus violate an extension of Loewenstein's rule to the gallosilicate system. However, in a subsequent paper [17] this was proven to be incorrect, in which the sodalite $Na_8Ga_6Si_6O_{24}(OH)_2.6H_2O$ was correctly identified. This crystallised in the space group $P\bar{4}3n$, indicating a perfectly ordered array of framework Ga and Si atoms. Extension of this method, using Ga_2O_3 and SiO_2 in the presence of NaOH at 100 °C, to entrap other anions did not prove possible.

In their study of the $Na_3[AlGeO_4].4H_2O$ system, Nenoff *et al.* [18] synthesised gallosilicate, aluminogermanate and gallogermanate sodalites using solutions of the precursors Na_5GaO_4, $Na_2Al_6O_2OH$, Na_2SiO_3 and Na_4GeO_4. HNO_3 was used to modify the pH, and reaction temperatures between 70 and 100 °C for 3-14 days were employed. Once more, the reaction conditions were not successfully applied to sodalites containing anionic enclathrates.

Hydrothermal reactions have proved far more successful for the preparation of framework modified sodalites. Perlmutter *et al.* [19] have investigated partial substitution of Ge into bromide sodalite at 300 °C and 2000-3000 psi for 24 hours, to yield

compositions described by $Na_8Al_6(Si_xGe_{1-x})_6O_{24}Br_2$, where x reaches a maximum of 0.46. Full Ge substitution using GeO_2 as the germanium source was not achieved.

Single crystals of $Na_8Al_6Ge_6O_{24}(OH)_2$ were obtained hydrothermally by Belokoneva *et al.* [20] using NaOH as the solvent in the temperature range 300-400 °C. Aluminogermanate halide sodalites were successfully synthesised by Fleet [21], although rather more drastic conditions were used. $NaAlGeO_4$ was first synthesised in sealed gold capsules from Na_2CO_3, Al_2O_3 and GeO_2 at 1473 K for 12 hours and 1073 K for 45 hours. This was used as the framework precursor, to which the required halide and water were added. These were then heated at 1048 K for 24 hours, followed by further heating cycles at lower temperatures if necessary. This reaction scheme is clearly unsuitable for thermally unstable anions. The method of McLaughlan and Marshall [22] for the enclathration of halide anions in modified frameworks involves reaction of the component oxides at temperatures in the order of 400 °C and the use of sealed platinum capsules of capacity 2 ml. This shows similarities to the scheme of Fleet, and thus excludes many anions of low or moderater thermal stability.

Sieger *et al.* [23] have extended the range of anions entrapped in aluminogermanate sodalites to include $(OH)^-$, $(NO_2)^-$, $(NO_3)^-$, $(ClO_4)^-$ and $B(OH)_4^-$. The synthesis involves reacting Al_2O_3, GeO_2, NaOH, H_2O and NaX, where X is the anion to be entrapped, at 180 °C in a Teflon autoclave under autogeneous pressure, although no detailed experimental conditions are given.

Newsam *et al.* [24] have reported the synthesis of gallosilicate chloride sodalite, in which $NaGaO_2$ is heated at 100 °C in NaOH in a polymethylpropylene flask for 1 hour; silica and NaCl are added, the mixture stirred for 10 minutes, and then transferred to a Teflon lined autoclave and heated to 180 °C for 48 hours. The initial treatment of gallium oxide with sodium hydroxide forms a sodium gallate precursor which is subsequently reacted with silica to produce a gallosilicate framework. This highlights the importance of choosing the most appropriate source of the framework cations, a point which will be examined in detail in the current work. It is desirable to select a reactive form of the framework species in an attempt to reduce reaction time, thus enhancing the possibility of entrapping anions which may possibly decompose under these reaction conditions.

Microwave technology is currently attracting growing interest because of the significant reductions in manufacturing cost due to energy and time saving, enhanced product uniformity, improved or unique microstructures resulting in better properties and also in development of new materials. In addition, due to the nature of microwave heating

the dynamics of the reactants in the liquid could change the reaction mechanism and allow new methods of controlling zeolite phases. Arafat *et al.* [25] have reported the microwave preparation of zeolite Y and ZSM-5, in which reaction times are drastically reduced. Zeolite Y crystallites were prepared in 10 minutes, whereas 10-50 hours are required by conventional heating techniques depending on the framework Si/Al ratio; ZSM-5 can also be produced in 30 minutes at 140 °C using microwave assisted technology. Other zeolites such as CoAPO-5 [26], ALPO-5 [27] and zeolite A [28] have also been prepared by microwave treatment of appropriate precursor gels. It is hoped to extend this work to prepare sodalites of various framework compositions containing a range of anions in the shortest possible time.

3.2.3 Non framework Cation Exchange

Sodalites can only be synthesised directly with sodium as the non-framework cation. Reactions with other cations such as lithium and potassium will lead to different zeolite structures due to the size of the cations templating different cages and channel systems [2, 9]. However, sodium can be replaced after synthesis by cation exchange. High temperature solid state exchange can be performed using alkali metal halides in the range 700-900 °C [29]. This is clearly applicable only to sodalites containing anions which have high thermal stability. If a sodalite containing a halide anion is treated with an alkali metal source containing a different halide, then halide exchange may occur. This has been observed in the ion exchange of sodium chloride sodalite treated with KBr: the resultant sodalite contains sodium and potassium cations, in addition to a mixture of chloride and bromide anions within the beta cages [2].

Alkali metal nitrates do not show this tendency to anion exchange, and also permit cation exchange at lower temperatures [30, 31], in the range 270-370 °C. Typically, an excess of an alkali metal nitrate is heated in the presence of the sodalite to just beyond its melting point for 2-3 hours. After cooling, the excess nitrate is washed free to yield the exchanged sodalite.

Low temperature solution exchanges are even more desirable when dealing with anions of poor thermal stability. A saturated solution of alkali metal chloride or acetate is heated with the sodalite to a reaction temperature generally between 40 and 100 °C, for 4-16 hours [2]. The excess salt is then simply washed free to leave the exchanged sodalite. The higher temperatures and longer reaction times are often used to obtain a greater degree of

cation exchange. These solution reactions are less harsh, but have not been successful when applied to framework substituted sodalites [32].

It would appear therefore that the solid state nitrate exchange method is the most versatile for sodalite cation exchange. In general solid state zeolite exchange reactions are preferred to solution methods for three reasons: firstly, they do not require handling of large volumes of salt solutions; secondly, they avoid the problem of discarding waste salt solutions; finally, they provide the opportunity to introduce metal cations into narrow pore cavities, which by aqueous methods would be hindered by large solvation shells of the cations.

3.2.4 Intra Cage Modifications

Once synthesised, certain sodalites are able to be modified by reaction of the anion within the beta cages. This is principally due to the gas porosity of sodalites at elevated temperatures[2, 3, 4, 10]. One example of this is the production of ClO_2^- sodalite from ClO_3^- sodalite by heating in air at 550 °C for 16 hours [32]. This cannot be achieved directly since $NaClO_2$ decomposes under the reaction conditions. Carbonate sodalite can be formed by the thermal decomposition of formate or acetate anions within the sodalite beta cages [33]; direct synthesis using the Hund [8] or Barrer [9] methods yields cancrinite rather than sodalite, and sodium carbonate does not display sufficient thermal stability for solid state reactions. It has also been reported [4] that treatment of chloride sodalite with H_2S at 900 °C yields a sulphur containing sodalite, which can then be oxidised by heating in air to yield ultramarine. Intra cage reductions in sodalites have been well documented, and include the formation of aluminate sulphide sodalite via the sulphate group [3].

3.3 SYNTHESIS OF ALUMINOSILICATE SODALITES

Aluminosilicate sodalites can be prepared by solid state, low temperature solution and hydrothermal reactions. In this study, synthesis has been undertaken using solid state and solution reactions, and the results obtained are outlined in turn below.

3.3.1 Solid State Methods

Direct solid state sintering was not used to any great degree in this work, due to the high temperatures and long reaction times compared with the structure conversion method of Chang [5], which was used to prepare sodalites containing anions of high thermal stability.

Zeolite Linde 4A, with a silicon to aluminium ratio of unity, was intimately ground with a five fold excess of the sodium salt to be entrapped and heated typically to 800 °C for 24 hours. An intermediate regrinding with a further equivalent weight of the salt ensured that the enclathrate was always present in sufficient excess.

Table 3.1 Summary of reactions using the Structure Conversion Method (SCM)

Cavity Salt	Temp./ °C	Time/h	Product	Structure type
NaCl	800	24	$Na_8(AlSiO_4)_6.Cl$	Sodalite
NaBr	800	24	$Na_8(AlSiO_4)_6.Br$	Sodalite
NaI	800	48*	$Na_8(AlSiO_4)_6.I_2$	Sodalite
Na_2MoO_4	800	24	$Na_8(AlSiO_4)_6.MoO_4$	Noselite
$Na_2Cr_2O_7$	800	24	$Na_8(AlSiO_4)_6.CrO_4$	Noselite

* After 24 hours a significant amount of nepheline was found to be present - this is consistent with the proposal of nepheline as the reaction intermediate [2].

In the case of the entrapped anion being monovalent the product crystallises with the sodalite structure in which every cage is occupied; doubly charged anions yield the noselite structure in which alternate cages are occupied. In the case of the chromate noselite, the starting material $Na_2Cr_2O_7$ is converted *in situ* to the $(CrO_4)^{2-}$ anion which is subsequently entrapped

as the framework is restructured to the sodalite topology. All of the products obtained were of very high crystallinity and were used as starting materials for experiments such as non-framework cation exchanges.

3.3.2 Low Temperature Solution Methods

The method outlined by Hund [8] involves reflux at low temperature under strongly basic conditions. It allows the synthesis of aluminosilicates containing salts which are unstable or volatile at the elevated temperatures used for structure conversion, and relies on the cavity salt being stable in alkali.

Aluminium powder (0.45 g) was dissolved in aqueous sodium hydroxide solution (8 M, 50 ml), and the solution filtered. To the filtrate was added the required sodium salt until saturation. The mixture was then heated to 120 °C and a solution of sodium silicate ("Waterglass", 30% SiO_2, 12% Na_2O, 6.2 g) in aqueous sodium hydroxide (8 M, 6 ml) was added dropwise over 30 minutes. The reaction mixture was then refluxed for 24 hours and the resultant solid product was filtered, washed with 200 ml of distilled water and dried overnight at 110 °C.

Table 3.2 Materials synthesised by the Hund method

Cavity salt	Amount/g	Product	Crystallinity
$NaMnO_4$	30	$Na_8(AlSiO_4)_6.(MnO_4)_2$	High
NaSCN	20	$Na_8(AlSiO_4)_6.(SCN)_2$	Poor
Na_2MoO_4	25	$Na_8(AlSiO_4)_6.MoO_4$	Good
NaI	30	$Na_8(AlSiO_4)_6.I_2$	Good
$NaVO_3$	25	$Na_8(AlSiO_4)_6.(OH)_2$	Poor
$Na_2S_2O_3.5H_2O$	25	$Na_8(AlSiO_4)_6.S_2O_3$	Average
$Na_2S_2O_5$	20	$Na_8(AlSiO_4)_6.(OH)_2$	Poor

The monovalent anions used all yielded sodalitic products, whilst the divalent anions entrapped provided cancrinitic materials. The bright purple permanganate sodalite has sharp,

intense peaks in the X-ray pattern indicating a sample of high crystallinity. The IR band at 910 cm^{-1} confirms the presence of the permanganate group within the framework.

The thiocyanate ion gives a sodalite of low crystallinity as indicated by the broad x-ray peaks: the $(SCN)^-$ ion does not promote sodalite formation particularly well, and as such hydroxide ions and water molecules are also incorporated into the structure. It is the parent material from which synthetic ultramaines can be made: heat treatment for 30 minutes at 600 °C yields ultramarine green containing the $(S_2)^-$ and $(S_3)^-$ chromophores, whilst the thermolysis product of heating at 800 °C for 2 hours is ultramarine blue containing the $(S_3)^-$ species. This may prove a suitable alternative for the synthesis of ultramarine, since it avoids the high temperatures and long reaction times currently used in its industrial production [34].

Iodide sodalite is obtained in good crystallinity, but the sample is still inferior to that using the structure conversion method outlined above. This is also true of the molybdate sample, although being a divalent anion, $(MoO_4)^{2-}$ gives the hexagonal cancrinite structure using the Hund method as opposed to the noselite obtained by SCM.

Sodium metavanadate yielded a sodalite that was principally hydroxide of low crystallinity, although the presence of other aluminosilicates such as nepheline, $NaAlSiO_4$, was observed. This may be due to the fact that metavanadate tends not to form discrete ions to any great extent [35]. Hydroxide sodalite was also obtained using $(S_2O_5)^{2-}$, which suggests that this ion is simply too large to be accommodated by the sodalite framework. The smaller $(S_2O_3)^{2-}$ ion was able to be enclathrated and provided a cancrinite as expected.

An alternative to the Hund method is that reported by Barrer [9]. 2 g kaolin was added to aqueous NaOH (4 M, 200 ml) and stirred with 10 g of the sodium salt at 80 °C for 5 days. The resultant powder product was filtered, washed with 200 ml of distilled water and dried overnight at 110 °C. Table 3.3 gives the products obtained using this method.

Table 3.3 Products synthesised by the Barrer method at 80 °C

Anion	Product	Product type	Crystallinity
$(S_2O_3)^{2-}$	$Na_8(AlSiO_4)_6.S_2O_3$	Cancrinite	Average
$(S_2O_5)^{2-}$	$Na_8(AlSiO_4)_6.(OH)_2$	Sodalite	Poor
Cl^-	$Na_8(AlSiO_4)_6.Cl_2$	Sodalite	High
OH^-	$Na_8(AlSiO_4)_6.(OH)_2$	Sodalite	Good
SCN^-	$Na_8(AlSiO_4)_6.(SCN)_2$	Sodalite	Poor

Both chloride and hydroxide ions are known to promote sodalite formation particularly well and the products using these species give samples of good crystallinity. It was hoped that the different crystallising conditions of this method may afford a higher quality thiocyanate sample, but as for the Hund method, the product was of low crystallinity.

Although the results of Barrer [9] indicated that certain divalent anions would produce sodalites, this was not the case with $(S_2O_3)^{2-}$ and a cancrinite was obtained. A sodalite containing the $(S_2O_3)^{2-}$ ion would be of considerable interest since reduction with hydrogen may provide an alternative synthetic route to ultramarine. As before, the $(S_2O_5)^{2-}$ ion was not entrapped.

The Barrer method outlined above was carried out at various temperatures, primarily to establish the lowest temperature at which the conversion of kaolinite to sodalite would occur. Reactions were carried out using NaCl as the salt to be entrapped. Samples were taken by means of removing 20 ml aliquots from the reaction medium at selected intervals and after being washed with distilled water and dried were analysed by PXD. The results from samples of significance are shown in Table 3.4.

It has been proposed [9, 11] that the transformation of kaolin at 80 °C occurs via zeolite A as the intermediate. Therefore a reaction at 80 °C using zeolite A as the starting material in place of kaolin was undertaken. This showed the formation of Na[AlSi]Cl sodalite after a reaction time of 48 hours.

Table 3.4 Temperature studies using the Barrer method

Temperature/°C	Time/days	Observations
80	3	x-ray amorphous product
	4	Na[AlSi]Cl formed
60	4	x-ray amorphous product
	6	Na[AlSi]Cl formed
40	9	Na[AlSi]Cl begins to form
	9 - 21	Na[AlSi]Cl increases as kaolin decreases
	21	≈ 90% Na[AlSi]Cl + ≈ 10% kaolin
25	≤ 21	kaolin only observed

Na[AlSi]Cl = $Na_8[AlSiO_4]_6.Cl_2$ sodalite.

The results obtained indicate the possibility of sodalite synthesis at 40 °C, and this may give scope for the entrapment of ions having low thermal stability, despite the fact that any products so obtained would contain unreacted kaolin as an impurity phase. Sodalite formation and kaolin diminution is not simultaneous at 60 and 80 °C; the reaction proceeds instead via an X-ray amorphous phase, proposed as zeolite A by Barrer and Schipper. The reaction from Zeolite 4A at 80 °C is consistent with this suggestion, with sodalite formation after 48 hours - this corresponds to the time taken for the transformation of the amorphous intermediate into sodalite using the Barrer method at 80 °C.

3.3.3 Non-Framework Cation Exchange of Aluminosilicate Sodalites

Replacement of sodium cations by other alkali metal cations has been well documented for aluminosilicate sodalites, and as such this has not been undertaken to any great degree in the current work. However, introduction of silver cations has been directed mainly to halide and halo-sodalites due to their interesting optical and electronic properties [36, 37, 38], and hence the range of sodalites examined is far narrower. Silver substitution has therefore been undertaken for various sodalites.

Silver nitrate (12 g) was dissolved in distilled water (20 mls) and the parent sodalite (1 g) was added. The solution was then heated to 100 °C for 24 hours and the solid filtered, washed with distilled water (200 mls) and dried overnight at 110 °C. In order to prevent

photodecomposition, the reaction vessel was coated in aluminium foil. The level of silver exchange was determined by dissolution of a known mass of the sodalite in 2 M HNO_3 followed by precipitation of the silver as AgCl using 1 M HCl. This precipitate was determined gravimetrically and the silver content calculated. Table 3.5 summarises the sodalites exchanged in this manner. The reaction can be represented as:

$$Na_8(AlSiO_4)_6.Y \rightarrow Na_{8-x}Ag_x(AlSiO_4)_6.Y$$

Table 3.5 Silver exchange of aluminosilicate sodalites.

Parent sodalite	Colour	Product	Colour
$Na_8(AlSiO_4)_6.MoO_4$	White	$Na_{1.8}Ag_{6.2}(AlSiO_4)_6.MoO_4$	Cream
$Na_8(AlSiO_4)_6.I_2$	White	$Na_{2.1}Ag_{5.9}(AlSiO_4)_6.I_2$	Cream
$Na_8(AlSiO_4)_6.CrO_4$	Yellow	$Na_{1.3}Ag_{6.7}(AlSiO_4)_6.CrO_4$	Rust
$Na_8(AlSiO_4)_6.(S_2)(S_3)$	Green	$Na_{1.3}Ag_{6.7}(AlSiO_4)_6.(S_2)(S_3)$	Yellow
$Na_8(AlSiO_4)_6.(S_3)_2$	Blue	$Na_{1.1}Ag_{6.9}(AlSiO_4)_6.(S_3)_2$	Green

The results obtained by silver exchange of the sodium sodalites show that nearly all of the sodium ions can be replaced by silver ions in sodalites. The white parent materials $Na_8(AlSiO_4)_6.I_2$ and $Na_8(AlSiO_4).MoO_4$ become cream coloured on exchange, indicating that silver exchange is not a particularly useful method for the introduction of colour into sodalitic materials. However, the colour changes on silver doping chromate sodalite and ultramarine are far more significant: ultramarine green becomes yellow, ultramarine blue yields a green material and the bright yellow chromate sodalite gives a rust coloured species. All of these changes are a result of a red shift in the UV/VIS. spectrum. These results show that silver doping is an effective technique for the modification of coloured species. Of particular note is the obtention of a yellow compound on exchange of ultramarine green - at present no suitable alternative exists for CdS, the yellow pigment currently used in industry [34], and this may prove a useful alternative. In terms of stability and toxicity ultramarines are well suited to industrial applications, but its potential is likely to be tempered by the fact that it would be expensive to produce on a large scale.

Powder x-ray diffraction on these materials shows that there is virtually no change in cell parameter compared with the parent unexchanged compounds. This is not surprising

considering the similarity in ionic radii of sodium and silver ions: 1.00 Å for Ag^+ compared with 0.99 Å for Na^+ [39]. There are, however, significant changes observed in the intensities of the peaks - this is particularly apparent for the (310) peak which is more intense than both the (222) and (321) reflections for the silver doped materials as opposed to the sodium species in which the (310) reflection is less intense than both of these.

3.4 SYNTHESIS OF FRAMEWORK MODIFIED SODALITES

The substitution of Ga for Al and Ge for Si in the sodalite framework has been previously reported [17-24]. The object of these framework substitutions in this work is twofold: firstly, to investigate the relationship between structural parameters and spectroscopic data for sodalites of different framework composition, and secondly to utilise the increased cage size afforded by larger framework cations in an attempt to enclathrate anions which cannot be normally incorporated into an aluminosilicate structure. Nenoff *et al.* [18] have demonstrated this increased cage size on substitution of Ge and Ga in their study of the $Na_3(ABO_4)_3.4H_2O$ sodalite system: compared with the parent aluminosilicate, the approximate increase in cage volume is 11.2 % for GaGe framework, 7.3 % for AlGe and 3.5 % for GaSi. These results show the potential for cage expansion and it was hoped to utilise the range of coloured anions which can be entrapped in sodalite beta cages. The sealed capsule methods of McLaughlan and Marshall [22] and Fleet [21] for the enclathration of halide anions in modified frameworks were considered rather drastic for use in this work and more convenient methods were sought involving lower temperatures and larger scale. Such a method has been used for the synthesis of gallosilicates, and is based on that reported by Newsam *et al.* [24]. Analogous routes to aluminogermanates and gallogermanates have also been investigated.

3.4.1 Hydrothermal Syntheses of Gallosilicate Sodalites

Initial preparations followed the method outlined by Newsam [24] for gallosilicate chloride sodalite. Gallia (Ga_2O_3, 4.17 g) was added to a solution of NaOH (1.78 g) in H_2O, and the solution heated at 100 °C for 1 hour in a polymethylpropylene flask. The silica source (SiO_2, 2.67 g) was added, followed by the sodium salt to be entrapped. The mixture was then transferred to a Teflon lined stainless steel bomb, and heated to the required temperature. The results obtained are summarised below in Table 3.6.

Table 3.6 Synthesis of Gallosilicate Sodalites via the Newsam Method

Anion	Weight Added/g	Temperature/ °C	Time/hrs	Anion Entrapped
SCN^-	10	180	48	OH^-
SCN^-	20	180	48	OH^-
SCN^-	20	180	24	OH^-
SCN^-	20	150	48	OH^-
Cl^-	15	180	48	OH^-
Cl^-	20	180	48	Cl^-
Br^-	20	180	48	Br^-
I^-	20	180	48	I^-
ClO_4^-	20	180	48	ClO_4^-
MnO_4^-	20	150	48	-
MnO_4^-	20	150	24	-

In the synthesis of gallosilicate sodalites, unless an approximately six fold excess of the sodium salt is used, the product obtained will be hydroxide rather than the required sodalite. The powder x-ray pattern of the hydroxide sodalite so obtained shows excellent agreement with that synthesised by McCusker *et al.* [17]. The chloride, bromide and iodide series were all successfully entrapped within a gallosilicate framework as was the perchlorate anion. However, thiocyanate and permanganate were not successfully entrapped and gave hydrosodalite and MnO_2 respectively. Although this route proved moderately successful and the products obtained were of reasonable crystallinity, several improvements were introduced. The method of preparing the sodium gallate precursor was altered: $NaGaO_2$ was presynthesised by stoichiometric solid state reaction of Na_2CO_3 and Ga_2O_3 at 800 °C for 48 hours. This allows the bulk preparation of precursor, and eliminates the inconvenient initial step for every reaction as required by the Newsam method. Secondly, the silicon source was changed from SiO_2, a fairly unreactive source of silicon, to Na_2SiO_3 which generally has much higher activity and is far more soluble in the reaction medium than silica. The time consuming dissolution stage of the silicon source is therefore also removed. It could thus be anticipated that gallosilicates would be synthesised more quickly and easily using these modifications.

1.39 g $NaGaO_2$, 2.46 g Na_2SiO_3, 15 g NaX, where X is the desired anion, were mixed with 5 mls. H_2O to form a gel, transferred to a 23 ml. Teflon lined autoclave (Parr 4349) and heated in the range 150-180 °C for 24-48 hrs. The vessel was then cooled in air, and the product isolated by filtration, washed with 200 mls distilled water, and dried overnight at 110 °C.

The products obtained were highly crystalline, and after only 24 hours reaction were superior to those synthesised after 48 hours using the Newsam method. A further modification was the introduction of base in an attempt to stabilise anions such as $(MnO_4)^-$ and SCN^-. This was successful for thiocyanate, but permanganate still decomposed to manganese (IV) oxide. It was therefore evident that less drastic conditions would have to be sought for its successful inclusion within the gallosilicate beta cage. Results obtained using this method are summarised below in Table 3.7.

Table 3.7 Gallosilicates synthesised hydrothermally by modified Newsam Method

Cavity Salt	Temp/°C	Time/h	Product
NaCl	180	48	$Na_8[GaSiO_4]_6.Cl_2$ {S}
NaBr	180	48	$Na_8[GaSiO_4]_6.Br_2$ {S}
NaI	180	48	$Na_8[GaSiO_4]_6.I_2$ {S}
$NaClO_4$	180	48	$Na_8[GaSiO_4]_6.(ClO_4)_2$ {S}
$NaMnO_4$	150	48	MnO_2
$NaMnO_4$	150	24	MnO_2
$NaMnO_4$	120	48	MnO_2
$NaMnO_4$	120	24	MnO_2
NaSCN	150	24	$Na_8[GaSiO_4]_6.(SCN)_2$ {S}
Na_2MoO_4	180	48	$Na_8[GaSiO_4]_6.MoO_4$ {C}
$Na_2S_2O_3$	180	48	$Na_8[GaSiO_4]_6.S_2O_3$ {C}
Na_2SO_4	180	48	$Na_8[GaSiO_4]_6.SO_4$ {C}

{S} = sodalite, {C} = cancrinite.

3.4.2 Hydrothermal Synthesis of Aluminogermanate Sodalites

A range of aluminogermanates were reported by Sieger *et al.* [23], and it was decided to attempt to repeat their synthetic method. The reactants GeO_2 (2 g), Al_2O_3 (0.98 g) and NaOH (1.53 g) were mixed with 20 g of the sodium salt to be entrapped and placed in a 45 ml Teflon lined stainless steel hydrothermal bomb (Parr 4347) along with the chosen solvent and heated to temperatures between 120 °C and 180 °C. A summary of the reactions studied is shown in Table 3.8 below.

Table 3.8 Hydrothermal reactions for aluminogermanates using the Sieger method

Anion	Temperature/ °C	Time/days	Solvent	Product
Cl^-	150	7	1,4-butanediol	no reaction
Cl^-	180	7	H_2O	M
Cl^-	180	14	H_2O	M
Br^-	150	14	1,4-butanediol	M
Br^-	180	14	H_2O	M
MnO_4^-	120	7	H_2O	M

M = mixed products.

For the halide aluminogermanate reactions, all products obtained were a mixture of phases, including unreacted starting materials and $NaAlGeO_4$.

This set of synthetic parameters did not lead to the successful formation of aluminogermanate sodalites. The preparation by Wiebcke *et al.* [40] of an aluminogermanate hydroxide sodalite was achieved using 16 M NaOH, and it is therefore possible that a greater excess of sodium hydroxide is required to rapidly dissolve the alumina and germania, and then allow recrystallisation of these reagents as sodalites with the anion acting as the synthetic template. The use of such strong base may be necessary to ensure that the hydroxide anion is present in sufficient excess to be exclusively entrapped. However, a strongly basic medium is not particularly desirable; from an industrial point of view the hazards and expense become problematic on a large scale, whereas from an experimental viewpoint competitive reactions between the desired anion and hydroxide tend not to give phase pure products. Despite these considerations, it was decided to examine the effect of

NaOH concentration in the synthesis of $Na_8[AlGeO_4]_6.Cl_2$. Reactions between 150 and 180 °C were attempted using 4 M, 8 M, 12 M and 16 M NaOH solutions; aluminogermanate chloride sodalite was not produced in any of these reactions, with the products being either unreacted GeO_2 or $NaAlGeO_4$.

In light of the results obtained from the gallosilicate reactions, certain modifications to the reaction pathway of Sieger *et al.* [23] were made, and sources of framework species were altered. $NaAlO_2$ and Na_2GeO_3 were introduced in an analogous manner to $NaGaO_2$ and Na_2SiO_3 for gallosilicates. This avoids the *in situ* formation of framework precursors via reaction of their oxides with sodium hydroxide, and thus removes one of the steps in the reaction scheme. This means that the time in which the sodium salt is present in the reaction medium before sodalite formation begins is significantly reduced, and thus the likelihood of decomposition is reduced. The consequent decrease in reaction time is also beneficial when considering reaction turnover and cost efficiency, since the framework precursors are able to be synthesised in bulk.

15 g of NaX, where X is the anion to be entrapped, was added to 0.91 g $NaAlO_2$, 1.85 g Na_2GeO_3 and 5 mls H_2O, transferred to a 23 ml. Teflon lined stainless steel bomb (Parr 4749) and heated to between 150 and 180 °C for the desired reaction time. The reaction milieu was of a gelatinous nature resulting from the small quantity of water used in an attempt to minimise the possibility of entrapment of water rather than the target anion. After the required heating cycle, the vessel was cooled to room temperature, the solid product collected by filtration, washed with 200 ml. distilled water to remove the excess salt and subsequently dried overnight at 110 °C.

In an analogous manner to gallosilicates, thiocyanate was able to be entrapped via the use of sodium hydroxide; the quantity used was minimised in order to avoid preferential enclathration of hydroxide which promotes sodalite formation to a greater degree than the linear thiocyanate anion. As seen previously, permanganate decomposed to MnO_2 whatever the concentration of base used. Results using this method are outlined in Table 3.9.

Table 3.9 Hydrothermal synthesis of aluminogermanates

Cavity Salt	Temp/°C	Time/h	Product
NaCl	180	48	$Na_8[AlGeO_4]_6.Cl_2$ {S}
NaBr	180	48	$Na_8[AlGeO_4]_6.Br_2$ {S}
NaI	180	48	$Na_8[AlGeO_4]_6.I_2$ {S}
$NaClO_4$	180	48	$Na_8[AlGeO_4]_6.(ClO_4)_2$ {S}
NaCl	180	8	$Na_8[AlGeO_4]_6.Cl_2$ {S}
NaCl	90	24	$Na_8[AlGeO_4]_6.Cl_2$ {S}
NaOH	180	24	$Na_8[AlGeO_4]_6.(OH)_2$ {S}
$NaMnO_4$	150	24	MnO_2
$NaMnO_4$	120	24	MnO_2
NaSCN	150	24	$Na_8[AlGeO_4]_6.(SCN)_2$ {S}
NaSeCN	90	24	$Na_8[AlGeO_4]_6.(OH)_{2-x}(SeCN)_x$ {S}
NaSeCN	120	24	$Na_8[AlGeO_4]_6.(OH)_{2-x}(SeCN)_x$ {S}
NaSeCN	150	24	$Na_8[AlGeO_4]_6.(OH)_{2-x}(SeCN)_x$ {S}
Na_2SO_4	180	48	$Na_8[AlGeO_4]_6.SO_4$ {C}
Na_2MoO_4	180	48	$Na_8[AlGeO_4]_6.MoO_4$ {C}
Na_2WO_4	180	48	$Na_8[AlGeO_4]_6.WO_4$ {C}
$Na_2Cr_2O_7$	180	48	$Na_8[AlGeO_4]_6.CrO_4$ {C}
$Na_2S_2O_3$	180	48	$Na_8[AlGeO_4]_6.S_2O_3$ {C}
$Na_2S_2O_5$	180	48	$Na_8[AlGeO_4]_6.S_2O_5$ {C}

{S} = sodalite, {C} = cancrinite.

The size increase of the aluminogermanate cage is utilised for the entrapment of the selenocyanate anion. This was not able to be entrapped by the aluminosilicate framework due to its bulk, but it has been successfully enclathrated using a bigger framework; the level of entrapment is relatively low with $x \approx 0.2$, but it does show the potential of larger cages to entrap a wider variety of anions compared with their aluminosilicate analogues. Even with such a small amount of selenocyanate within the cages, significant colouration can be obtained via thermal decomposition to polyselenide radicals $(Se_n)^-$. This will be detailed in Chapter Six. A further example of the use of the larger aluminogermanate cage

is provided by the entrapment of the metabisulphite anion, $(S_2O_5)^{2-}$, which like selenocyanate is simply too large to be incorporated into an aluminosilicate cage. The entrapment of divalent anions within aluminogermanates show that this framework type shows the same sort of versatility as aluminosilicates, and indeed in addition to the cancrinites formed with divalents, further structural variation in the form of the losod framework has been proven [32].

3.4.3 Hydrothermal Synthesis of Gallogermanate Sodalites

Following the success of the gallosilicate and aluminogermante sodalites, the synthesis of gallogermante sodalites was attempted. Such frameworks incorporate both of the larger framework cations studied, and have the potential to afford the largest cages, as shown by Nenoff *et al.* [18]. It was therefore envisaged that provided suitable synthetic conditions could be developed, gallogermanate sodalites would be able to entrap anions which were too voluminous to be enclathrated within the other frameworks studied.

Table 3.10 Synthesis of gallogermanate sodalites

Cavity Salt	Temp/°C	Time/h	Product
NaCl	180	48	$Na_8[GaGeO_4]_6.Cl_2$ {S}
NaBr	180	48	$Na_8[GaGeO_4]_6.Br_2$ {S}
NaI	180	48	$NaGaGeO_4$
NaI	150	48	$Na_8[GaGeO_4]_6.I_2$ {S}
$NaClO_4$	150	48	M
$NaMnO_4$	120	24	MnO_2
NaSCN	150	24	$Na_6[GaGeO_4]_6.8H_2O$ {S}
Na_2SO_4	180	48	$Na_6[GaGeO_4]_6.8H_2O$ {S}

{S} = sodalite, M = mixture of $Na_8[GaGeO_4]_6.(ClO_4)_2$ and $NaGaGeO_4$.

The framework precursors $NaGaO_2$ (1.39 g) and Na_2GeO_3 (1.85 g) were mixed with 15 g of the appropriate cavity salt and 5 mls. H_2O to form a gel, which was subsequently heated to the desired reaction temperature in a Teflon lined Parr 4349 23 ml. hydrothermal bomb. After the reaction was complete, the vessel was cooled, and the solid product

collected by filtration, washed with 200 mls. distilled water and dried overnight at 100 °C. The results obtained are summarised in Table 3.10 above.

From the results obtained it is evident that gallogermanates are far more sensitive to synthetic conditions than gallosilicates and aluminogermanates. This is highlighted by the experiments using iodide and perchlorate: the temperature had to be reduced to 150 °C for iodide to be successfully entrapped, and phase pure gallogermanate perchlorate sodalite could not be obtained despite several attempts. As before permanganate decomposed to manganese (IV) oxide, whilst thiocyanate and sulphate anions yielded only hydrosodalite. From the results thus far obtained, it was clear that the aluminogermanate framework was the largest system that would allow a wide range of anions to be entrapped.

3.4.4 Low Temperature Solution Synthesis

A modified Hund preparation was used in an attempt to synthesise gallosilicate and aluminogermanate chloride sodalites. Gallia (Ga_2O_3, 1.58 g) was used in place of Al powder in gallosilicate synthesis, and Na_2GeO_3 (3 g) used instead of Na_2SiO_3 in aluminogermanate sodalite synthesis. Na_2GeO_3 was presynthesised by stoichiometric solid state reaction of GeO_2 and Na_2CO_3 at 800 °C for 72 hours.

The powder products obtained from these reactions were of excellent crystallinity but the cell parameters of the phases were smaller than those reported in the literature: 8.941 Å compared with 8.961 Å of Newsam for gallosilicate chloride sodalite [24], and 8.934 Å compared with 9.044 Å of Sieger *et al.* for aluminogermanate chloride sodalite [23]. (The equivalent aluminosilicate chloride sodalite, $Na_8(AlSiO_4)_6.Cl_2$, has a cell parameter of 8.881 Å [2].) Refinement of the products was problematic using pure GaSi and AlGe frameworks, and it was thought likely that leaching of B into the GaSi and Si into the AlGe frameworks from the borosilicate vessels used in the reactions had taken place.

Reactions under the same reaction conditions at 120 °C using polymethylpropylene flasks were carried out, but no products were obtained after 4 days reaction. Previous studies of gallium and germanium containing sodalites by Schipper *et al.* [11] and Barrer *et al.* [15] were subject to this same problem of reaction between sodium hydroxide and the glass reaction vessel; their experimental procedures were repeated in polymethylpropylene flasks to eliminate this possibility, but in all cases no products were obtained, even with reaction times of seven or more days. The synthetic conditions of Nenoff *et al.* [18] for

hydrosodalites were not able to be modified to allow the incorporation of anionic species. Alternative methods for these syntheses were thus sought.

The conditions which had proved successful for hydrothermal synthesis were adapted to solution. Stoichiometric amounts of the appropriate framework precursors were added to the required cavity salt and refluxed in 10 mls. H_2O in a polymethylpropylene flask at 120 °C for 24 hours. Aluminogermanates could be readily synthesised in the absence of additional base, gallosilicates yielded impure sodalites, and gallogermanates gave hydrosodalites only. The addition of base to stabilise anions such as permanganate and thiocyanate (4 M and 1 M NaOH respectively) was also successful. The incorporation of divalent anions was not achieved with any of the framework types using this method. Once again, the relative ease of formation of aluminogermante sodalites is clear compared with gallosilicates and gallogermanates.

Table 3.11 Solution syntheses of framework substituted sodalites

Reagents	Product
$NaAlO_2 + Na_2GeO_3 + NaCl$	$Na_8[AlGeO_4]_6.Cl_2$ {S}
$NaAlO_2 + Na_2GeO_3 + NaOH + NaSCN$	$Na_8[AlGeO_4]_6.(SCN)_2$ {S}
$NaAlO_2 + Na_2GeO_3 + NaOH + NaMnO_4$	$Na_8[AlGeO_4]_6.(MnO_4)_2$ {S}
$NaAlO_2 + Na_2GeO_3 + Na_2SO_4$	$Na_6[AlGeO_4]_6.8H_2O$ {S}
$NaGaO_2 + Na_2SiO_3 + NaCl$	$Na_8[GaSiO_4]_6.Cl_2$ {S} + I
$NaGaO_2 + Na_2SiO_3 + NaOH + NaSCN$	$Na_8[GaSiO_4]_6.(SCN)_2$ {S} + I
$NaGaO_2 + Na_2SiO_3 + NaOH + NaMnO_4$	$Na_8[GaSiO_4]_6.(MnO_4)_2$ {S} + I
$NaGaO_2 + Na_2SiO_3 + Na_2SO_4$	$Na_6[GaSiO_4]_6.8H_2O$ {S}
$NaGaO_2 + Na_2GeO_3 + NaCl$	$Na_6[GaGeO_4]_6.8H_2O$ {S}
$NaGaO_2 + Na_2GeO_3 + NaOH + NaSCN$	$Na_6[GaGeO_4]_6.8H_2O$ {S}
$NaGaO_2 + Na_2GeO_3 + NaOH + NaMnO_4$	$Na_6[GaGeO_4]_6.8H_2O$ {S}
$NaGaO_2 + Na_2GeO_3 + Na_2SO_4$	$Na_6[GaGeO_4]_6.8H_2O$ {S}

I = unknown impurity.

3.4.5 Solid State Reactions

The synthesis of gallium and germanium containing sodalites was attempted via solid state reaction in an analagous manner to the aluminosilicates. Stoichiometric quantitities of Na_2CO_3, Al_2O_3/Ga_2O_3 and SiO_2/GeO_2 were reacted with an excess of the sodium salt to be entrapped. In addition, the framework precursors successfully used in hydrothermal reactions were also introduced, namely $NaAlO_2/NaGaO_2$ and Na_2SiO_3/Na_2GeO_3. Reaction times investigated were 24,48 and 72 hours at temperatures in the range 800-1000 °C. None of these reactions yielded the target sodalite phases.

3.4.6 Non-Framework Cation Exchange of Framework Substituted Sodalites

Exchange of non-framework cations has been well documented for aluminosilicate sodalites, but their framework substituted analogues have not been rigorously investigated. Henderson and Taylor [41] have reported cation exchange on aluminogermanate, gallosilicate and gallogermanate halide sodalites, but from the cell parameters of the parent sodium sodalites, it would appear that they are not of ideal stoichiometry $Na_8[ABO_4]_6X_2$. This arises from the fact that the parent sodalites were prepared in borosilicate vessels, for which leaching via the sodium hydroxide medium used can readily occur. The results obtained in the current work would therefore appear more reliable. Previous studies using solution exchanges have been unsuccessful, and thus nitrate melt reactions were chosen as the method of exchange.

The parent sodium sodalite (0.5 g) was mixed with 2 g of the appropriate nitrate and heated to the required temperature just beyond the melting point of the nitrate. After approximately 3 hours, the reaction was air cooled, the product washed with 200 mls. H_2O to remove the excess nitrate and dried overnight at 110 °C. The results so obtained are summarised in Table 3.12.

Table 3.12 Non-framework cation exchange of framework substituted sodalites

Parent Sodalite	Exchange salt	Temp./°C	Time/hrs	Product
Na[GaSi]Cl	$LiNO_3$	240	3	Li[GaSi]Cl
Na[GaSi]Br	$LiNO_3$	240	3	Li[GaSi]Br
Na[GaSi]I	$LiNO_3$	240	3	Li[GaSi]I
Na[GaSi]Cl	KNO_3	370	16	K[GaSi]Cl
Na[GaSi]Br	KNO_3	370	16	K[GaSi]Br
Na[GaSi]I	KNO_3	370	16	K[GaSi]I
Na[AlGe]Cl	$LiNO_3$	240	2	Li[AlGe]Cl
Na[AlGe]Br	$LiNO_3$	240	3	Li[AlGe]Cl
Na[AlGe]I	$LiNO_3$	240	3	Li[AlGe]Cl
Na[AlGe]Cl	KNO_3	370	16	K[AlGe]Cl
Na[AlGe]Br	KNO_3	370	16	K[AlGe]Br
Na[AlGe]I	KNO_3	370	16	K[AlGe]I
Na[GaGe]Cl	$LiNO_3$	240	2	-
Na[GaGe]Br	$LiNO_3$	240	2	-
Na[GaGe]I	$LiNO_3$	240	2	-
Na[GaGe]Cl	KNO_3	370	16	Na[GaGe]Cl
Na[GaGe]Br	KNO_3	370	16	Na[GaGe]Br
Na[GaGe]I	KNO_3	370	16	Na[GaGe]I

Table 3.12 shows how the gallosilicate and aluminogermanate sodalites can readily undergo exchange of non-framework cations by nitrate melt. This is particularly the case with lithium for which full exchange can be obtained within three hours reaction. It is interesting to note that for the aluminogermanate chloride material, a reaction time of three hours caused decomposition of the sample to nepheline, whilst a reaction time of two hours yielded a fully ion exchanged aluminogermanate chloride sodalite. It is possible that full lithium exchange occured after two hours at which point reaction of the excess lithium nitrate present in the mixture with $Li_8[AlGeO_4]_6.Cl_2$ causes the sodalite to collapse. The

reason that the chloride collapsed whereas the bromide and iodide were stable could well be due to the fact that the smaller anion results in framework bond angles more highly strained than for the other halides. This will be described in Chapter Five.

The propensity of the gallogermanates to resist ion exchange may be related to the difficulty encountered in synthesising sodalites containing anions other than the halides. Lithium exchange destroys the sodalite leaving the nepheline analogue, $NaGaGeO_4$, as the principal product, whereas potassium leaves the sodalite intact but unexchanged. The reason for this is not clear, although it does appear as though the gallogermanate framework will only support a very limited range of cell parameters and framework bond angles, manifested by the successful incorporation of only three anions and only one type of non-framework cation.

3.5 MICROWAVE SYNTHESIS OF SODALITES

Typical solution, hydrothermal and solid state sodalite syntheses involve reaction times of 24 hours and upwards, and although shorter experiments can yield sodalites, they remain relatively time consuming. The use of microwave radiation to promote sodalite crystallisation has been studied and permits rapid product formation. Consequently, high experimental turnover and vastly reduced levels of power consumption are possible.

Stoichiometric amounts of the appropriate framework precursors $NaAlO_2$, Na_2GeO_3 and $Na_2SiO_3.5H_2O$ were mixed with 4g of the sodium salt to be entrapped and 1.5 ml of H_2O, transferred to a 23 ml. Teflon lined Parr 4781 microwave digestion bomb and heated in a domestic microwave oven at various power levels for a range of reaction times. The exact experimental conditions used are summarised in Table 3.13.

Table 3.13 Summary of microwave synthesis of sodalites

Cavity salt	Heat Treatment	Product	Crystallinity
NaCl	1000W, 60s;½ pwr, 10 min	$Na_8[AlGeO_4]Cl_2$	High
NaCl	1000W, 60s;½ pwr, 5 min	$Na_8[AlGeO_4]Cl_2$	Average
NaCl	1000W, 60s	$Na_8[AlGeO_4]Cl_2$	Good
NaCl	1000W, 50s	$Na_8[AlGeO_4]Cl_2$	Average
NaCl	1000W, 40s	$Na_8[AlGeO_4]Cl_2$	Good
NaCl	1000W, 30s	$Na_8[AlGeO_4]Cl_2$	Excellent
NaCl	1000W, 20s	$Na_8[AlGeO_4]Cl_2$	Excellent
NaCl	1000W, 10s	$Na_8[AlGeO_4]Cl_2$	Good
NaCl	1000W, 30s	$Na_8[AlSiO_4]Cl_2$	Poor
NaBr	1000W, 30s	$Na_8[AlSiO_4]Br_2$	Poor
NaI	1000W, 30s	$Na_8[AlSiO_4]I_2$	Poor
NaSCN	1000W, 30s	$Na_8[AlSiO_4](SCN)_2$	Poor

½ pwr = half power: refers to the 'duty cycle' in which full power is applied for 15s, followed by no power for 15 s.

Table 3.13 shows how aluminogermanate chloride sodalite was successfully synthesised using a varity of microwave heat treatments. The highest quality sample was

that obtained after 20s at 1000W. However, the sample obtained after only 10 s is still of good quality, and shows the potential for extremely rapid sodalite synthesis. This particular heat treatment would appear to be the most suitable for anions of limited thermal stability.

The aluminosilicate sodalites produced are of poor crystallinity, although their formation does show the potential for the preparation of sodalites of different framework composition using this method. Relatively little research has been undertaken using microwave radiation, but the preliminary results obtained here do indicate that this line of work is one which may be worth pursuing. At present it is unclear whether or not the small scale reactions presented here could feasibly be scaled up to an industrial level, but certainly if large batch process could be designed in which reaction times are a fraction of those required using conventional heating methods, dramatic energy cuts could be envisaged.

3.6 CONCLUSIONS

Hydrothermal reactions have been shown to be particularly suited to the preparation of framework modified sodalites. The reaction schemes devised within this work show how the same precursor type can be employed in the synthesis of both gallium and germanium substituted sodalites. In terms of ease of anion entrapment, aluminogermanates are more readily formed than gallosilicates which are in turn better than the gallogermanates. This can be illustrated by the fact that no divalent anions can be entrapped within gallogermanates, and the only anions entrapped to form monophasic products are the halides. The range of anions entrapped within gallosilicate framework is far smaller than that for the aluminogermanates: low temperature solution reactions have also been far more successful with aluminogermanates than their gallosilicate counterparts.

A comparison with the methods reported in the literature reflects favourably on the methods used herein. The range of anions able to be entrapped is far more diverse than those outlined using other techniques; the use of NaOH as required by Sieger *et al.* [23] is not necessary unless the particular anion to be enclathrated requires a basic medium for stabilisation. The temperatures and pressures at which aluminogermanates will form is also significantly reduced from that of Sieger *et al.* [23], with successful syntheses as low as 90 °C.

The synthetic method devised by Fleet [21] for aluminogermanates is rather drastic, using sealed gold capsules heated at temperatures in the order of 800 °C producing pressures of approximately 0.2 GPa to yield single crystals. Since the crystallographic results of this work agree so closely with those of Fleet (outlined in detail in Chapter Five) it can be stated that the reduction of reaction pressure and temperature does not impair the formation of highly crystalline aluminogermanate sodalites. It should be remembered of course that single crystal syntheses often involve significantly different experimental conditions than those applicable to the preparation of bulk powdered materials. It was the intention of this study to reduce reaction temperature and pressure so as to devise synthetic procedures which are applicable to the enclathration of anions of relatively low thermal stability such as permanganate. Reactions were undertaken using the halide anions in order to optimise general synthetic procedures which then could be used to entrap more complex species within the sodalite cage. The success of these methods can easily be gauged by comparing them with literature reports such as that of Fleet for the aluminogermanates. In his study, Fleet reported that the experimental method successfully

used for aluminogermanate sodalite synthesis could not be extended to prepare gallosilicates or gallogermanates; he attributed the wider range of thermal stability of the aluminogermanates to the smaller framework cage. Although this would explain the failure to synthesise the larger gallogermanates, gallosilicate sodalites are smaller than aluminogermantes and thus according to this reasoning should display a greater range of themal stability than their aluminogermanate analogues. This is clearly not the case and so the ease of formation of the aluminogermanates cannot be explained by the size of the framework alone. The ionic radius of both aluminium and germanium is 0.39 Å in tetrahedral coordination [39], and it may be that this feature gives the largest clue to the relative stability of framework compositions. It is perhaps feasible that sodalites are most easily formed when the framework cations have the smallest size mismatch: this would explain the experimental observation that aluminogermanates are easier to synthesise than gallosilicate or aluminogermanate sodalites. The aluminosilicates, however, have a large difference in the T and T' cationic radii and their facile synthesis does seem to contradict this proposition, although it may well be the case that several factors are involved in governing sodalite formation, one of which is size of framework cations.

An alternative explanation could be that since gallium and germanium are considerably larger than aluminium and silicon, they will have more of a tendancy to adopt six fold coordination and thus not promote sodalite formation to any great degree. This effect will be increased when gallium and germanium are combined in the reaction medium. The obtention of gallogermanate sodalites would therefore be far more synthetically challenging than those required to form frameworks containing either gallium or germanium, which is indeed the case as observed via experiment.

3.7 REFERENCES

[1] D.W. Breck, 'Zeolite Molecular Sieves, Structure, Chemistry and Uses', Wiley-Interscience, New York (1974).

[2] G. Wong, *Ph.D. Thesis*, University of Southampton (1990).

[3] M.E. Brenchley, *Ph.D. Thesis*, University of Southampton (1994).

[4] J.S. Prener and R. Ward, *J. Am. Chem. Soc.*, **72**, 2780 (1950).

[5] I.F. Chang, *J. Electrochem. Soc.*, **121**, 815(1974).

[6] G. Engelhardt, J. Felsche and P. Sieger, *J. Am. Chem. Soc.*, **114**, 1173 (1992).

[7] F. Hund, *Z. Anorg. Allg. Chem.*, **509**, 153 (1984).

[8] F. Hund, *Z. Anorg. Allg. Chem.*, **511**, 225 (1984).

[9] R.M. Barrer, J.F. Cole, and H. Sticher, *J. Chem. Soc.*, A**10**, 2475 (1968).

[10] R.M. Barrer, 'Hydrothermal Chemistry of Zeolites', Academic Press, London (1982).

[11] P.J. Schipper, C.Z. van Doorn and P.T. Bolwijn, *J. Am. Ceramic Soc.*, **55**, 256 (1972).

[12] W.A. van Erp, H.W. Kouwenhoven and J.M. Nanne, *Zeolites*, **7**, 286 (1987).

[13] L.T. Todd and C.E. Stroud, *Mater. Res. Bull.*, **15**, 595 (1980).

[14] R.R. Neurgaonkar and F.A. Hummel, *Mat. Res. Bull.*, **11**, 61 (1976).

[15] R.M. Barrer, J.W. Baynham, F.W. Bultitude and W.M. Meier, *J. Chem. Soc.*, 195, (1959).

[16] K. Suzuki, Y. Kiyozumi, S. Shin and S. Ueda, *Zeolites*, **5**, 11 (1985).

[17] L.B. McCusker, W.M. Meier, K. Suzuki and S.Shin, *Zeolites*, **6**, 388 (1986).

[18] T.M. Nenoff, W.T.A. Harrison, T.E. Gier, N.L. Keder, C.M. Zaremba, V.I. Srdanov, J.M. Nicol and G.D. Stucky, *Inorg. Chem.*, **33**, 2472 (1994).

[19] M.S. Perlmutter, L.T. Todd and E.F. Farrell, *Mat. Res. Bull.*, **9**, 65 (1974).

[20] E.L. Belokoneva, L.N. Dem'yanets, T.G. Uvarova and N.V. Belov, *Sov. Phys. Crystallogr.*, **27**(5), 597 (1982).

[21] M.E. Fleet, *Acta Cryst.*, C**45**, 843 (1989).

[22] S.D. McLaughlan and D.J. Marshall, *Phys. Lett.*, **32A**, 343 (1970).

[23] P. Sieger, G. Engelhardt, and J. Felsche, *JCPDS Powder diffraction file*, Pattern Numbers **43-241/249**, International Centre for Diffraction Data, Newtown Square Corporate Campus, 12 Campus Boulevard, Newtown Square, Pennsylvania 19073-3273, U.S.A. (1991).

[24] J.M. Newsam and J.D. Jorgensen, *Zeolites*, **7**, 569 (1987).

[25] A. Arafat, J.C. Jansen, A.R. Ebaid and H. van Bekkum, *Zeolites*, **13**, 162 (1993).

[26] U. Lohse, R. Bertram, K. Jancke, I. Kurzawski, B. Parlitz, E. Loeffler and E. Schreier, *J. Chem. Soc. Faraday Trans.*, **91**, 1163 (1995).

[27] I. Girnus, K. Jancke, R. Vetter, J. Richter-Mendau and J. Caro, *Zeolites*, **15**, 33 (1995).

[28] X. Meng, W. Xu, S. Tang and W. Pang, *Chin. Chem. Lett.*, **3**, 69 (1992).

[29] D. Taylor, *Contrib. Mineral. Petrol.*, **51**, 39 (1975).

[30] J. Godber and G.A. Ozin, *J. Phys. Chem.*, **92**, 4980 (1988).

[31] A. Stein, G.A. Ozin and G.D. Stucky, *J. Am. Chem. Soc.*, **114**, 8119 (1992).

[32] P.J. Mead, *Ph.D. Thesis*, University of Southampton (1996).

[33] P. Sieger, A.M. Schneider, M. Wiebcke, P. Behrens, J. Felsche and G. Engelhardt, *Chem. Mater.*, 7, 163 (1995).

[34] G. Buxbaum (ed.), "Industrial Inorganic Pigments", VCH, Weinheim, Federal Republic of Germany (1993).

[35] F.A. Cotton and G. Wilkinson, 'Advanced Inorganic Chemistry', Fifth Edition, Wiley-Interscience, New York (198).

[36] G.A. Ozin, A. Kuperman and A. Stein, *Adv. Mater.*, **1**, 69 (1989).

[37] A. Stein, G.A. Ozin and G.D. Stucky, *J. Soc. Photogr. Sci. Technol. Japan*, **53**(4), 322 (1990).

[38] G.D. Stucky and J.E. MacDougall, *Science*, **247**, 669 (1990).

[39] R.D. Shannon and C.T. Prewitt, *Acta Cryst.*, **A32**, 751 (1976).

[40] M. Wiebcke, P. Sieger, J. Felsche, G. Englehardt, P. Behrens and J. Schefer, *Z. Anorg. Allg. Chem.*, **619**, 1321 (1993).

[41] C.M.B. Henderson and D. Taylor, *Spectrochim. Acta*, **35A**, 929 (1979).

Chapter Four

SYNTHETIC STRATEGIES

4.1 INTRODUCTION

The previous chapter outlined the general synthetic procedures for sodalites of different framework composition. This section primarily deals with anions which may be able to be entrapped within sodalites to yield materials with pigment properties offering alternatives to those currently used in industry. A review of small coloured anions will be undertaken, their synthesis discussed and the most appropriate method of attempted entrapment for each within the sodalite cage highlighted. In addition, non-coloured anions which can be entrapped and subsequently treated to yield a coloured product will be investigated. The selection of anions for attempted entrapment will be rationalised according to their individual properties. The adaptation of the general synthetic procedures as required for specific anions will be discussed. The success of the methods will be reviewed and, in those cases where the target material was not successfully prepared, the reasons for this will be discussed.

For a particular anion to be successfully entrapped within an aluminosilicate framework it must possess certain properties: stability to temperatures in the order of 800 °C as required for solid state reactions (e.g. Cl^-) [1, 2], or stability to base (e.g. SCN^-) required for the low temperature methods of Hund and Barrer [3, 4]. The anion must also be relatively small, and, if four coordinate, have tetrahedral rather than square planar symmetry to promote sodalite formation. Such requirements exclude coloured anions such as the ruby red $[Fe(CN)_5NO]^{2-}$ from use in sodalite based pigments. Isomorphous substitution of framework aluminium and silicon, principally to increase cage size to allow the incorporation of voluminous anions, will also be detailed.

4.2 TRANSITION METAL OXO-ANIONS

Anions of the transition elements would appear to be particularly suited to the application of sodalite pigments on account of their colour. Simple coloured transition metal oxo-anions such as $(CrO_4)^{2-}$, $(MnO_4)^-$, $(RuO_4)^-$, $(RuO_4)^{2-}$ and $(FeO_4)^{2-}$ are obvious choices for entrapment, and indeed the yellow chromate (VI) and purple manganate (VII) sodalites have already been reported [5, 6]. This latter species is another example of the extra stability afforded by entrapment within sodalites: alkali metal permanganates typically decompose at temperatures in the order of 200 °C whilst $Na_8(AlSiO_4)_6.(MnO_4)_2$ is stable to 600 °C, at

which point the formation of manganate from permanganate can be seen. These anions are classified below according to the particular transition metal in question.

4.2.1 Manganese

The heptavalent state is best known in the form of the purple permanganate anion, $(MnO_4)^-$. The sodium and potassium salts are made on a large scale by electrolytic oxidation of basic solutions of the manganate anion, $(MnO_4)^{2-}$. $KMnO_4$, solubilised by crown ethers or cryptands in benzene, is a widely used oxidant [7]. Indeed, the reduction of manganese (VII) to lower oxidation states is one of the major problems encountered when attempting to entrap the permanganate anion in sodalites; formation of $(MnO_4)^{2-}$ and MnO_2 is commonly observed if the experimental conditions are not fully optimised. It is stabilised in basic solution, and its alkali metal salts are typically stable to temperatures in the region of 160-200 °C. It could therefore be envisaged that the entrapment of the permanganate anion could be achieved via a solution method such as that of Hund [3]; its temperature stability is clearly insufficient for enclathration via high temperature solid state techniques. The aluminosilicate permanganate sodalite has been successfully prepared using the Hund method, with the strongly basic reaction medium ideally suited to the stability requirements of the permanganate anion.

Manganese (VI) is commonly known only in one environment, namely the deep green manganate anion, $(MnO_4)^{2-}$ [8]. This is formed by oxidising MnO_2 in fused KOH with KNO_3, air or other oxidising agents, by evaporating $KMnO_4$ and KOH solutions, or by refluxing a strongly basic solution of permanganate at 140 °C. Only two salts, K_2MnO_4, and several hydrated forms of Na_2MnO_4 have been isolated in a pure form. Both of these are very dark green, and thus framework materials containing the manganate ion would be potential replacements for greens such as cobalt chrome aluminates. The manganate anion is stable only in very basic media; in acid, neutral or only slightly basic solutions it readily disproportionates in a kinetically complex way according to the equation:

$$3(MnO_4)^{2-}_{(aq)} + 4H^+_{(aq)} \rightarrow 2MnO_4^-{}_{(aq)} + MnO_{2(s)} + 2H_2O$$

In this work, the manganate anion was prepared by refluxing $NaMnO_4$ in 15M NaOH for two hours at 140 °C [9]. In a similar manner to permanganate, low temperature solution methods provide the best possibility of entrapping the manganate ion. Once again, the Hund

method provides the ideal environment for the enclathration of $(MnO_4)^{2-}$ within an aluminosilicate framework and yields yield a deep green cancrinite. The entrapment of divalent anions within framework substituted sodalites has not proven possible using the low temperature solution methods of this work; since hydrothermal reactions lead to the formation of MnO_2, the enclathration of manganate anions within gallium and germanium containing materials is simply not viable. Thermal treatment of permanganate sodalite has been reported to yield a deep green material [10], which would correspond to the thermal degradation of $(MnO_4)^-$ to $(MnO_4)^{2-}$, although this is in fact accompanied by significant simultaneous formation of MnO_2 which effectively negates its resultant pigmentary attributes.

There are few authenticated examples of compounds containing pentavalent manganese [11]. The oxychloride $MnOCl_3$, which decomposes above 0 °C to $MnCl_3$ and is easily hydrolysed, is formed by reducing $KMnO_4$ dissolved in HSO_3Cl with sucrose. The oxo-anion $(MnO_4)^{3-}$ and Mn^V esters have often been cited as intermediates in the reduction of MnO_4^- but with little evidence. Unstable manganate (V) and (VI) intermediates have been detected in the reduction of MnO_4^- by $(SO_3)^{2-}$. Olazcuaga [12] reported the synthesis of the dark green γ-Na_3MnO_4 by heating Na_2O and MnO_2 at 700 °C for 15 hours under O_2; heating this material for 8 days at 300 °C produced β-Na_3MnO_4, which like the gamma analogue is both dark green and hygroscopic. However, since the encapsulation of trivalent anions within sodalites has not been successful, $(MnO_4)^{3-}$ is not of use for sodalite based pigments. It would therefore appear that manganese (V) is not stable to a sufficient degree as a mono- or divalent anion to allow its entrapment within the sodalite beta cage by any of the synthetic methods previously outlined. It could possibly be envisaged that partial intracage reduction of Mn(VII) or Mn(VI) could lead to the formation of Mn(V), although it is more likely that reduction directly to MnO_2 would occur.

4.2.2 Vanadium

Vanadium possesses several stable oxo-anions in varying oxidation states ranging from +3 to +5 [11]. The metavanadate anion, $(VO_3)^-$, and orthovanadate $(VO_4)^{3-}$, both contain vanadium in the pentavalent state and display sufficient stability in base to suggest that the Hund method would be suitable for their incorporation in an aluminosilicate framework. However, neither are particularly suitable for sodalites: the metavanadate

structure is composed of chains rather than discrete ions, whereas orthovanadate is a trivalent anion and hence does not promote sodalite formation to any great degree. In addition, neither of these sodium salts are coloured and are therefore of no use as replacements for the coloured pigments currently employed.

4.2.3 Chromium

As already indicated, the chromate (VI) anion is bright yellow and is stable to both basic media and high temperature, allowing a choice of solution or solid state methods for its entrapment in the sodalite structure. Since it is divalent, the Hund method [3] would afford the more open cancrinite structure whereas structure conversion [2] yields a noselite in which divalent anions are found in alternate cages. The latter is therefore the chosen synthetic method, since cancrinites tend to be less stable both chemically and thermally due to their less compact framework. The method outlined by Barrer [4] also yields a cancrinite with the chromate anion. The chromate anion can be synthesised *in situ* from chromium trioxide or the dichromate anion. In solutions above pH 6, CrO_3 forms the tetrahedral yellow chromate ion $(CrO_4)^{2-}$; between pH 2 and 6, $(HCrO_4)^-$ and the orange-red dichromate ion $(Cr_2O_7)^{2-}$ are in equilibrium; and at pH values below one the main moiety formed is H_2CrO_4 [11]. The equilibria are the following:

$$HCrO_4^- \Leftrightarrow CrO_4^{2-} + H^+$$
$$H_2CrO_4 \Leftrightarrow HCrO_4^- + H^+$$
$$Cr_2O_7^{2-} + H_2O \Leftrightarrow 2HCrO_4^-$$

In addition the following base-hydrolysis equilibria exist:

$$Cr_2O_7^{2-} + OH^- \Leftrightarrow HCrO_4^- + CrO_4^{2-}$$
$$HCrO_4^- + OH^- \Leftrightarrow CrO_4^{2-} + H_2O$$

In the hydrothermal preparations used in this work, $(CrO_4)^{2-}$ is formed *in situ* using $(Cr_2O_7)^{2-}$ in the presence of 8 M NaOH. The chromate source in the Structure Conversion Method [2] was $Na_2Cr_2O_7.2H_2O$, which when reacted with Zeolite 4A at 800 °C forms $(CrO_4)^{2-}$ *in situ* which is subsequently entrapped within the sodalite beta cages as the zeolite is restructured. Both solution and solid state methods yield bright yellow aluminosilicate framework materials.

Gallium and germanium containing sodalites have not been prepared successfully using solid state methods. Hydrothermal reactions have therefore been employed in order to synthesise gallosilicate and aluminogermanate chromate materials: these are of the cancrinite rather than sodalite structure as found for the aluminosilicates. The anion source in these cases was sodium dichromate which produced the $(CrO_4)^{2-}$ anion *in situ* as described above. Both of these bright yellow cancrinites were successfully prepared at 180 °C with a reaction time of 48 hours; their respective UV/VIS spectra are compared with the aluminosilicate analogue in Chapter Six.

The toxicity associated with chromium does, however, mean that such materials cannot be widely used as industrial alternatives to yellow currently used, despite the extra chemical stability afforded to the anion by the framework in which it is entrapped.

4.2.4 Ruthenium

The dark green perruthenate ion, RuO_4^-, has insufficient temperature stability to allow high temperature sodalite synthesis (decomposing at 440 °C in vacuo), and aqueous alkaline solutions of the sodium salt are unstable, with Ru (VII) being reduced to Ru (VI). This decomposition involves coordination of OH^- groups to Ru, and the production of H_2O_2.

Sodium ruthenate(VI) is very similar indeed to sodium ferrate, and is prepared analogously by oxidation of $RuCl_3$ with sodium hypochlorite [11]:

$$3NaOCl + 2RuCl_3 + 10NaOH \rightarrow 2Na_2RuO_4 + 9NaCl + 23H_2O$$

The orange tetrahedral $(RuO_4)^{2-}$ ion is moderately stable in mild alkali, but coordinates two OH^- to become six coordinate, and thus cannot be accommodated by the sodalite cage [9]. However, since no decomposition was observed at 120°C over the reaction time of 24 hours, it would appear that ruthenate(VI) does have sufficient temperature stability to make sodalite synthesis in non-basic media a possibility. The oxidation of ruthenium trichloride usually involves using an excess of sodium hydroxide to give the ruthenate anion. Reactions in which the oxidation of ruthenium trichloride were attempted in the absence of base and using a stoichiometric amount of hydroxide were unsuccessful; the characteristic colour of the ruthenate anion was only observed when excess base was present. It is therefore not suited to sodalite formation since the coordination of hydroxyl groups in solution could not be prevented.

4.2.5 Iron

The FeO_4^{2-} ion is of particular interest due to its red/purple colour, non-toxic nature and base stability but it does possess poor thermal properties. Attempted synthesis of ferrate (VI) sodalite using a modified Hund method at 80 °C [9] resulted in the thermal decomposition of the iron (VI) to iron (III). Since 12 M NaOH solution was used to stabilise the ferrate anion, this decomposition was attributed to thermal instability rather than pH effects. A lower temperature sodalite synthesis would therefore be required. Results obtained using the method of Barrer [13] at various temperatures, as outlined in the previous chapter, indicate the possibility of sodalite formation as low as 40 °C, and thus synthesis of ferrate sodalite at 40 °C was attempted.

Na_2FeO_4 was prepared as outlined by Audette *et al.* [13]. 200 ml NaOCl (14% w/v Cl) was cooled in an ice/salt bath, and solid NaOH was slowly added until saturation. The temperature of the solution was maintained below 20 °C at all times during this addition. The solution was then filtered. To the filtrate 25 g of $Fe(NO_3)_3.9H_2O$ was added with stirring, and the temperature of the solution held below 25 °C. The solution was then stirred at 0 °C for 90 minutes, filtered into 50 ml of ice cold 12 M NaOH solution, and the residue washed with 100 ml 12 M NaOH. The reaction corresponds to the equation:

$$3NaOCl + 2Fe(NO_3)_3.9H_2O + 10NaOH \rightarrow 2Na_2FeO_4 + 6NaNO_3 + 3NaCl + 23H_2O$$

Further purification can be achieved by treating the solid with 10 ml. benzene, then three to five times with 20 ml. portions of aldehyde-free ethanol, and finally stirring for 20 min with 1000 ml ethanol. This last treatment is repeated three times. The product is then washed with 50 ml ether and dried in vacuo. However, the initial reaction was undertaken principally to investigate the stability of the ferrate and therefore no attempt at purification was made at this stage.

To the solution prepared as above, 2 g of kaolinite was added. The reaction mixture was heated with stirring to 40 °C. After a period of 3 days there was visible decomposition of the purple ferrate(VI) to a brown coloured species. The reaction was stopped and the solid product collected by filtration, washed with 100 ml of 10 M NaOH solution (to avoid further decomposition of any remaining ferrate) and dried overnight at 80 °C. Analysis by powder X-ray diffraction showed the formation of Fe_2O_3, confirming the decomposition of Fe(VI) to Fe(III).

In an attempt to further stabilise the iron (VI), a ferrate solution saturated with NaOH was prepared, and a second experiment performed as above at 40 °C. Once again decomposition to iron (III) was observed. The decomposition of Fe(VI) to Fe(III) has been observed for the sodium ferrate at 40 °C in an analogous manner to reactions previously undertaken at 80 °C. This decomposition can be described by the equation:

$$2\ (FeO_4)^{2-} + 10H^+ \rightarrow 2Fe^{3+} + 3/2O_2 + 5H_2O$$

A reaction in which the sodium ferrate solution was frequently replaced with a fresh solution of the salt was also undertaken, but replacing the ferrate solution every 24 hours still led to significant ferrate composition. Although there were no obvious visible signs of decomposition and the reaction milieu maintained the purple/red colour characteristic of the ferrate anion, upon filtration to remove the old solution solid Fe_2O_3 was obtained. In an attempt to speed up the reaction, Zeolite A was used as the starting material in place of kaolinite. Once again the problem of decomposition was encountered: the formation of sodalite could not be achieved before reduction of iron (VI) to iron (III) occurred.

4.2.6 Summary of Transition Metal Oxo-Anions Suitable for Sodalite Entrapment

Table 4.1 below summarises the attempted synthesis of sodalites containing transition metal oxo-anions.

Table 4.1 Transition metal oxo anions in sodalite synthesis

Anion	Colour	Base Stable	Temp. Stable	Method of entrapment	Product
$(RuO_4)^-$	green	N	N	-	-
$(RuO_4)^{2-}$	orange	N	N	-	-
$(FeO_4)^{2-}$	red/purple	Y	N	Barrer	$Fe_2O_3.H_2O$
$(MnO_4)^-$	purple	Y	N	Hund	$Na_8[AlSiO_4]_6(MnO_4)_2$
$(MnO_4)^{2-}$	green	Y	N	Hund	$Na_8[AlSiO_4]_6(MnO_4)$
$(CrO_4)^{2-}$	yellow	Y	Y	SCM/Soln	$Na_8[AlSiO_4]_6(CrO_4)$

The term "base stable" is used to indicate whether the anion possesses sufficient base stability for the Hund [3] or Barrer [4] methods to be appropriate for enclathration; similarly "temp. stable" refers to whether or not the sodium salt has the necessary thermal stability to make the high temperature solid state routes to sodalite formation a viable option.

4.3 TRANSITION METAL OXYHALIDES

Another group of coloured anions are the transition metal oxyhalides, such as the yellow $(VO_2Cl_2)^-$. The halogen in such species is normally introduced by treatment of the transition metal oxo-anion with the corresponding acid [14]. Sodalite synthesis in alkali therefore appears inappropriate since hydrolysis back to the parent compound would be expected, and is indeed observed in basic media: in the case of the yellow dichlorodioxovanadate anion decomposition back to the metavanadate is seen with HCl also evident. Other anions such as the orange chlorochromate, CrO_3Cl^-, are hydrolysed by water in the same manner and in this case $CrO_3(OH)^-$ is formed [11]. In a similar manner to these examples, all of the transition metal oxyhalides tend to hydrolyse in water or base. High temperature routes are hence the best possibility for entrapment in these cases. The dioxodichlorovanadate (V) sodium salt was prepared by the treatment of a solution of sodium metavanadate with 25% HCl:

$$NaVO_{3(aq)} + HCl_{(aq)} \rightarrow NaVO_2Cl_{2(aq)} + H_2O$$

An attempt to isolate this species by rotary evaporation of the water present led to decomposition to a dark solid, which contained VO_2. Solid state entrapment therefore would not be appropriate since isolation of the salt was not achieved. It would therefore appear that the alternative is to simply add the required framework precursors, i.e. $NaAlO_2$ and Na_2SiO_3, and attempt to form a sodalite in acidic media. A solution preparation was attempted using $NaAlO_2$ and Na_2SiO_3 and an acidic solution of $NaVO_2Cl_2$ at 120 °C for 24 hours, but decomposition to V_2O_5 was observed. The entrapment of oxyhalide anions was thus deemed particularly problematic, and other coloured anions were thus sought.

The fluorooxo transition metal anions show less tendency to hydrolyse, but since their formation generally involves use of HF solutions, their projected use as industrial pigments can be effectively ruled out, and hence their syntheses were not attempted.

4.4 CHALCOGENOMETALLATES

In their highest oxidation states, the transition metals V, Nb, Ta, Mo, W and Re form strongly coloured tetrahedral thioanions. Chalcogenometallates can be prepared by solid state reactions (e.g. Th_3VSe_4 [15]) from the constituent elements, or by reaction of H_2S/H_2Se with a solution (e.g. Na_2MoS_4 [16]) of the oxometallate. Many of these compounds were investigated as early as the nineteenth century [17-19] but their isolation and purification have only been reported in the last thirty years; for example, the thiomolybdates $(MoOS_3)^{2-}$ [20] and $(MoO_3S)^{2-}$ [21]. Selenometallates tend to be far more air sensitive than thiometallates and are thus of less interest in the synthesis of new pigments.

Table 4.2 Thio- and Seleno- Metallates Colours

Anion	Colour
$(VS_4)^{3-}$	red/violet
$(VSe_4)^{3-}$	violet
$(NbS_4)^{3-}$	red/brown
$(TaSe_4)^{3-}$	brown
$(MoS_4)^{2-}$	red
$(MoSe_4)^{2-}$	blue/violet
$(WS_4)^{2-}$	yellow

The vanadium, niobium and tantalum chalcogenometallates are all trivalent and are not as potentially useful in sodalite synthesis as their divalent analogues. Although the entrapment of a trivalent ion has been reported by Barrer [4] the results are unsubstantiated, and there have been no subsequent reports of sodalite synthesis using trivalent anions. In particular the thiomolybdates and thiotungstates which are stable in base and display colours ranging from yellow to red depending on the sulphur content, may be suitable for entrapment. Thiotungstates require far more extensive treatment with H_2S than do thiomolybdates [22], and so thiomolybdates were chosen for an in-depth study as potential replacements for the cadmium yellows and reds.

The thiomolybdates $(MoO_{4-x}S_x)^{2-}$, where x=1-4, were synthesised using the methods described by Laurie *et al.* [16] and McDonald *et al.* [22]. The reaction of hydrogen sulphide with molybdates is consecutive:

$$(MoO_4)^{2-} \rightarrow (MoO_3S)^{2-} \rightarrow (MoO_2S_2)^{2-} \rightarrow (MoOS_3)^{2-} \rightarrow (MoS_4)^{2-}$$

The difficulty is to stop the reaction at the desired stage and selectively obtain the required product. The thiomolybdates can be prepared directly from sodium molybdate [23], but all of the series are readily soluble and so the distinction of products is only possible by means of *in situ* spectroscopic studies, and contamination of one particular product by another member of the series is common. The syntheses via the ammonium salts avoids this problem by utilising the different solubilities in ammonia. In the case of the tetrathiomolybdate the synthesis follows closely that of Kruss [19] reported in the nineteenth century. McDonald *et al.* [22] recommended heating to 50-60 °C during the H_2S treatment, but since the reaction is exothermic this was not necessary. The product, obtained as the 3.5 hydrate, is extremely water soluble and must be stored over a desiccant to avoid slow decomposition to MoS_2. This is the case with all of the sodium thiomolybdates which display limited stability in air. In each case the ammonium salt was prepared first, with subsequent conversion to the sodium analogue by dissolution in NaOH. This allows the separation of the different members of the series as a function of their varying solubilities in ammonia.

4.4.1 Synthesis of $(NH_4)_2MoS_4$

Ammonium paramolybdate, ($(NH_4)_6Mo_7O_{24}.4H_2O$, 10 g) was dissolved in a mixture of distilled water (30 ml) and ammonia (100 ml, specific gravity 0.88). H_2S was bubbled rapidly through the solution for approximately 30 minutes, and the solution cooled to 0 °C. Red crystals of the product deposited on cooling and were isolated by filtration, washed with ethanol and dried in vacuo.

4.4.2 Synthesis of $(NH_4)_2MoOS_3$

Na_2MoO_4 (8.0 g) was dissolved in a mixture of NH_4OH (30 ml, specific gravity 0.88) and H_2O (18 ml) and the solution cooled in an ice-bath after filtration. H_2S was passed rapidly over the surface of the solution, causing the precipitation of $(NH_4)_2(MoO_2S_2)$. The

delivery tube must not be immersed in the solution as this will favour the formation of the tetrathio salt. The gas flow was continued until the majority of the precipitate had redissolved, and the reaction mixture was then filtered into ice-cold ethanol (700 ml). The solid product was collected by filtration, washed with EtOH and Et_2O and dried in vacuo.

4.4.3 Synthesis of $(NH_4)_2MoO_2S_2$

$(NH_4)_6Mo_7O_{24}.4H_2O$ (10 g) was dissolved in a mixture of NH_4OH (25 ml, specific gravity 0.88) and H_2O (15 ml) and the solution cooled in an ice-bath after filtration. H_2S was passed slowly over the surface of the solution causing the precipitation of the required product. To maximise the yield, the flow of H_2S from the reaction flask was monitored and when it significantly increased, the H_2S was halted. After a further 5 minutes at 0 °C, the product was filtered, washed with EtOH and Et_2O and dried in vacuo.

4.4.4 Synthesis of $(NH_4)_2MoO_3S$

$(NH_4)_6Mo_7O_{24}.4H_2O$ (10 g) was dissolved in a mixture of NH_4OH (25 ml, specific gravity 0.88) and H_2O (15 ml) and the solution cooled in an ice-bath after filtration. H_2S was passed slowly over the surface of the solution causing the precipitation of the orange $(NH_4)_2MoO_2S_2$. At the first sign of precipitation, the flow of gas was halted. The solution was filtered into ice cold EtOH and the precipitated solid was isolated by filtration, washed with EtOH and Et_2O and dried in vacuo.

4.4.5 Formation of $Na_2(MoO_{4-x}S_x)^{2-}$

$(NH_4)_2MoS_4$ (10 g) was dissolved in ice-cold aqueous NaOH (1.7 g, 20 ml). The resultant H_2O and NH_3 were removed by rotary evaporation and then vacuum pumping. The red solid was dissolved in acetone (120 ml) and the solution filtered. Diethylether (300 ml) was added to the filtrate causing the precipitation of the product, which was filtered, washed with ether (3 x 20 ml) and then dried in vacuo. In each case, the ammonium salts were converted to their sodium analogues by dissolution in aqueous NaOH, as outlined for the tetrathiomolybdate. The reaction is as:

$$(NH_4)_2MoS_4 + 2NaOH \rightarrow Na_2MoS_4 + 2H_2O + 2NH_3$$

The infra-red band at 480 cm^{-1} was assigned to ν_1(Mo-S,) with the bands at 1650 and 3450 cm^{-1} attributed to the H_2O present. The lack of Mo-O bands at approximately 865 cm^{-1} for the tetrathiomolybdate also indicated that the complete replacement of O by S had taken place. The powder X-ray diffraction pattern taken over the range 10-60 ° showed excellent agreement with that reported by Laurie *et al.* [16]. The thermogravimetric and differential thermal analyses traces show loss of the associated water up to 100 °C followed by decomposition at 210 °C. The thermal stability in N_2 rather than air shows no significant improvement. This contrasts with the dithiomolybdate, for which decomposition in air is observed at 200 °C whereas under N_2 it is stable to 420 °C. The thermal stability of thiomolybdates under H_2S has been studied by Konings *et al.* [24] and shows that it is no greater than under N_2. The extra stability of the dithiomolybdate under N_2 could possibly be utilised for structure conversion: sodium chromate sodalite has been synthesised at 400 °C [25] showing that structure conversion can take place at relatively low temperatures. However, synthesis of the parent molybdate sodalite from 4A at 400 °C was not successful, with the 4A starting material remaining unreacted.

4.4.6 Entrapment of Thiomolybdates Within Sodalites

For each of the thiomolybdates prepared as above, the Hund method was used in an attempt to incorporate the anions within an aluminosilicate framework. In each case, on washing with distilled water, white products were obtained showing that none of the series had been enclathrated in the framework. In each case the powder products were a mixture of aluminosilicates, with the major phase being analcime, $Na(Si_2Al)O_6.H_2O$. There was no observed decomposition of the products during these reactions and therefore the failure to entrap the thiomolybdate anions can be attributed to size constraints of the sodalite cage.

Since the aluminosilicate beta cage has been demonstrated to be too small to accommodate anions of the thiomolybdate series their enclathration within sodalites containing gallium and germanium was attempted. Previous synthetic studies, outlined in Chapter Three, had shown that divalent anions could not be incorporated into gallogermanate sodalites; aluminogermanate cages were therefore the largest in which divalents could be successfully entrapped. The syntheses of materials with general formula $Na_8[AlGeO_4]_6(MoO_{4-x}S_x)$ were therefore attempted. The appropriate sodium salt was mixed with stoichiometric amounts of $NaAlO_2$ and Na_2GeO_3, 10 mls of 4M NaOH solution, and transferred to a Teflon lined autoclave. Reaction times between 24 and 72 hours and

temperatures in the range 120 - 180 °C were investigated. In each case, the thiomolybdate salt was washed free leaving a white aluminogermanate hydroxide sodalite as the product. Once again, no decomposition was observed and it was therefore concluded that the aluminogermanate cage was not of sufficient volume to permit enclathration of thiomolybdate anions.

4.4.7 High Temperature Hydrogen Sulphide Reactions

Following the failure to entrap the thiomolybdates in aluminosilicate sodalites using direct solution methods, an indirect method via secondary synthetic treatment of molybdate noselite with hydrogen sulphide was examined. High temperature reactions using H_2S have proved a useful route for the introduction of sulphur into sodalites in the synthesis of ultramarines [1], in which $Na_8(AlSiO_4)_6.Cl_2$ is heated under H_2S at 900 °C for 2 hours, totally replacing the Cl by S, which is then oxidised to form S_n^- ions within the framework. Analogous reactions in which the one or more of the oxygens of the molybdate group are replaced by S were therefore attempted. 0.25 g of molybdate noselite, $Na_8[AlSiO_4]_6.MoO_4$, in an alumina boat was placed in a tube furnace and the system flushed with nitrogen at ambient temperature for 30 minutes. H_2S was then passed over the sample under heating to the reaction temperature, for 1 hr at the reaction temperature, and during cooling back to room temperature. Experiments were performed at 50 °C intervals in the range 650 - 950 °C: at temperatures up to and including 900 °C the parent sodalite was unchanged, whereas at 950 °C decomposition to nepheline, $NaAlSiO_4$, was observed. Analogous reactions using $Na_8[AlGeO_4]_6.MoO_4$ were equally unsuccessful.

For each of the products obtained using the high temperature reaction with H_2S method, there was a darkening of the colour of the product compared with the white starting material. This became increasingly apparent as the temperature was increased. It was thought that this was due to the formation of molybdenum trisulphide from bulk sodium molybdate on the surface of the sodalite, since it has been reported that reaction of Na_2MoO_4 and H_2S yields MoS_3 [26].

4.5 THIOCYANATE SYSTEMS

Ultramarines are widely used in industry as pigments and dyes, but they are synthesised on a large scale using high temperatures and rather lengthy reaction times [27]. Their synthesis using less drastic conditions is therefore of considerable interest: such a route is the entrapment of thiocyanate anions within the sodalite beta cage. The thermolysis product of these sodalites is the sulphur containing ultramarine, $Na_8[AlSiO_4]_6.(S_n)_2$, where n = 2-4. The synthesis of thiocyanate containing sodalites has been investigated using the solution methods of Hund [3] and Barrer [4], in addition to hydrothermal reactions. Since these anions are linear, they do not promote sodalite formation particularly well, and a major problem is enclathration of the hydroxide anion which is necessary to prevent decomposition of the thiocyanate anion during the course of the experiment. A range of synthetic conditions have therefore been studied in order to optimise the incorporation of the desired anion. The synthesis of framework modified sodalites containing the thiocyanate anion has also been investigated in order to examine the change in colour associated with the sulphur radicals as a consequence of framework substitution. Their hydrothermal preparation involves the use of the minimum amount of base possible in order to stabilise the thiocyanate anion whilst avoiding the problem of preferential hydroxide entrapment due to the presence of a large excess of $(OH)^-$. This corresponds to 5 mls 1 M NaOH solution, 15g of NaSCN with 0.91 g $NaAlO_2$/1.39 g $NaGaO_2$ and 2.36 g $Na_2SiO_3.5H_2O$/1.85 g Na_2GeO_3, which allows the $(SCN)^-$ to be entrapped with no signs of hydroxide anions within the beta cages. If insufficient NaOH is present then the thiocyanate is not entrapped at all and hydrosodalite is the product obtained. Too large an excess of NaOH simply leads to obtention of hydroxide sodalites since the hydroxide anion has been experimentally shown to be particularly suited to sodalite formation.

Following the successful preparation of thiocyanate sodalites, investigation of the heat treatments required to produce ultramarine was undertaken This involved heating at different temperatures for varying lengths of times, in addition to examining the effects of heating the sodalite under different atmospheres. These particular thermal conditions and the products obtained are described in detail in Chaper Six. The basic intra-cage reaction corresponds to an initial thermal degradation of the thiocyanate anion, followed by oxidation of the sulphur to forms radicals of the form $(S_n)^-$ with subsequent expulsion of the N and C components as gaseous products. The degree of oxidation of the sulphur, and hence the

colour obtained, is governed by the heat treatment involved, with ultimate conversion to $(SO_4)^{2-}$ as the oxidation is completed.

4.6 SELENOCYANATE SODALITE

Sodium thiocyanate is widely obtainable, whereas the selenocyanate is commercially available as the potassium analogue. Ion exchange prior to use must therefore be undertaken, since the sodium form must be used if sodalite is to be formed. 25 g of KSeCN was dissolved in 25 mls H_2O and passed through an ion exchange column containing Amberlite 120 Na resin using nitrogen gas to increase the flow of solution through the column. The column was then washed through with 100 mls H_2O to ensure that all of the $(SeCN)^-$ had been collected. The column was subsequently regenerated using NaCl solution and washed thoroughly with H_2O: the washings were tested with $AgNO_3$ which precipitates any chloride anions as AgCl. the washing process was continued until there was no evidence of AgCl. The ion exchange process was repeated three times to ensure complete exchange of potassium by sodium had taken place.

The resultant selenocyanate solution was then rotary evaporated to yield a buff coloured solid. This was then transferred to a Teflon lined autoclave (Parr 4347) containing stoichiometric amounts of the framework precursors $NaAlO_2$ and Na_2GeO_3, in addition to 5 mls of 2 M NaOH solution. The hydroxide solution was present in an attempt to stabilise the $(SeCN)^-$ anion in the same way as had been seen for the $(SCN)^-$ anion. Attempted entrapment of this ion in an aluminosilicate sodalite simply led to the formation of hydroxide sodalite, with the failure to enclathrate $(SeCN)^-$ attributed to size constraints of the aluminosilicate beta cage. The aluminogermanate framework was hence selected as it provides the best chance of entrapment, since it forms easily and allows the enclathration of a large range of anions, in addition to being somewhat larger than its aluminosilicate or gallosilicate equivalents. Reaction temperatures between 90 and 180 °C all lead to the formation of $Na_8[AlGeO_4]_6(OH)_{2-x}(Se_n)_x$, where x tends to be approximately 0.2. In an exactly analogous manner to the thiocyanate anion, thermal treatment yields a sodalite containing the $(Se_n)^-$ species. Since the level of Se in the cage is small, the colour obtained does not reach the blood red which would correspond to $Na_8[AlGeO_4]_6$ $(Se_n)_2$, although orange can be easily obtained. In order to increase the amount of $(SeCN)^-$ in the sodalite it would appear that an even larger cage is required such as that provided by gallogermanates. However, at this time synthetic methods allow only very few anions to be successfully incorporated within gallogermanate framework sodalites.

4.7 THIOSULPHATE SYSTEMS

An alternative route to ultramarines is via the enclathration of the thiosulphate anion $(S_2O_3)^{2-}$. This ion can be entrapped via solution or hydrothermal methods, but the product crystallises with the cancrinite structure [4, 28]. It has been shown previously that certain cancrinites can be thermally converted to sodalites, and it was hoped that this can be achieved for the thiosulphate anion. Ultramarine is produced either by irradiation or thermal treatment of the cancrinite, with the specific nature of the S_n species, and hence the colour, dependent on the temperature and the time of the treatment. It has been shown [28] that irradiation of the sample with X-rays such as CuKα yields a yellow colour and a band is observed in the UV/VIS spectrum at 406 nm characteristic of the $^2\Pi_{1/2u} \leftarrow {}^2\Pi_{3/2g}$ transition of the S_2^- radical. It has been suggested that the formation of these radicals involves cleavage of the S-S bond in the $(S_2O_3)^{2-}$ anion, which is relatively weak in comparison with the bond strength in diatomic molecules, with additional subsequent formation of S^- and SO_3^- fragments. The formation of such radicals can be understood on the basis of the disorder of the thiosulphate group within the cancrinite channels by a cooperative mechanism involving one thiosulphate group with "up" and "down" orientation:

$$O_3S\text{-}S^{2-}\ (up) + S\text{-}SO_3^{2-}\ (down) \rightarrow O_3S^- + S^{2-} + SO_3^{2-}$$

$$O_3S\text{-}S^{2-}\ (up) + O_3S\text{-}S^{2-}\ (up) \rightarrow O_3S^- + S^- + O_3S\text{-}S^{2-}$$

$$\rightarrow O_3S^{2-} + S + O_3S\text{-}S^{2-}$$

The latter case involving only one orientation would mean that a S or S^- fragment would have to pass a $(S_2O_3)^{2-}$ anion or a SO_3^- moiety, which is severely restricted due to steric hindrance. No evidence of the formation of S_3^- via irradiation was observed.

Thermal treatment, however, does permit the formation of both S_2^- and S_3^- species. Heating at 1000 °C in argon or 800 °C in air or oxygen provide similar results. After approximately 30 minutes a green sample is obtained which contains both the S_2^- and S_3^- radicals, with a further 30 minutes yielding the blue shade consisting of S_3^- exclusively within the framework cavities. Such thermal treatment does not convert the cancrinite

framework to sodalite. These results mirror those originally reported by Hund [3]. The formation of S_3^- radicals can be explained by a thermally activated diffusive mechanism which permits the S/S^- fragments to migrate within the open cancrinite channels.

The interest in the thiosulphate anion is caused by the fact that upon thermal degradation or reduction, a sodalite or cancrinite with more sulphur per cage than the thiocyanate analogue would be obtained. It is the aim to synthesise thiosulphate cancrinites and simultaneously convert the anion to the $(S_n)^-$ species and transform the cancrinite to a sodalite framework, giving a sulphur rich sodalite which would consequently possess extremely rich shades. The synthesis of thiosulphate cancrinites with different framework compositions will be detailed in Chapter Six. It could perhaps be envisaged that the different thermal stabilities of the various framework types may allow conversion of cancrinite to sodalite systems. Thermal studies showed how a coloured cancrinite containing sulphur could be achieved but no structural conversion of cancrinite to sodalite was achieved.

In addition to investigating the suitability of $(S_2O_3)^{2-}$ as an ultramarine precursor, the $(S_2O_5)^{2-}$ anion was also studied. Attempted entrapment within an aluminosilicate framework using the Hund or Barrer methods [3, 4] produced only hydroxide sodalite due to the size of the metabisulphite anion. In a similar manner to the selenocyanate anion, it was hoped that the aluminogermanate beta cage would afford the extra volume required to enclathrate $(S_2O_5)^{2-}$; the resultant product could then be heat treated, giving another alternative preparation for ultramarine. $Na_8[AlGeO_4]_6(S_2O_5)$ was prepared but was of extremely poor crystallinity, and as for thiosulphate materials, was not successfully converted to a sodalite.

4.8 CONCLUSIONS

The transition metal oxo-anions provide suitable anions for entrapment within sodalites in the form of $(MnO_4)^-$, $(MnO_4)^{2-}$ and $(CrO_4)^{2-}$, all of which yield intensely coloured materials. It is perhaps the permanganate sodalite which generates the most interest in terms of potential as an industrial pigment, since the manganate compound crystallises with the more open cancrinite structure resulting in diminished thermal stability and hygroscopic tendencies, whilst the regulations concerning chromium severely restrict its use. It has also been shown that the deep red ferrate ion, $(FeO_4)^{2-}$, does not possess the necessary thermal stability for sodalite enclathration and decomposition to Fe_2O_3 even at temperatures as low as 40 °C is observed. The perruthenate and ruthenate anions are equally unsuitable since $(RuO_4)^-$ is thermally unstable and $(RuO_4)^{2-}$ coordinates hydroxyl groups to become octahedrally coordinated, a geometry which does not permit sodalite formation.

The chalcogenometallates, and in particular the anions of the thiomolybdate series, appear suitable for application as sodalite pigments in terms of their intense colours, base stability and sufficient temperature stability to envisage entrapment via solution methods. However, the size constraints of the sodalite beta cage prevent encapsulation, despite the introduction of gallium and germanium in order to create a sodalite with increased cell volume.

Sodalites containing the $(XCN)^-$ anion, where X represents the chalcogen S or Se, have been successfully prepared and can be simply converted to the respective ultramarine by thermal treatment. The resultant shade of ultramarine may be altered by variation in the particular heat process which controls the level of oxidation of the S/Se within the cages. The aluminogermanate selenocyanate sodalite highlights how the larger cage afforded by the substitution of germanium for silicon can be utilised to incorporate anions which are simply too voluminous to be encapsulated within aluminosilicates. Although the level of selenium entrapped is relatively low due to the bulk of the selenocyanate, the orange colour obtained does provide alternatives to the cadmium sulphoselenides. This route to ultramarines also avoids the use of the lengthy process used to synthesise ultramarine directly involving high temperatures in the order of 500 °C and above.

Alternative precursors to ultramarines are frameworks containing $(S_2O_3)^{2-}$ or $(S_2O_5)^{2-}$. In an analogous manner to the thio- and selenocyanate sodalites, intra-cage thermal degradation leads to the formation of polysulphide radicals responsible for the

colouration. The divalent anions produce the cancrinite structure which is not converted to sodalite by thermal treatment: it was hoped that the cancrinites could be restructured to form the more condensed sodalite either at the same time as the original anion is decomposed, or by subsequent heating once the sulphur radicals had been produced. This transformation was not observed with the cancrinite retaining its structure until the temperature is raised above 800 °C causing complete collapse of the framework. In a similar way to the selenocyanate anion, metabisulphate, $(S_2O_5)^{2-}$, is able to be encaged via introduction of germanium instead of aluminium. The resultant cancrinite has properties similar to the $(S_2O_3)^{2-}$, and hence can be converted to an ultramarine analogue by heating.

4.9 REFERENCES

[1] J.S. Prener and R. Ward, *J. Am. Chem. Soc.*, **72**, 2780 (1950).

[2] I.F. Chang, *J. Electrochem. Soc.*, **121**, 815(1974).

[3] F. Hund, *Z. Anorg. Allg. Chem.*, **511**, 225 (1984).

[4] R.M. Barrer, J.F. Cole, and H. Sticher, *J. Chem. Soc.*, A**10**, 2475 (1968).

[5] G. Wong, *Ph.D. Thesis*, University of Southampton (1990).

[6] M.T. Weller and K.E. Haworth, *J. Chem. Soc., Chem. Commun.*, **10**, 373 (1991).

[7] H. Bock and D. Jaculi, *Angew. Chem. Int. Ed. Engl.*, **23**, 305 (1984).

[8] R.J.H. Clark, *Inorg. Chem.*, **24**, 2088 (1985).

[9] M.E. Brenchley, *Ph.D. Thesis*, University of Southampton (1994).

[10] J.L. Guth, M. Bourdeaux and R. Wey, German Patent, 2120645 71118 (1987).

[11] F.A. Cotton and G. Wilkinson, "Advanced Inorganic Chemistry", Fifth Edition, Wiley-Interscience, New York (1988).

[12] R. Olazcuaga, *Rev. Chim. Mineral.*, **13**, 9 (1976).

[13] R.J. Audette and J.W. Quail, *Inorg. Chem.*, **11**, 1904 (1972).

[14] E. Ahlborn, E. Diemann and A. Muller, *J. Chem. Soc. Chem. Commun.*, 378 (1972)

[15] C. Crevecoeur, *Acta Cryst.*, **17**, 757 (1964).

[16] S.H. Laurie, C.E. Pratt and J.H.L. Yong, *Inorg. Chim. Acta*, **93**, L57 (1984).

[17] J.J. Berzelius, *Poggendorffs Ann. Phys. Chem.*, **7**, 262 (1826).

[18] J.J. Berzelius, *Poggendorffs Ann. Phys. Chem.*, **8**, 269 (1826).

[19] G. Kruss and K. Ohnmais, *Ber. Dtsch. Chem. Ges.*, **23**, 2547 (1890).

[20] A. Muller, E. Diemann and U. Heidborn, *Z. Anorg. Allg. Chem.*, **371**, 136 (1969).

[21] A. Muller, H. Dornfeld, H. Schulze and R.C. Sharma, *Z. Anorg. Allg. Chem.*, **468**, 193 (1980).

[22] J.W. McDonald, G.D. Friesen, L.D. Rosenheim and W.E. Newton, *Inorg. Chim. Acta*, **72**, 205 (1983).

[23] C.A. Kelleher and J. Mason, *Int. J. Biochem.*, **18(7)**, 629 (1986).

[24] A.J.A. Konings, A. Valstar, V.H.J. de Beer and R. Prins, *J. Catal.*, **76**, 473 (1982).

[25] P.J. Mead, *Personal Communication*, University of Southampton (1995).

[26] A. Muller, E. Diemann R. Jostes and H. Bogge, *Angew. Chem. Int. Ed. Engl.*, **20**, 934 (1981).

[27] G. Buxbaum (ed.), "Industrial Inorganic Pigments", VCH, Weinheim, Federal Republic of Germany (1993).

[28] G.G. Lindner, W. Massa and D. Reinen, *J. Solid State Chem.*, **117**, 386 (1995).

Chapter Five

CHARACTERISATION OF HALIDE SODALITES

5.1 INTRODUCTION

The structural properties of the sodalites synthesised in the current work have been investigated by powder x-ray diffraction. Initial determination of phase composition, sample purity and cell size were performed over the 2θ range 20-60 ° with a 20 minute run time. More detailed examination over the 2θ range 20-120 ° with an acquisition time of 900 minutes was performed using the Rietveld method. This allows the accurate determination of structural parameters such as cell parameter and framework bond angles. Selected samples have additionally been examined by powder neutron diffraction, which has the ability to locate light atoms more precisely than is possible using x-rays as the radiation source. This is particularly valuable for the framework oxygen atoms, those samples for which lithium has been exchanged for sodium as the non-framework cation, and the distinction of framework cations such as Al and Si which are adjacent to one another in the periodic table. These can be difficult to fix with a high degree of certainty using powder x-ray data alone.

In addition to determining the exact stoichiometry of individual samples, the derived structural data allows certain trends to be studied. For a particular framework composition, the effect of enclathrating different anions within the sodalite beta cage can be examined. As the size of the central anion increases the manner in which the framework is adapted to maintain chemically sensible bond distances is able to be determined. It has been reported [1, 2] that most of the framework expansion which is required as the anion size increases is principally accommodated by tetrahedral tilting and variation in the T-O-T framework bond angle, which is in turn controlled by the position of the framework oxygen atoms. The accurate location of these oxygen atoms is thus vital, and highlights the need for neutron diffraction.

For a particular entrapped anion, it is also interesting to compare how the structural properties of frameworks of various composition differ from each other. This can be simply monitored by examining the structural parameters derived for aluminosilicate, gallosilicate, aluminogermanate and gallogermanate halide sodalites. The effect of ion exchange on their properties is also examined.

For the sodalites of varying composition studied in this work, the main trends to be examined are the following:

i) to what extent does the framework expand upon introducing larger anions;

ii) how does the framework T-O-T angle change with cell size;

iii) does the intra-framework tetrahedral angle, O-T-O, deviate significantly from the ideal value of 109.48 °;

iv) for a particular framework composition, are framework T-O distances constant as the anion is changed;

v) similarly, do the Na-O and Na-X, where X is the entrapped anion, deviate significantly as the framework composition changes, and is there a noticeable trend in the manner in which such deviations, if any, occur.

This chapter details the individual structural refinements of halide containing sodalites and compares how the framework type affect the resultant structural parameters. A general review of the sodalite structure is given in Chapter Eight, in which information regarding sodalites containing a much wider range of anions has been collated to give a more complete picture of the factors governing sodalite structural chemistry.

5.2 SODIUM SODALITES

The halide series of sodalites provide an ideal system for the study of sodalite composition: these extremely simple enclathrated anions reside at the centre of the beta cage and thus do not complicate the study of how the framework changes with composition. The structure is shown in Figure 5.1 The effect on the framework, in addition to non-framework cations, can be easily studied both as a function of halide for a given framework composition and as a function of framework components for a given halide anion. Due to their simplicity, the halide series of sodalites allow structural data to be easily extracted from powder diffraction measurements and can give reliable indications on how more complex zeolitic species will be altered by framework doping, particularly when these diffraction data are allied to spectroscopic information such as MASNMR chemical shift values. Correlations relating structural parameters with spectroscopic results will be dealt with in detail in Chapter Seven.

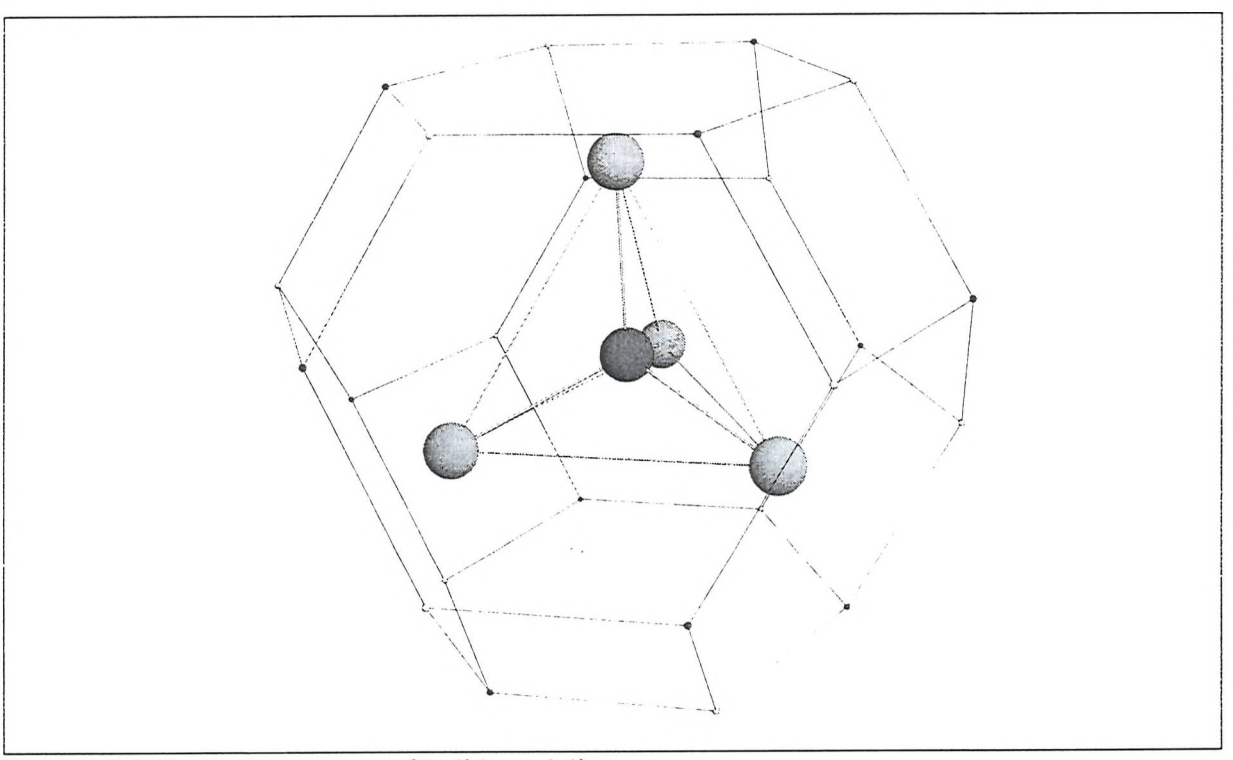

Figure 5.1 General structure of halide sodalites.

All of the halide series, $Na_8[ABO_4].X_2$, where A = Al and Ga, B = Si and Ge, and X = Cl, Br and I, were synthesised by hydrothermal methods described in Chapter Three. The aluminogermanates and gallogermanates were prepared using the precursor Na_2GeO_3 in conjunction with $NaAlO_2$ and $NaGaO_2$ as appropriate. The gallosilicates were

prepared using a modified version of the method reported by Newsam [3], in which $NaGaO_2$ was hydrothermally reacted with an aqueous solution containing a stoichiometric amount of SiO_2 and an excess of the sodium salt to be entrapped. All powder samples were examined by neutron diffraction on the POLARIS instrument at ISIS, at d-spacings between 0.67 and 3.08 Å, except $Na_8[GaGeO_4].I_2$ for which data were collected on D2B at ILL, Grenoble. Run times on POLARIS were approximately 2 hours and D2B acquisition time was 4 hours. All materials were refined using the GSAS Powder Diffraction Suite of Larson and Von Dreele [4]. All peaks in the PXD pattern could be indexed using a primitive lattice indicating the space group $P\bar{4}3n$ consistent with their aluminosilicate sodalite analogues. Aluminium or gallium and silicon or germanium were placed on the 6(c) (¼, ½, 0) and 6(d) (¼, 0, ½) sites respectively, the halide on the 2(a) (0, 0, 0), sodium on the 8(e) (x, x, x) site with $x \approx 0.18$ and the framework oxygen, O(1), on the 24(i) (x, y, z) site with $x \approx 0.14$, $y \approx 0.15$, $z \approx 0.45$.

5.2.1 T.o.f. PND/PXD study of Gallosilicate Sodalites

Relatively few examples of full gallium substitution for aluminium in the sodalite structure exist in the literature. In 1961 Selbin and Mason [5] reported the syntheses of several gallium containing molecular sieves, including one possessing the sodalite structure. This was not structurally characterised to any great degree, with the only significant difference observed from the aluminium analogue being an increase in intensity of the diffraction line at 28.2 °, 2θ. However, since they did not observe an increase in cell parameter associated with the introduction of gallium, it is debatable whether the introduction of a significant level of Ga for Al was achieved; indeed, it would seem likely that dissolution into the reaction medium of the vessel constituents by the sodium hydroxide present and their subsequent incorporation into the sodalite framework occurred. This also appears to be the case in the work reported by Schipper *et al.* [6]. The results of McCusker *et al.* [7] and Newsam [3] do indicate full gallium substitution in the hydroxide and chloride sodalite systems respectively and, in agreement with the results obtained in this work, the materials crystallise in the cubic space group $P\bar{4}3n$. The method of Newsam was that on which the gallosilicate syntheses were based, with the gallium source changed from Ga_2O_3 to $NaGaO_2$.

The starting model for each of the gallosilicate halide sodalites was the aluminosilicate halide analogues [1]: these give a good initial model for the structures which facilitates the Rietveld process. Scale factor and background parameters were then introduced, followed by lattice parameters, zero point correction and sample displacement thus pinpointing reflection positions. Atomic positions were next incorporated to generate peak intensities, initially of the framework species followed by non-framework ions; variation of isotropic thermal parameters accounts for atomic vibrations and peak shape parameters for sample broadening.

The final refinement parameters for the gallosilicate halides are shown in Table 5.1, and derived bond distances and angles are given below in Table 5.2.

Table 5.1 Final refinement parameters, atomic positions and thermal parameters ($Å^2$) with estimated errors in parentheses from powder neutron diffraction data for sodium gallosilicate halide sodalites

		$Na_8[GaSiO_4]_6.X_2$		
		Cl	Br	I
a(Å)		8.9603(6)	9.0000(3)	9.0742(3)
R_{wp}/R_{exp}		3.18/1.88	4.40/2.76	3.71/2.10
Ga	B	1.49(2)	0.89(5)	0.89(3)
Si	B	1.51(3)	0.25(5)	0.68(5)
X	B	4.16(5)	3.36(4)	4.22(6)
O	x	0.1354(2)	0.1366(3)	0.1387(1)
	y	0.1498(5)	0.1504(1)	0.1527(2)
	z	0.4283(4)	0.4329(1)	0.4394(1)
	B	2.23(3)	1.47(3)	1.51(3)
Na	x	0.1722(3)	0.1808(3)	0.1936(2)
	B	3.18(1)	3.52(1)	2.21(7)

The chloride and iodide samples refined satisfactorily as would be expected given the simple nature of their structures; a cell parameter of 8.9603 Å for the chloride material is in good agreement with the 8.961 Å reported by Newsam [3]. Refinement of the bromide

sample was less facile, due to the presence of an impurity in the sample, manifested most clearly by a shoulder on the most intense peak, the (2 1 1) located at $2\theta = 24$ °. It is likely that this shoulder is caused by the formation of a gallosilicate hydrosodalite. There are two possibilities in this case: that these two sodalites exist as separate phases i.e. the product is predominantly Na[GaSi]Br with a second phase, Na[GaSi]H_2O, present as an impurity; secondly, that the bulk sample is a sodalite containing both bromide anions and water molecules, and that these two species are unhomogeneously distributed between the beta cages within the material giving rise to rather broad diffraction maxima caused by a distribution of cell parameters. In this latter case, it would be expected that the maximum intensity of the peak would coincide with a cell parameter corresponding to an average sodalite in which the beta cage is not occupied solely by water molecules or bromide ions but a mixture of the two. The cell parameter therefore would not be that corresponding to full occupancy of the beta cages by bromide ions.

Table 5.2 Selected derived framework bond distances (Å) and angles (°) from powder neutron diffraction data for sodium gallosilicate sodalites at 298 K with estimated errors in parentheses.

	Multiplicity	Cl	Br	I
Ga-O	4	1.800(4)	1.819(2)	1.802(1)
Si-O	4	1.634(2)	1.595(7)	1.630(1)
Na-O	3	2.318(3)	2.333(2)	2.317(2)
Na-A	1	2.662(3)	2.841(2)	3.094(1)
O-Ga-O	4	108.81(9)	108.56(8)	108.39(5)
O-Ga-O	2	110.80(9)	111.31(2)	111.66(9)
O-Si-O	4	107.43(5)	107.31(9)	107.03(5)
O-Si-O	2	113.64(9)	114.00(2)	114.47(11)
Ga Tilt		25.6(1)	24.0(1)	21.7(1)
Si Tilt		27.9(1)	26.2(2)	23.(1)
Ga-O-Si		133.43(8)	137.24(6)	138.37(9)
O-Na-O	3	102.27(8)	107.13(7)	109.20(8)
O-Na-A	3	115.96(4)	111.72(12)	109.74(8)

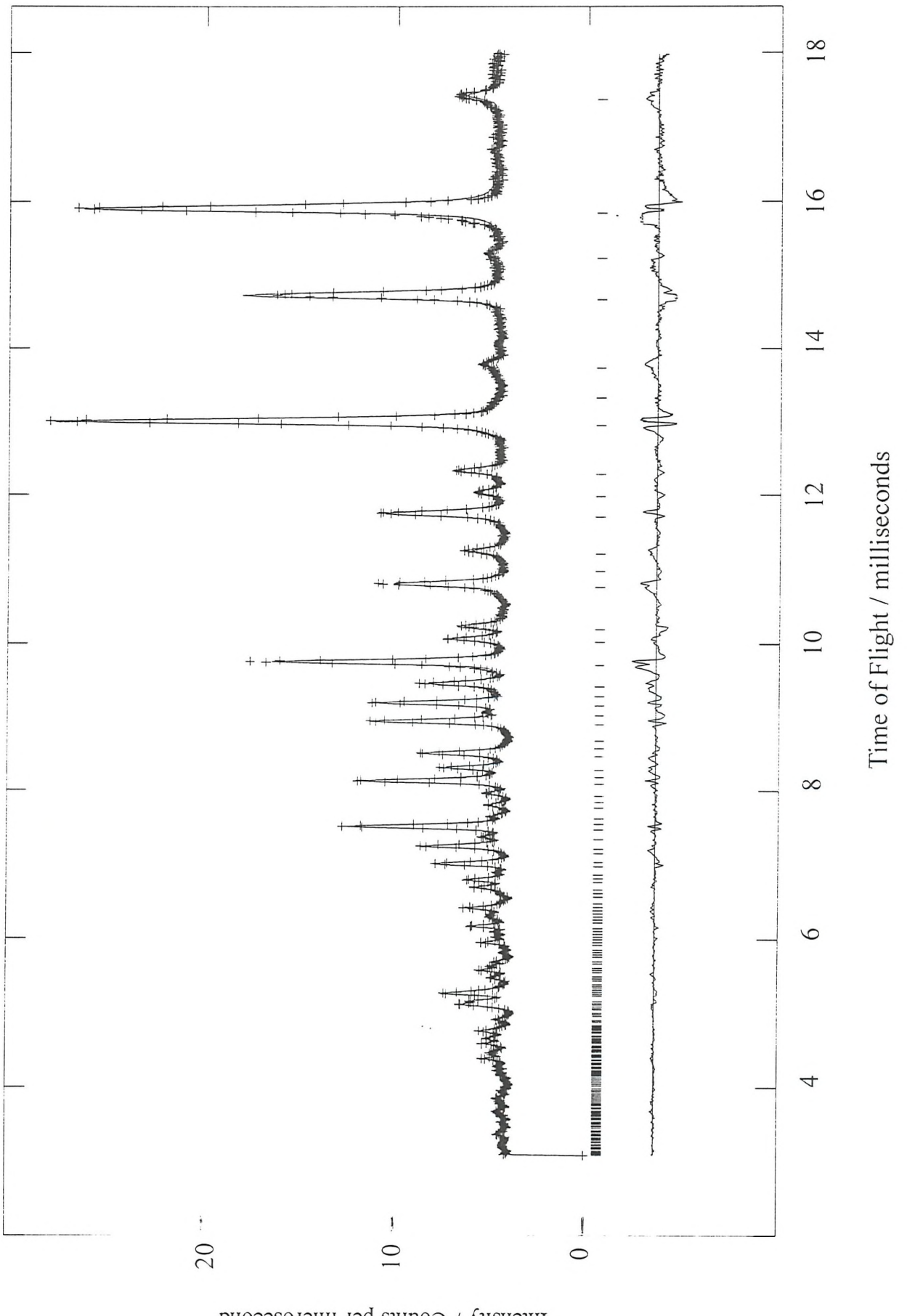

Figure 5.2 298 K T.o.f. PND fit for $Na_8[GaSiO_4]_6.Cl_2$

However, examination of the sample shows that the shoulder occurs to one side of the peak only, and it would therefore seem likely that this is caused by a second phase whose diffraction maxima happen to partially overlap with the bromide containing majority phase. The reason for the inclusion of a higher level of water in the bromide sample compared with the chloride and iodide samples synthesised under the same conditions is unclear; a possible explanation is a slight variation in water content of the reaction medium. It would appear logical that augmenting the level of water in the reagents would promote hydrosodalite formation to a greater degree; there is of course an optimum water stoichiometry - too much water will lead to entrapment of water in preference to the desired anion, whereas too small a quantity means that the reaction approaches that akin to the solid state, which has not proven successful for the synthesis of framework substituted sodalites. Despite the hydrosodalite impurity, the refinement still yields results which are in line with the chloride and iodide samples. Attempted modelling of the hydrosodalite impurity as a second phase in the bromide material did not prove successful, despite using the results of Nenoff *et al.* [8] in their investigation of the $Na_3[ABO_4]_3.4H_2O$ system. This may have been caused by a different water content in the impurity compared with their material which was synthesised under significantly different experimental conditions, outlined in Chapter Three. A second reason could be that, despite the ability of neutron diffraction to locate light atoms, the positions of hydrogen atoms are extremely difficult to pinpoint.

Upon examination of the data several trends are apparent. As expected, the unit cell expands as the halide size is increased. This cell expansion is accompanied by increase of the framework Ga-O-Si bond angle, and a decrease in the tetrahedral tilt angles: this is in accordance with previous studies which have also shown that cell contraction is accommodated by cooperative rotations of the TO_4 tetrahedra manifested by increasingly large tetrahedral tilting and decrease in framework T-O-T bond angle. As the halide is changed from chloride to bromide to iodide, the O-Ga-O (x4) intra-tetrahedral bond angle decreases whereas the O-Ga-O (x2) angle increases, with the same trend existing for the Si angles. This same change in halide size is also accompanied by smooth changes in the O-Na-O and O-Na-A angles which increase and decrease respectively, so that it is the gallosilicate iodide sodalite which displays the least deviation from the ideal tetrahedral angle of 109.48 °.

Table 5.3 Final refinement parameters, atomic positions and thermal parameters ($Å^2$) with estimated errors in parentheses from powder x-ray diffraction data for sodium gallosilicate halide sodalites

		$Na_8[GaSiO_4]_6.X_2$		
		Cl	Br	I
a(Å)		8.9600(6)	8.9997(3)	9.0857(6)
R_{wp}/R_{exp}		3.18/1.88	4.40/2.76	3.71/2.10
Ga	B	1.37(3)	1.42(5)	2.56(9)
Si	B	1.14(5)	1.19(8)	0.85(7)
X	B	3.67(9)	3.62(9)	4.61(9)
O	x	0.1347(3)	0.1356(5)	0.1366(11)
	y	0.1510(3)	0.1537(5)	0.1575(12)
	z	0.4282(4)	0.4313(5)	0.4386(11)
	B	1.97(9)	0.97(6)	1.48(8)
Na	x	0.1729(3)	0.1802(4)	0.1937(7)
	B	2.53(9)	2.47(9)	2.50(4)

Although it has been reported that there is a shortening of the T-O bond as the cell expands and the T-O-T angle becomes more linear [1, 2], this is not evident with these data; the data set is too small to allow any firm trend to be proposed since the changes would be small. This will be discussed for a large data range in Chapter Eight.

Synthetic studies following the data collection revealed a strong influence of the silicon source on the resultant material; products far superior in crystallinity and purity could be obtained using Na_2SiO_3 instead of SiO_2, a more reactive framework precursor. However, this information was not available at the time of neutron data collection, and as such the products studied were not of the optimum quality. Thus for the gallosilicate products, the materials were resynthesised at a later date using the improved synthetic conditions and refined from powder x-ray data collected over the 2θ range 20-120 ° with a step size of 0.02 °.

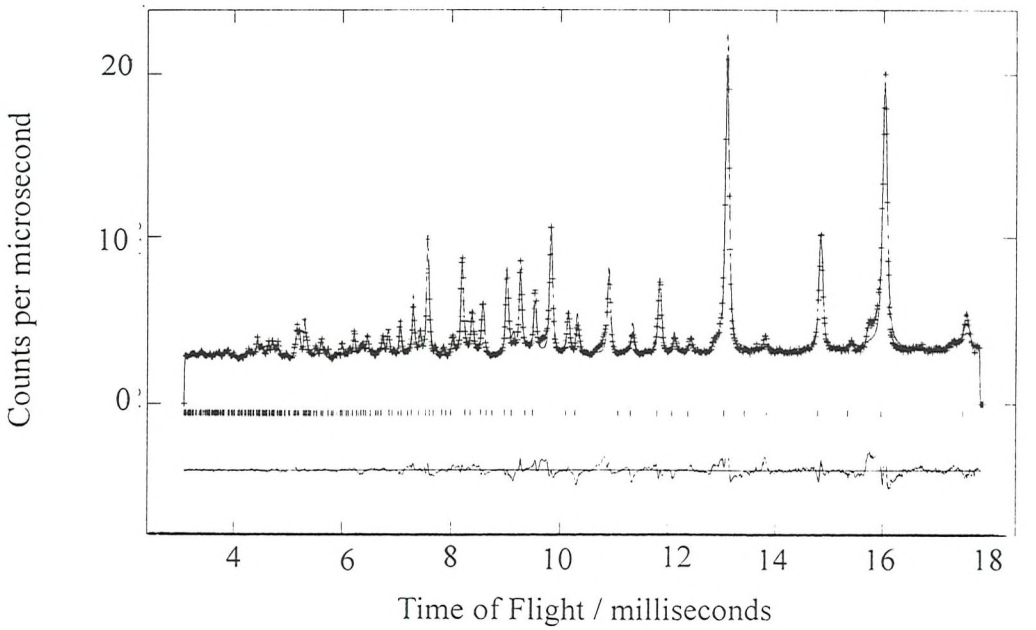

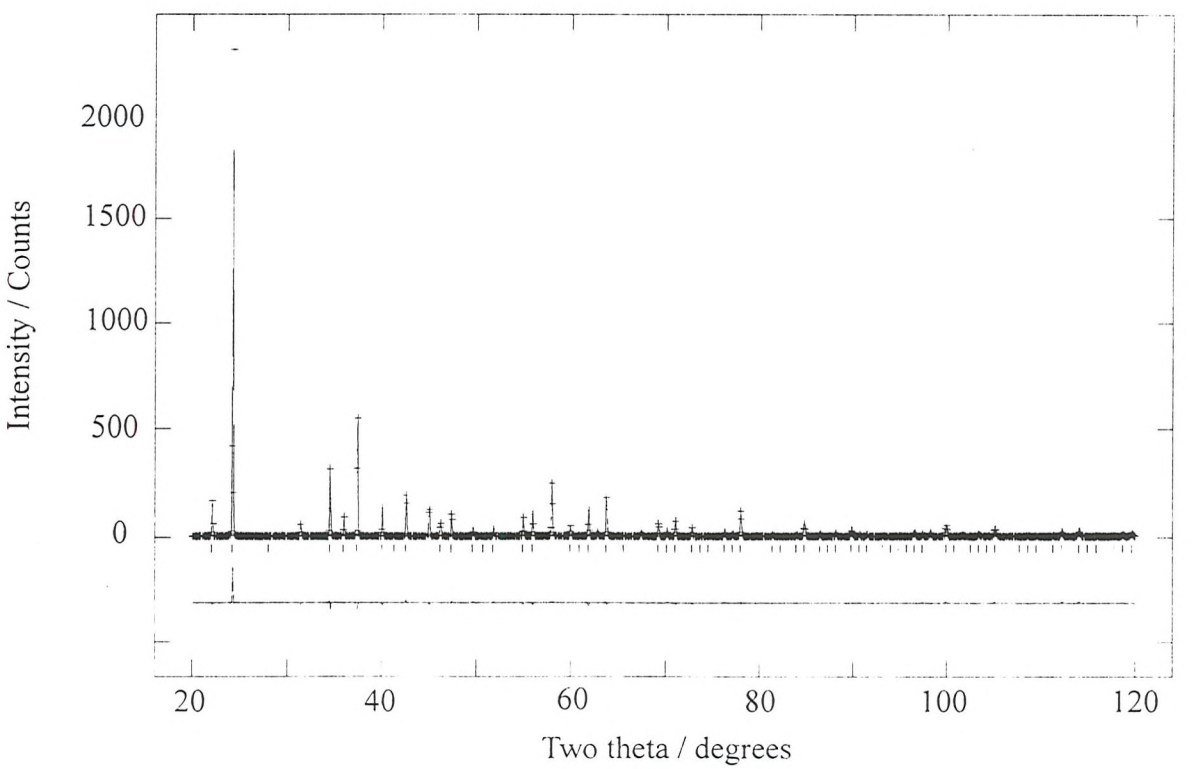

Figure 5.3 T.o.f. PND fit (top) and PXD fit (bottom) at 298 K for $Na_8[GaSiO_4]_6.Br_2$

Table 5.4 Selected derived framework bond distances (Å) and angles (°) from powder x-ray diffraction data for sodium gallosilicate sodalites at 298 K with estimated errors in parentheses.

	Multiplicity	Cl	Br	I
Ga-O	4	1.817(3)	1.835(30)	1.849(2)
Si-O	4	1.628(3)	1.610(3)	1.599(1)
Na-O	3	2.317(4)	2.328(5)	2.309(2)
Na-A	1	2.679(4)	2.783(5)	3.048(2)
O-Ga-O	4	108.81(9)	108.33(8)	108.10(1)
O-Ga-O	2	110.80(9)	111.78(9)	112.26(1)
O-Si-O	4	107.23(9)	106.45(6)	106.05(1)
O-Si-O	2	114.04(9)	115.70(9)	116.56(1)
Ga Tilt		25.4(1)	24.1(1)	21.3(1)
Si Tilt		28.1(1)	26.9(1)	24.2(1)
Ga-O-Si		133.3(2)	134.8(2)	137.2(1)
O-Na-O	3	102.5(2)	103.8(2)	108.8(1)
O-Na-A	3	115.8(1)	114.7(3)	110.2(1)

Refined structural parameters are summarised in Tables 5.3 and 5.4 above. A comparison of the data sets for these compounds does indeed show the superior nature of the materials synthesised using Na_2SiO_3 as the silicon source. This is highlighted by examination of the region surrounding the most intense (2 1 1) reflection, where the appearance of hydrosodalite is most easily observed. The $Na_8[GaSiO_4].Br_2$ made with SiO_2 shows an obvious shoulder to lower two theta which can be attributed to hydrosodalite. This does not appear to any significant degree, bearing in mind the detection limit of $\leq 5\%$ of the instrumentation, for the sample prepared using Na_2SiO_3. It should also be borne in mind whilst making comparisons between neutron and x-ray diffraction data that neutron diffraction is far more accurate in determining the location of light atoms like oxygen and as such the values of the derived gallium-oxygen bond lengths would be expected to be more reliable than those yielded by x-rays. The increase in sample quality of samples prepared using this second method is also displayed by other

materials in the series. A comparison of the structural parameters extracted from the data sets is interesting for the gallosilicates.

Whilst the cell parameters of the compounds are extremely similar, the gallium-oxygen bond lengths of the materials prepared from SiO_2 are somewhat shorter than the 1.82 Å expected from ionic radii considerations. This is not the case for those gallosilicates synthesised from Na_2SiO_3, for which the refined bond lengths correlate well with those values predicted from ionic radii.

5.2.2 T.o.f. PND study of Aluminogermanate Sodalites

Refinement of the aluminogermanate series of halide sodalites was undertaken using the results of Fleet [9] as starting models, and employed the same refinement technique as previously outlined for the gallosilicates.

Table 5.5 Final refinement parameters, atomic positions and thermal parameters ($Å^2$) with estimated errors in parentheses from powder neutron diffraction data at 298 K for sodium aluminogermanate halide sodalites

		$Na_8[AlGeO_4]_6.X_2$		
		Cl	Br	I
a(Å)		9.0425(4)	9.0914(9)	9.1735(1)
R_{wp}/R_{exp}		2.62/1.60	2.72/1.93	2.67/2.52
Al	B	0.72(2)	0.66(2)	0.54(1)
Ge	B	0.67(1)	0.74(1)	0.66(2)
X	B	2.64(2)	2.91(3)	3.35(1)
O	x	0.1428(2)	0.1444(1)	0.1455(1)
	y	0.1441(1)	0.1453(1)	0.1475(1)
	z	0.4277(3)	0.4319(2)	0.4384(1)
	B	1.16(1)	1.19(1)	1.10(2)
Na	x	0.1733(1)	0.1818(1)	0.1935(1)
	B	1.91(3)	1.88(3)	1.93(2)

Since the results of Fleet agree so closely with those presented in this work, the refinements proceeded extremely quickly with all of the profile fits matching the experimental data almost exactly, yielding low thermal parameters and small chi-squared values. The cell parameters reported by Fleet [9] are 9.0438 Å for Na[AlGe]Cl, 9.0949 Å for Na[AlGe]Br and 9.1755 Å for Na[AlGe]I; these results are also in concordance with those reported by McLaughlan and Marshall [10] whose cell constant for Na[AlGe]Cl was 9.037 Å. The final refined parameters for the materials prepared in the work are presented in Tables 5.5 and 5.6.

Table 5.6 Selected derived framework bond distances (Å) and angles (°) from powder neutron diffraction data for sodium aluminogermanate halide sodalites at 298 K with estimated errors in parentheses.

	Multiplicity	Cl	Br	I
Al-O	4	1.748(3)	1.748(2)	1.752(1)
Ge-O	4	1.734(1)	1.734(2)	1.728(2)
Na-O	3	2.329(3)	2.326(1)	2.328(2)
Na-A	1	2.711(2)	2.857(1)	3.075(2)
O-Al-O	4	107.84(2)	107.65(2)	107.41(3)
O-Al-O	2	112.78(4)	113.18(4)	113.82(6)
O-Ge-O	4	107.72(2)	107.54(2)	107.27(2)
O-Ge-O	2	113.03(4)	113.41(4)	113.89(4)
Al Tilt		26.6(1)	25.1(1)	22.7(1)
Ge Tilt		26.9(1)	25.3(1)	23.0(1)
Al-O-Ge		132.98(3)	134.81(3)	137.52(4)
O-Na-O	3	102.39(4)	105.08(4)	108.71(6)
O-Na-A	3	115.86 (4)	113.58(4)	110.21(5)

The synthetic method devised by Fleet for aluminogermanates is rather drastic, using sealed gold capsules heated at temperatures in the order of 800 °C producing pressures of approximately 0.2 GPa to yield single crystals. Since the crystallographic results of this work agree so closely with those of Fleet it can be stated that the reduction

of reaction pressure and temperature does not impair the formation of highly crystalline aluminogermanate sodalites. It should be remembered of course that single crystal syntheses often involve significantly different experimental conditions than those applicable to the preparation of bulk powdered materials. It was the intention of this study to reduce reaction temperature and pressure so as to devise synthetic procedures which are applicable to the enclathration of anions of relatively low thermal stability such as permanganate. Reactions were undertaken using the halide anions in order to optimise general synthetic procedures which then could be used to entrap more complex species within the sodalite cage. The success of these methods can easily be gauged by comparing them with literature reports such as that of Fleet for the aluminogermanates. In his study, Fleet reported that the experimental method successfully used for aluminogermanate sodalite synthesis could not be extended to prepare gallosilicates or gallogermanates; this is not the case for the preparative method of this work, which allows both gallium and germanium to be incorporated into the sodalite framework.

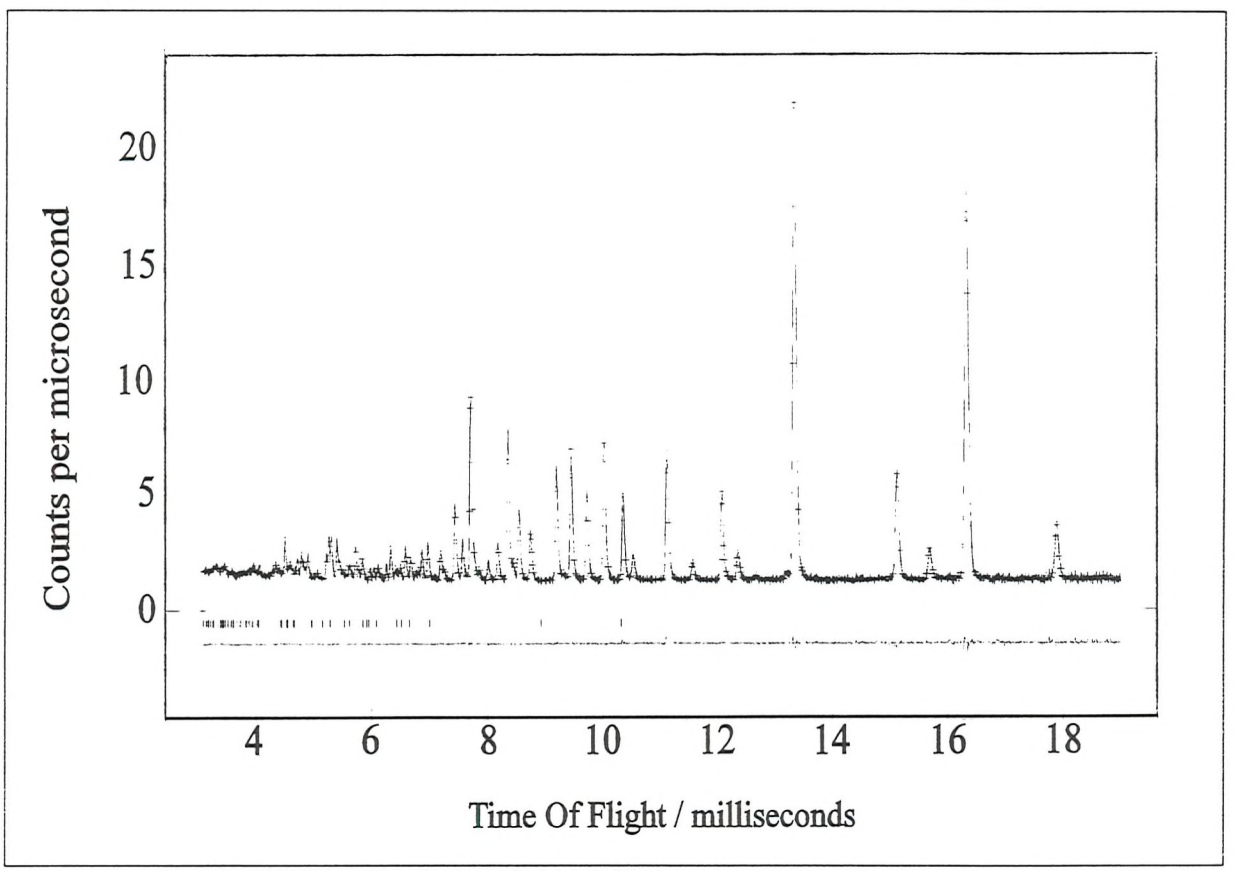

Figure 5.4 T.o.f. PND profile fit for Na[AlGe]I.

The chloride sodalite was found by Fleet to show slight (12 %) disorder of the framework components, whereas the bromide and iodide species had fully ordered

tetrahedral frameworks. This was attributed to the high annealing temperature, 1048 K, of the chloride; for the hydrothermally synthesised aluminogermanate sodalites prepared in this work there was no post-synthetic annealing and as such no disorder was observed at all.

It is apparent from examining the structural parameters that the most significant factor effecting the structure of the sodium aluminogermanate sodalites is spatial accommodation of the halide anion. There is a systematic change in the structural parameters in proportion to the relative size of the halide anion in an analogous fashion to the gallosilicates. This is manifested by progressive changes in variables such as unit cell parameter and T-O-T framework bond angles. Halide substitution in the order Cl, Br, I leads to the expansion and straightening of the aluminogermanate framework to accommodate the larger anions as is expected. There is a significant change within the O-Na-O and O-Na-X bond angles which approach the ideal tetrahedral angle of 109.48 ° in the iodide sample. The final fit to the data for $Na_8[AlGeO_4]_6.I_2$ is shown in Figure 5.4.

5.2.3 T.o.f. PND study of Gallogermanate Sodalites

The gallogermanate series of sodalites has been studied to a far lesser extent than the gallosilicates or aluminogermanates: this can be explained by the fact that their synthesis is considerably more difficult, with what appears to be rather a narrow range of thermal stability. In a similar manner to the gallosilicates and aluminogermanates the size of the halide anion at the cage centre dictates the level of relative collapse observed in the framework. Refinement was again straightforward with the results of the aluminogermanate refinements used for the starting models. Expansion of the unit cell is accompanied by the usual increase in framework bond angle, the factor which compensates most for the variation in framework size.

Table 5.7 Final refinement parameters, atomic positions and thermal parameters ($Å^2$) with estimated errors in parentheses from powder neutron diffraction data for sodium gallogermanate halide sodalites

		$Na_8[GaGeO_4]_6.X_2$		
		Cl	Br	I
a(Å)		9.1159(6)	9.1725(6)	9.2669(5)
R_{wp}/R_{exp}		4.61/2.76	4.44/2.55	4.97/3.45
Ga	B	1.95(1)	1.02(2)	1.38(2)
Ge	B	1.14(3)	2.09(4)	1.22(4)
X	B	3.16(3)	3.54(4)	3.96(3)
O	x	0.1410(3)	0.1417(2)	0.1454(3)
	y	0.1447(3)	0.1461(2)	0.1458(2)
	z	0.4197(1)	0.4230(1)	0.4293(1)
	B	2.11(1)	2.16(1)	1.86(1)
Na	x	0.1701(2)	0.1776(2)	0.1887(2)
	B	2.63(2)	2.86(4)	2.86(5)

In the iodide material the Ga-O distance is rather shorter than those for the chloride and bromide samples. This material was examined using the neutron source at the ILL, Grenoble, compared with the POLARIS source at RAL which was used for all of the other framework substituted halide sodalites examined in this work. Once more deviation form the ideal tetrahedral angle for O-Na-O and O-Na-X becomes smaller as halide size is increased.

Table 5.8 Selected derived framework bond distances (Å) and angles (°) from powder neutron diffraction data for sodium gallogermanate halide sodalites at 298 K with estimated errors in parentheses.

	Multiplicity	Cl	Br	I
Ga-O	4	1.806(3)	1.812(2)	1.798(1)
Ge-O	4	1.763(3)	1.760(2)	1.762(1)
Na-O	3	2.303(2)	2.293(1)	2.230(1)
Na-A	1	2.685(3)	2.821(2)	3.029(1)
O-Ga-O	4	107.62(4)	107.50(3)	107.10(2)
O-Ga-O	2	113.25(8)	113.50(7)	114.32(2)
O-Ge-O	4	107.25(4)	107.06(3)	107.06(2)
O-Ge-O	2	114.02(9)	114.42(7)	114.41(3)
Ga Tilt		29.0(1)	27.8(1)	25.9(1)
Ge Tilt		29.7(1)	28.5(1)	25.9(1)
Ga-O-Ge		129.09(5)	130.47(4)	133.20(2)
O-Na-O	3	101.61(8)	104.26(7)	107.85(3)
O-Na-A	3	116.50(6)	114.29(6)	112.03(7)

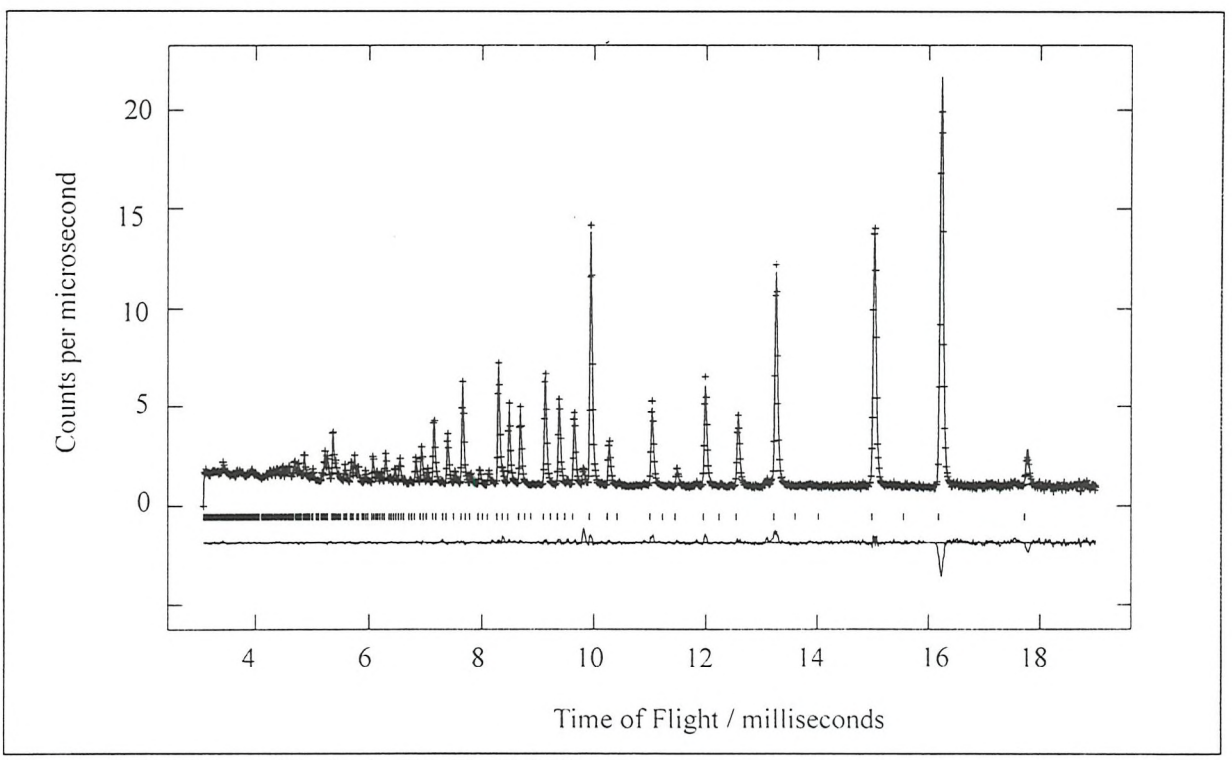

Figure 5.5 PND profile fit for Na[GaGe]Cl.

5.3 LITHIUM EXCHANGED HALIDE SODALITES

All of the framework substituted sodium halide sodalites were subjected to lithium exchange by the nitrate melt method. This generally involved heating at 270 °C with an excess of nitrate for 3 hours, with the excess salt subsequently washed free with distilled water. After this initial treatment, all materials were heated at 500 °C overnight to improve their crystallinity. Products were initially examined by powder x-ray diffraction and then further studied by powder neutron diffraction where appropriate.

5.3.1 T.o.f. PND study of Lithium Gallosilicate Halide Sodalites

The parent sodium gallosilicate materials used were those prepared using Na_2SiO_3 as the framework precursor. As stated previously, this is the method which provides the samples of highest crystallinity, and since exchange of non-framework cations is often associated with a reduction in the crystallinity of sodalites, obtaining parent samples of the highest crystallinity possible was deemed to be important. The disadvantage of this is that direct comparison of the sodium and lithium halide sodalites is made more difficult since the samples were synthesised using different methods. This does not affect the comparison of materials with different framework composition.

A dramatic reduction in cell parameter is observed following the introduction of lithium on the sodium sites. This is due to the fact that full exchange was possible, as indicated by refinement using lithium as the sole occupant of the 8(e) (x, x, x) cation site. This was the case for all of the halide materials, and refinement proceeded very smoothly, yielding excellent fits to the experimental data, as indicated by the profile fit shown in Figure 5.6. Cell contraction is accompanied by a decrease in framework Ga-O-Si angle amounting to approximately 12 ° compared with the parent sodium materials for each of the halide samples studied. Although in theory T-O-T angles of 109.5 ° are possible these are never experimentally observed, and the values obtained herein are some of the lowest ever reported for sodalites. Neutron diffraction studies were performed on $Li_8[AlSiO_4]_6.Cl_2$ and $Li_8[AlSiO_4]_6.Br_2$ by Wong [1] which revealed cell parameters of 8.444 Å and 8.508 Å and framework bond angles of 124.5 ° and 126.4 ° respectively.

Table 5.9 Final refinement parameters, atomic positions and thermal parameters ($Å^2$) with estimated errors in parentheses from powder neutron diffraction data for lithium gallosilicate halide sodalites

		$Li_8[GaSiO_4]_6.X_2$		
		Cl	Br	I
a(Å)		8.5362(6)	8.5776(5)	8.6489(5)
R_{wp}/R_{exp}		2.62/1.60	2.72/1.93	2.67/2.52
Ga	B	0.55(4)	0.51(4)	0.99(1)
Si	B	0.19(2)	0.27(4)	0.08(2)
X	B	2.50(4)	2.10(4)	2.49(9)
O	x	0.1269(1)	0.1282(1)	0.1319(2)
	y	0.1456(1)	0.1466(1)	0.1472(2)
	z	0.4027(1)	0.4051(1)	0.4102(1)
	B	0.78(3)	0.81(4)	1.04(5)
Li	x	0.1744(4)	0.1818(1)	0.1897(1)
	B	2.94(8)	1.88(3)	2.59(2)

Table 5.9 above summarises the refinement parameters, and Table 5.10 below selected bond distances and angles for the lithium exchanged gallosilicate halide sodalites. Table 5.10 shows how the gallium and silicon bond distances are close to those expected, although in the iodide sample the Ga-O bond is a little shorter, and the Si-O bond a little longer than those predicted from the respective ionic radii [11]. In a similar manner to the parent sodium sodalites, a smooth variation of intra-tetrahedral bond angles is evident. The O-T-O (x4) angles decrease and the O-T-O (x4) angles increase as the cell becomes larger. It is also clear that the O-Ga-O angles are those which display the greatest deviation from the ideal tetrahedral value of 109.48 °C.

Table 5.10 Selected derived framework bond distances (Å) and angles (°) from powder neutron diffraction data for lithium gallosilicate halide sodalites at 298 K with estimated errors in parentheses.

	Multiplicity	Cl	Br	I
Ga-O	4	1.827(1)	1.826(2)	1.808(1)
Si-O	4	1.630(1)	1.631(1)	1.641(1)
Li-O	3	2.006(2)	1.996(2)	2.006(3)
Li-A	1	2.578(6)	2.692(5)	2.841(6)
O-Ga-O	4	109.32(3)	109.10(3)	108.63(5)
O-Ga-O	2	109.78(7)	110.22(7)	111.17(1)
O-Si-O	4	107.39(4)	107.21(4)	107.06(5)
O-Si-O	2	113.72(8)	114.09(7)	114.41(9)
Ga Tilt		33.8(1)	32.9(1)	31.2(1)
Si Tilt		37.5(2)	36.5(1)	34.3(1)
Ga-O-Si		121.48(5)	122.56(5)	124.81(8)
O-Li-O	3	106.9(2)	109.2(1)	111.4(2)
O-Li-A	3	111.9(2)	114.3(2)	112.0(2)

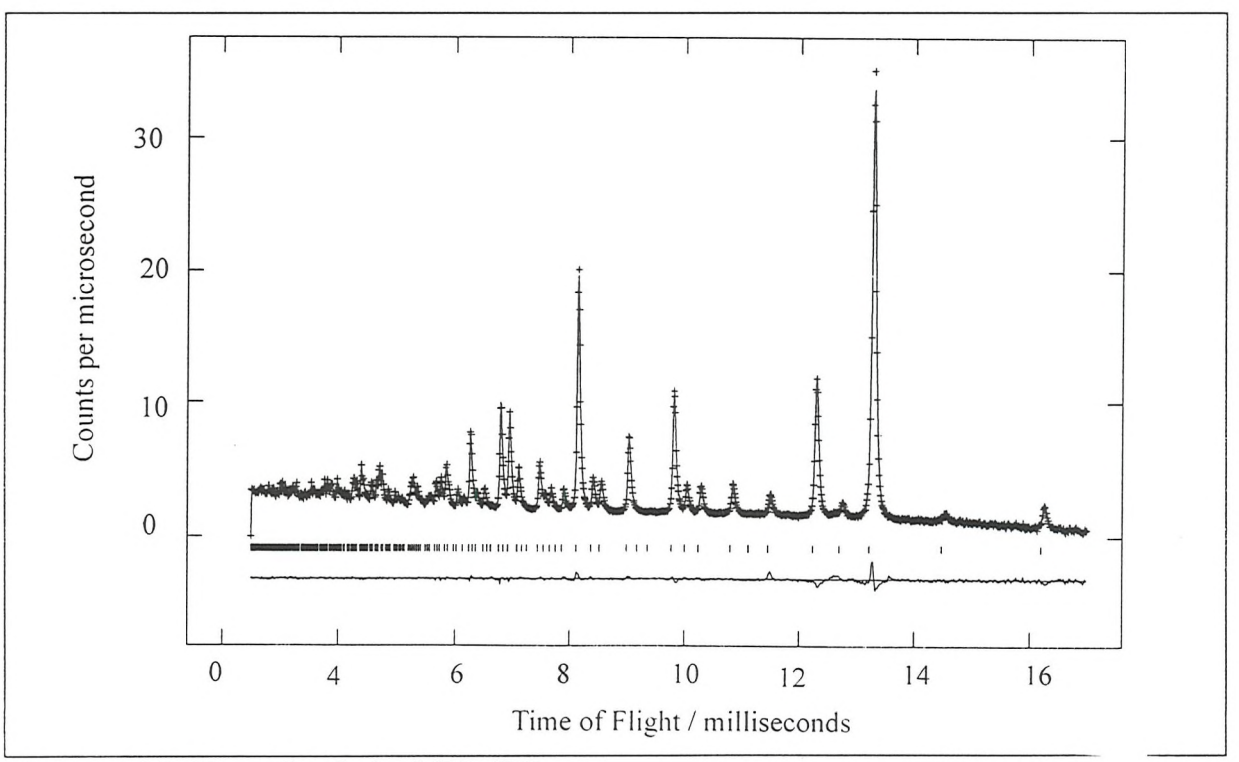

Figure 5.6 PND profile fit for Li[GaSi]Br.

5.3.2 T.o.f. PND study of Lithium Aluminogermanate Halide Sodalites

The aluminogermanate bromide and iodide samples were successfully exchanged after 3 hours at 270 °C using $LiNO_3$, but the chloride was destroyed. The reason for this was unclear: it is possible that since the chloride is the smallest of the series, prolonged treatment resulting in a high level of lithium exchange producing a structure which possesses bond angles too strained to be conducive to the sodalite structure. Treatment with $LiNO_3$ for 2 hours does yield a lithium exchanged sodalite, which can be refined successfully using full lithium occupancy on the 8(e) (x, x, x) site. It would therefore appear that a fully lithium exchanged aluminogermanate chloride sodalite can be obtained if the reaction is stopped at the appropriate time, 2 hours. Treatment for 3 hours is therefore effectively reacting $Li_8[AlGeO_4]_6.Cl_2$ with $LiNO_3$ which results in the collapse of the sodalite framework.

Table 5.11 Final refinement parameters, atomic positions and thermal parameters ($Å^2$) with estimated errors in parentheses from powder neutron diffraction data for lithium aluminogermanate halide sodalites

		$Li_8[AlGeO_4]_6.X_2$		
		Cl	Br	I
a(Å)		8.6848(9)	8.6786(5)	8.7505(5)
R_{wp}/R_{exp}		2.62/1.60	2.72/1.93	2.67/2.52
Al	B	0.47(15)	0.44(11)	0.31(12)
Ge	B	0.43(7)	0.44(4)	0.53(7)
X	B	6.43(9)	2.59(5)	2.44(5)
O	x	0.1396(2)	0.1377(2)	0.1399(1)
	y	0.1374(2)	0.1399(2)	0.1416(2)
	z	0.4052(1)	0.4054(1)	0.4094(1)
	B	0.86(8)	0.75(9)	0.78(7)
Li/Na	x	0.1830(4)	0.1828(3)	0.1928(2)
	B	3.30(12)	2.21(8)	1.99(8)

Refinement was undertaken in an exactly analogous manner as the exchanged gallosilicates, and proceeded smoothly for all samples with full lithium occupancy on the non-framework cation sites. Calculated and observed profiles are shown for the bromide in Figure 5.7 and matched extremely closely indicating that the input data accurately reflected the actual characteristics of the samples investigated. These structural parameters are summarised in Tables 5.11 and 5.12 below. The level of cell contraction is again high, and framework Al-O-Ge angles are only marginally bigger than those for the gallosilicate exchanged sodalites. Examination of cell parameters as given in Table 5.11 shows how the bromide sample is in fact slightly smaller than the chloride, which is the opposite to that which was expected. It seems likely that the decreased contraction of the chloride analogue is linked to the shortened reaction time which was necessary to prevent complete collapse of the aluminogermanate framework; however. this would in turn suggest that the level of lithium exchange was lower in the chloride than the bromide.

Table 5.12 Selected derived framework bond distances (Å) and angles (°) from powder x-ray diffraction data for lithium aluminogermanate halide sodalites at 298 K with estimated errors in parentheses.

	Multiplicity	Cl	Br	I
Al-O	4	1.762(2)	1.760(2)	1.759(2)
Ge-O	4	1.738(2)	1.736(2)	1.740(2)
Li-O	3	2.006(2)	2.006(2)	2.002(1)
Li/Na-A	1	2.753(6)	2.748(4)	2.922(4)
O-Al-O	4	107.95(4)	107.86(3)	107.48(3)
O-Al-O	2	112.56(9)	112.74(6)	113.53(6)
O-Ge-O	4	107.72(3)	107.64(3)	107.30(3)
O-Ge-O	2	113.04(9)	113.21(7)	113.90(6)
Al Tilt		34.6	34.1	32.6
Ge Tilt		34.2	34.5	32.9
Al-O-Ge		122.64(6)	122.69(4)	124.36(4)
O-Li-O	3	109.5(2)	109.3(1)	112.3(1)
O-Li-A	3	109.5(2)	114.3(1)	112.0(1)

Refinement did not suggest this, since variation of the lithium occupancy on the 8(e) (x, x, x) site did not reveal any significant deviation from unity. Despite this, a small amount of residual sodium on the site would seem the likeliest explanation for the larger cell parameter. The larger thermal parameter for lithium in the chloride material, in conjunction with a long cation to chloride distance (Table 5.12), supports this proposition of a small amount of residual sodium in the aluminogermanate chloride material. The size difference in the lithium exchanged chloride and bromide sodalites is small, and the chloride version still shows a marginally smaller Al-O-Ge angle than the bromide.

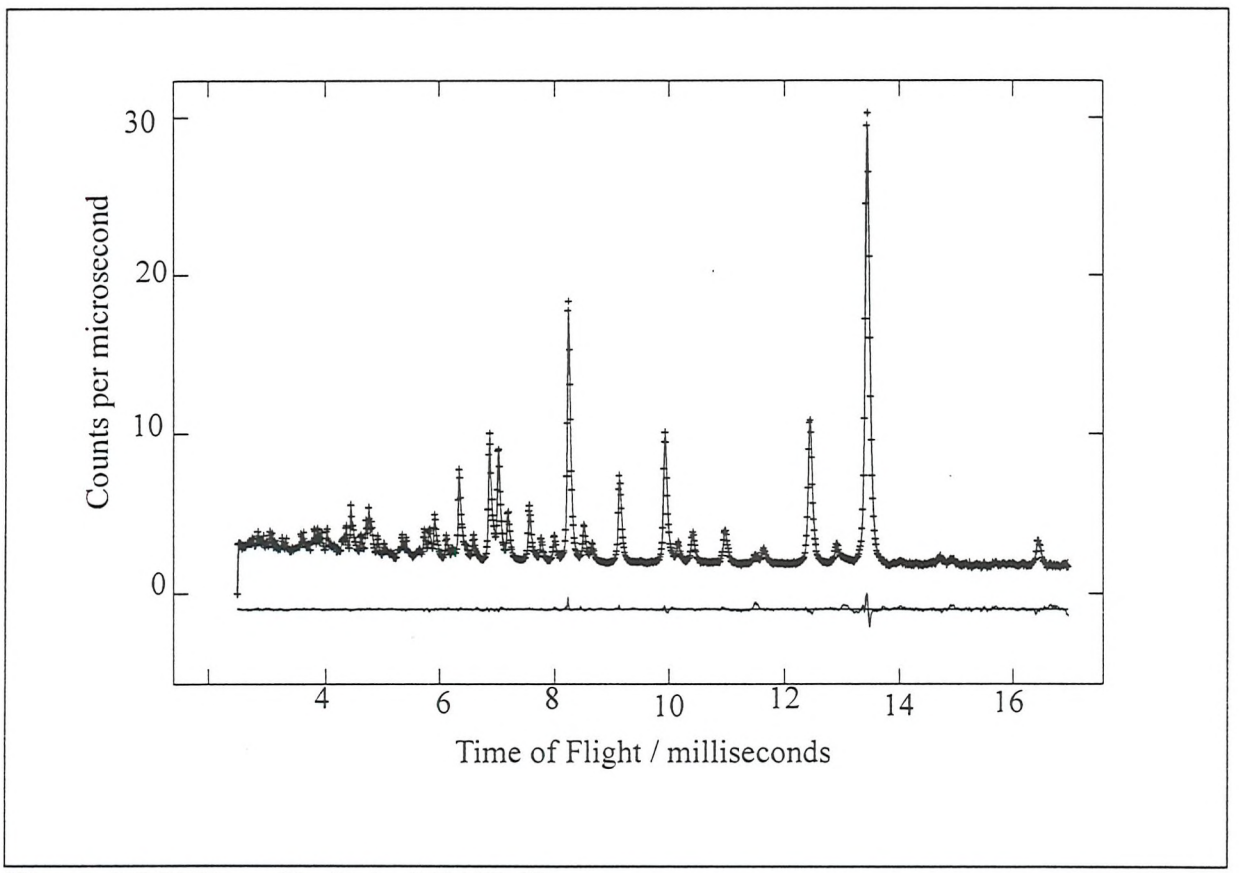

Figure 5.7 PND profile fit for Li[AlGe]Br.

5.3.3 Attempted Lithium Exchange of Gallogermanate Halide Sodalites

The same treatment for the gallogermanate series did not result in successful ion exchange for any of the halides. All of the materials subject to lithium nitrate melt treatment were destroyed, despite shortening the time in which the samples were in contact with the $LiNO_3$. It does appear as though the gallogermanate framework cannot contract sufficiently to support replacement of sodium by lithium. In the same way as for the aluminogermanate chloride sodalite, since the analysis is performed *ex-situ*, it is

difficult to determine the point at which framework collapse occurred. It is possible that lithium exchange occurred to some degree in the gallogermanate sodalite structure, and this sodalite is then destroyed by further heating with $LiNO_3$ when the lithium exchange reaches a level which cannot be supported by the gallogermanate sodalite structure. *In-situ* work would certainly prove extremely useful in the study of the mechanism of cation exchange and framework collapse.

5.4 POTASSIUM EXCHANGED HALIDE SODALITES

In an analogous manner to lithium exchange, all of the framework substituted sodium halide sodalites were subjected to potassium exchange by the nitrate melt method. This involved heating at 370 °C with an excess of potassium nitrate for 16 hours, with the excess salt washed free with distilled water. After this initial treatment, all materials were heated at 500 °C overnight to improve their crystallinity. Products were examined by powder x-ray diffraction. Gallosilicate and aluminogermanate materials were able to undergo replacement of sodium by potassium thus allowing significant increase in cell size, whereas gallogermanates showed no tendency to exchange whatsoever. Reaction times of 16 hours led to destruction of the gallogermanate framework, whereas short reaction times in the order of 2-3 hours simply left the materials unaltered. Exchange was also attempted using stoichiometric amounts of nitrate: it could be envisaged that the use of a large excess of nitrate created conditions which were too drastic to allow the gallogermanate framework to survive. However, once again short reactions left the starting materials unaltered whereas overnight runs destroyed the framework. In a similar manner to lithium exchange, it would appear that the gallogermanates have such a narrow stability range that exchange via nitrate melt is not possible. Further studies on the manner of cation exchange on gallogermanates are necessary to widen the scope of structural parameters adopted.

Full Rietveld refinement of PXD data was undertaken on these samples, and the resultant data are summarised in Tables 5.12 to 5.16. As expected, insertion of potassium into the sodalite structure yields expanded cells, although using nitrate melt, the level of substitution is somewhat lower than for lithium despite reaction times of 16 hours rather than the 3 hours used for lithium exchange. This reduced tendency to exchange may be explained in part by a lower rate of diffusion of the larger potassium ions throughout the sodalite lattice. Despite multiple treatments with potassium nitrate, no increased level of exchange was attained. This observation is in line with the results of Mead [12].

The potassium exchanged sodalites were refined with both sodium and potassium on the 8(e) site: initially on the same site until the refinement became stable, and then split to account for the different cation preferences. An overall charge of +8 on the cation site was maintained to retain overall electroneutrality. The fractional occupancies entered into the initial model were those determined using flame photometry, and were subsequently

varied to yield the values quoted in the tables below. The refinement procedure was analogous to the other halide sodalites.

Table 5.13 Final refinement parameters, atomic positions and thermal parameters ($Å^2$) with estimated errors in parentheses from powder x-ray diffraction data for potassium gallosilicate halide sodalites

		$M_8[GaSiO_4]_6.X_2$		
		$Na_{3.6}K_{4.4}Cl$	$Na_{4.1}K_{3.9}Br$	$Na_{3.8}K_{4.2}I$
a(Å)		9.103(9)	9.188(5)	9.284(5)
R_{wp}/R_{exp}		10.73/7.41	12.02/8.73	11.56/8.62
Ga	B	0.94(8)	0.73(9)	1.01(12)
Si	B	1.32(5)	1.27(6)	0.94(9)
X	B	3.92(12)	4.08(9)	3.73(8)
O	x	0.1403(3)	0.1412(5)	0.1430(2)
	y	0.1520(4)	0.1529(6)	0.1544(7)
	z	0.4371(3)	0.4398(3)	0.4421(3)
	B	1.98(4)	1.32(3)	1.77(4)
Na	x	0.1830(4)	0.1858(3)	0.1928(2)
	B	2.21(4)	2.87(6)	1.90(6)
K	x	0.2324(10)	0.2395(9)	0.2571(12)
	B	3.61(5)	2.63(4)	3.98(4)

Inspection of Table 5.16 shows how the positions adopted by the sodium and the potassium are significantly different. The sodium ions reside in similar positions to the parent sodium sodalites, and are strongly coordinated to three of the framework oxygens and the central halide giving approximately tetrahedral coordination. In contrast, the potassium cations are situated much further from the cage centre located approximately in the centre of the six rings. This leads to coordination to all of the framework oxygens in the six ring, as opposed to the three bound to sodium.

Table 5.14 Selected derived framework bond distances (Å) and angles (°) from powder x-ray diffraction data for potassium gallosilicate halide sodalites at 298 K with estimated errors in parentheses.

	Multiplicity	Cl	Br	I
Ga-O	4	1.833(6)	1.842(5)	1.829(5)
Si-O	4	1.612(5)	1.609(4)	1.596(7)
Na-O	3	2.329(3)	2.317(2)	2.322(4)
Na-A	1	2.681(3)	2.773(4)	3.061(3)
O-Ga-O	4	107.9(4)	107.6(3)	107.2(3)
O-Ga-O	2	111.3(9)	111.8(6)	112.8(6)
O-Si-O	4	107.1(3)	106.9(3)	106.6(3)
O-Si-O	2	114.7(9)	115.1(7)	115.5(6)
Ga Tilt		22.48(2)	21.49(3)	20.56(3)
Si Tilt		24.15(2)	23.09(1)	22.04(1)
Ga-O-Si		138.7(6)	141.5(4)	144.2(4)

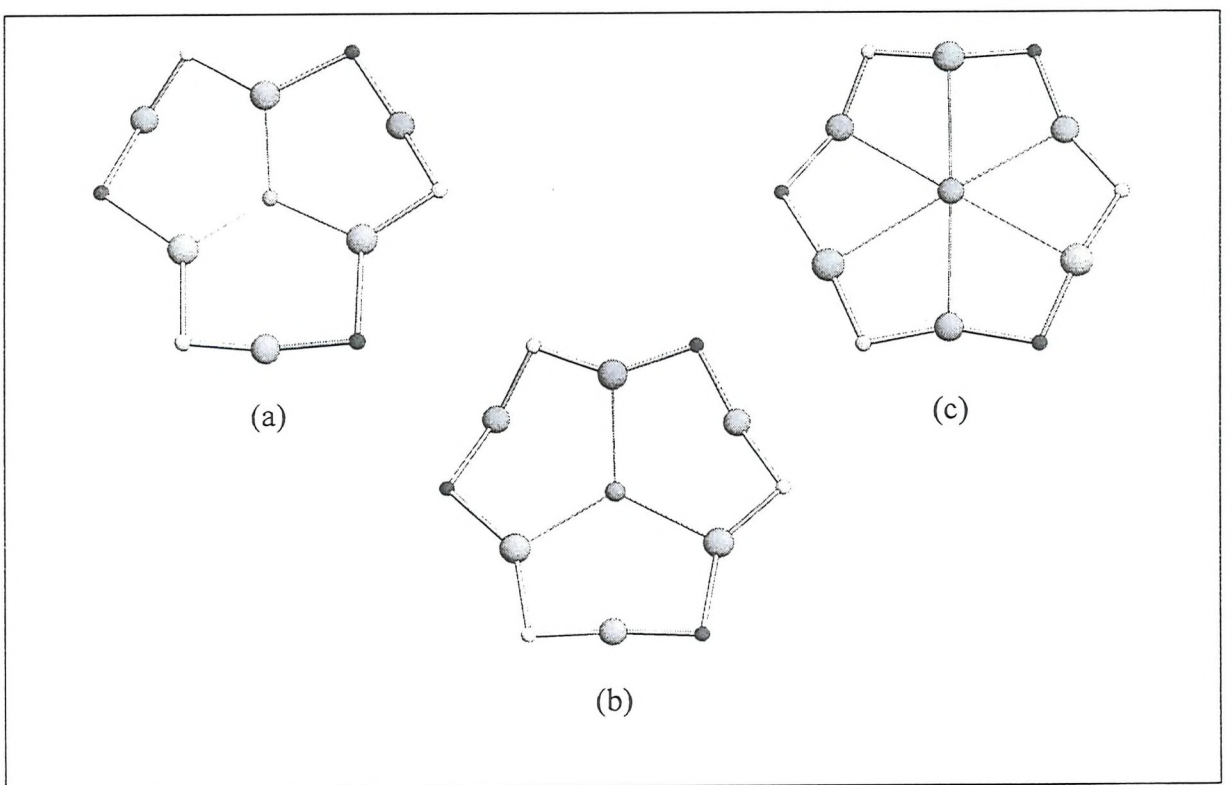

Figure 5.8 Cation co-ordination of **(a)** lithium, **(b)** sodium and **(c)** potassium sodalites.

In a similar way to the gallosilicate materials, potassium exchange of aluminogermanates produces sodalites containing both sodium and potassium as the non-framework cations. The potassium ions are once more located towards the centre of the six ring window in six fold coordination with the framework oxygens defining the ring, whereas the sodiums reside nearer to the cage centre to coordinate to only three oxygens. This is represented by Figure 5.8, which shows the different positions and coordinations adopted when the cation is lithium, sodium or potassium.

Table 5.15 Final refinement parameters, atomic positions and thermal parameters ($Å^2$) with estimated errors in parentheses from powder x-ray diffraction data for potassium aluminogermanate halide sodalites

		$M_8[AlGeO_4]_6.X_2$		
		$Na_{3.3}K_{4.7}Cl$	$Na_{3.8}K_{4.2}Br$	$Na_{3.6}K_{4.4}I$
a(Å)		9.270(9)	9.328(5)	9.372(5)
R_{wp}/R_{exp}		2.62/1.60	2.72/1.93	2.67/2.52
Al	B	0.51(7)	1.09(11)	0.76(12)
Ge	B	0.73(7)	0.89(4)	1.01(7)
X	B	2.71(9)	3.01(5)	3.13(5)
O	x	0.1444(2)	0.1472(2)	0.1493(1)
	y	0.1465(2)	0.1487(2)	0.1527(2)
	z	0.4310(2)	0.4331(2)	0.4402(2)
	B	0.93(8)	1.63(9)	1.78(7)
Na	x	0.1830(4)	0.1828(3)	0.1928(2)
	B	1.79(12)	2.21(8)	1.93(8)
K	x	0.2435(7)	0.2569(9)	0.2673(14)
	B	2.67(9)	2.63(8)	1.98(8)

Table 5.16 Selected derived framework bond distances (Å) and angles (°) from powder x-ray diffraction data for potassium aluminogermanate halide sodalites at 298 K with estimated errors in parentheses.

	Multiplicity	Cl	Br	I
Al-O	4	1.759(21)	1.758(15)	1.743(15)
Ge-O	4	1.741(20)	1.745(15)	1.736(15)
Na-O	3	2.330(23)	2.327(16)	2.323(14)
Na-A	1	2.739(6)	2.862(4)	3.0814)
K-O		2.592(15)	2.621(12)	2.998(16)
O-Al-O	4	107.8(4)	107.3(3)	107.1(3)
O-Al-O	2	112.9(9)	113.4(6)	113.9(6)
O-Ge-O	4	107.5(33)	107.1(3)	106.8(3)
O-Ge-O	2	114.2(9)	113.8(7)	113.4(6)
Al Tilt		25.22(2)	24.22(3)	21.39(2)
Ge Tilt		25.54(2)	24.44(4)	21.83(2)
Al-O-Ge		140.6(6)	142.2(4)	143.7(4)

5.5 CONCLUSIONS

The halide sodalites have been shown to be an excellent system for the study of structural variation as a function of composition due to their simplicity. Rietveld refinement of powder neutron data for all parent sodium sodalites provides structural parameters indicating that framework collapse is directly linked to a decrease in framework T-O-T bond angle.

Full lithium exchange has been achieved for gallosilicate and aluminogermanate sodalites using the nitrate melt method after 2-3 hours reaction time. This melt method is particularly effective for lithium exchange of framework substituted sodalites for which low temperature solution exchange has proven ineffective. It is likely that the short reaction time is a consequence of the size of the lithium cation which can diffuse quickly through the sodalite framework. The high temperatures involved in exchange using alkali metal halides are avoided, hence widening the range of materials which can be treated to include sodalites of limited thermal stability. PND data allows the extent of cell contraction to be monitored and shows how Ga-O-Si and Al-O-Ge bond angles approaching 120 ° have been obtained highlighting the degree of collapse accompanying lithium introduction.

In a similar way, expansion of the gallosilicate and aluminogermanate cells is possible via potassium exchange, although the level of exchange obtained, determined using flame photometry and powder x-ray diffraction, is significantly lower than that with lithium. In an analogous manner to lithium, it is likely that the larger size of the potassium ion will lead to poor diffusion and hence reduced tendency to exchange.

In contrast, gallogermanates show no tendency to exchange with either lithium or potassium, confirming the narrow band of structural parameters accessible using the synthetic techniques employed in this work. This follows the failure to synthesise monophasic gallogermanate sodalites with any anions other than halides. Further synthetic studies are thus required in order to prepare gallogermanates with a wider range of structural parameters, permitting correlations to be extended.

As previously indicated, in the halide series there is no noticeable shortening of the T-O bond lengths as cell size increases, but this is due to the narrow range of data; correlations presented in Chapter Eight for a whole range of sodalite compositions does show the general relationship between T-O bond length and cell parameter as reported by several authors.

Trends relating bond angles and cell parameter are much more evident within the halide series. As the cell parameter is increased for a particular framework composition there are definite trends observed: the O-T-O (x4), O-Na-A and tetrahedral tilt angles decrease, whereas the O-T-O (x2), the T-O-T and the O-Na-O angles increase. This general statement holds true whatever the framework composition and once more shows the consistency of the sodalite structure.

5.6 REFERENCES

[1] G. Wong, *Ph.D. Thesis*, University of Southampton (1990).

[2] M.E. Brenchley, *Ph.D. Thesis*, University of Southampton (1994).

[3] J.M. Newsam and J.D. Jorgensen, *Zeolites*, **7**, 569 (1987).

[4] A.C. Larson and R.B. Von Dreele, Generalized Structure Analysis System, MS-H805, Los Alamos, NM 87545 (1990).

[5] J. Selbin and R.B. Mason, *J. Inorg. Nucl. Chem,* **20**, 222 (1961).

[6] P.J. Schipper, C.Z. van Doorn and P.T. Bolwijn, *J. Am. Ceramic Soc.*, **55**, 256 (1972).

[7] L.B. McCusker, W.M. Meier, K. Suzuki and S.Shin, *Zeolites*, **6**, 388 (1986).

[8] T.M. Nenoff, W.T.A. Harrison, T.E. Gier, N.L. Keder, C.M. Zaremba, V.I. Srdanov, J.M. Nicol and G.D. Stucky, *Inorg. Chem.*, **33**, 2472 (1994).

[9] M.E. Fleet, *Acta Cryst.*, C**45**, 843 (1989).

[10] S.D. McLaughlan and D.J. Marshall, *Phys. Lett.*, **32A**, 343 (1970).

[11] R.D. Shannon and C.T. Prewitt, *Acta Cryst.*, **A32**, 751 (1976).

[12] P.J. Mead, *Ph.D. Thesis*, University of Southampton (1996).

Chapter Six

SODALITES CONTAINING COMPLEX ANIONS

6.1 INTRODUCTION

The previous chapter outlined sodalites containing simple halide anions and compared their structural properties. The current chapter will review sodalites containing more complex anions such as $(SCN)^-$, $(SeCN)^-$ and$(XO_4)^-$, where X=Cl and Mn. Although the anions themselves are not necessarily regarded as complex entities, their entrapment within sodalites leads to systems which may be considered complex due to the disorder associated with the central anion within the beta cages. The permanganate species are highly coloured, and the effect of framework composition and non-framework cation exchange on the colour properties will be examined. Thiocyanate and selenocyanate containing sodalites can be thermally degraded to yield ultramarines containing the $(S_n)^-$ and $(Se_n)^-$ radicals responsible for colouration. The effect of temperature and time on these intra-cage modifications can be followed by UV/VIS and FT-IR spectroscopy and will be detailed below. In addition, divalent anions including $(XO_4)^{2-}$, where X=S, Mn, Mo, W and Cr, as well as $(S_2O_3)^{2-}$ and $(S_2O_5)^{2-}$ can be entrapped, although these tend to yield the more open cancrinite structure. Cancrinites are in general rather more hygroscopic and less thermally stable than their sodalite equivalents and are therefore of less potential use as pigments. However, it has been shown that certain cancrinites can be thermally restructured to form sodalites whilst retaining the integrity of the entrapped anion [1]. This will be detailed for the different framework types.

6.2 SODALITES CONTAINING $(XO_4)^-$ ANIONS

The first synthesis of a sodalite containing the $(ClO_4)^-$ anion was reported by Barrer and Coie in 1970 [2], but little characterisation was performed; the same work also included an aluminosilicate permanganate material, but this crystallised with the cancrinite structure. The Hund method [3] was successfully used by Weller and Haworth [4] to prepare aluminosilicate perchlorate and permanganate sodalites, with the structure determination of these materials subsequently detailed by Brenchley and Weller [5]. This communication also reported the lithium and potassium exchanged analogues with Rietveld refinement of powder neutron data at both 4 and 300 K allowing the orientational disorder of the central anions to be examined. The effect of introducing gallium and germanium into the framework on these materials is discussed below.

6.2.1 The Permanganate Anion

As indicated in Chapter Four, the permanganate anion is stable only in strongly basic solutions to temperatures in the order of 160-200 °C, and is thus perfectly suited to entrapment within an aluminosilicate framework via the Hund method. Hydrothermal syntheses attempted in the current work resulted in decomposition to MnO_2; solution methods were thus used in the attempted synthesis of gallium and germanium permanganate containing sodalites. Aluminogermanate and gallosilicate permanganate sodalites were successfully synthesised by the method devised in this study, using the framework precursors $NaAlO_2/NaGaO_2$ and Na_2SiO_3/Na_2GeO_3 as appropriate. In each case, the presence of the permanganate anion was confirmed by the observation of the IR active ν_3 mode at 911 cm^{-1}. The gallosilicate sample was poorly crystalline and contained a significant amount of impurity, as had been observed for other gallosilicates synthesised using solution reactions. The addition of 4 M NaOH to the reaction medium allowed the permanganate to retain stability throughout the reaction, and prevented any significant decomposition to MnO_2. The formation of manganese (IV) oxide causes an appreciable difficulty since upon filtration it is collected alongside the sodalite phase as the residue. It has been reported [6] that heating MnO_2 with 10 M NaOH solution can reoxidise the manganese (IV) to manganese (VII), but this did not appear to be successful to any great degree. The synthesis of a gallogermanate permanganate sodalite was not successful: hydrothermal methods led to MnO_2 and the low temperature solution synthesis yielded only hydrosodalite. This is in line with the other gallogermanate reactions in this work: solution synthesis always produced hydrosodalite, and the halide series were the only anions successfully entrapped to give phase pure sodalites. This indicates the sensitivity of gallogermanates to synthetic conditions, although it is not known why such a limited number of anions can be entrapped within the gallogermanate beta cage.

Neutron diffraction was performed on the aluminogermanate permanganate sodalite on D2B with an acquisition time of four hours. Full Rietveld refinement was performed in the space group $P\bar{4}3n$ using the GSAS package of Larson and Von Dreele [7] with the structure of $Na_8[AlSiO_4]_6(MnO_4)_2$ as the starting model [5]. The refinement process was the same as that for the halide sodalites, with scale factor and background parameters initially introduced, followed by lattice parameters, zero point correction and sample displacement thus pinpointing reflection positions. Atomic positions were next incorporated to generate peak intensities, initially of the framework species followed by

non-framework ions. Manganese was placed at the cage centre on the 2(a) (0, 0, 0) site; the permanganate oxygen was found to be disordered and the 24(i) (x, y, z) site, with $x \approx 0.15$, $y \approx 0.07$, $z \approx 0.00$, was chosen to represent this disorder as was utilised for the aluminosilicate analogue. The occupancy on this site was set to one-third, and the oxygen position and temperature factors were then refined. Since there is substantial disorder associated with this site, refinement of atomic coordinates was accompanied by damping constraints, with the x, y and z coordinates only allowed to vary 25% of the maximum. The application of this constraint prevents the continual alternation from one possible anion geometry to another within the sodalite cage. The refined thermal parameters of the permanganate oxygen are rather high, but this is not unexpected, and indeed was observed for the aluminosilicate analogue. This is caused by the considerable thermal motion associated with the disorder of the anion apparent at ambient temperature. It would have been interesting to acquire powder neutron data at 4 K, and this would have resulted in what could be described as a "quenched" thermal motion of the anion at the cage centre; certainly as the temperature is decreased, much less thermal motion would be expected and would be reflected by a lower refined thermal parameter for the permanganate oxygen. This was the case for the aluminosilicate permanganate sodalite which was studied at 300 K and at 4 K by Brenchley and Weller [5]. The framework was initially refined, followed by the sodium cations, the manganese located at the cage centre and lastly the anion oxygens. The refinement proceeded smoothly and a chi-squared value of 2 was achieved. The final refinement parameters are shown in Table 6.1 and selected derived bond distances and angles in Table 6.2; the profile fit is shown in Figure 6.1.

Table 6.1 Final refinement parameters, atomic positions and thermal parameters ($Å^2$) with estimated errors in parentheses from powder neutron diffraction data at 298 K for sodium aluminogermanate permanganate sodalite

Atom	Site	Occupancy	x	y	z	B
Na	8(e)	1	0.2127	0.2127	0.2127	3.53(9)
Al	6(c)	1	0.25	0	0.5	0.24(7)
Ge	6(d)	1	0.25	0.5	0	0.37(4)
O(1)	24(i)	1	0.1469(3)	0.1491(3)	0.4465(2)	1.31(4)
Mn	2(a)	1	0	0	0	4.5(3)
O(2)	24(i)	0.333	0.149(2)	0.072(2)	0.013(2)	14.6(7)

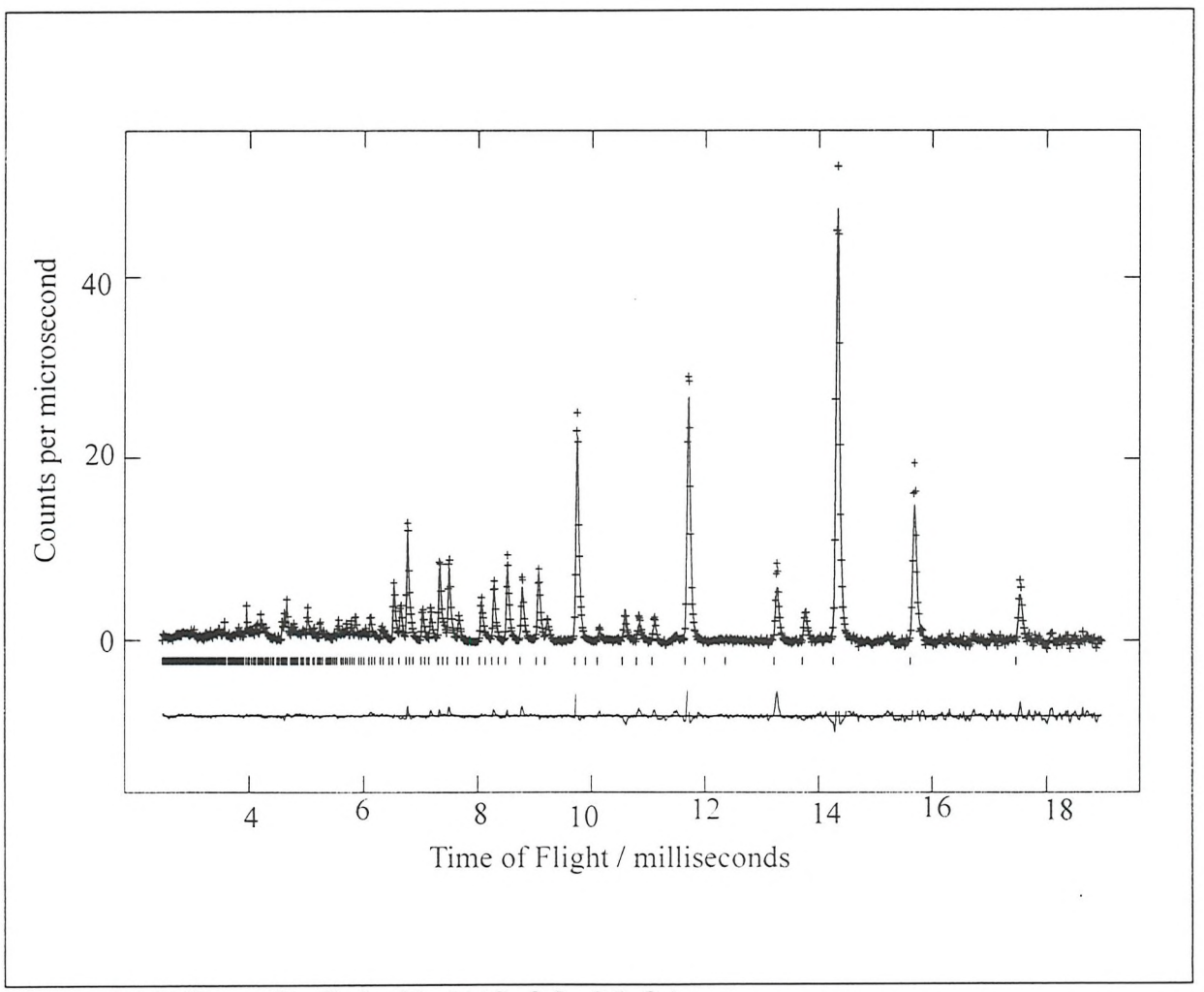

Figure 6.1 PND profile fit for $Na_8[AlGeO_4]_6.(MnO_4)_2$

Table 6.2 Selected derived framework bond distances (Å) and angles (°) from powder neutron diffraction data for sodium aluminogermanate permanganate sodalite at 298 K with estimated errors in parentheses.

Parameter	Final Refinement Value
Al-O(1)	1.750(4)
Ge-O(1)	1.723(3)
Na-O(1) x3	2.324(2)
Na-O(1) x3	3.066(2)
Mn-O(2)	1.539(2)
Na-O(2) 1/3 x 3	2.53(2)
Al-O(1)-Ge	141.0(1)
O(1)-Al-O(1) x2	113.9(2)
O(1)-Al-O(1) x4	107.3(1)
O(1)-Ge-O(1) x2	114.3(2)
O(1)-Ge-O(1) x4	107.1(1)

a = 9.2576(9) Å; R_{wp}/R_{exp} = 5.72/3.02

Examination of the data shows that the Al-O(1) and Ge-O(1) distances are in good agreement with those expected from consideration of their respective ionic radii. The results are also in excellent concordance with other sodalites of the aluminogermanate system, as well as those reported by Brenchley and Weller for the aluminosilicate permanganate sodalite [5]. The coordination of the sodium atoms to the framework oxygen shows that there are three strong bonds of ≈ 2.32 Å, which is the predicted value for a standard sodium to oxygen bond, and three somewhat weaker interactions at a distance of ≈ 3.07 Å. This illustrates the point made in the opening chapter concerning the varying coordination of the non-framework cations to the framework oxygens, which can be regarded as three or six depending on the particular species involved, in addition to the single bond to the entrapped anion at the cage centre. The structure is shown in Figure 6.2.

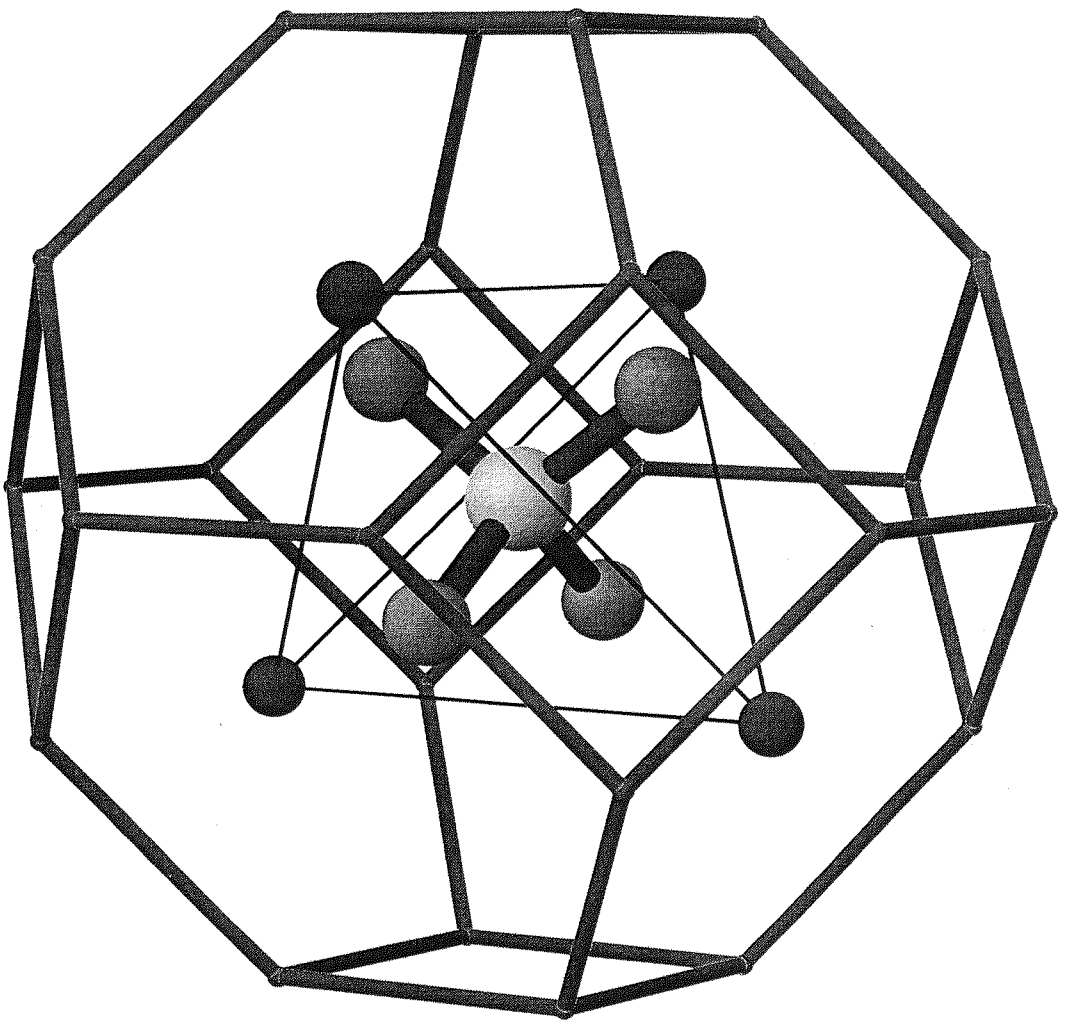

Figure 6.2 Structure of $Na_8[AlGeO_4]_6.(MnO_4)_2$

The UV/VIS spectrum of $Na_8[AlGeO_4]_6(MnO_4)_2$ is shown in Figure 6.3, which includes the corresponding $Na_8[AlSiO_4]_6(MnO_4)_2$ data for comparison. It is evident that the characteristic absorption of the permanganate anion, caused by charge transfer $O \rightarrow Mn$ within the anion, is not appreciably altered by variation in framework composition.

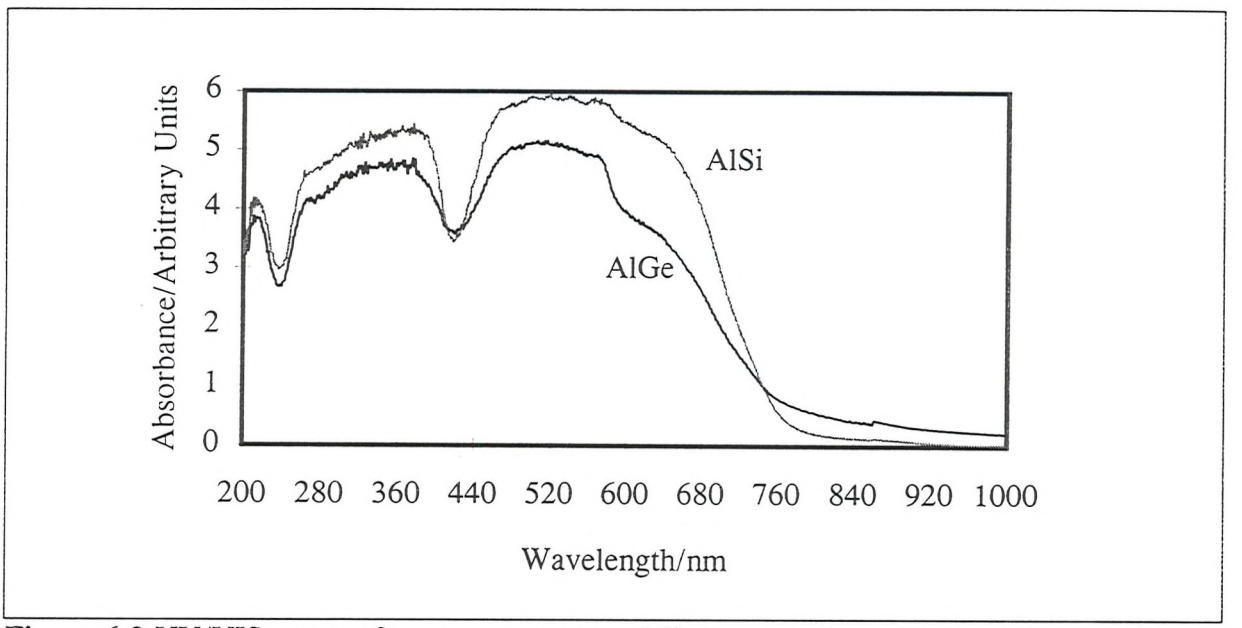

Figure 6.3 UV/VIS spectra for permanganate sodalites.

6.2.2 The Perchlorate Anion

The perchlorate anion, $(ClO_4)^-$, shows many similarities to the permanganate anion described above. However, sodium perchlorate displays considerably higher thermal stability than sodium permanganate: indeed it can be readily synthesised using hydrothermal routes with no decomposition of the anion. In addition, the perchlorate anion does not need to be stabilised within the reaction medium by the addition of sodium hydroxide. These considerations mean that sodalites containing perchlorate can be prepared rather more easily than the permanganate analogue. Aluminogermanate perchlorate sodalite was prepared by hydrothermal reaction of a gelatinous mixture of $NaAlO_2$, Na_2GeO_3 and a large excess of $NaClO_4$ at 180 °C for 24 hours. Sodium gallosilicate perchlorate sodalite was initially prepared using SiO_2 and $NaGaO_2$ as the framework precursors in a similar fashion to the halide analogues. Both of these materials were examined by powder neutron diffraction on POLARIS. The gallosilicate sample was subsequently resynthesised using Na_2SiO_3 and $NaGaO_2$ since these framework precursors were found to yield considerably improved materials. This latter sample was characterised by Rietveld refinement of powder x-ray diffraction data. The gallogermanate perchlorate sodalite could not be prepared phase pure, with high levels of impurity encountered in all attempts. The reason for this failure remains unclear.

Table 6.3 Final refinement parameters, atomic positions and thermal parameters ($Å^2$) with estimated errors in parentheses from powder neutron diffraction data for sodium aluminogermanate perchlorate sodalite at 298 K

Atom	Site	Occupancy	x	y	z	B
Na	8(e)	1	0.2042(2)	0.2042(2)	0.2042(2)	3.02(6)
Al	6(c)	1	0.25	0	0.5	0.64(8)
Ge	6(d)	1	0.25	0.5	0	0.71(5)
O(1)	24(i)	1	0.1472(2)	0.1484(2)	0.4439(2)	1.35(8)
Cl	2(a)	1	0	0	0	3.66(4)
O(2)	24(i)	0.333	0.135(1)	0.051(2)	0.013(2)	12.0(5)

a = 9.2305(4) Å; R_{wp}/R_{exp} = 2.78/2.02

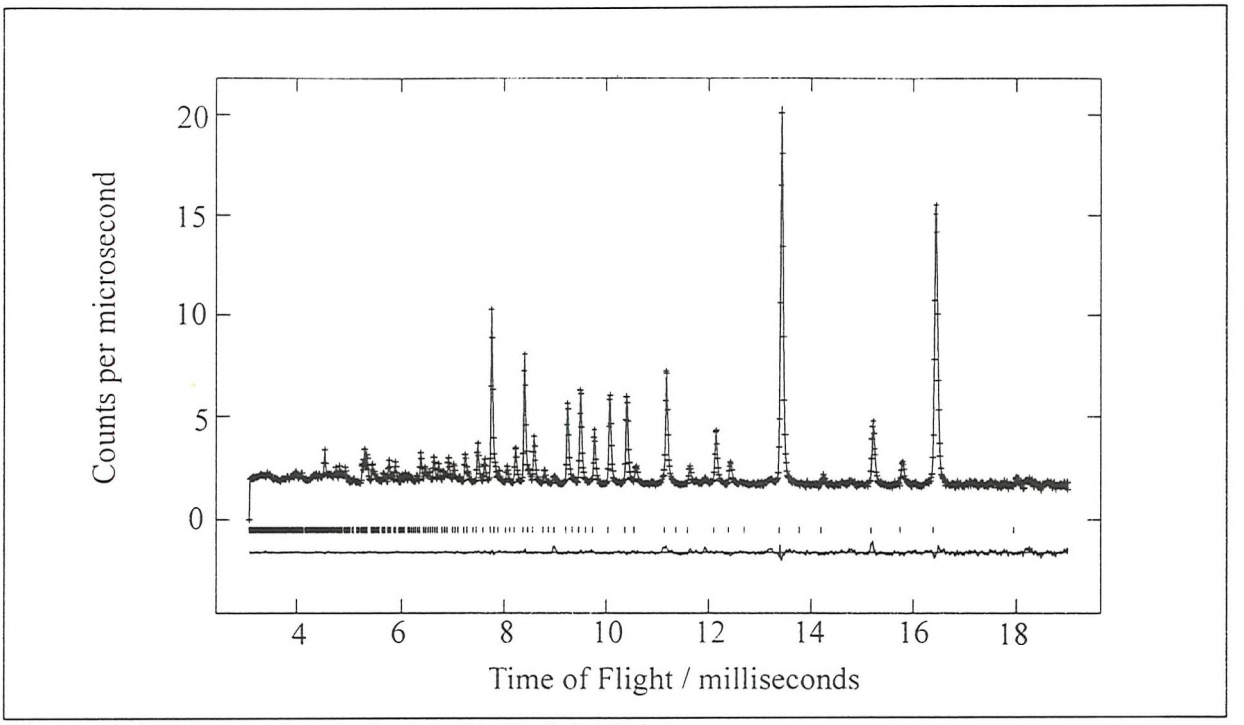

Figure 6.4 PND profile fit for $Na_8[AlGeO_4]_6(ClO_4)_2$.

The structural refinement procedure was exactly analogous to that employed for the aluminogermanate permanganate sodalite, with the 24(i) (x, y, z) once again chosen to model the disorder of the central anion. Refinement of the framework proceeded smoothly, and was followed by the non-framework cations and the central perchlorate. Once more, the perchlorate oxygen, O(2), displayed a high temperature factor, explained as before by the level of thermal motion associated with rotation of the anion.

Table 6.4 Selected derived framework bond distances (Å) and angles (°) from powder neutron diffraction data for sodium aluminogermanate perchlorate sodalite at 298 K with estimated errors in parentheses.

Structural Parameter	Final Refinement Value
Al-O(1)	1.746(2)
Ge-O(1)	1.730(2)
Na-O(1) x 3	2.332(1)
Na-O(1) x 3	3.084(1)
Cl-O(2)	1.335(6)
Na-O(2) 1/3 x 3	2.54(2)
Al-O(1)-Ge	139.77(6)
O(1)-Al-O(1) x 2	114.10(8)
O(1)-Al-O(1) x 4	107.21(4)
O(1)-Ge-O(1) x 2	114.36(7)
O(1)-Ge-O(1) x 4	107.08(4)

Structural parameters for gallosilicate perchlorate sodalite are detailed in Tables 6.5 and 6.6 below, from which a comparison between neutron and x-ray data can be made. Of particular note is the temperature factor of the perchlorate oxygen, O(2). PND yields a high value as for the aluminogermanate due to thermal motion; however, PXD data provides a far lower value which is in fact lower than those for sodium and chloride. Since the gallosilicate cage is somewhat smaller than the aluminogermanate, the tetrahedral anion has less room to rotate freely, and hence a slight reduction in the O(2) temperature factor would not be surprising. However, the difference between the perchlorate O(2) thermal factors in the aluminogermanate and gallosilicate materials is very large indeed, and is much greater than would be expected. Indeed, for the aluminosilicate analogue at 300 K reported by Brenchley and Weller [5] the thermal parameter is 12.01 $Å^2$.

Table 6.5 Final refinement parameters, atomic positions and thermal parameters ($Å^2$) with estimated errors in parentheses from powder neutron and x-ray diffraction data for sodium gallosilicate perchlorate sodalite at 298 K

		$Na[GaSiO_4]_6(ClO_4)_2$	
		PND	PXD
a(Å)		9.1350(6)	9.1490
R_{wp}/R_{exp}		1.69/0.92	10.43/7.67
Ga	B	1.05(7)	2.37(8)
Si	B	0.53(6)	1.27(5)
Cl	B	4.31(8)	5.25(13)
O(1)	x	0.1400(2)	0.1395(6)
	y	0.1536(2)	0.1599(7)
	z	0.4453(2)	0.4455(7)
	B	1.86(4)	2.27(9)
Na	x	0.2047(3)	0.2068(5)
	B	3.72(9)	4.05(11)
O(2)	x	0.139(1)	0.132(2)
	y	0.046(2)	0.057(2)
	z	0.018(1)	0.056(1)
	B	13.0(4)	3.5(26)

The Cl-O(2) bond distances are rather short as previously observed for aluminosilicates, which were attributed to the rotational nature of the central anion causing compression of the Cl-O(2) bond. Such short Cl-O(2) distances were also observed by Mead in his study of chlorate containing sodalites [8]. There are noticeable differences between the derived bond distances and angles from PND and PXD data. The Ga-O and Si-O distances are rather different, as are the intra-tetrahedral O(1)-Ga-O(1) and O(1)-Si-O(1), with the PXD data showing greater deviation from the ideal tetrahedral value.

Table 6.6 Selected derived framework bond distances (Å) and angles (°) from powder neutron and x-ray diffraction data for sodium gallosilicate perchlorate sodalite at 298 K with estimated errors in parentheses.

Structural Parameter	PND Refinement Value	PXD Refinement Value
Ga-O(1)	1.793(1)	1.845(5)
Si-O(1)	1.627(1)	1.597(4)
Na-O(1) x3	2.318(2)	2.307(7)
Na-O(1) x3	3.044(2)	3.027(6)
Cl-O(2)	1.345(1)	1.407(12)
Na-O(2) 1/3 x 3	2.568(1)	2.855(4)
Ga-O(1)-Si	140.78(3)	139.6(4)
O(1)-Ga-O(1) x2	111.98(1)	113.6(5)
O(1)-Ga-O(1) x4	108.23(2)	107.5(2)
O(1)-Si-O(1) x2	114.33(2)	117.9(6)
O(1)-Si-O(1) x4	106.94(4)	105.4(3)

6.3 FRAMEWORKS CONTAINING $(XO_4)^{2-}$ ANIONS

The preparation of framework materials containing divalent anions has been well documented for aluminosilicates [8, 9, 10]. As outlined in Chapter Three, hydrothermal or solution sodalite reactions in which monovalent anions are replaced by divalents generally give rise to cancrinites rather than the more condensed sodalite structures. This is illustrated by the Hund method [3], which always yields cancrinites whatever the divalent anion used; the Barrer method [11] is reported to give sodalites with certain anions such as $(SO_3)^{2-}$, but such results we not obtained within the scope of the work herein, and once more cancrinites were formed. High temperature solid state reactions for aluminosilicates do yield the sodalite topology: the introduction of divalent anions simply results in the occupation of alternate cages by the anion, with the remainder of the beta cages containing only M^{4+} clusters. The entrapment of divalents within modified frameworks had not previously been extensively studied prior to the development of the synthetic methods of this work. Using the methods devised herein, Mead [8] was able to successfully entrap the carbonate anion within an aluminogermanate framework forming the losod structure, and it was hoped to entrap a much wider range of divalent anions within gallosilicate, aluminogermanate and gallogermanate frameworks. Since solid state methods had not proven successful for the synthesis of framework substituted sodalites, it was expected that the hydrothermal and solution routes employed would lead to the formation of cancrinites. In an analogous manner to aluminosilicates it was then the intention to transform the cancrinite structure into that of sodalite via thermal treatment without destruction or modification of the central anion.

Before the entrapment of coloured tetrahedral divalent anions was attempted, it was decided to optimise the general conditions using the $(SO_4)^{2-}$, $(MoO_4)^{2-}$ and $(WO_4)^{2-}$ anions. Since they can be readily enclathrated by aluminosilicate frameworks via high temperature, hydrothermal or low temperature routes, they pose no synthetic problems associated with thermal stability, base sensitivity or steric hindrance. Experimental parameters varied were temperature and time, and it transpired that the best chance of entrapping divalents involved a reaction time of 48 hours at a temperature in the range 150-180 °C using the general hydrothermal method utilised for entrapment of monovalents. All of the three divalent anions could be entrapped within both gallosilicate and aluminogermanate frameworks, although there was no success using a gallogermanate framework. Shorter reactions were not successful and simply resulted in the formation of nephelenic species. It could therefore be envisaged that these nepheline species, $NaGaSiO_4$ or $NaAlGeO_4$, act as intermediates in the

formation of frameworks containing divalent species. No detailed study of the reaction mechanism for such species was however performed, and as such this proposal remains somewhat speculative. All of these anions gave rise to cancrinites, and the presence of the anionic species was confirmed using IR spectroscopy. The sulphate group was confirmed by the υ_3 band at 1105 cm^{-1}, molybdate by υ_3 at 837 cm^{-1}, and tungstate by υ_3 at 839 cm^{-1}. These values are in good agreement with those found in the literature [12].

The bright yellow chromate(VI) anion can readily be enclathrated within aluminosilicates, either by the structure conversion method of Chang [13] or by the Hund method [3]. Both products retain the vivid colour characteristic of the free sodium salt, but vary in their structures as previously indicated. The thermal and base stability of chromate(VI) allow both high temperature and low temperature solution methods to be employed in its entrapment. In the attempted syntheses of gallium and germanium containing samples, sodium dichromate was used in the presence of strong base to form sodium chromate, Na_2CrO_4, *in situ* around which the framework could form. Gallosilicate and aluminogermanate chromate materials were successfully synthesised using hydrothermal reactions at 180 °C for 48 hours. Both of the synthesised samples were characterised by powder x-ray diffraction which revealed that they possessed the cancrinite rather than sodalite topology. Infra-red spectroscopy confirmed the presence of the $(CrO_4)^{2-}$ moiety via observation of the ν_3 IR active band at 896 cm^{-1}.

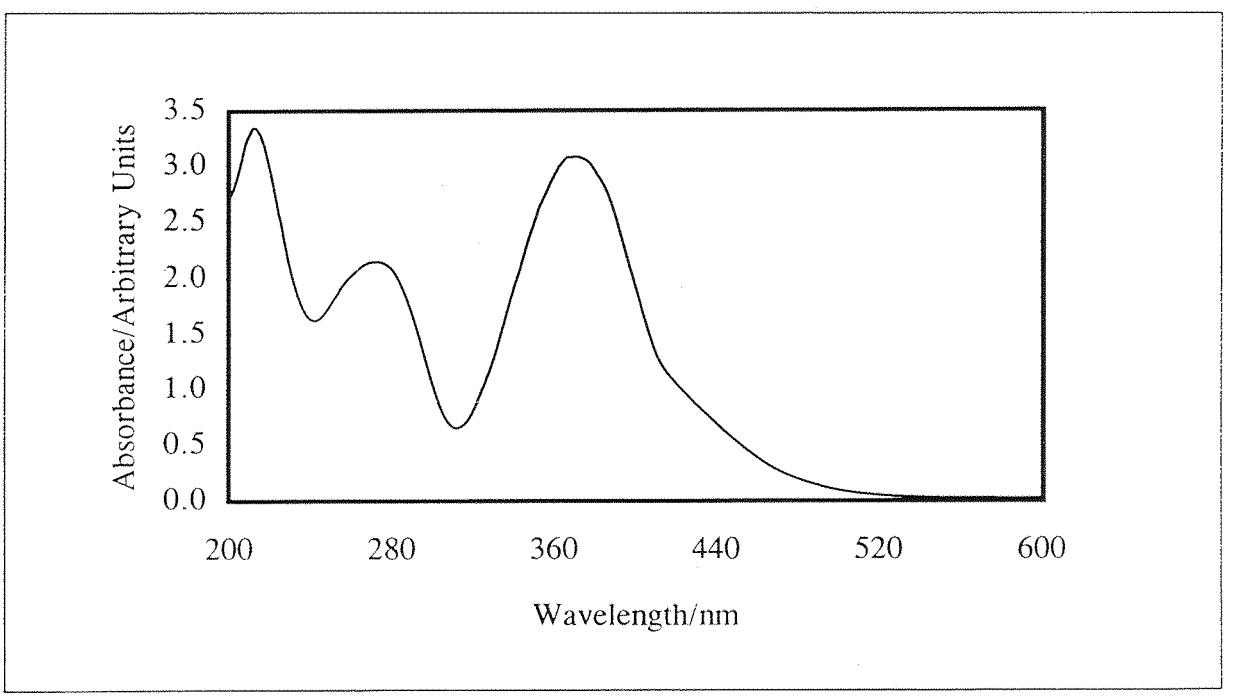

Figure 6.5 UV/VIS spectrum of gallosilicate chromate cancrinite

UV/VIS spectroscopy was also undertaken and the characteristic absorption of the chromate anion could readily be seen. Silver doping of the sodium aluminosilicate noselite allowed the colour to be modified via a red shift in the UV/VIS by approximately 70 nm yielding a rust coloured material. This is an excellent example of how sodalite colours can be tailored to suit the requirements of the individual, and provides another reason to support the choice of such framework materials for pigment applications. Figure 6.5 shows the UV/VIS spectra of the gallosilicate chromate material.

Both the gallosilicate and aluminogermanate chromate samples were of relatively poor crystallinity, and since they were cancrinites no structural characterisation via use of the Rietveld method was attempted. Thermal treatment in order to obtain gallosilicate and aluminogermanate chromate sodalites did not prove successful: at 800 °C both were destroyed after 16 hours, whereas treatments involving lower temperatures or shorter times simply left the samples unaltered.

Attempts were also made to synthesise gallium and germanium containing sodalites in which the manganate(VI) anion, $(MnO_4)^{2-}$, was entrapped. However, hydrothermal syntheses led to decomposition to MnO_2, and solution synthesis proved unsuccessful in the enclathration of divalent anions. Efforts to entrap $(MnO_4)^{2-}$ within gallium and germanium containing frameworks were thus abandoned.

6.4 THIOCYANATE SODALITES

As described in Chapter One the industrial preparation of sulphur ultramarine is rather a time consuming process and produces materials of rather low crystallinity, although it does yield products of extremely strong shades [14]. In this work the preparation of a number of thiocyanate sodalites which act as ultramarine precursors has been studied. Ultramarine is the thermolysis product of thiocyanate sodalite, and the effect of temperature and time on the materials has been investigated. In addition, the atmosphere under which the precursor is converted to ultramarine may alter the colourific properties of the resultant sodalite and hence was also examined.

6.4.1 Preparation

Aluminosilicate thiocyanate sodalites were synthesised by the method of Hund [3]. The gallosilicate and aluminogermanate analogues were synthesised hydrothermally as described in Chapter Three, with the addition of 1 M NaOH to the starting mixture to prevent decomposition of the $(SCN)^-$ anion under reaction. Reactions were initially attempted without the inclusion of this base and resulted in the formation of hydrosodalites. The choice of the minimum quantity of base required to stabilise the anion was made in order to circumvent the formation of hydroxysodalite, which can often form preferentially to thiocyanate. This is often the case for aluminosilicate thiocyanates prepared by solution: diffraction maxima obtained by PXD are often broad due to the sodalite cages containing water molecules, hydroxide and thiocyanate anions. The incorporation within the beta cage of species other than the desired anion makes structural refinement problematic, and thus the levels of these undesired moieties in the starting gel were kept to a minimum.

6.4.2 Structural Characterisation

Aluminosilicate thiocyanate sodalite has previously been characterised using neutron diffraction data [9], but there have been no structural investigations of framework substituted sodalites containing the thiocyanate anion. Detailed structural studies were not performed on the gallosilicate sample due to the presence of a significant amount of hydrosodalite impurity coupled with relatively poor crystallinity. This makes refinement

particularly problematic considering the difficulty of suitably modelling the disordered thiocyanate anion. In contrast, the aluminogermanate material prepared was of excellent crystallinity, possessing narrow, sharp peaks in the x-ray diffraction pattern which also showed no indication of a hydrosodalite phase as observed for the gallosilicate analogue. This sample was therefore selected for analysis by powder neutron diffraction. Data were collected on D2B at ILL, Grenoble with an acquisition time of six hours.

The starting model used was that proposed by Wong [9] for aluminosilicate thiocyanate sodalite. Aluminium and germanium were placed on the 6(c) (¼, ½, 0) and 6(d) (¼, 0, ½) sites respectively, sodium on the 8(e) (x, x, x) site with $x \approx 0.18$ and the framework oxygen, O(1), on the 24(i) (x, y, z) site with $x \approx 0.14$, $y \approx 0.15$, $z \approx 0.45$. The structural model proposed for the thiocyanate group was one in which the $(SCN)^-$ group was centred with carbon on (0, 0, 0) and sulphur/nitrogen on (x, 0, 0). two different sites were allowed along (x, 0, 0) with $x \approx 0.15$ and $x \approx 0.17$ to account for the sulphur and nitrogen species. Occupation of this site would permit the $(SCN)^-$ ion to adopt one of three possible orientations along each coordinate axis in each cage. The location of the anion was difficult which can be attributed to disorder within the beta cage. This disorder could well arise from a rapidly rotating species, and thus low temperature studies would prove extremely useful. This would reduce rotation permitting more definite location of the cavity species.

Refinement of the framework proceeded smoothly, with acceptable temperature factors for all components. The non-framework ions were then introduced to the refinement process: sodium first followed by the linear $(SCN)^-$ anion. This process enabled the sodium to be relatively easily pinpointed, although location of the anion was far more difficult: all components of the anion showed high thermal parameters indicative of disorder caused by rapid rotation within the beta cage. The coordinates of the anion were also allowed to vary and yielded values of the x parameter characteristic of the relative sizes of the sulphur and nitrogen ions. Occupancies were also varied but showed no significant deviation from their preset values and as such were removed from the refinement process. Table 6.7 summarises the final refinement parameters, whilst Table 6.8 shows selected bond lengths and angles. The final profile fit to the data for $Na_8[AlGeO_4]_6(SCN)_2$ is shown in Figure 6.6.

Table 6.7 Final refinement parameters, atomic positions and thermal parameters ($Å^2$) with estimated errors in parentheses from powder neutron diffraction data at 298 K for sodium aluminogermanate thiocyanate sodalite

Atom	Site	Occupancy	x	y	z	B
Na	8(e)	1	0.1995(4)	0.1995(4)	0.1995(4)	3.97(8)
Al	6(d)	1	0.25	0	0.5	1.27(7)
Ge	6(c)	1	0.25	0.5	0	1.37(7)
O	24(i)	1	0.1466(2)	0.1476(2)	0.4412(2)	1.95(5)
C	2(a)	1	0	0	0	16.3(9)
S	12(f)	0.167	0.2061(4)	0	0	14.0(9)
N	12(f)	0.167	0.1468(6)	0	0	12.8(9)

a = 9.22567(7) Å

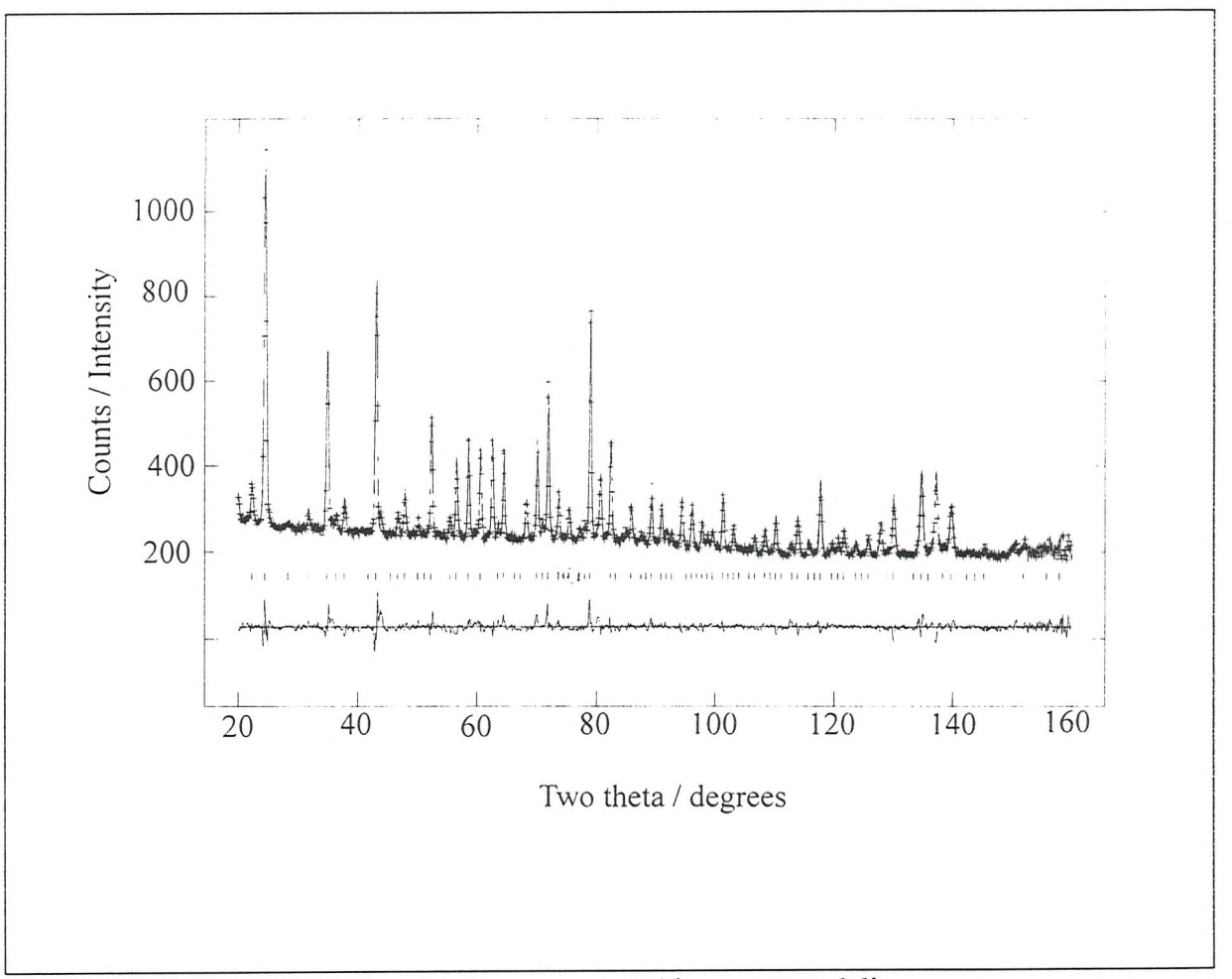

Figure 6.6 PND profile fit for aluminogermanate thiocyanate sodalite.

Table 6.8 Selected derived framework bond distances (Å) and angles (°) from powder neutron diffraction data for sodium aluminogermanate thiocyanate sodalite at 298 K with estimated errors in parentheses.

Parameter	Final Refinement Value
Al-O	1.747(4)
Ge-O	1.737(3)
Na-O x3	2.333(1)
Na-O x3	3.112(2)
Na-S	2.703(2)
Na-N	2.648(2)
C-S	1.802(1)
C-N	1.254(1)
Al-O(1)-Ge	138.74(3)
O(1)-Al-O(1) x2	113.87(6)
O(1)-Al-O(1) x4	107.32(5)
O(1)-Ge-O(1) x2	114.10(4)
O(1)-Ge-O(1) x4	107.22(8)

The work of Wong [9] reports structural data for aluminosilicate thiocyanate sodalite, and it is interesting to make a comparison between that and the results obtained in this study. A framework bond angle Al-O-Si of 143.06 ° compares with that of 138.74 ° for Al-O-Ge; this illustrates the greater relative cell collapse of the aluminogermanate framework compared with its aluminosilicate derivative for the same enclathrated anion as expected. A cell parameter of 9.0732 Å for the aluminosilicate was obtained, whereas the aluminogermanate refined cell was 9.2257 Å, and once again the size increase on substituting silicon by germanium is that which is expected. For the aluminosilicate thiocyanate sample, no details regarding refined parameters for the $(SCN)^-$ anion were given, and thus no comparison can be drawn.

A PND study of NaSCN at 9 K has been carried out by Bats *et al.* [15], and allows a comparison between bond distances for thiocyanate as the free salt and as contained in the sodalite. In the sodium salt, the C-N and C-S distances are 1.178 and 1.647 Å respectively, compared with 1.254 and 1.802 Å for the sodalite. It is clear that the bond

distances for the thiocyanate anion within the sodalite are somewhat longer than for the free salt. Na-N and Na-S distances found in the sodium salt are 2.582 and 2.891 Å, compared with 2.647 and 2.703 Å respectively for the sodium sodalite. The sodium to nitrogen distances are in reasonable agreement, although the sodium to sulphur distance in the sodalite is rather shorter than that of the free salt. The distances pertaining to the thiocyanate anion entrapped within the aluminogermanate beta cage are in general agreement with those of the free salt, with the discrepancies highlighting the difficulty in accurately locating the disordered anion within the sodalite cage at ambient temperature. A low temperature PND study would prove extremely useful in pinpointing the position of the $(SCN)^-$ anion.

6.4.3 Thermal Properties of Thiocyanate Sodalites

It has been previously documented that aluminosilicate thiocyanate [9] sodalites can be thermally degraded to form ultramarines, the colour of which are directly related to the particular heating conditions employed. In this work a variety of thermal treatments were carried out, to establish the conditions appropriate to forming the differing colours available form the thiocyanate species. In addition to the initial heat treatments in air, the effect of altering the atmosphere in which the oxidation is carried out has been studied.

Table 6.9 Thermal treatment of $Na_8[AlSiO_4]_6.(SCN)_2$ monitored by UV/VIS spectroscopy

Time/hours	S_2^-/S_3^- Ratio	Colour
0	-	white
0.25	3	green
0.5	2.5	green/blue
1	2	blue/green
2	1.5	blue
5	0.7	dark blue
16	-	white

The work of Wong has shown that 800 °C is a suitable temperature at which to perform the thermal treatment, and thus this was the temperature at which the comparison

of heating times and atmospheres was carried out. These heat treatments were followed by UV/VIS spectroscopy, and in particular the relative intensities of the S_2^- band at ≈ 400 nm and the S_3^- band at ≈ 600 nm. Initially thermal treatments were carried out in a box furnace by placing the sample directly into a furnace preset at 800 °C and then removing the sample after the required time period; i.e. there was no gradual heating or cooling of the sample. Results are displayed in Table 6.9.

A comparison of individual intensities of the S_2^- and S_3^- bands cannot be made for different samples, since the actual intensity is governed by parameters such as particle size. Since such parameters may differ significantly from one sample to another, direct comparison cannot be considered valid: i.e. the level of absorbance of a certain band cannot be directly compared with that in a different sample. Comparison between these bands for one particular sample can, however, be made and yields relevant information regarding the degree of oxidation of the $(SCN)^-$ anion which has taken place. The level of oxidation, monitored by the ratio of S_2^-/S_3^- in the UV/VIS spectrum dictates the colour of the material: as the amount of S_3^- radical rises the sample takes on a progressively bluer shade. At a given temperature the level of S_3^- increases with heating time due to gradual oxidation of the sulphur; at 800 °C this reaches a maximum value after 5 hours and then begins to tail off as oxidation continues through to $(SO_4)^{2-}$ at which point the colour fades from blue to white. This corresponds to complete oxidation of the $(SCN)^-$ anion via $(S_n)^-$ through to S(VI) in $(SO_4)^{2-}$ observed after 16 hours at 800 °C. An interesting point to note is that the sodalite has been converted to a noselite in which there are divalent sulphate anions in alternate cages. The presence of sulphate was confirmed using IR spectroscopy.

The oxidation of thiocyanate can also be followed by IR spectroscopy. Before heating, the IR spectrum shows an intense band at 2071 cm^{-1} corresponding to the C≡N stretch of the $(SCN)^-$ anion. As heating commences, evolution of a band at ≈ 2170 cm^{-1} is observed, caused by the C≡N stretch of the $(OCN)^-$, which is formed at the expense of the $(SCN)^-$ anion as oxidation proceeds. There is simultaneous diminution of the $(SCN)^-$ anion and augmentation of the $(OCN)^-$ anion. It is believed that the $(OCN)^-$ then reacts with the SO_2 which is produced to form $(S_n)^-$ with release of the carbon and nitrogen as gases in the form of CO_2 and NO_2. These bands disappear totally after five hours at 800 °C, as the carbon and nitrogen have been expelled from the beta cages.

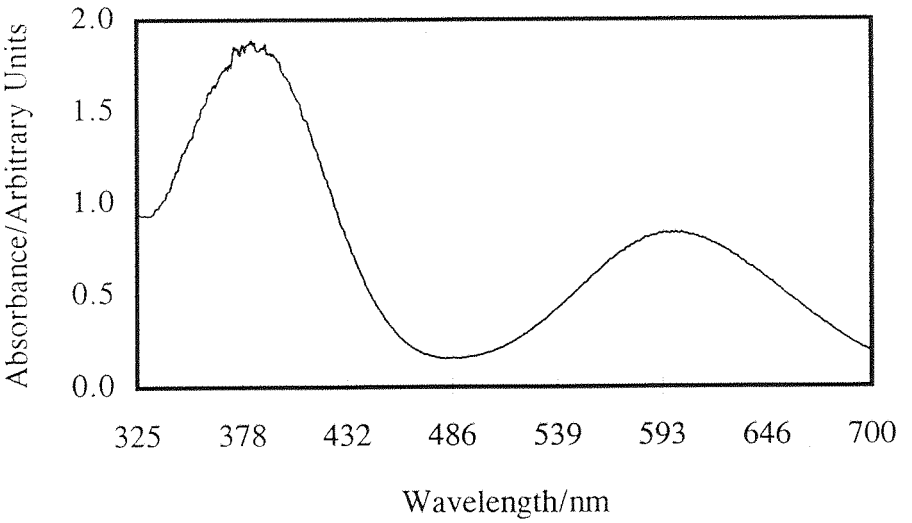

t=1 h

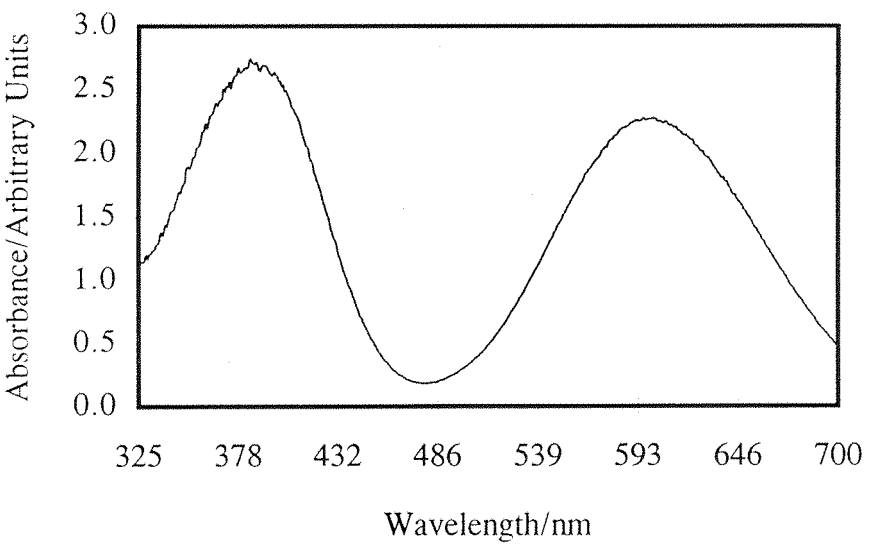

t=2.5 h

Figure 6.7 UV/VIS spectra of heat treated aluminosilicate thiocyanate sodalites

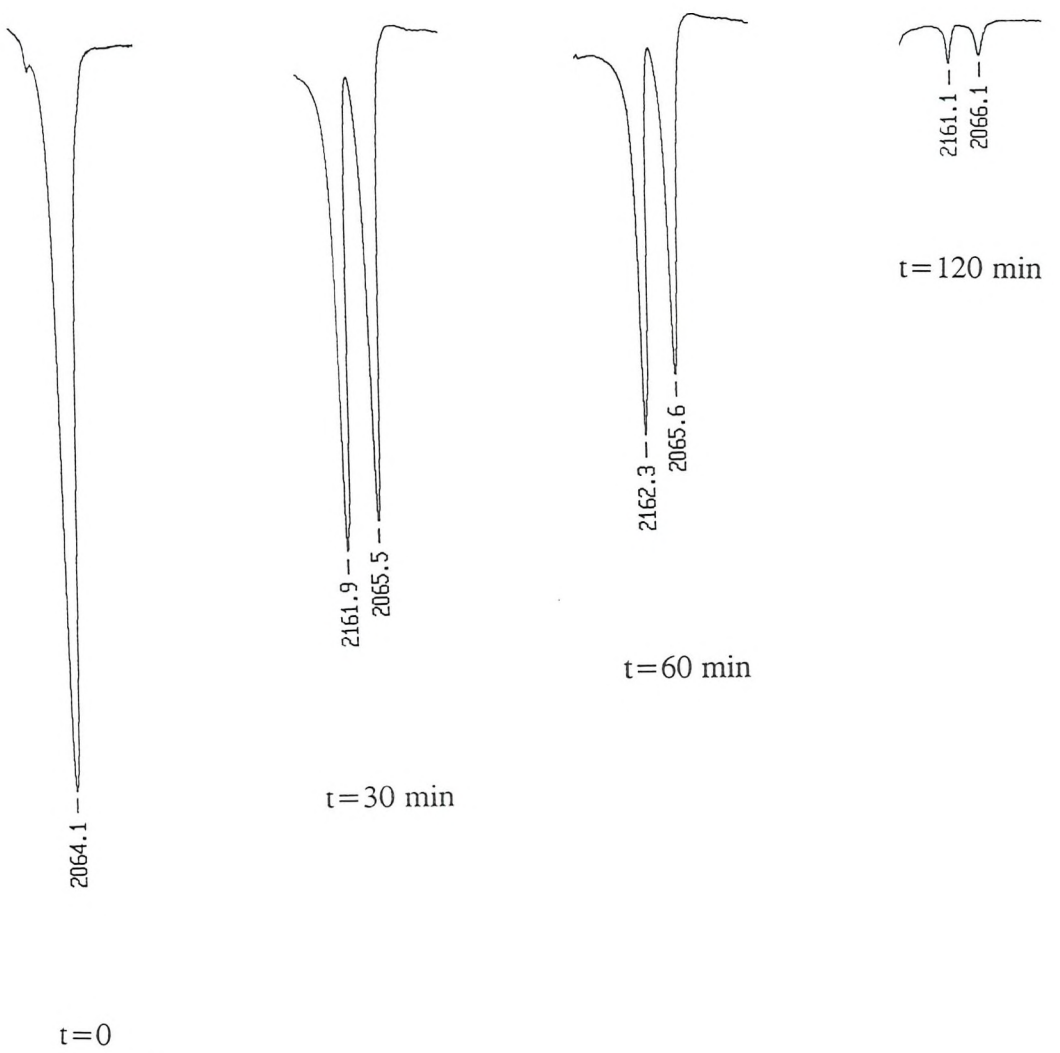

Figure 6.8 IR spectra of heat treated aluminosilicate thiocyanate sodalites

For the study of variation of atmosphere on the thiocyanate sodalite, reactions had to be performed in a fundamentally different manner from those in a box furnace. The use of H_2S meant that the sample could not simply be removed at 800 °C after the required time period since it would create a safety hazard: opening of the tube furnace at 800 °C would allow oxygen from the air to enter the reaction which would create an explosive mixture with the H_2S present. Thus reactions under different atmospheres were carried out in a tube furnace in which the temperature was raised from ambient to 800 °C, held at that temperature for one hour, and then cooled to room temperature before the sample was removed. Clearly, direct comparison cannot be made with the results shown in Table 6.10 since the sample is subjected to thermal treatment during the processes of heating and cooling. A control experiment using air as the reaction atmosphere was thus carried out.

Table 6.10 Thermal treatment of $Na_8[AlSiO_4]_6.(SCN)_2$ under different atmospheres

Atmosphere	S_2^-/S_3^- Ratio	Colour
Air	0.9	Blue
N_2	-	White
O_2	0.8	Dark blue
H_2S/O_2	0.7	Dark blue

For the case where the atmosphere was H_2S, the sample was subjected to the procedure described above, and the sample removed. It was then reheated under oxygen in the same manner. The purpose of this particular experiment was to ascertain whether additional sulphur could be introduced within the beta cages thus giving rise to a more intensely coloured ultramarine. The results of this study are presented in Table 6.10. It can be seen that heating under nitrogen does not yield an ultramarine, which is exactly as expected since there can be no oxidation of the $(SCN)^-$ anion. Under an O_2 atmosphere increased oxidation of the sulphur compared with air over the same reaction period leads to a deeper colour and greater predominance of the S_3^- radical. Treatment with hydrogen sulphide prior to reaction under oxygen slightly darkens the shade of the resultant material: although the sample clearly has been heated for double the length of time as the other samples, H_2S is a reducing agent and as such there ought to be no preliminary oxidation of the thiocyanate sodalite before treatment with oxygen. Comparison between the samples heated under pure oxygen and hydrogen sulphide/oxygen can thus be justified.

In general the oxidative decomposition of thiocyanate sodalite can be represented by the following reaction scheme:

$$Na_8[AlSiO_4]_6.(SCN)_2.xH_2O \text{ white}$$
$$\downarrow 200\ ^\circ C$$
$$Na_8[AlSiO_4]_6.(SCN)_2 \text{ white}$$
$$\downarrow 500\ ^\circ C$$
$$Na_8[AlSiO_4]_6.(SCN,\ OCN,\ S_3^-,\ S_2^-) \quad \text{blue/green}$$
$$\downarrow 600\ ^\circ C$$
$$Na_8[AlSiO_4]_6.(S_3^-,\ S_2^-) \text{ blue}$$
$$\downarrow 850\ ^\circ C$$
$$Na_8[AlSiO_4]_6.(SO_4) \text{ white}$$

From the results obtained it is clear that the shade can be easily tailored to suit the colourific requirements of the material. Variation of both temperature and time allows the level of oxidation to be controlled in much the same way as the present industrial preparative conditions for ultramarine are controlled via kiln temperature [14]. However, thiocyanate sodalite is quickly and easily synthesised, followed by rapid conversion to ultramarine making this a viable alternative to the current method of ultramarine production. It could possibly be envisaged that a batch process could be used in which the expended reactants are simply replaced systematically ensuring that the reaction medium at all times has a sufficient quantity of each reagent to allow reaction to proceed, with the products periodically removed by filtration.

Aluminogermanate and gallosilicate thiocyanate sodalites were also prepared and subjected to thermal degradation in order to produce ultramarine analogues. In a similar manner to aluminosilicate thiocyanate sodalite, heat treatment produces the $(OCN)^-$ anion within the beta cage with S_2^- and S_3^- also observed using UV/VIS spectroscopy. However, the deep colour attainable for the aluminosilicate was not able to be obtained using either the gallosilicate or aluminogermanate samples. This was not surprising for the gallosilcate since PXD had clearly shown the sample to be a mixture of hydro- and thiocyanate sodalites. The reason for the paler shade of the aluminogermanate compared with the aluminosilicate is not clear; a cell parameter of 9.23 Å compared with 9.09 Å for the

aluminosilicate material does indicate that a large level of the $(SCN)^-$ ion has been successfully entrapped within the beta cage as does the strong absorption in the IR spectrum. Once again prolonged heating gives rise to complete oxidation of the sulphur leading to the formation of $Na_8[AlGeO_4]_6.(SO_4)$. However, for the aluminogermanate and gallosilicate sodalites this process reaches completion much more quickly than for the aluminosilicate at the same temperature. The IR spectrum for $Na_8[AlGeO_4]_6.(SCN)_2$ is shown in Figure 6.9. At 800 °C, a pale green colour is obtained after five minutes, a further five minutes producing a light blue. This colour remains unchanged for a further 45 minutes, after which the colour fades to white as oxidation through to $(SO_4)^{2-}$ is completed.

The gallosilicate sample shows almost identical thermal properties as the aluminogermanate with the same degree of reduced temperature stability compared with the parent aluminosilicate material.

6.4.4 Silver Doping Studies

The replacement of sodium by silver as for the chromate materials allows the colour of ultramarines to be tailored to the desired shade caused by a red shift in the UV/VIS spectrum. Introduction of silver can be varied via the reaction temperature of the aqueous exchange, carried out normally at 100 °C. Reduction in reaction temperature slows the exchange process and allows the amount of silver doping to be controlled. UV/VIS spectra, as shown in Figure 6.10, in which ultramarine blue has been treated to show how varying the degree of silver exchange allows the spectral shift, and hence the observed colour, to be tailored.

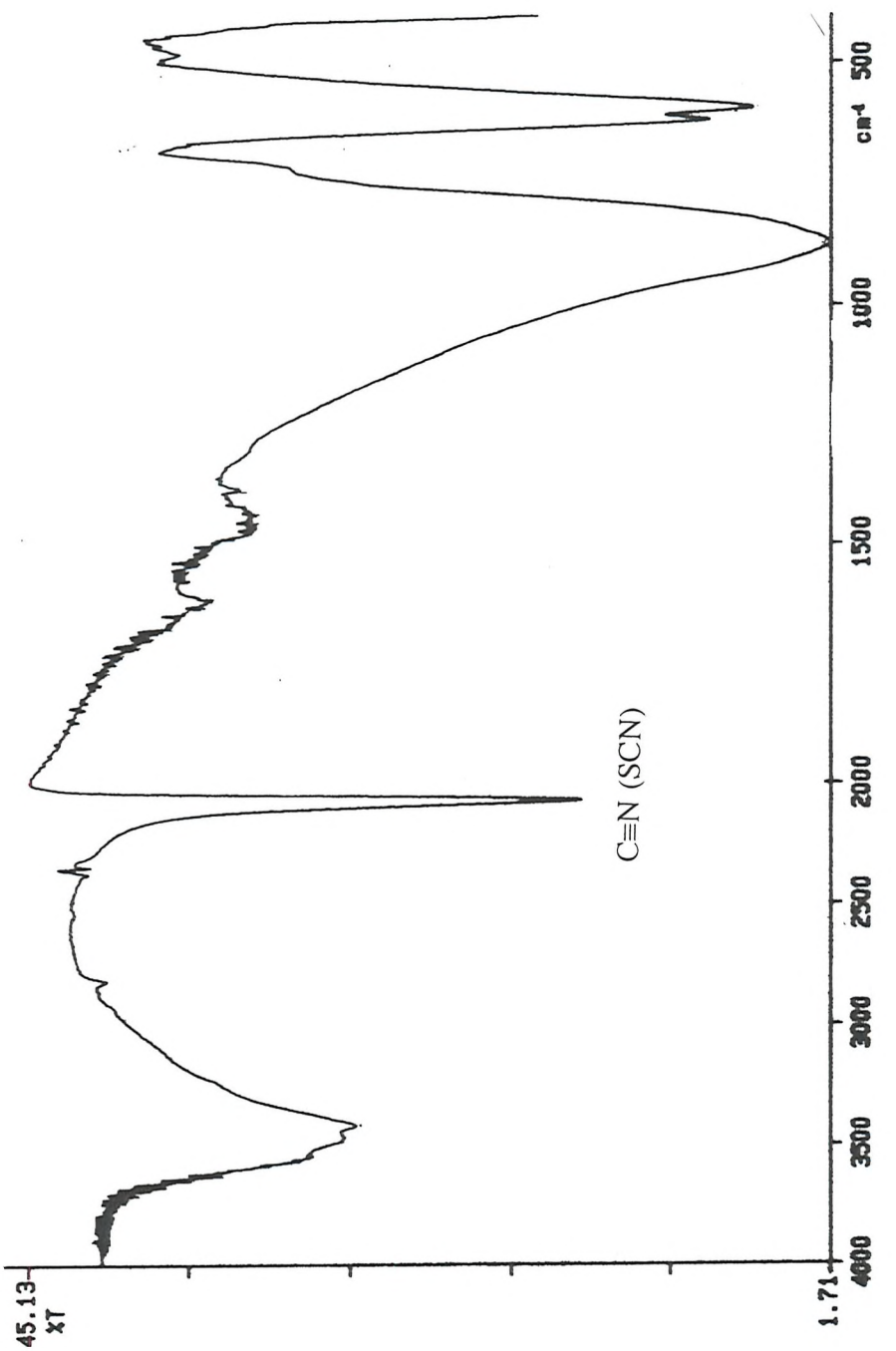

Figure 6.9 IR spectrum of aluminogermanate thiocyanate sodalite

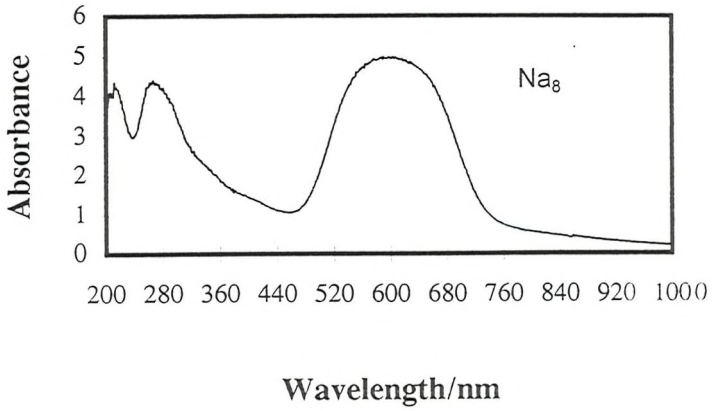

λ_{max} 590 nm

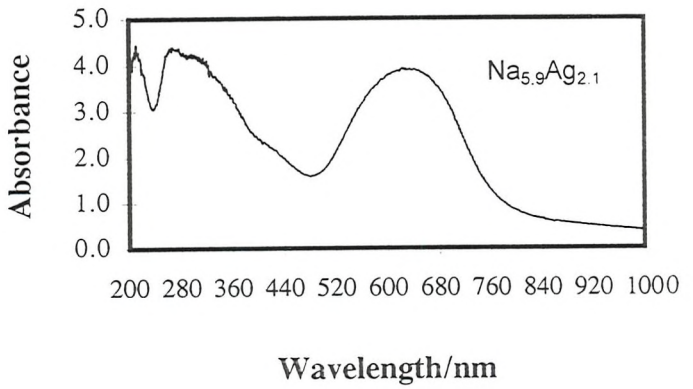

λ_{max} 626 nm

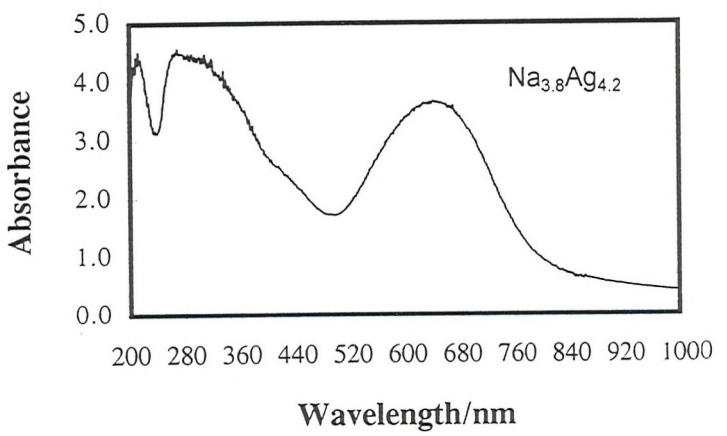

λ_{max} 637 nm

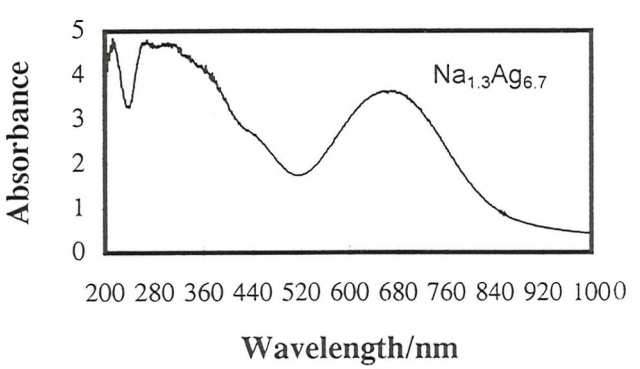

λ_{max} 674 nm

Figure 6.10 UV/VIS spectra of silver exchanged ultramarine blue.

6.5 ALTERNATIVE SULPHUR ULTRAMARINE PRECURSORS

The entrapment of $(S_2O_3)^{2-}$ results in the formation of cancrinites for aluminosilicates, gallosilicates and aluminogermanate framework materials. In a similar way to thiocyanate sodalites thermal treatment of these white parent materials can lead to colouration caused by the formation of polysulphide radicals in the cavities. However, the process of thermal degradation for the two precursors is rather different. As outlined above, thiocyanates decompose via $(OCN)^{\cdot}$ which then reacts with SO_2 within the sodalite cages to form $(S_n)^{\cdot}$ radicals within the framework voids. For the thiosulphate cancrinite however, it is proposed that a thermally activated diffusion of sulphur species through the open channel network occurs, resulting in the formation of polysulphide radical anions [16].

As for the thiocyanates, 800 °C was selected for the thermal treatment; this is the same as that used by Lindner and Reinen in their study of sodium aluminosilicate thiosulphate cancrinite[16]. Heating is accompanied by a gradual colour change through pale green to blue as time approaches one hour. This corresponds to the optimum reaction time under air at 800 °C for the production of a material analogous to ultramarine blue. Structural studies performed on intermediate phases show that the cancrinite structure is preserved during the production of the polysulphide species. It was hoped that in addition to thermally degrading the $(S_2O_3)^{2-}$ anion, the cancrinite structure could be converted to sodalite leaving a more condensed framework; however, no evidence was obtained for this conversion, and continued heating simply led to the destruction of the framework after 16 hours at 800 °C.

Analogous processes were observed for thermal treatment of gallosilicate and aluminogermanate thiosulphate cancrinites, with again no evidence of conversion to sodalitic framework structure observed. UV/VIS spectroscopy allows the process of thermal degradation to be followed and spectra of the blue shade obtained are analogous to those obtained using thiocyanate as the precursor.

The increased size of the aluminogermanate beta cage allows the metabisulphite anion, $(S_2O_5)^{2-}$, to be entrapped via hydrothermal synthesis. This is confirmed by the cancrinitic nature of the product as seen by PXD, and by the IR bands characteristic of $(S_2O_5)^{2-}$ observed at 1138 cm^{-1}. However, despite several attempts at its synthesis, a product of high crystallinity was not obtained. No structural characterisation was performed; thermal treatment to yield ultramarine at 800 °C in air produced only a very

pale bluish tinge and thus aluminogermanate metabisulphite cancrinite could not be classed as a precursor to ultramarine.

6.6 SELENIUM ULTRAMARINE

Sodalites containing selenium are far less well documented than their sulphur analogues due to the difficulty in their synthesis. Lindner and Reinen [17] reported the hydrothermal synthesis of selenium ultramarine in 1994 at 600 °C by direct preparation from SiO_2, Al_2O_3, NaOH and elemental Se, or alternatively from Kaolin, SiO_2, Na_2CO_3, charcoal and Se powder at 780 °C. More recently, Lindner *et al.* [18] successfully introduced selenium into the cancrinite network using hydrothermal methods. The experimental procedure involved sealing SiO_2, Al_2O_3, NaOH, NaCl and Se in a gold capsule and heating to 600 °C, creating autogeneous pressure of 1 kbar. After 14 days reaction, analysis showed the product to be a cancrinite with a slight impurity corresponding to selenium ultramarine. The cooling process was shown to affect the relative proportions of the two materials, with the level of sodalite increasing as the vessel is cooled more rapidly. They proposed that the red/brown colouration was caused by the presence of $(Se_2)^{2-}$ and $(Se_2)^{-}$ within the channels. Such methods for the production of selenium pigments are rather drastic, and large scale preparation could not be feasibly envisaged. Synthetic processes which would yield selenium ultramarine at lower temperature and pressure were sought. Since thiocyanate sodalite has been shown to be a suitable precursor to sulphur ultramarine, an analogous procedure based on selenocyanate was attempted.

The main problem associated with this method is the size of the anion. Whereas the entrapment of Se alone does not present particular problems for the aluminosilicate beta cage, the $(SeCN)^{-}$ anion is considerably bigger and hence levels of encapsulation would therefore be expected to be low. It has already been seen that the $(SCN)^{-}$ anion does not promote sodalite formation to any great degree, and hence experimental conditions must be carefully tailored if the preparation of hydroxysodalite is to be avoided. Such problems are expected to be more prevalent with the larger Se containing anion.

An additional inconvenience is the pre-treatment necessary to form the sodium selenocyanate. The potassium analogue is commonly available, whereas the sodium version is not, and hence ion exchange is necessary. Whilst this is not a problem, it does add to the required experimental time. The Hund method [3] was used in an attempt to form aluminosilicate selenocyanate sodalite, but despite several attempts to optimise the experimental procedure, each time hydroxysodalite was obtained. This was attributed to size constraints of the aluminosilicate cage, and hence the synthesis of an

aluminogermanate selenocyanate was attempted. This was undertaken at 150 °C using hydrothermal means, and the resultant sodalite contained a mixture of hydroxide and selenocyanate anions; this was confirmed using IR spectroscopy, with the C≡N stretch of the $(SeCN)^-$ anion clearly visible at 2071 cm^{-1}. Subsequent experiments showed that the temperature could be reduced to 90 °C without detriment to the product.

Following synthesis, heat treatment of the selenocyanate material was undertaken. Since 800 °C had been shown to be a suitable temperature for the decomposition of the thiocyanate, this was the temperature selected for the Se species. The sample was heated in an alumina boat at 800 °C in air and examined at five minute intervals. In an analogous manner to the $(SCN)^-$ sodalite, oxidation proceeded via $(Se_n)^-$ as the species responsible for the colouration. Further oxidation with heating was observed until a white powder was obtained: this corresponded to the $(SeO_3)^{2-}$ species in contrast to $(SO_4)^{2-}$ as seen for the sulphur material, indicating that oxidation does not proceed to such a degree using selenium. The transformation to $Na_8[AlGeO_4]_6.SeO_3$ occurred after 60 minutes at 800 °C, indicating that this compound does show the necessary thermal stability for application with PVC or ceramic materials.

The blood red colour of selenium ultramarine was not able to be matched using this experimental route, since the level of selenium incorporation within the sodalite was low. However, despite this factor, an orange colour was attained, and could well provide an alternative to the cadmium sulphoselenides which are presently in widespread use. Throughout the heat treatment the integrity of the sodalite framework was kept intact.

Figure 6.11 shows the IR spectrum for $Na_8[AlGeO_4]_6.(Se_n)_2$ with spectra for the heat treated materials also presented. UV/VIS spectroscopy has been used to confirm that the species responsible for the colour is the $(Se_2)^-$ species identified by its characteristic absorption bands at ≈ 365 nm and ≈ 495 nm.

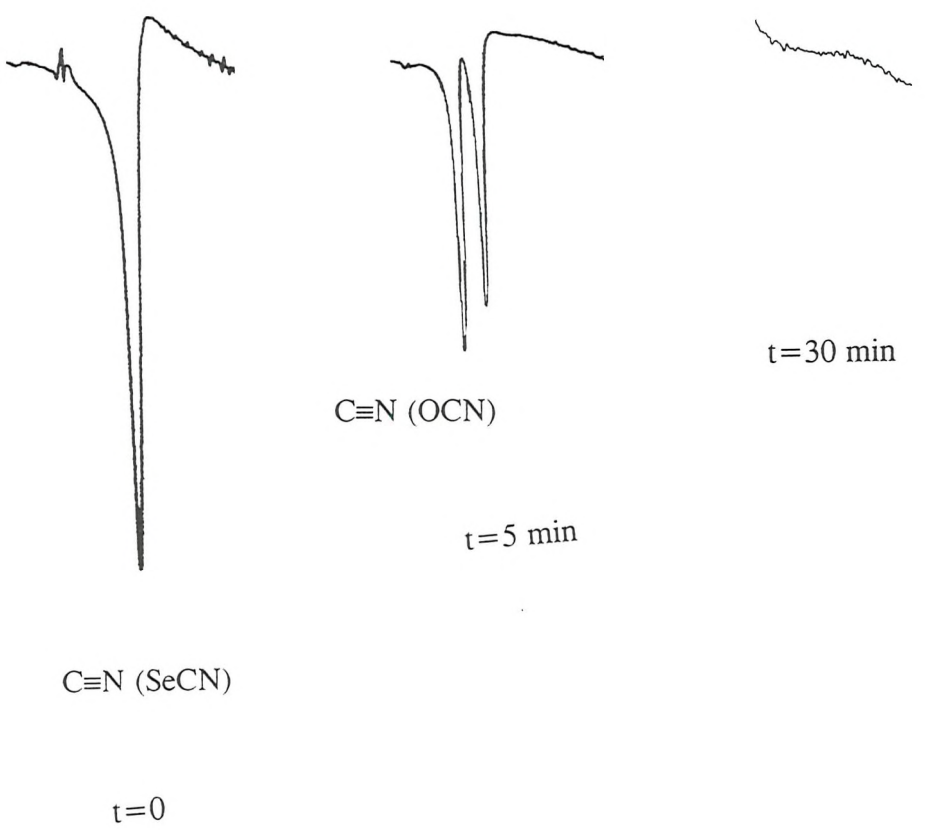

Figure 6.11 IR spectra for heat treated aluminogermanate selenocyanate sodalite

6.7 CONCLUSIONS

Aluminosilicate sodalites have been shown to be extremely suited to the entrapment of a wide range of ions including halides, tetrahedral oxo-anions and the linear thiocyanate and selenocyanate anions. This provides the opportunity to produce coloured materials like the deep purple permanganate sodalite, the bright yellow chromate noselite and the dark green manganate cancrinite. The thiocyanate sodalites have been shown to be excellent precursors to ultramarine, shown in Figure 6.12, and the heat treatment can be varied to prepare different ultramarine shades.The versatility of the sodalite structure is illustrated by its ability to accommodate various non-framework cations via post synthetic treatment of the parent sodium sodalites. This in turn allows coloured materials to be tailored to the desired shades by careful control of the conditions employed for ion exchange. Whilst potassium and lithium introduction change the shade a little , silver exchange has a far more dramatic inluence on the colour: ultramarine green becomes yellow, ultramarine blue becomes green and chromate yellow is turned rust coloured all by the simple replacement of sodium by silver in the cages. These colour changes can be curtailed somewhat if intermediate shades are required by reduction in reaction time, reaction temperature or the concentration of the silver nitrate used.

Isomorphous replacement of aluminium and silicon by gallium and germanium has been completed to yield a large range of sodalite and cancrinite materials. The reason for the success in preparing so many different framework materials can be put down to the synthetic methods devised in this work which entail both hydrothermal and low temperature solution methods. This permits sensitive anions such as permanganate to be readily entrapped: hydrothermal reaction results in decomposition to manganese (IV) oxide, whereas the adaption to solution allows the anion to be successfully stabilised. Ultramarine equivalents containing gallium and germanium have been prepared and the variation in optical properties followed by UV/VIS spectroscopy. The increased cage size of the aluminogermanate over the aluminosilicate has been exploited to form a sodalite containing the selenocyanate anion. This species can be thermally altered by intra-cage decomposition of the anion to form a seleniun ultramarine. Although the level of selenium encapsulated is low due to the bulk of the $(SeCN)^-$ anion, the orange colour obtained is certainly significant and perhaps subsequent experimental variation may allow this level of enclthration to be augmented.

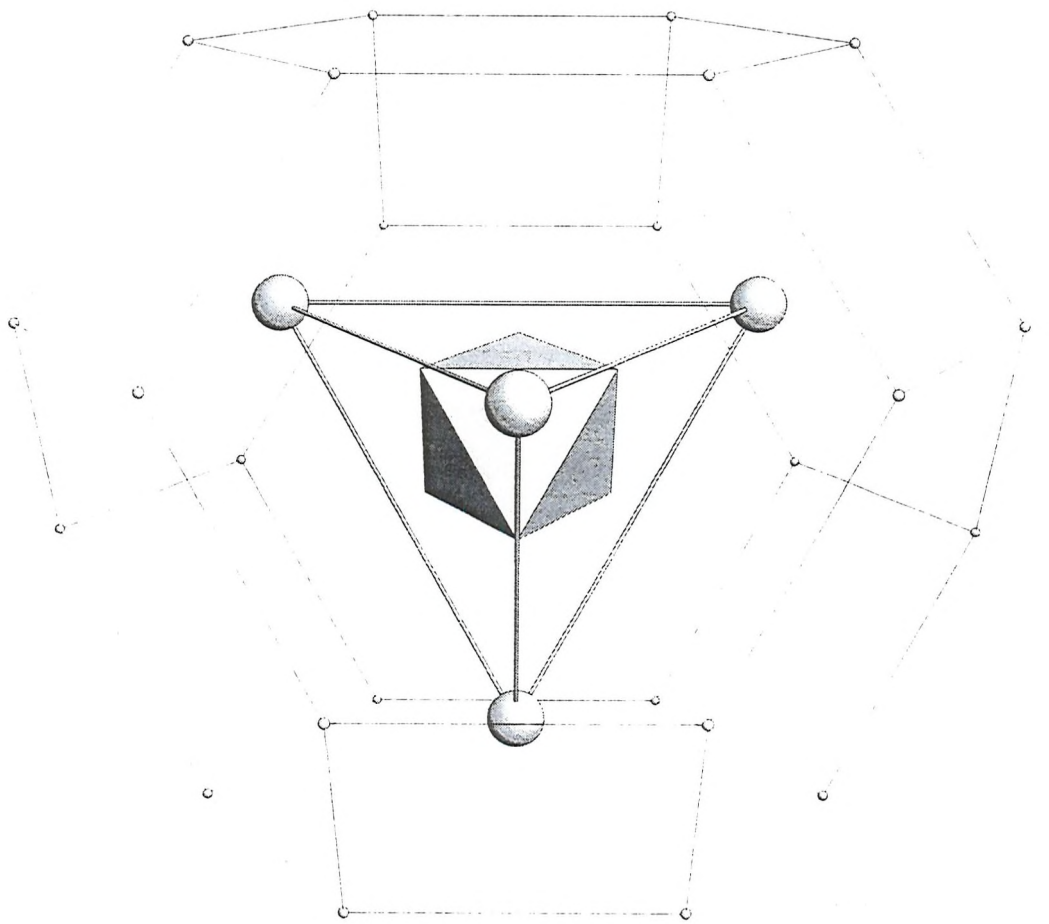

Figure 6.12 Representation of ultramarine

Diffraction studies on these framework modified sodalites have illustrated how their structure mirrors those adopted by the aluminosilicate analogues in terms of rotational disorder associated with the central anion.

6.8 REFERENCES

[1] S.E. Dann, *Personal communication*, University of Southampton (1996).

[2] R.M. Barrer, J.F. Cole, and H. Sticher, *J. Chem. Soc.*, A**10**, 2475 (1968).

[3] F. Hund, *Z. Anorg. Allg. Chem.*, **511**, 225 (1984).

[4] M.T. Weller and K.E. Haworth, *J. Chem. Soc., Chem. Commun.*, **10**, 373 (1991).

[5] M.E. Brenchley and M.T. Weller, *Zeolites*, **14**, 682 (1994).

[6] F.A. Cotton and G. Wilkinson, "Advanced Inorganic Chemistry", Fifth Edition, Wiley-Interscience, New York (1988).

[7] A.C. Larson and R.B. Von Dreele, Generalized Structure Analysis System, MS-H805, Los Alamos, NM 87545 (1990).

[8] P.J. Mead, *Ph.D. Thesis*, University of Southampton (1996).

[9] G. Wong, *Ph.D. Thesis*, University of Southampton (1990).

[10] M.E. Brenchley, *Ph.D. Thesis*, University of Southampton (1994).

[11] R.M. Barrer, J.F. Cole, and H. Sticher, *J. Chem. Soc.*, A**10**, 2475 (1968).

[12] K. Nakamoto, "Infrared and Raman Spectra of Inorganic and Coordination Compounds", Third Edition, Wiley-Interscience, New York (1978).

[13] I.F. Chang, *J. Electrochem. Soc.*, **121**, 815(1974).

[14] G. Buxbaum (ed.), "Industrial Inorganic Pigments", VCH, Weinheim, Federal Republic of Germany (1993).

[15] J.W. Bats, P. Coppens and A. Kvick, *Acta Cryst.*, **B33**, 1534 (1977).

[16] G.G. Lindner, W. Massa and D. Reinen, *J. Solid State Chem.*, **117**, 386 (1995).

[17] G.G. Lindner and D. Reinen, *Z. Anorg. Allg. Chem.*, **620**, 1321 (1994).

[18] G.G. Lindner, K. Hoffmann, K. Witke, D. Reinen, C. Heinemann and W. Koch, *J. Solid State Chem.*, **126**, 50 (1996).

Chapter Seven

SPECTROSCOPIC INVESTIGATIONS

7.1 INTRODUCTION

Structural characterisation of framework materials is commonly achieved via PXD and PND. These methods allow the elucidation of parameters such as atomic positions, bond distances and bond angles. Although these methods yield important data, characterisation should not be limited to diffraction alone. Spectroscopic techniques such as MASNMR, FT-IR and UV/VIS also have much to offer and when used in conjunction with diffraction give comprehensive information regarding the materials in question. It is vital to use all the characterisation tools available, since the interpretation of a data set from a solitary measurment can often lead to false conclusions being drawn, a problem which is easily circumvented by consideration of supplementary information. Spectroscopic techniques have been shown to yield results which can be readily correlated with results derived from diffraction, with structural parameters such as framework bond distances and angles having a marked effect on MASNMR chemical shift and IR absorption bands. In addition to providing complementary data to diffraction studies, these spectroscopic methods are invaluable for the study of poorly crystalline or amorphous materials. It is these two techniques which will be detailed in this chapter; UV/VIS spectroscopy has already been discussed for specific materials in the previous chapter.

7.2 MAGIC ANGLE SPINNING NUCLEAR MAGNETIC RESONANCE (MASNMR) SPECTROSCOPY

Despite the wealth of information provided by powder x-ray and neutron diffraction, they are bulk techniques and as such only yield information relating to the average structure of the material under investigation. In addition, x-ray diffraction does not locate the positions of light atoms very accurately, and cannot readily differentiate between atoms which are adjacent to one another in the periodic table such as aluminium and silicon; since the majority of zeolite materials contain silicon and aluminium in their frameworks, this can prove a major problem. Neutron diffraction permits these species to be distinguished far more easily, and also allows the location of light atoms to be more readily defined. However, it cannot provide detailed information concerning the local environment of framework cations.

NMR spectroscopy is governed by local chemical environment rather than long range periodicity, and thus provides an excellent complementary technique to diffraction methods. ^{29}Si and ^{27}Al MASNMR spectroscopy have been widely applied to zeolitic systems, yielding information concerning framework ordering, framework composition, determination of distinct crystallographic sites, factors including acidity, mechanisms for dealumination, and correlations between chemical shift and framework structure. ^{29}Si is a particularly favourable nucleus since it has a low natural abundance giving a dilute spin system and has $I=½$ which reduces the problems associated with quadrupolar broadening and allows the determination of local silicon environments in most cases. The majority of MASNMR investigations have thus been directed towards the ^{29}Si nucleus, although more recently with the advent of computer software to delineate and simulate quadrupolar effects, other nuclei such as ^{27}Al and ^{71}Ga have also been successfully probed. Non-framework species can also be explored to yield data regarding co-ordination and mobility of M^+ exchangeable cations in addition to co-ordination, geometry and mobility of guest molecules or anions [1-6].

The most useful parameter available from MASNMR spectra for characterising framework structures is the chemical shift which may be directly related to a number of local structural features. The most important factors include the nature of the neighbouring tetrahedral cations (T'), the T-O-T' bond angle and the T-O distance though additional factors, for example the distribution of non framework cations in the vicinity of the NMR active nucleus, may also be of influence.

In order to parameterise the various structural effects on chemical shift it is necessary to study a comprehensive range of materials. This may be done in the sodalite system where it is possible to enclathrate a wide variety of anions within this framework type; this allows the comparison of chemical shift data for a particular value of cell parameter, T-O-T' angle or T-O distance and thus permits a more accurate elucidation of the direct effect of tetrahedral framework cation type on resonance position.

This work reports the MASNMR data for a large series of sodalite framework species $M_8[ABO_4]_6.X_2$, where A = Al and Ga, and B = Si and Ge, and correlations of these data with selected structural parameters. The differing effects of particular framework factors such as geometric and electrostatic on the chemical shift for ^{29}Si, ^{27}Al and ^{71}Ga can thus be resolved.

7.2.1 Previous Studies on ^{29}Si MASNMR Spectroscopy

The study of Lipmaa [7, 8] on silicate systems revealed that, as in the case of solution spectra, ^{29}Si chemical shift values fall within distinct ranges. These are governed by the number of silicon atoms attached at the vertices of a particular SiO_4 tetrahedron, denoted by Q^{4-n}, where n = 0-4, and represents the number of adjacent silicon atoms.

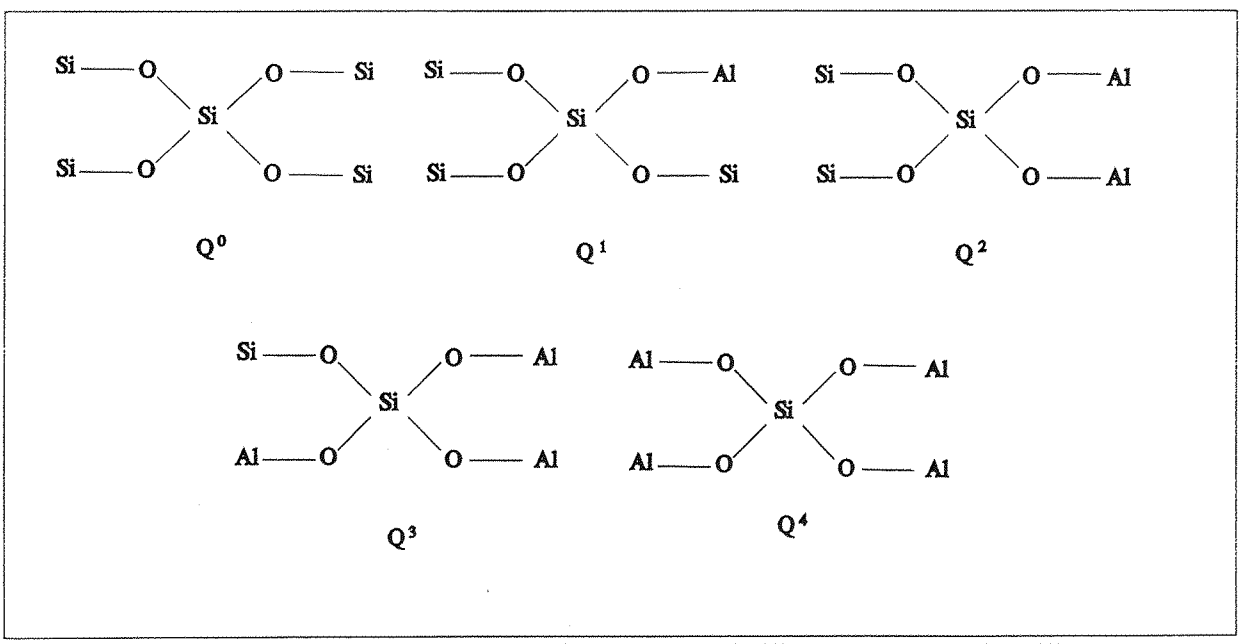

Figure 7.1 MASNMR chemical shift environments for silicates and aluminosilicates

For zeolites the ^{29}Si spectra depend on whether the four atoms at the corners of the SiO_4 tetrahedron are Si or Al. The resultant chemical shift ranges have been shown to a first

approximation to be independent of non-framework cations present or the specific zeolite structure, and are determined only by the local silicon environment. The five possible cases according to this idea are displayed in Figure 7.1, with the corresponding chemical shift ranges presented in Figure 7.2.

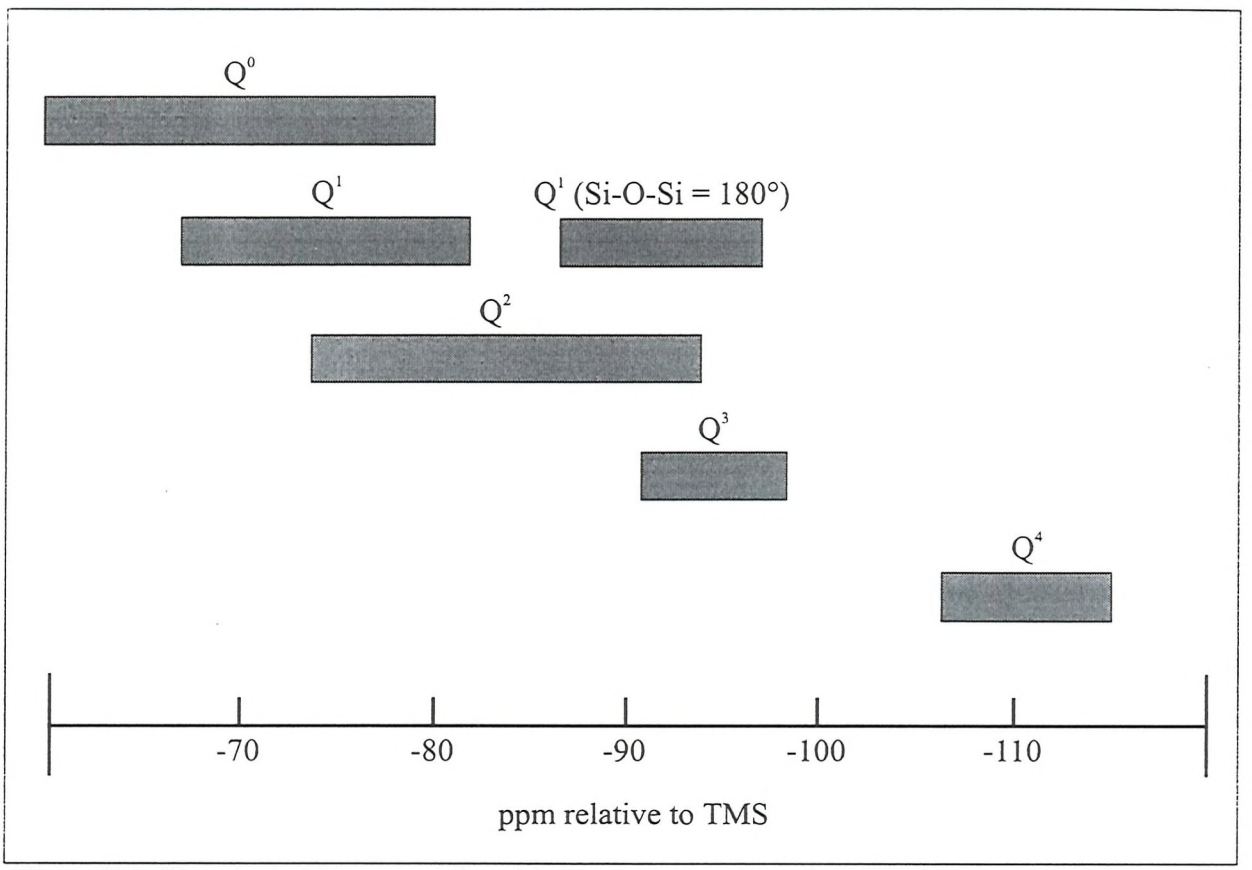

Figure7.2 Chemical shift ranges for silicates and aluminosilicates

According to Loewenstein's first rule [9], whenever two tetrahedra are linked via a common oxygen bridge the centre of only one of them can be occupied by Al, the other centre being occupied by Si or another small ion of electrovalence four or more such as phosphorous; despite certain exceptions such as the pure aluminates, this rule generally holds extremely well. The second rule proposed by Loewenstein says that whenever two aluminium ions are directly adjacent to the same oxygen at least one of them must have a coordination number of greater than four towards the oxygen. The application of these rules to zeolites implies a framework silicon to aluminium ratio of unity or above; in the case when this ratio is unity, Loewnstein's rules preclude any disorder of these framework species, resulting in a single Q^4 silicon environment and a single peak in the MASNMR spectrum. This is the case for the aluminosilicates and gallosilicates studied in this work, for which the ratio of Si:Al or Si:Ga is unity.

For aluminosilicates, the ^{29}Si chemical shift, δ, has been related to the average T-O-T bond angle, θ, for zeolites [10, 11] and for aluminosilicate sodalites by Weller and Wong [12]:

$$\delta \text{ / ppm} = 1.89 - 0.631\,\theta \text{ / }^{\circ} \qquad 7.1$$

Ramdas and Klinowski [13] examined the effect of aluminium content and average intra framework atomic distance on δ for a range of zeolitic compounds including TMA silica sodalite and proposed the following relationship:

$$\delta \text{ / ppm} = 143.03 + 7.95n - 20.34\,S\,d_{TT} \text{ / Å} \qquad 7.2$$

where n is the number of aluminiums surrounding each silicon, S d_{TT} is the sum of the four average Si-T distances around each $Si(OAl)_n(OSi)_{4-n}$ unit assuming Si-O(1) and Al-O(1) bond lengths of 1.62 and 1.75 Å respectively and hence defined as:

$$S\,d_{TT} \text{ / Å} = [3.37n + 3.24(4-n)]\sin(\theta/2) \qquad 7.3$$

The introduction of aluminium for silicon is stated as altering the paramagnetic contribution to δ (the 7.95n term), but does not appear highly significant for aluminosilicate sodalites compared with the deshielding of the silicon nucleus through electron withdrawal from the shared oxygen as the aluminium content is augmented.

The effective electronegativity of the four oxygens in the T-O framework bonds has been linked to the ^{29}Si chemical shift by Radeglia and Engelhardt [17, 18]. They used their previous observation [19] that the electronegativity of the oxygen depends on the s-hybridisation of the oxygen orbitals in the T-O bonds, in conjunction with the relation between the degree of s hybridisation and T-O-T bond angle proposed by Klessinger *et al.* [20] to form the correlation:

$$\delta \text{ / ppm} = \delta_0 \text{ / ppm} + an + b\cos\theta \text{ / } \cos(\theta - 1) \qquad 7.4$$

where δ_0, a and b are constants.

Sheriff and Grundy merged the correlation of Weller and Wong with that of Radeglia and Engelhardt for silicate materials [18]. The distance and angle of the mid-point of an adjacent T-O bond is related to δ, and linked also to the bond valence of the adjacent framework

atom. The degree of s hybridisation is then introduced to yield a correlation corresponding to the formula:

$$\delta \text{ / ppm} = -56.06 + 650.08\ \chi \qquad 7.5$$

with χ defined as:

$$\chi = \Sigma\ s\ ((1 - 3\cos^2\alpha)/3\ R^2)\ (\cos\theta / (\cos\theta - 1))) \qquad 7.6$$

where α is the angle between the T-O bond and Si-(T-O mid-point) and s is the bond valence defined as [19]:

$$s = \exp[(r_0 - r)/0.37] \qquad 7.7$$

where r_0 is the T-O distance taken from Brown and Altermatt [19] and r is the refined T-O bond distance.

7.2.2 Previous Studies on ^{27}Al MASNMR Spectroscopy

Similar correlations to ^{29}Si between chemical shift and structural parameters are evident for MASNMR spectra of the aluminium nucleus. However, since it possesses a quadrupolar moment, spectral line broadening can often be a problem; this can be reduced by using high spinning rates, or by the use of more complex techniques such as double angle or dynamic angle spinning spectroscopy. In general however, less research has been carried out on ^{27}Al due to spectral complication.

Jacobsen *et al.*[20] have adapted the relationships described above for ^{29}Si to aluminosilicate sodalites, correlating δ (^{27}Al) with T-O-T angle and the sum of the four Si-T distances:

$$\delta \text{ / ppm} = 163.982 - 0.724\ \theta / ^\circ \qquad 7.8$$

$$\delta \text{ / ppm} = 261.14 - 15.67\ S\ d_{TT} / \text{Å} \qquad 7.9$$

where S d_{TT} is as previously defined.

Other correlations have been proposed, including the quadrupolar line broadening with tetrahedral distortion angle to measure asymmetry in the AlO_4 tetrahedra [21, 22].

7.2.3 Previous Work on ^{71}Ga MASNMR Spectroscopy

For the physical characterisation of solids, application of ^{69}Ga or ^{71}Ga MASNMR spectroscopy still remains in a relatively early stage of development. Ga MASNMR spectra in the literature are scarce, and those which have been cited generally display severe quadrupolar line broadening. It was, however, utilised successfully by Zhong and Bray [23] in their characterisation of caesium gallate glasses which revealed different Ga MASNMR bands for tetrahedrally and octahedrally coordinated gallium, indicating that Ga MASNMR could be an effective tool in the analysis of solids. Ione *et al.* [24] used ^{69}Ga for a study on gallosilicate zeolites; other studies such as that of Timkin *et al.* [25], who employed both ^{69}Ga and ^{71}Ga, illustrated the importance of high MASNMR spinning frequencies to reduce the chemical shift anisotropy effects on line widths. Of the two gallium isotopes, ^{71}Ga is more attractive because of its smaller quadrupolar moment, although it has a lower natural abundance: 39.6 % compared with 60.4 % for ^{69}Ga.

The recent study by Mead [26] on selected gallosilcate samples prepared by the synthetic method of this work showed linear trends between resonance position and structural parameters; however, these data were referenced with respect to 3 M $Ga(NO_3)_3$ rather than 1 M $Ga(NO_3)_3$ which is the accepted Ga standard. These data have now be corrected to the true values, as have those recently reported relating to this work [27, 28]. The correlations are still linear but described by different parameters.

For the gallosilicates and gallogermanates of this work, the gallium environment is so close to being perfectly tetrahedral that this problem does not manifest itself to any significant degree, and as such no correction was deemed necessary for our data. The ^{71}Ga data sets displayed broader peaks than found for silicon or aluminium, but with typical symmetrical peak halfwidths of only 20 ppm, the comparison with the few spectra reported in the literature is favourable.

7.3 FOURIER-TRANSFORM INFRA RED (FT-IR) SPECROSCOPY

One of most important applications of infra-red spectroscopy is the characterisation of enclathrates or adsorbates in zeolite systems; however, a great deal of information can also be extracted by the study of the framework constituents themselves. The spectra are dependent on the topology of the framework, the ratio of the framework cations and the nature of the non-framework cations present within the system for purposes of charge balance. Theoretically, it is possible to use the recorded spectra as fingerprints for certain zeolite structural types and for determining the factors which affect framework structures. It has also been possible to show that certain infra-red absorptions are characteristic of particular zeolite building blocks such as double four rings and double six rings [29]. Such information may be useful as an initial indication of framework topology before diffraction studies are performed, and even more so when the materials are of poor crystallinity. The study of systems such as sodalite where there is a common framework structure allows certain relationships beteween IR band positions and structural parameters such as T-O bond length and T-O-T bond angle to be developed.

Flanigen *et al.* [29] realised that vibrations in zeolites derive from strongly coupled TO_4 tetrahedra, and cannot therefore be assigned to indivivdual AlO_4 or SiO_4 units. It was thus proposed that the vibrations were internal TO_4 vibrations whose frequencies are independent of framework type, or external vibrations of this tetrahedral unit which are affected by local framework geometry such as T-O-T angle. Although zeolites are of high symmetry and the resultant IR spectra appear relatively simple, interpretation is not particularly facile due to the large number of atoms in the unit cell, and is further confused by the fact that not all of the possible vibrations are IR active. Studies undertaken on isolated tetrahedral units in order to improve the situation were carried out by Blackwell [30, 31], in which the double ring modes between 500 and 650 cm^{-1} were identified. These were in general accord with the results of Flanigen [29], although whether these results can be reliably used to interpret the overall zeolite structute is uncertain. Recent simulation work carried out by De Man *et al.* [32] on a selection of silica polymorphs including sodalite attempted to elucidate the framework vibrational modes. The simulated results were in good agreement with those experimentally obtained and the contributions of the Si-O-Si and SiO_4 structural units were studied. IR spectra of zeolites are further complicated by the fact that there are relatively few observed vibrational features and this causes great difficulty in comparing experimental and simulated patterns. The scarcity of

experimental data is generally caused by low intensity or the failure to successfully resolve bands.

The feldspars were examined by Iiishi, Tomisaka, Kato and Umegaki [33] and they deduced that the absorptions arising from the vibrations of the non-framework cations and the framework oxygens occur below 250 cm^{-1}. In their study of the IR spectra of various anhydrous members of the halide sodalite family, Henderson and Taylor [34, 35] found that the strong IR absorption bands for aluminosilicate sodalites in the range 300-1200 cm^{-1} arise almost entirely from the framework. It is therefore these bands which should be senstive to changes in the framework: they also investigated gallium and germanium substituted sodalites, although these were prepared by the method of Schipper [36], and are thus subject to leaching of the borosilicate glassware via the strongly basic reaction medium. The results from these particular compounds should thus be treated with care, although they may provide general pointers of use to the fully gallium and germanium substituted sodalites prepared in this work.

A serious difficulty associated with the interpretation of the IR spectra of silicates is the unambiguous assignment of absorption bands. Assignments are therefore largely empirical, although supported by several calculations for model structures. The assignments in this work are those used by Henderson and Taylor [34, 35], which were based initially on the general assignments for pyrosilicates by Lazarev [37]and Farmer [38] and for framework silicates by Iiishi *et al.* [33] and Moenke [39]. These are:

υ_{as} T-O-T (asymmetric stretching mode)	900-1200 cm^{-1}
υ_{s} T-O-T (symmetric stretching mode)	550-850 cm^{-1}
δ O-T-O (bending mode)	400-550 cm^{-1}
δ T-O-T (bending mode)	<300 cm^{-1}

The spectra in this work were recorded above 400 cm^{-1} and hence the δ(T-O-T) bending modes were not observed.

Initial correlations by Henderson and Taylor [34, 35] between positions of IR absorptions and structural parameters such as cell size, framework T-O-T angles and T-O distances will be further examined in this work.

7.4 SPECTROSCOPIC DATA COLLECTION

All of the spectroscopic data collected as a part of this work were collected at the University of Southampton. Details of the apparatus used were given in Chapter Two, but are re-iterated here for clarity.

7.4.1 MASNMR Spectroscopy

Powdered samples were run on a Bruker AM300 spectrometer at Southampton. The Bruker machine consisted of a 7 Tesla superconducting magnet with a multinuclear probe ranging between ^{31}P at 121 MHz to ^{2}H at 46 MHz. The spinning rates used were between 2.5 and 6 kHz. The magic angle was set using the ^{79}Br resonance in solid KBr and the pulse length calibrated using a secondary reference sample of 3-(trimethyl silyl)-1-propane sulphonic acid. ^{29}Si, ^{27}Al and ^{71}Ga spectra were obtained at a field of 59.584 MHz relative to TMS, saturated Al(acac) in benzene and 1 M $Ga(NO_3)_3$ respectively using a 4 μS 90 ° pulse with the decay acquired for 49.0 μS (200-300 transients).

7.4.2 FT-IR Spectroscopy

All FT-IR spectra were recorded using a Perkin Elmer FT-IR 1710 spectrometer equipped with a Perkin Elmer 3600 data station which was employed to perform peak location on all bands observed. Materials to be analysed were intimately ground with spectroscopic grade KBr and pressed into a thin disc, and spectra acquired over the range 4000-400 cm^{-1} with a resolution of 2 cm^{-1}. In Chapter Six, details of IR band positions relating to entrapped anions were given; in this section it is the positions of the bands relating to framework modes which are discussed. The study of framework absorption bands as a function of sodalite composition allows the effect of ionic subtitution to be resolved.

7.5 MASNMR SPECTROSCOPY RESULTS AND DISCUSSION

The synthetic methods devised in this work have permitted the preparation of sodalites with great compositional variety which in turn allows the study of the effect of ionic substitution on MASNMR spectral band positions. The observed chemical shift values can be related to structural parameters as outlined in the background study above. However, much of the work previously undertaken concentrated on aluminosilicate materials since these are by far the easiest to prepare. Investigations of gallium and germanium containing sodalites in the literature are scarce, and this work attempts, at least partially, to fill this void. The new relationships derived within this study will be compared with their aluminosilicate counterparts and the validity of extending the aluminosilicate correlations to other framework compositions will be investigated.

Since by their nature sodalites are amongst the simplest framework materials, it is hoped that the effect of gallium and germanium framework substitution on spectral band positions can be resolved, and that the conclusions drawn can be related to more complex zeolite systems in which full or partial framework substitution has taken place. The importance of understanding the consequences of introducing gallium and germanium into the framework is apparent in those cases where materials are of poor crystallinity for which diffraction methods may not be able to provide detailed structural information. Alternative characterisation techniques such as MASNMR spectroscopy hence assume an even greater significance, and indeed can often be the only viable data source. This work presents complementary data derived from diffraction and spectroscopic techniques and relates the two for aluminosilicate, gallosilicate, aluminogermanate and gallogermanate framework compositions. Preliminary gallosilicate and aluminogermanate data were analysed by Mead [26] using the synthetic procedures described herein, and the extended data now available allows these relationships to more fully detailed, whilst that relating to the gallogermanates provides correlations not previously reported. The gallogermanate data set is particularly limited and as such should not be over interpreted, but it does provide indications as to the effect of replacing both aluminium and silicon in the sodalite framework.

Table 7.1(a) MASNMR Chemical Shifts for Halide Sodalites

Sodalite	a/Å	θ/°	Chemical shift/ppm		
			^{27}Al	^{29}Si	^{71}Ga
Li[GaSi]Cl	8.54	122.5	-	-68.5	201.7
Na[GaSi]Cl	8.96	133.7	-	-78.8	182.2
K[GaSi]Cl	9.10	138.7	-	-82.4	175.5
Li[GaSi]Br	8.58	122.6	-	-69.6	202.2
Na[GaSi]Br	9.00	135.9	-	-80.2	179.6
K[GaSi]Br	9.19	141.5	-	-84.7	170.9
Li[GaSi]I	8.65	124.8	-	-71.4	199.5
Na[GaSi]I	9.09	138.8	-	-82.3	178.1
K[GaSi]I	9.28	144.2	-	-87.2	165.8
Li[AlGe]Cl	8.68	123.0	76.2	-	-
Na[AlGe]Cl	9.04	133.1	69.7	-	-
K[AlGe]Cl	9.27	140.6	63.7	-	-
Li[AlGe]Br	8.68	122.9	76.1	-	-
Na[AlGe]Br	9.13	134.9	68.2	-	-
K[AlGe]Br	9.33	142.2	62.5	-	-
Li[AlGe]I	8.75	124.3	74.2	-	-
Na[AlGe]I	9.18	137.5	66.1	-	-
K[AlGe]I	9.37	143.7	61.6	-	-
Na[GaGe]Cl	9.12	129.0	-	-	198.1
Na[GaGe]Br	9.17	130.5	-	-	194.7
Na[GaGe]I	9.27	133.2	-	-	189.4

Table 7.1(b) MASNMR Chemical Shifts of Complex Sodalites

Sodalite	a/Å	θ/°	Chemical shift/ppm		
			^{27}Al	^{29}Si	^{71}Ga
Na[AlSi]SCN	9.07	143.1	58.5	-90.0	-
Na[AlGe]SCN	9.23	138.7	64.5	-	-
Li[AlSi]MnO_4	8.72	129.9	67.0	-80.7	-
Na[AlSi]MnO_4	9.11	149.2	57.9	-90.6	-
K[AlSi]MnO_4	9.27	152.2	53.8	-94.5	-
Na[AlGe]MnO_4	9.25	142.0	63.4	-	-
Li[AlSi]ClO_4	8.74	132.4	66.5	-81.9	-
Na[AlSi]ClO_4	9.09	147.5	58.5	-90.2	-
K[AlSi]ClO_4	9.34	156.6	52.1	-97.3	-
Na[GaSi]ClO_4	9.15	140.3	-	-84.1	172.5
Na[AlGe]ClO_4	9.23	141.5	64.4	-	-

The data used to plot these correlations pertain to this work, in addition to results reported by Mead [26], Wong [40] and Brenchley [41] to ensure there are sufficient points to allow valid conclusions to be drawn. The data set thus incorporates anions including halides, halates, tetrahedral oxo-anions such as perchlorate and permanganate, and the organic anions formate and acetate. In addition, potassium and lithium exchanged sodalites complement the parent sodium sodalites studied.

7.5.1 ^{29}Si MASNMR Spectroscopy

Results relating to aluminosilicates have effectively been used in the current study as a control against which new relationships for framework modified materials can be compared. Chemical shift values have been plotted against five structural parameters: unit cell size, framework bond angle θ, sin(θ/2), secant(θ), and the degree of s hybridisation given by the relationship cosθ/cos(θ-1). The resultant relationships are presented in Figure 7.3. In each case linear regression analysis has been performed which not only gives the equation relating the dependent and independent variables, but also the linear correlation constant showing how well the data are described by the straight line in question. This

shows how consistent the data set is, and how reliably the correlation can be used to extract structural parameters for materials via knowledge of the MASNMR chemical shift values alone. The results are presented in Table 7.2 below. Figure 7.3 relates the negative ^{29}Si chemical shift as well as the negative secant for presentation purposes, but this is taken into account in the equations given below to simply yield relationships allowing resonance position to be calculated directly. The ^{29}Si chemical shift, δ, is hence given by the equation:

$$\delta = mx + c$$

where m is the gradient, c is the intercept on the y axis, and x is the variable; R is the linear correlation coefficient.

Table 7.2 Linear correlations of ^{29}Si resonance frequency with structural parameters

Framework		Cell	θ	$\cos\theta/(\cos\theta-1)$	$\sin(\theta/2)$	$\sec\theta$
AlSi	m	-24.34	-0.63	-166.34	-210.58	-30.41
	c	130.86	1.94	-14.57	111.40	126.65
	R	0.993	0.993	0.984	0.986	0.981
GaSi	m	-25.02	-0.79	-159.81	-215.71	-24.06
	c	145.00	26.47	-13.75	119.48	114.17
	R	0.999	0.998	0.998	0.998	0.996

Figure 7.3 demonstrates that the correlations proposed for aluminosilicates can be extended to frameworks containing silicon and another tetrahedral cation. It is clear from the R values that the relationships are followed extremely closely with the best correlations being for cell constant and T-O-T angle for aluminosilicates, and cell constant for the gallosilicates. The results also demonstrate that gallosilicates not only conform to the same trends as do the aluminosilicates but often show improved linear correlation over aluminosilicates. However, the range of gallosilicate sodalites is smaller than that for aluminosilicates; a similar number of samples may give rather more scatter and hence a slighty reduced R constant.

Figure 7.3. (a)-(e) ^{29}Si MASNMR shift vs structural parameters.

The resonance position of ^{29}Si is shifted upfield by approximately 2.5 ppm from $Si(OAl)_4$ to $Si(OGa)_4$ at a given T-O-T angle; this fits in with the general observation [27] that as the silicon nearest neighbour is changed from Si to Ga to Al to Be, δ is shifted downfield due to its neighbour's increasing electron withdrawal from the bridging oxygen. This deshields the silicon nucleus. It is also apparent that δ becomes more negative with increased T-O-T angle in each of these systems. This is explained by the larger s orbital contribution to the Si-O bond deshielding the silicon as the angle increases.

The results of Newsam [11] for a range of zeolites with a framework aluminium to silicon ratio of unity agree extremely closely with those reported herein illustrating that such relationships may indeed prove extremely useful in the characterisation of zeolites in general. A previous study on gallosilicate sodalites [42] reported that δ was shifted by 10 ppm on replacement of aluminium by gallium but this value does not allow for the changing T-O-T angle associated with the inclusion of gallium in the framework. Replacement of aluminium by the larger gallium will, with fixed tetrahedral ion sites, necessitate a decrease in the Si-O-Al/Ga bond angle to accommodate the longer Ga-O distance (Al-O= 1.74 Å, Ga-O-1.82 Å). This decrease in the bond angle can be predicted from these bond length considerations and by comparing angles in a series of sodalites with GaSi and AlSi frameworks. This decrease in bond angles averages about 6 degrees which would account for a decrease in chemical shift of 6 ppm. The additional change observed between Al $(OSi)_4$ and $Ga(OSi)_4$ frameworks must derive from the direct replacement of Al by Ga i.e. an electrostatic effect. This amounts to about 4 ppm for the four sites.

7.5.2 ^{27}Al MASNMR Spectroscopy

Figure 7.4 shows ^{27}Al chemical shift plotted against the same five structural parameters as for ^{29}Si resonances, with the linear regression results summarised in Table 7.3 below.

Table 7.3 ^{27}Al MASNMR chemical shift versus structural parameters

Framework		Cell	θ	cosθ/(cosθ-1)	sin(θ/2)	secθ
AlSi	m	-24.14	-0.62	-162.48	-203.02	-30.17
	c	277.53	149.69	132.41	253.03	22.29
	R	0.994	0.989	0.986	0.990	0.981
AlGe	m	-20.77	-0.64	-133.92	-175.09	-20.26
	c	256.24	154.70	123.01	229.51	38.73
	R	0.984	0.991	0.990	0.988	0.986

The aluminium spectra collected in this work show very little second order quadrupolar broadening producing very narrow, sharp resonances of typical halfwidth 3-5 ppm. This is because the aluminosilicate and aluminogermanate sodalites contain aluminium in an environment for which the charge distribution is close to cubic in symmetry, thus reducing line broadening.

In an analogous manner to ^{29}Si, δ becomes more negative as the T-O-T angle, and hence s orbital contribution to the oxygen, increases. In addition, for the more electropositive silicon the chemical shift is higher than that for germanium at the same T-O-T, with both of these being more negative compared with the pure aluminates [22, 27].

Linear regression fits show that aluminosilicates are best fitted using the unit cell size as the structural parameter whereas aluminogermanates are most effectively correlated using the T-O-T as the independent variable.

Figure 7.4. (a)-(e) ^{27}Al MASNMR shift vs structural parameters.

7.5.3 ^{71}Ga MASNMR Spectroscopy

In an analogous manner to the silicon and aluminium spectra, the chemical shift values relating to the ^{71}Ga nucleus have been plotted against certain structural parameters. The graphs resulting from this study are displayed in Figure 7.5, with the linear correlation values summarised in Table 7.4. The data are in general agreement with the 184 ppm reported by Timken and Oldfield [25] for gallosilicate hydrosodalite.

Table 7.4 Linear Correlation of ^{71}Ga MASNMR results with structural parameters

Framework		Cell	θ	cosθ/cos(θ-1)	sin(θ/2)	secθ
GaSi	m	-50.56	-1.64	-336.19	-453.51	-50.01
	c	635.14	402.29	319.64	599.64	109.19
	R	0.999	0.998	0.996	0.997	0.995
GaGe	m	-57.29	-2.06	-435.53	-571.06	-67.89
	c	720.33	463.52	366.24	713.45	90.20
	R	0.998	0.999	0.999	0.999	0.999

The relationships derived for ^{29}Si can now be extended to include the ^{71}Ga nucleus, and δ can be successfully correlated with cell parameter, the T-O-T angle θ, sin(θ/2), sec(θ) and cos(θ)/cos(θ - 1). The best fit to the experimental data for the gallosilicate materials is achieved with the expression involving cell parameter; for the gallogermanates all the data sets correlate excellently. However, it must be remembered that there are so few data points available that these gallogermanate relationships can only be regarded at this stage as indicators of trends which must be more fully explored.

The effects of quadrupolar interactions have not been resolved for the gallium data: the gallosilicates display broader peaks than gallogermanates for which linewidths are particularly narrow (Figure 7.6). Timkin et al. [25] found that the observed and corrected ^{71}Ga chemical shift values for gallosilcate hydro-hydroxy sodalite differ by 2 ppm. For the gallosilicate spectra, the band width is approximately 25 ppm: quadrupolar interactions would mean that the reported values in Table 7.1 are shifted from the true value by approximately 2 ppm. However, the empirical trends shown still hold satisfactorily.

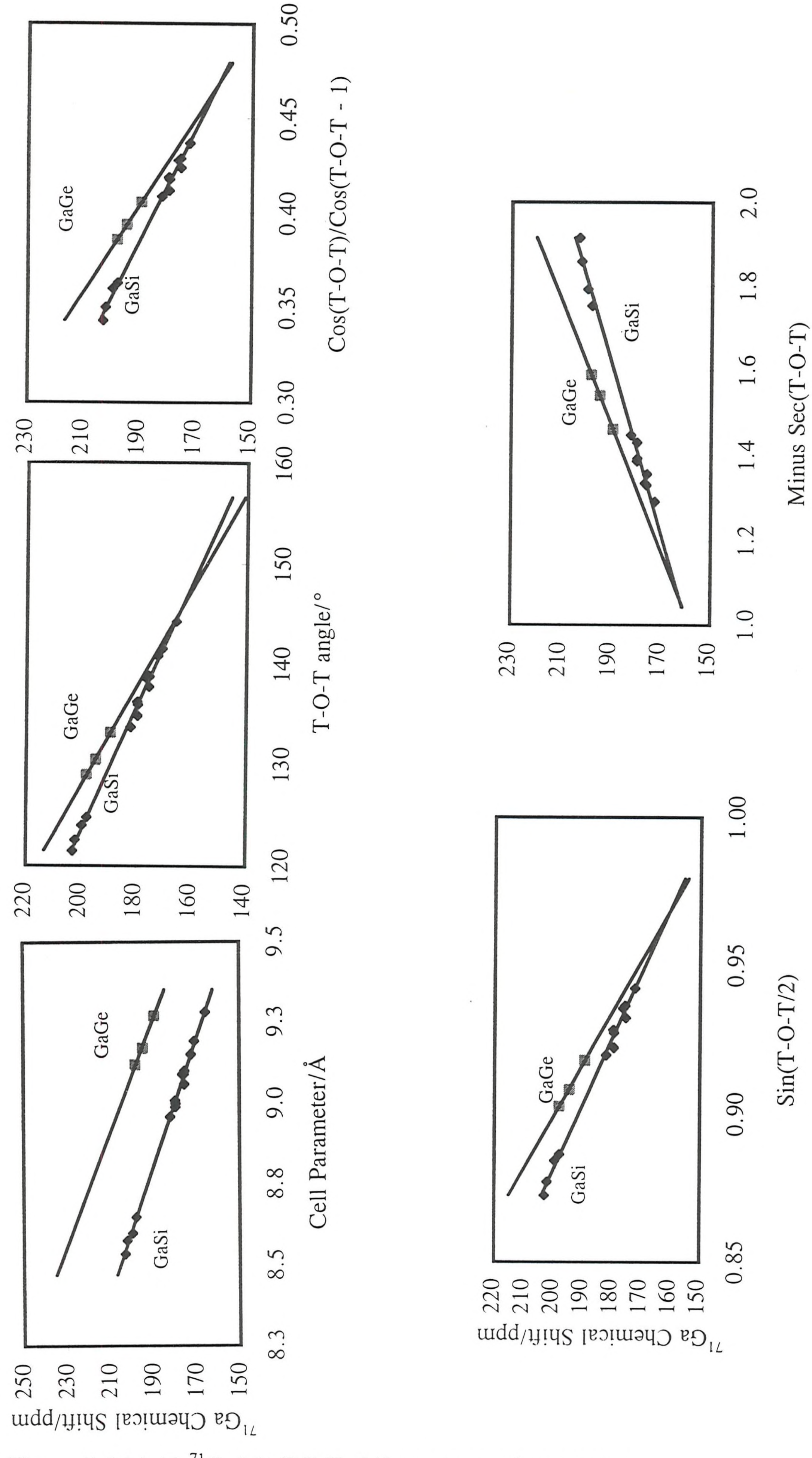

Figure 7.5 (a)-(e) ^{71}Ga MASNMR shift vs structural parameters.

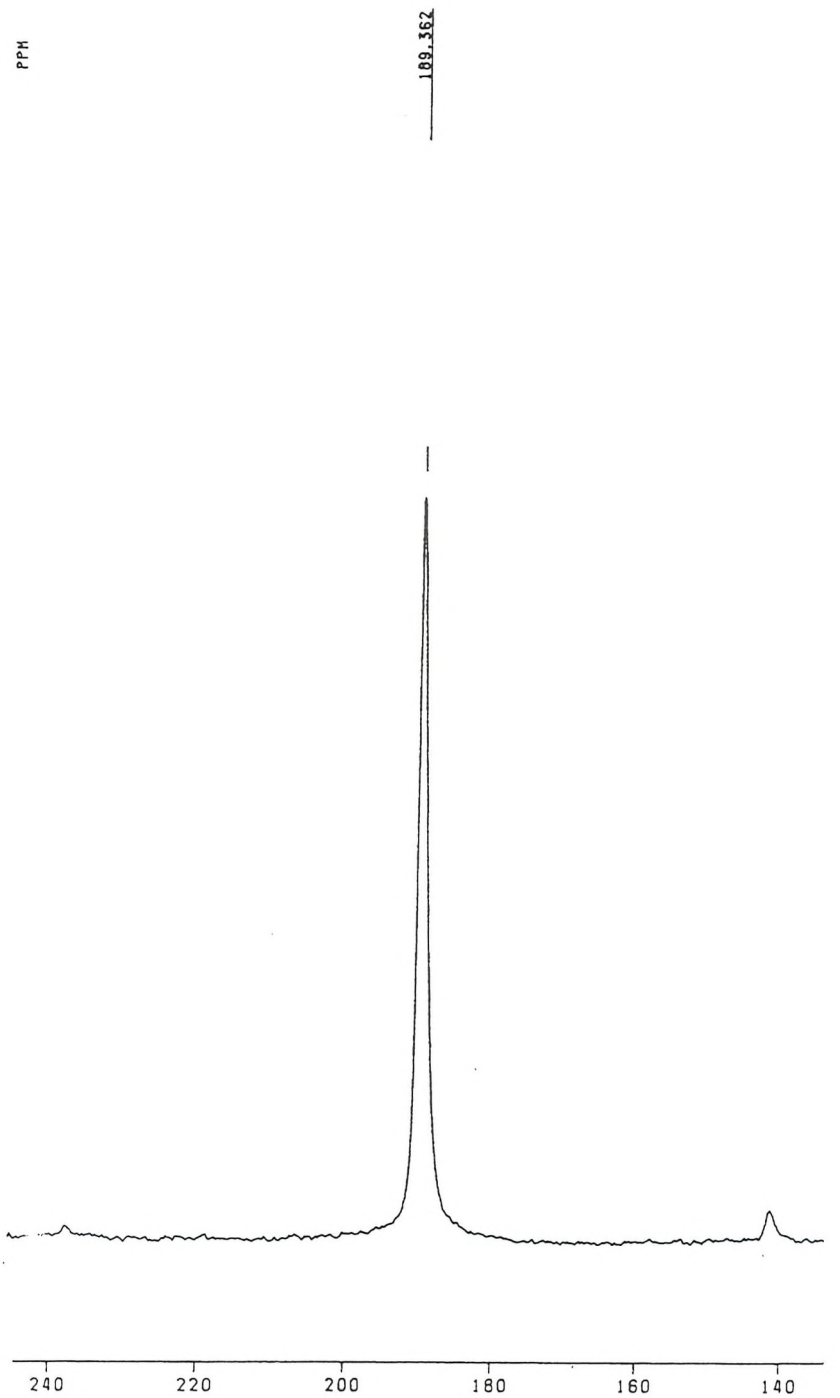

Figure 7.6 ^{71}Ga MASNMR spectrum for $Na_8[GaGeO_4]_6.I_2$.

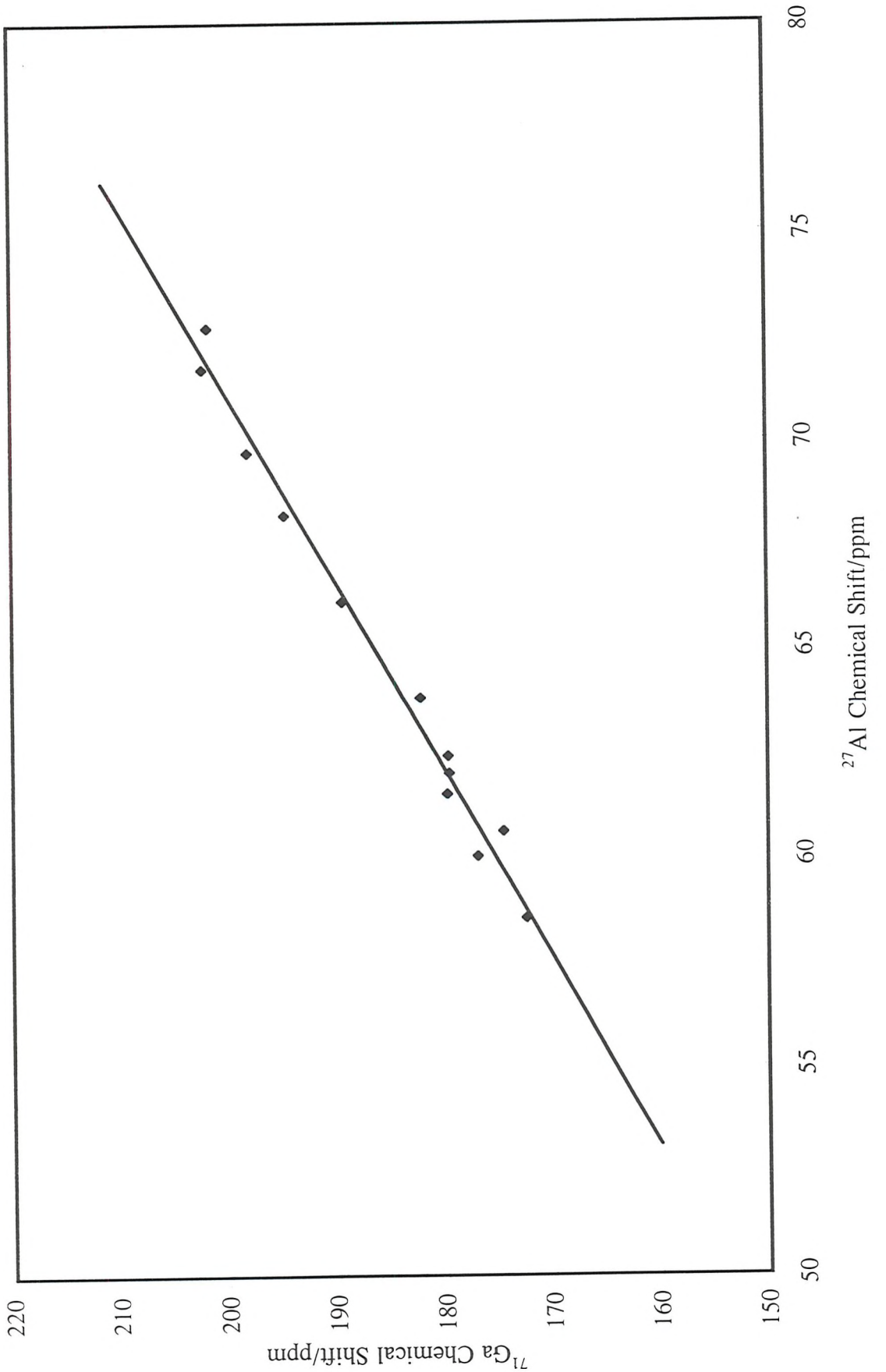

Figure 7.7 ^{71}Ga vs ^{27}Al MASNMR shifts for $M_8[(Al/Ga)SiO_4]_6.X_2$.

For a series of compounds $M_8[(Al/Ga)SiO_4]_6X_2$ with the same M and X the ^{27}Al chemical shift is plotted against the ^{71}Ga chemical shift. This is shown in Figure 7.7. In allowing for relaxation in the local structure as gallium dopes for aluminium such a correlation may then be used to relate the chemical shifts of gallium and aluminium on the same site in a framework material. Application of this correlation may need allowance for changes in Al-O-T and Ga-O-T bond angles which may not be the same in all framework materials as found between a pair of sodalites and as assumed in this graph but the correlations plotted in Figures 7.4 and 7.5 could be used to correct for this. Using these graphs structural information can then be extracted for poorly crystalline or amorphous phases, doped zeolites or solid solutions.

7.6 FT-IR RESULTS AND DISCUSSION

FT-IR spectra on all of the framework substituted sodalites have been recorded and the results reported herein; aluminosilicate data are also included for comparison. Mead investigated the IR spectra of certain framework modified sodalites, but had extremely limited data available and hence the correlations derived may not be entirely reliable [26]. This work has allowed the number of gallium and germanium containing sodalites to be increased hence permitting IR trends to be meaningfully reported. The data of Mead are included to supplement this data, and would be expected to fit the relationships of this work since they were obtained using the synthetic methods used here, and as such are not susceptible to the type of problems encountered by Henderson and Taylor [35]. These relate to their syntheses of gallium and germanium substituted sodalites which were performed in basic media using borosilicate glass reaction vessels: the resultant cell parameters indicate that full occupancy of the framework sites by gallium and/or germanium had not been achieved, suggesting that leaching of the vessel components had taken place. This resultant spectral band positions cannot therefore be relied upon to any great degree. Their results will be compared with those obtained here. In addition to not achieving full gallium and germanium substitution on the sodalite framework tetrahedral sites, Henderson and Taylor were not able to successfully achieve complete replacement of sodium by lithium and as such could not extend their spectroscopic investigations as fully as those reported here. The IR band positions are summarised in Table 7.5 below.

In an analogous manner to MASNMR spectroscopy the affect of varying the framework components may be monitored by forming correlations between IR band positions and structural parameters such as cell parameter and framework T-O-T angle derived from powder diffraction data. These are presented graphically below, and the corresponding linear regression parameters are also summarised to give an indication of how well the data is described using linear relationships.

Table 7.5(a) IR Band Positions for Halide Sodalites

Sodalite	a/Å	θ/°	Wavenumber/cm^{-1}				
			υ_{as1}	υ_{as2}	υ_{s1}	υ_{s2}	υ_{s3}
Li[GaSi]Cl	8.54	122.5	927	-	671	655	593
Na[GaSi]Cl	8.96	133.7	945	-	646	633	556
K[GaSi]Cl	9.10	138.7	950	-	634	620	544
Li[GaSi]Br	8.58	122.6	930	-	668	653	589
Na[GaSi]Br	9.00	135.9	943	863	642	627	552
K[GaSi]Br	9.19	141.5	954	-	630	616	535
Li[GaSi]I	8.65	124.8	933	-	664	648	583
Na[GaSi]I	9.09	138.8	948	876	636	621	539
K[GaSi]I	9.28	144.2	958	-	623	609	528
Li[AlGe]Cl	8.68	123.0	-	832	675	656	-
Na[AlGe]Cl	9.04	133.1		863	640	615	-
K[AlGe]Cl	9.27	140.6	-	881	614	585	-
Li[AlGe]Br	8.68	122.9	-	834	674	655	-
Na[AlGe]Br	9.13	134.9	-	871	626	596	-
K[AlGe]Br	9.33	142.2	-	888	607	576	-
Li[AlGe]I	8.75	124.3	-	838	667	647	-
Na[AlGe]I	9.18	137.5	-	871	626	596	-
K[AlGe]I	9.37	143.7	-	889	605	574	-
Na[GaGe]Cl	9.12	129.0	-	792			
Na[GaGe]Br	9.17	130.5		801			
Na[GaGe]I	9.27	133.2		811			

Table 7.5(b) IR Bands Positions for Complex Sodalites

Sodalite	a/Å	θ/°	Wavenumber/cm^{-1}				
			υ_{as1}	υ_{as2}	υ_{s1}	υ_{s2}	υ_{s3}
Na[AlSi]SCN	9.07	143.1	996	-	722	695	655
Na[AlGe]SCN	9.23	138.7	-	877	619	591	-
Li[AlSi]MnO_4	8.72	129.9	957	-	749	725	680
Na[AlSi]MnO_4	9.11	149.2	1005	-	720	692	653
K[AlSi]MnO_4	9.27	152.2	1020	-	706	680	639
Na[AlGe]MnO_4	9.25	142.0	-	879	617	588	-
Li[AlSi]ClO_4	8.74	132.4	960	-	747	-	677
Na[AlSi]ClO_4	9.09	147.5	1002	-	723	695	657
K[AlSi]ClO_4	9.34	156.6	995	-	-	672	628
Na[GaSi]ClO_4	9.15	140.3	959	-	631	618	532
Na[AlGe]ClO_4	9.23	141.5	-	876	620	513	-

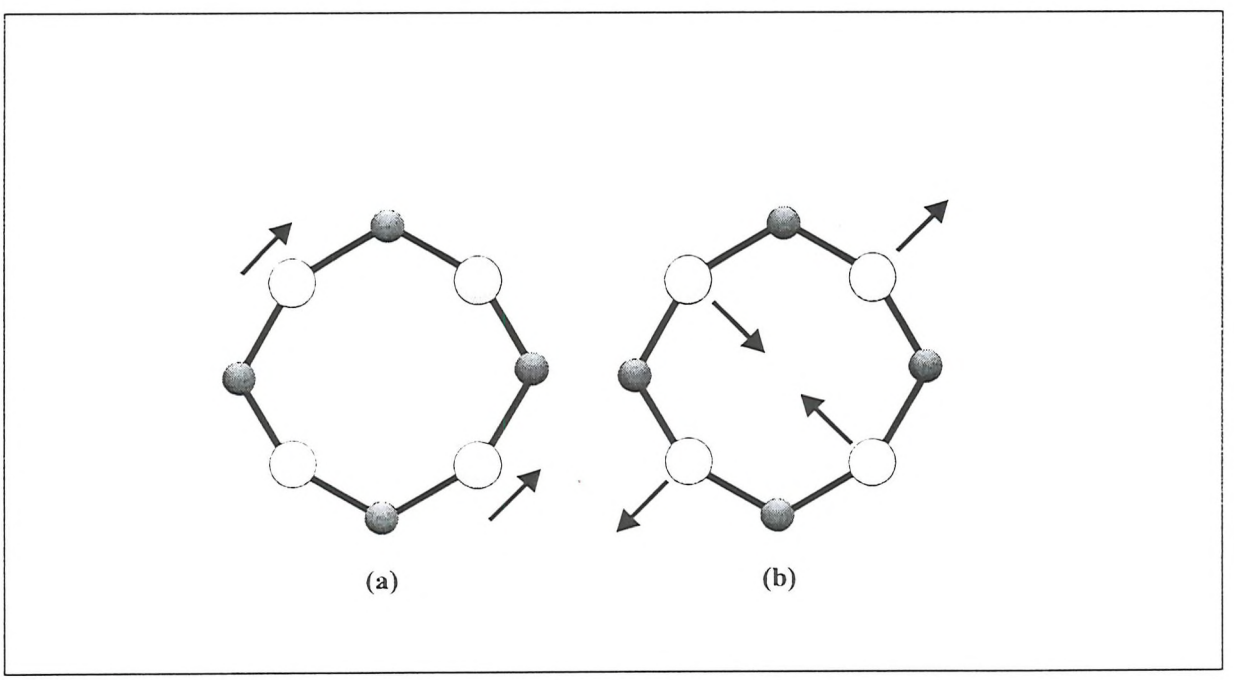

Figure 7.8(a) ν_{as1} IR active stretching mode **(b)** ν_{s1} IR active bending mode

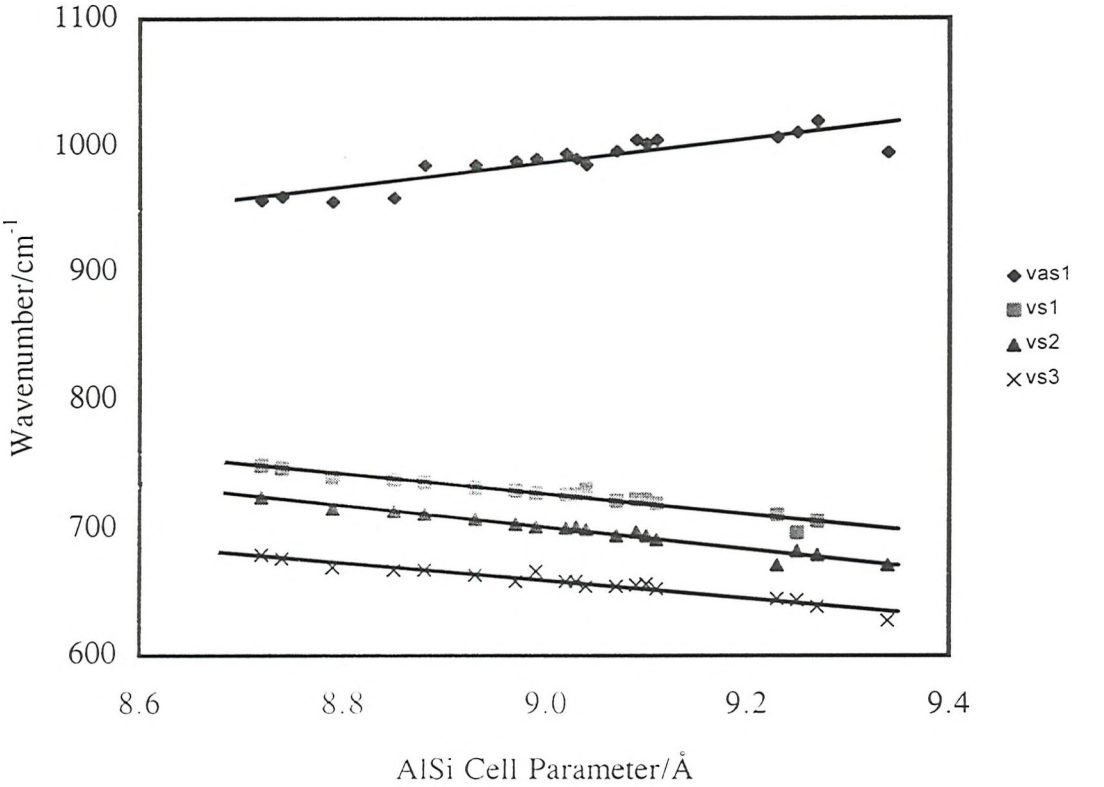

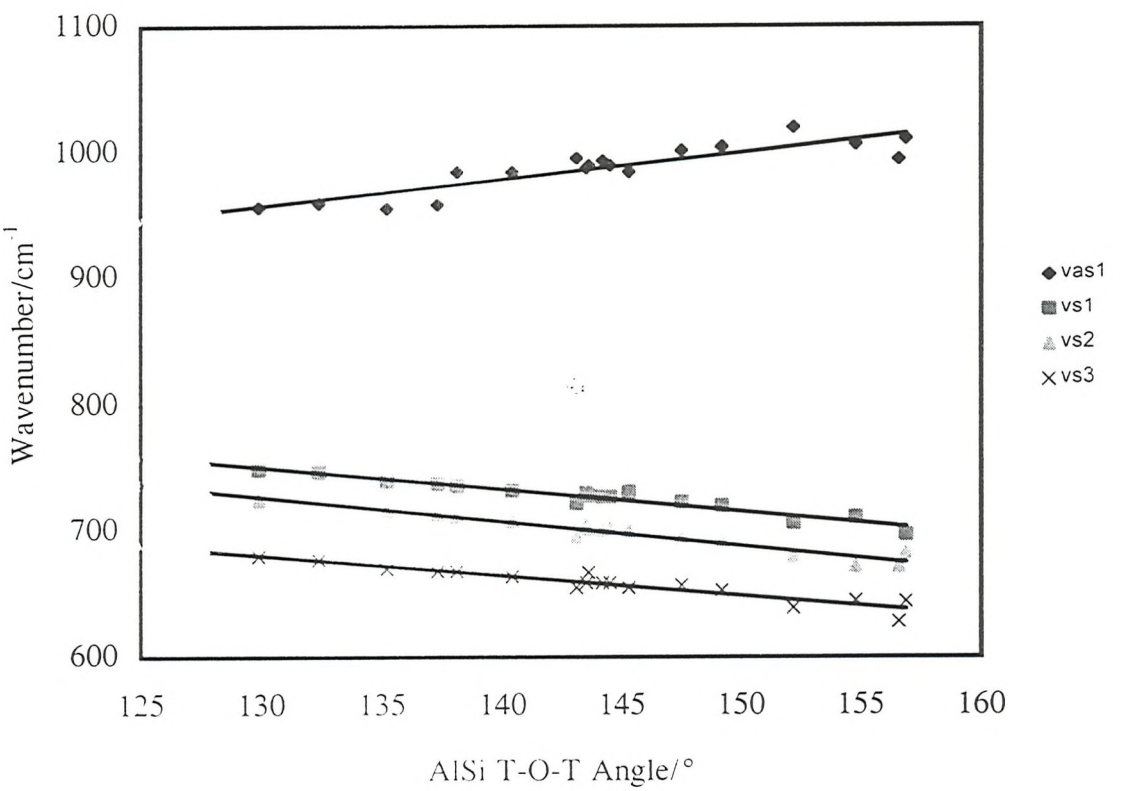

Figures 7.9(a) IR band vs M[AlSi]X cell **(b)** IR band vs M[AlSi]X T-O-T angle

The graphs for aluminosilicates show how as cell parameter or framework T-O-T angle is increased the asymmetric bands are shifted to higher wavenumber, whilst the symmetric bands all move to lower wavenumber. Linear regression results for these trends are given in Table 7.6, and show how the relationships can be adequately described by equations of the form y = mx + c, where y is the wavenumber, m is the gradient, x is the correlated variable and c is the intercept on the y axis. The linear regression constant, R, shows how well the linear correlations are fitted. Henderson and Taylor [34, 35] have described how the asymmetric bands are strongly linked to the T-O-T asymmetric mode shown in Figure 7.8. As the T-O-T angle is increased the T-O bond is shortened which results in a shift of the asymmetric band to higher energy. In contrast, the symmetric bands contain more local bending mode character and as such, the T-O bond compression is reduced with increased T-O-T angle giving band shifts to lower energy. This is entirely in accord with the results shown in Figure 7.9.

Equivalent relationships are seen for the gallium and germanium framework substituted sodalites, in which smooth linear trends are also obtained. The main differences from aluminosilicate materials are in the band positions at a particular value of cell parameter or T-O-T angle, and in the number of observable framework modes. Where aluminosilicates have generally one asymmetric and two to three symmetric T-O-T bands, aluminogermanate sodalites show only two υ_s(T-O-T) bands, gallosilicates two to three, and the gallogermanates only one. At a particular cell parameter or T-O-T angle, with respect to aluminosilicates, the aluminogermanate υ_{as}(T-O-T) bands are shifted to lower energy by approximately 130 cm^{-1} and υ_s(T-O-T) by 85 cm^{-1}; gallosilicate υ_{as}(T-O-T) bands to lower wavenumber by approximately 40 cm^{-1} and υ_s(T-O-T) bands by 80 cm^{-1}; the gallogermanate asymmetric band is lowered by approximately 200 cm^{-1}, and the symmetric band by 160 cm^{-1}.

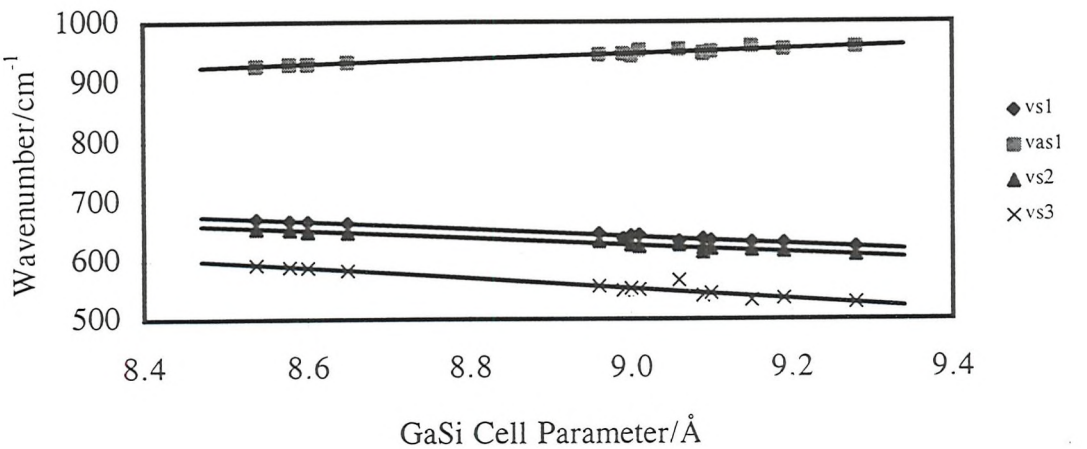

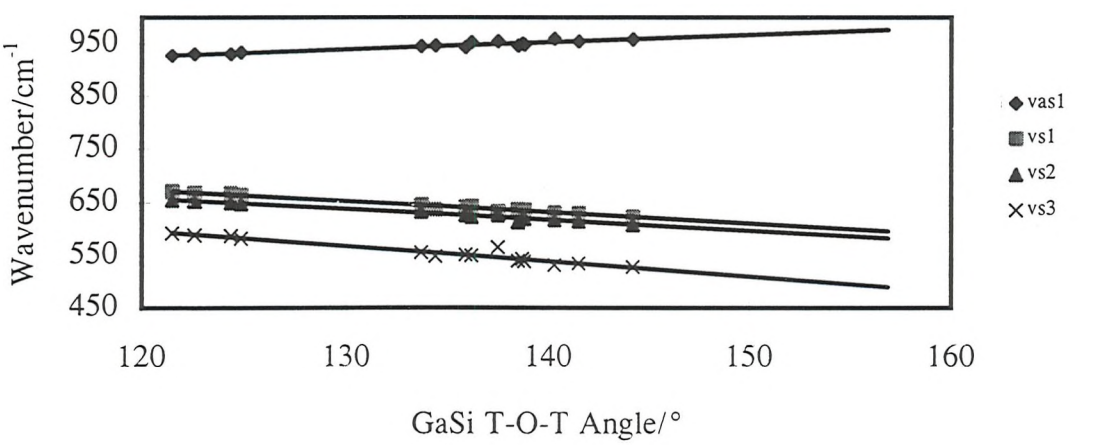

Figures 7.10(a) IR band vs M[GaSi]X cell **(b)** IR band vs M[GaSi]X T-O-T angle

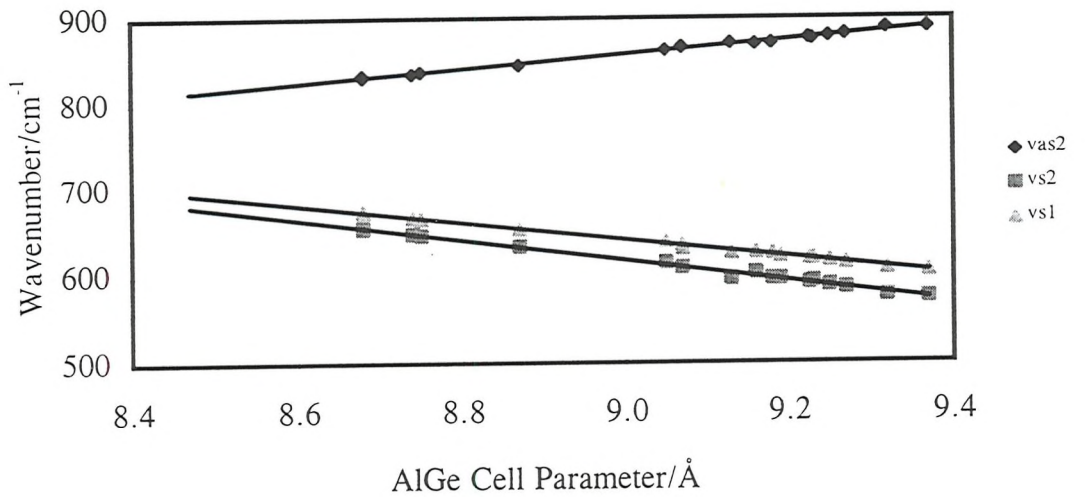

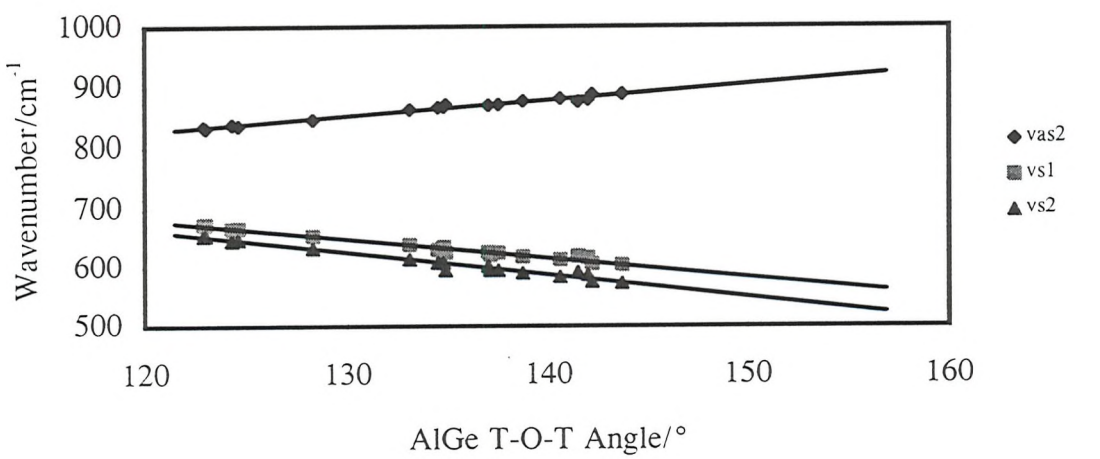

Figures 7.11(a) IR band vs M[AlGe]X cell **(b)** IR band vs M[AlGe]X T-O-T angle

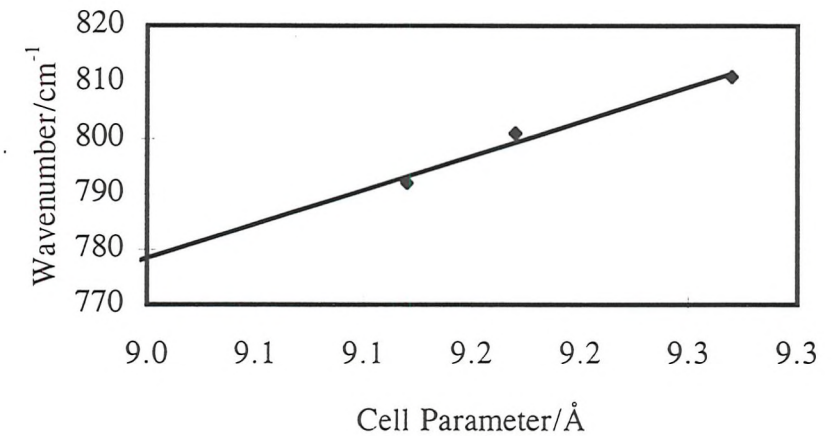

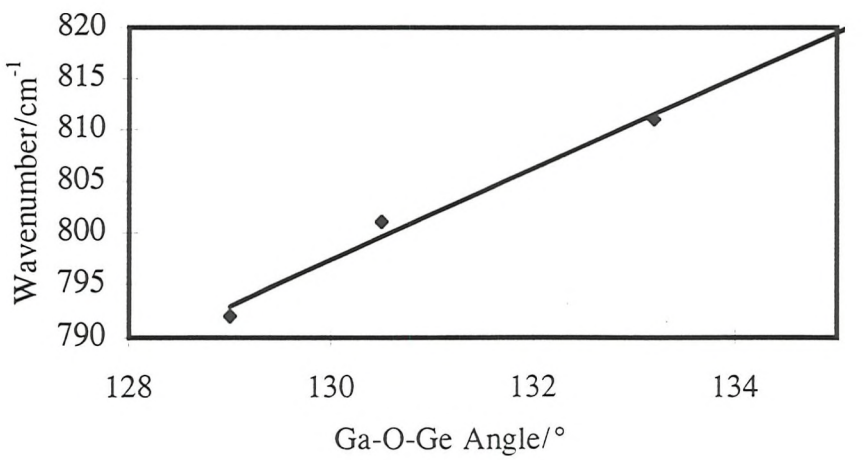

Figures 7.12(a) IR band vs M[GaGe]X cell **(b)** IR band vs M[GaGe]X T-O-T angle

Table 7.6 Linear Regression results for IR Absorption Bands Versus Cell Parameter

Framework		υ_{as}	υ_{s1}	υ_{s2}	υ_{s3}
AlSi	m	111.82	-78.12	-86.34	-68.97
	c	-18.36	1430.50	1478.70	1280.40
	R	0.930	0.948	0.970	0.958
GaSi	m	39.98	-65.15	-62.32	-86.98
	c	586.70	1227.30	1187.20	1335.60
	R	0.876	0.964	0.942	0.871
AlGe	m	82.90	-100.31	-119.64	-
	c	112.56	1544.70	1694.70	-
	R	0.988	0.987	0.984	-

In addition to the straightforward plots of wavenumber versus cell parameter or framework T-O-T angle, Henderson and Taylor [34, 35] proposed that the position of the main IR absorption band could be related to the average T-O framework bond length. Figure 7.13 shows how the data accumulated using all of the aluminosilicate, gallosilicate, aluminogermanate and gallogermanate materials fits in with this relation. It can be seen that despite a fair degree of scatter, the general trend is that upon increased T-O distance the energy of the principal IR band is lowered gradually. It is also interesting to note that the gallosilicates all lie above the line whereas the aluminogermanates all lie a little below the fitted trendline. The fact that this correlation holds reasonably well for all framework compositions indicates that the mass of the framework ion does not significantly affect the position of the main absorption band.

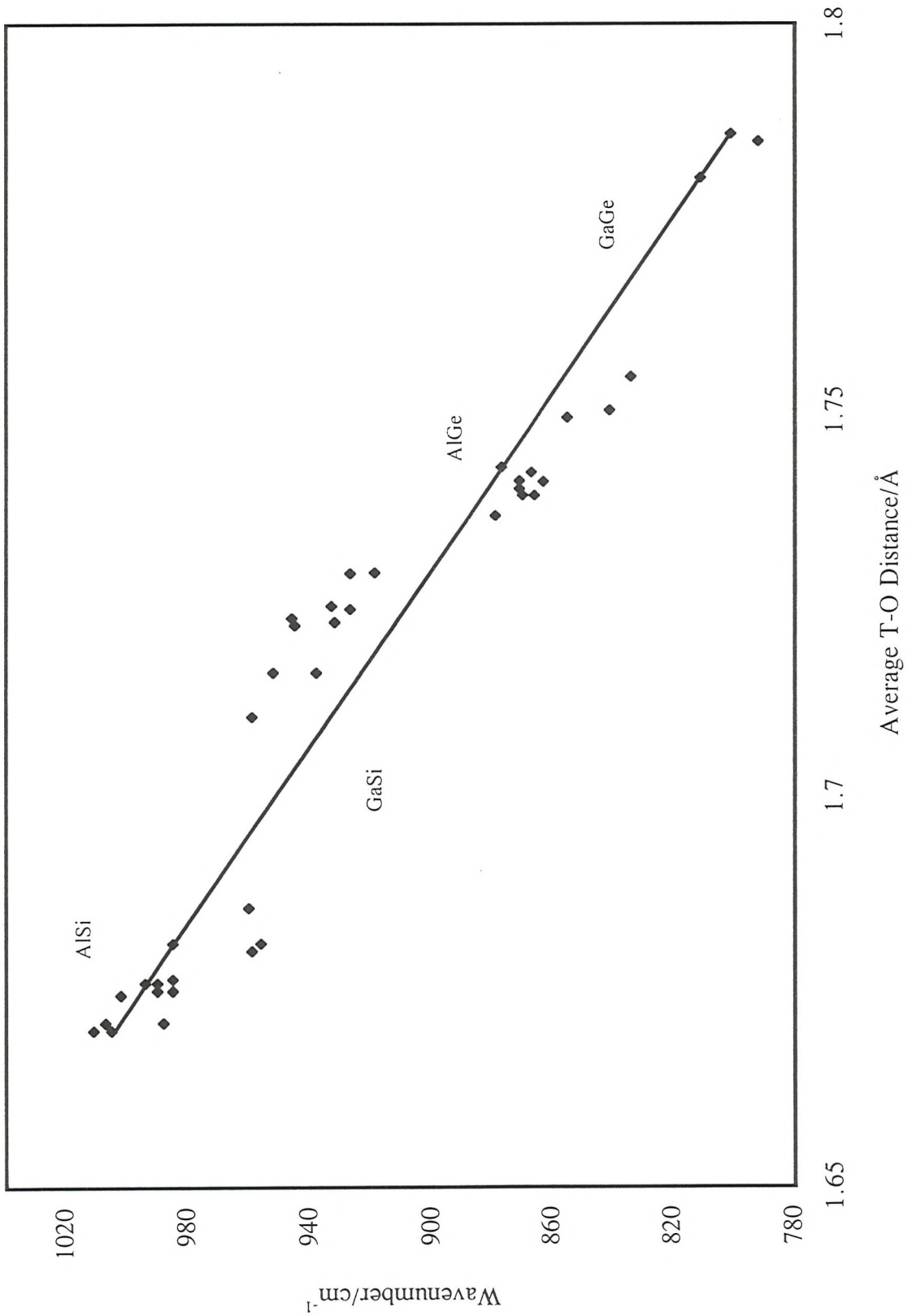

Figure 7.13(a) Principle IR band vs T-O distance for all framework types

7.7 CONCLUSIONS

MASNMR spectroscopy has been used to confirm the framework ordering indicated by Rietveld refinement in the space group $P\bar{4}3n$ and to provide correlations between chemical shift and a variety of structural parameters. These are in good agreement with those previously reported for aluminosilicates, and have been extended to cover gallosilicate, aluminogermanate and gallogermanate sodalites. Such correlations may allow structural parameters to be directly extracted using spectroscopic information alone. It is also hoped that structural information pertaining to zeolites in which partial doping of gallium and germanium has been undertaken may be able to be deduced from MASNMR data, since direct structural characterisation from diffraction is often complicated. Although these relationships only cover materials with a one to one ratio of framework atoms they may be expanded to include zeolitic species in which partial isomorphous substitution on framework sites has been achieved. In general there is a linear relationship between the chemical shift change and n for a series of compounds $T(OT'_1)_{4-n}(OT'_2)_n$. Hence, for example, the chemical shift changes seen in replacing four aluminiums by four galliums may be divided by four to get the expected change for a single site substitution. In addition the correlations reported in this work may be used to determine the site of isomorphous replacement in complex framework structures. For example replacement of aluminium by gallium in a complex aluminosilicate zeolite structure can be studied by ^{29}Si, ^{27}Al and ^{71}Ga MASNMR spectroscopy. At low levels of substitution little change would be expected in the ^{29}Si spectrum. However, comparison of the chemical shifts for ^{27}Al and ^{71}Ga in equivalent structures may allow determination of the site of substitution. Correlations such as those shown in Figure 7.7 may be used to this end. Furthermore, it is also envisaged that solid solutions of sodalites with frameworks comprising (Al/Ga, Si/Ge) will be able to be characterised. At present, such sodalite solid solutions have not been experimentally obtained, but this may simply be due to a lack of suitable synthetic conditions. In addition to aiding the structural elucidation of partially substituted framework materials, amorphous or poorly crystalline samples could be analysed using spectroscopy in conjunction with the relationships proposed here.

FT-IR spectroscopy has permitted correlations similar to those of MASNMR to be obtained, although they are less well defined. Particular variations in IR absorption cannot be assigned to one structural component alone, but general trends are still able to be observed. The correlations described are generally in agreement with those proposed by

Creighton *et al.* [43, 44] with regard to change in band position as a function of cell edge or T-O-T framework bond angle. The results presented here are in accord with the observation that the position of IR absorption bands depends mainly on framework structure. Wavenumbers are determined by bond distances and angles of the framework and are not affected greatly by bonds between framework oxygens and cavity ions; however, it must be remembered that the size of the cavity ions controls the degree of framework collapse. The trend relating wavenumber and average framework T-O bond length is seen to hold for all the framework types prepared herein. This suggests that the mass of the framework cation does not appear to significantly influence the relationship. In their spectroscopic study of sodalite materials, Henderson and Taylor [35] acknowledged the fact that their trends were severely hindered by a lack of structural data: the synthesis and characterisation a wide range of sodalites as a part of this work has overcome this problem and the resultant spectroscopic/structural correlations can be considered to be rather more reliable than those initially proposed.

Extending the series even further, particularly by preparing a variety of gallogermanates would be beneficial, and would reveal whether the linearity observed holds for a wider range of cell sizes and T-O-T angles. It is quite feasible that the correlations seen here are a linear portion of what is described by a curve over a larger data range. The extrapolation of these trends must therefore be undertaken with great care; Henderson and Taylor proposed a gentle curve relating wavenumber and cell parameter, although their data does show a large degree of scatter and a relatively large degree of extrapolation has been undertaken. In addition to an increase in the number of data points, further work concerning IR frequency calculations for a model structure would prove informative.

7.8 REFERENCES

[1] P.B. Kempa, G. Engelhardt, J.C. Buhl, J. Felsche, G. Harvey and C. Baerlocher, *Zeolites*, **11**, 558 (1991).

[2] N.C. Nielsen, H. Bildsøe, H.J. Jakobsen and P. Norby, *Zeolites*, **11**, 622 (1991).

[3] R. Jelinek, B.F. Chmelka, A. Stein and G.A. Ozin, *J. Phys. Chem.*, **96**, 6744 (1992).

[4] G. Engelhardt, H. Koller, P. Sieger, W. Depmeier and A. Samoson, *Solid State Nucl. Magn. Reson.*, **1**, 127 (1992).

[5] G. Engelhardt, J. Felsche and P. Sieger, *J. Am. Chem. Soc.*, **114**, 1173 (1992).

[6] P. Sieger, A.M. Schneider, M. Wiebcke, P. Behrens, J. Felsche and G. Engelhardt, *Chem. Mater.*, 7, 163 (1995).4292

[7] E. Lippmaa, M. Magi, A. Samoson, G. Engelhardt and A. Grimmer, *J. Am. Chem. Soc.*, **102**, 4889 (1980).

[8] E. Lippmaa, M. Mägi, A. Samoson, M. Tarmak and G. Engelhardt, *J. Am. Chem. Soc.*, **103**, 4992 (1981).

[9] W. Löwenstein, *Am. Miner.*, **39**, 92 (1954).

[10] J.M. Thomas, J. Klinowski, S. Ramdas, B.K. Hunter and D.T.B. Tennakoon, *Chem. Phys. Lett.*, 1547 (1983).

[11] J.M. Newsam, *J. Phys. Chem.*, 91, 1259 (1987).

[12] M.T. Weller and G. Wong, *J. Chem. Soc. Chem. Commun.*, **16**, 1103 (1988).

[13] S. Ramdas and J. Klinowski, *Nature*, **308**, 521 (1984).

[14] G. Engelhardt and R. Radeglia, *Chem. Phys. Lett.*, **108**, 271 (1984).

[15] R. Radeglia and G. Engelhardt, *Chem. Phys. Lett.*, **114**, 28 (1985).

[16] G. Engelhardt, R. Radeglia, H. Jancke, E. Lippmaa and M. Mägi, *Org. Magn. Reson.*, **5**, 51 (1973).

[17] M. Klessinger, 'Elektronenstruktur Organischer Moleküle', 283, Verlag Chemie, Weinheim (1982).

[18] B.L. Sherriff and H.D. Grundy, *Nature*, **332**, 819 (1988).

[19] I.D. Brown and D. Altermatt, *Acta Cryst.*, B**41**, 244 (1985).

[20] H.S. Jacobsen, P. Norby, H. Bildsøe and H.J. Jakobsen, *Zeolites*, **9**, 491 (1989).

[21] G. Engelhardt and W.J. Veeman, *Chem. Soc. Chem. Commun.*, 622 (1993).

[22] M.T. Weller, M.E. Brenchley, D.C. Apperley and N.A. Davies, *Solid State Nucl. Magn. Reson.*, **3**, 103 (1994).

[23] J. Zhong and P.J. Bray, *J. Non-Cryst. Solids*, **94**, 122 (1987).

[24] K.G. Ione, L.A. Vostrikova and V.M. Mastikhin, *J. Mol. Catal.*, **31**, 355 (1985).

[25] H.K.C. Timken and E. Oldfield, *J. Am. Chem. Soc.*, **109**, 7669 (1987).

[26] P.J. Mead, *Ph.D. Thesis*, University of Southampton (1996).

[27] M.T. Weller, S.E. Dann, G.M. Johnson and P.J. Mead, *Proc. 11th Int. Zeol. Conf.*, in press.

[28] G.M. Johnson and M.T. Weller, *Proc. 11th Int. Zeol. Conf.*, in press.

[29] E.M. Flanigen, K. Hassan and H.A. Szymanski, *Adv. Chem. Ser.*, **101**, 201 (1971).

[30] C.S. Blackwell, *J. Phys. Chem.*, **83**, 3251 (1979).

[31] C.S. Blackwell, *J. Phys. Chem.*, **83**, 3257 (1979).

[32] A.J.M. de Man and R.A. van Santen, *Zeolites*, **12**, 269 (1992).

[33] K. Iiishi, T. Tomisaka, T. Kato and Y. Umegaki, *Neues. Jb. Miner. Abh.*, **115**, 98 (1971).

[34] C.M.B. Henderson and D. Taylor, *Spectrochim. Acta*, **33**A, 283 (1977).

[35] C.M.B. Henderson and D. Taylor, *Spectrochim. Acta*, **35**A, 929 (1979).

[36] P.J. Schipper, C.Z. van Doorn and P.T. Bolwijn, *J. Am. Ceramic Soc.*, **55**, 256 (1972).

[37] A.N. Lazarev, "Vibrational Spectra and Structure of Silicates", translated from Russian by G.D. Archard, ed. V.C. Farmer, Consultants Bureau, New York (1972).

[38] V.C. Farmer, "The Infra Red Spectra of Minerals", Chapter 13, Mineralog. Soc., London (1972).

[39] H.H.W. Moenke, "The Infra Red Spectra of Minerals", Chapter 16, Mineralog. Soc., London (1972).

[40] G. Wong, *Ph.D. Thesis*, University of Southampton (1990).

[41] M.E. Brenchley, *Ph.D. Thesis*, University of Southampton (1994).

[42] S. Hayashi, K. Suzuki, S. Shin, K. Hayamizu and O. Yamamoto, *Bull. Chem. Soc. Jpn.*, **58**, 52 (1985).

[43] J.A. Creighton, H.W. Deckman and J.M. Newsam, *J. Phys. Chem.*, **98**, 448 (1994).

[44] J.A. Creighton, H.W. Deckman and J.M. Newsam, *J. Phys. Chem.*, **95**, 2099 (1994).

Chapter Eight

STRUCTURAL PROPERTIES OF SODALITES

8.1 INTRODUCTION

Structural properties of individual sodalites containing specific anions have been discussed in Chapters Five and Six. In this chapter, an overall review of the sodalite structure will be given, in which data concerning all framework compositions and anion types has been accumulated. A wide range of data is thus available, and when combined with results previously reported may allow the effect of composition on sodalite structure to be more fully understood. Although the sodalite topology is relatively simple and the fully expanded structure is well understood [1, 2, 3], there remain several questions which have not been satisfactorily answered, including the factors which determine why certain anions are preferentially entrapped within sodalite cages. Clearly the size and geometry of the anion is important, but for a certain framework composition the reasons for particular anions promoting the sodalite structure more readily than others are not clear. Structural considerations may also be useful in determining why certain framework types are easier to synthesise than others: do those that form readily have some particular parameters in common which are not present in frameworks which are synthetically far more challenging.

The study of a large range of sodalite data may provide pointers as to the favoured anions for entrapment, the preferred size of sodalites for different framework compositions and the ability of the sodalite structure to adapt to anion sizes. The extent to which certain structural parameters such as tetrahedral tilts and framework bond angles can deviate from the ideal may also provide information regarding which sodalites can realistically be expected to form. The data from this study will be compared with previous experimental and theoretical data, and the differences discussed. It is important to observe how the data collected in this work fits into correlations previously reported[3]: this not only tests the validity of the relationships for new data sets, but also gives an indication of the integrity of the values obtained. Most of the current work concentrates on framework substituted sodalites, whilst the correlations of the literature pertain principally to aluminosilicates; the extension of these relationships to materials of different framework composition will therefore be investigated. Discrepancies may arise from several sources: it is possible that gallium and germanium containing sodalites do not conform to the same trends as aluminosilicates; the new data obtained may highlight a deficiency in the previously proposed models; in addition, if the results of this work do not fit the trends for aluminosilicates, it may indicate that the parameters extracted from the diffraction profiles are flawed in some manner.

Such models may be used in a predictive nature to highlight the limits of each individual framework type. For example, as the tetrahedral tilt angles tend towards zero or the framework T-O-T bond angle reaches a value of 160.5 ° the resultant sodalite structure will correspond to the maximum possible cell size. The actual value of the unit cell will vary with particular framework composition, but these values can never be exceeded. In a similar way, maximum framework collapse is governed by the minimum framework bond T-O-T angle of 109.5 ° and maximum tilt angles of 45 °.

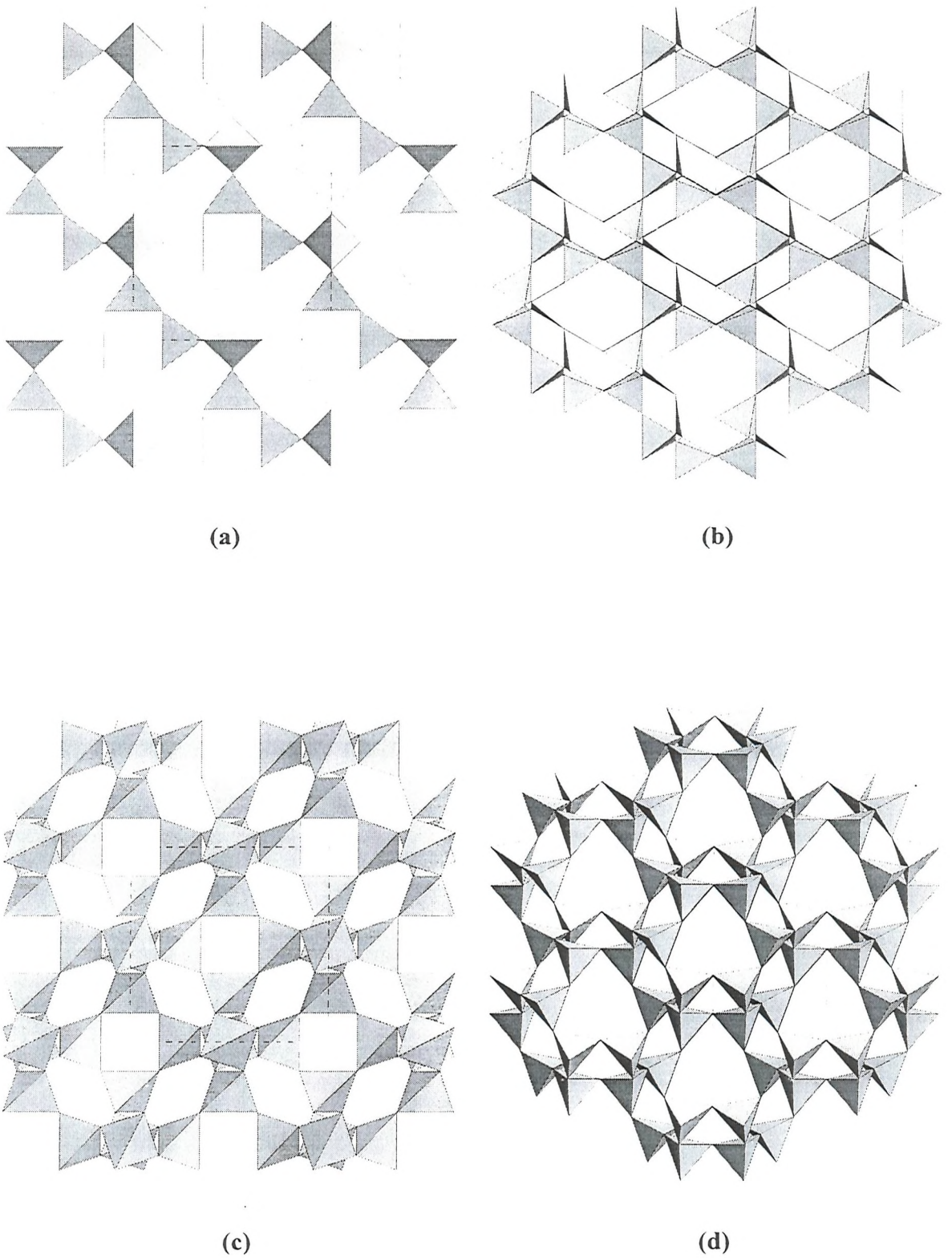

Figure 8.1 Structure of sodalite showing TO4 tetrahedra **(a)** and **(b)** fully expanded **(c)** and **(d)** partially collasped frameworks.

8.2 PREVIOUS STRUCTURAL STUDIES

Many studies have been directed towards the sodalite structure due to its relative simplicity compared with other zeolitic systems. Early work such as that of Taylor [5, 6] concentrated on correlations involving simple structural parameters like unit cell size and framework bond angle. Subsequent work probed the detailed nature of the sodalite structure more deeply allowing the prediction of structural parameters with a knowledge of cell parameter and non-framework anion and cation radii [1, 6-8]. The vast majority of research has centred on aluminosilicate sodalites, since the synthetic methods outlined in the literature allow the preparation of a wider range of materials than those for framework substituted sodalites. Beagley and Titiloye [3] have reviewed this work on aluminosilicates, and have extended their models to include framework modified species. In this chapter the previously proposed correlations and theoretical models will be examined and compared with the values corresponding to materials synthesised in the current work.

Distortion of the framework tetrahedra from the ideal O-T-O value of 109.48 ° has been examined for sodalite materials, with aluminate sodalites shown by Depmeier [2] to display appreciable deviation from this value. This was attributed to the high ionic character of the aluminate framework compared with its aluminosilicate analogue, for which the O-T-O angle shows virtually no distortion from the ideal. For sodalites such as aluminates where there is only one tetrahedral framework component, framework collapse from the fully expanded space group $Im\bar{3}m$ to $I\bar{4}3m$ occurs via tetrahedral tilting about the $\bar{4}$ axis [1-10]. This is represented in Figure 8.1. This tilt angle can be readily calculated if the T-O bond distance and cell parameter of the sodalite are known, using the equation:

$$a / Å = 4t(2/3)^{½}\cos\phi_{av} + 4t(1/3)^{½} \qquad 8.1$$

where a is the cell parameter and ϕ_{av} is the average tilt angle. The two assumptions made in derivation of this equation are that the average T-O distance, t, and the O-T-O angle do not change significantly with cell size. This equation yields an average tilt angle which describes sodalites whose frameworks either contain only a single tetrahedral atom or are disordered. Sodalites with an ordered array of tetrahedral framework atoms adopt the space group $P\bar{4}3n$ and the tetrahedral tilt angles for each tetrahedral species become slightly different since the symmetry of the framework oxygen site is lowered as shown in Figure 8.2. In such cases in order to accurately describe the mechanism of framework collapse it is necessary to

distinguish between the two tetrahedral tilt angles. This is achieved using the framework oxygen positions, shown in equations 8.2 and 8.3 for silicon and aluminium respectively.

$$\tan\phi_{Si} = (1/2 - z)/x \qquad 8.2$$

$$\tan\phi_{Al} = (1/2 - z)/y \qquad 8.3$$

where ϕ_{Si} and ϕ_{Al} are the tetrahedral tilt angles and x, y, z the atomic co-ordinates of the framework oxygen.

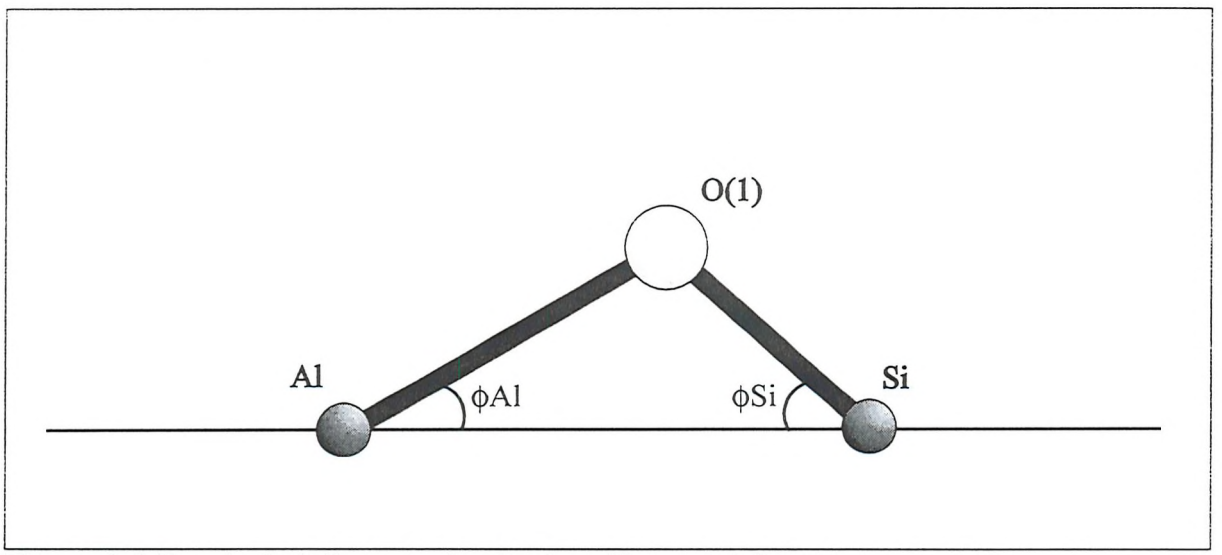

Figure 8.2 Tetrahedral tilt angles in alumino-silicate sodalite.

In addition to being linked to tilt angle, the cell parameter is also related to the framework T-O-T bond angle as described by equation 8.4:

$$\text{T-O-T} / ^\circ = 2\sin^{-1}[(a/t)/(32)^{1/2}] \qquad 8.4$$

where a is the cell parameter. Using these equations it is possible to calculate the maximum possible values of T-O-T angle and cell parameter, which correspond to zero tilt angles. This is perfectly logical, since tilt angles describe sodalite cell collapse; when these are zero there is no framework collapse and thus the unit cell reaches its maximum expansion corresponding to maximum possible linearity of the T-O-T bond angle.

$$a_{max} / \text{Å} = 5.575\ t \qquad 8.5$$

$$\text{T-O-T} = 5.575\ t / (32)^{1/2}\ t = 160.5\ ^{\circ} \qquad 8.6$$

It is noteworthy that the maximum T-O-T angle of 160.5 ° is independent of framework composition, while the maximum cell parameter is governed solely by the average T-O bond length. The minimum cell parameters and T-O-T angles are described by the closest approach possible between framework oxygens in neighbouring tetrahedra. This occurs when the tilt angle is 45 ° and the T-O-T angle is 109.5 ° producing oxygen co-ordinates of (0.125, 0.125, 0.375).

It has also been reported that altering the framework T-O-T angle should cause a corresponding change in the T-O bond distance due to variation of the oxygen hybridisation [11]; increasing the T-O-T angle bond linearity from 109.5 ° to 120 ° and onwards towards 180 ° changes the bridging oxygen hybridisation from sp^3 to sp^2 and towards sp. Augmenting the degree of s orbital character results in a stronger bond which should thus be manifested by a decrease in the T-O bond length as the unit cell expands. The relationship between T-O distance and T-O-T angle can also be explained by π-bonding interactions; as the T-O-T angle becomes more linear the degree of π-bonding increases due to improved overlap of the $d\pi$- and $p\pi$-bonding orbitals and hence the bond becomes stronger and shorter [12]. However, the study of this phenomenon is not trivial: the range of cell parameters available using only aluminosilicate frameworks is relatively limited, and thus in order to obtain a large data set it is necessary to alter the framework components. The introduction of larger less electropositive cations changes the charge density at the oxygen. The oxygen becomes less polarised resulting in shorter stronger bonds with increased sodalite cell parameter [4]. Resolving these contributions is not straightforward, and this must be borne in mind before conclusions can be drawn.

8.3 RESULTS AND DISCUSSION

The structural parameters presented herein are all derived from powder diffraction studies of x-ray or neutron data. The majority of the refinements in this work relate to powder neutron diffraction and as such the derived data should be accurately enough defined to permit correlations to be investigated. Neutron diffraction allows the more accurate location of light atoms, and thus correlations involving sodium and oxygen atoms are much more likely to be valid if PND has been used in their determination. Table 8.1 below shows selected structural parameters derived from PND arranged by framework type.

The effect of framework substitution on cell size will be investigated, in addition to the mechanisms by which the sodalite structure adapts to compensate for the change in size of entrapped anions, non-framework and tetrahedral framework cations. As suggested previously, detailed analysis of the sodalite structure for the various framework types may also give indications as to why certain materials are easier to prepare: it is feasible that those which present synthetic difficulties possess highly strained or distorted bond angles corresponding to highly collapsed or expanded cells.

The theory behind framework substitution was that upon incorporation of larger T atoms bigger sodalites are produced, and it was the intention to profit from this increased cell size by entrapping anions which could not be enclathrated in the traditional aluminosilicate sodalite beta cage. In order to optimise the conditions for the preparation of these materials, synthetic studies were initially concentrated on the halides since these anions add no complexity to the system in terms of geometry, and both thermal and base stability. This also provides the opportunity to study sodalite structure as a function of ionic size since the coordination requirements for the halides are identical.

Table 8.1 Selected Structural Data from PND Data for Framework Modified Sodalites

Sodalite	a/Å	θ/°	$\phi_{Al/Ga}$/°	$\phi_{Si/Ge}$/°	(Al/Ga)-O/Å	(Si/Ge)-O/Å
Li[GaSi]Cl	8.54	121.5	33.8	37.5	1.827	1.630
Li[GaSi]Br	8.58	122.6	32.9	36.5	1.826	1.631
Li[GaSi]I	8.65	124.8	31.2	34.3	1.808	1.641
Na[GaSi]Cl	8.96	133.7	25.4	28.1	1.817	1.628
Na[GaSi]Br	9.00	135.9	24.1	26.9	1.835	1.610
Na[GaSi]I	9.09	138.8	21.3	24.2	1.849	1.599
$Na[GaSi]ClO_4$	9.15	140.8	19.6	21.3	1.793	1.627
Li[AlGe]Cl	8.68	122.6	34.6	34.2	1.762	1.738
Li[AlGe]Br	8.68	122.7	34.1	34.5	1.760	1.736
Li[AlGe]I	8.75	124.4	32.6	32.9	1.759	1.740
Na[AlGe]Cl	9.04	133.1	26.6	26.9	1.748	1.734
Na[AlGe]Br	9.13	134.9	25.1	25.3	1.748	1.734
Na[AlGe]I	9.18	137.5	22.7	23.0	1.752	1.728
Na[AlGe]SCN	9.23	138.7	21.7	21.9	1.749	1.737
$Na[AlGe]ClO_4$	9.23	141.5	20.7	20.9	1.746	1.730
$Na[AlGe]MnO_4$	9.26	142.0	20.3	20.0	1.750	1.723
Na[GaGe]Cl	9.12	129.0	29.0	29.7	1.806	1.763
Na[GaGe]Br	9.17	130.5	27.8	28.5	1.816	1.760
Na[GaGe]I	9.27	133.2	25.9	25.9	1.798	1.763

8.3.1 Cell Expansion Via Framework Substitution

The halide series of sodalites provides an ideal data set for the examination of the effect of size of both the halide and the tetrahedral framework cation. It has been possible to prepare aluminosilicate, gallosilicate, aluminogermanate and gallogermanate chloride, bromide and iodide sodalites. It was expected that, for a particular entrapped anion, the introduction of larger framework cations would yield more voluminous sodalite cages and hence larger unit cells. Although increase in cell size is observed this is relatively small compared with the percentage increase in the ionic radius of the framework components. This data is presented below in Table 8.2. Percentage increases are given relative to aluminosilicates and hence the percentage increases of these sodalites are necessarily zero.

Table 8.2 Unit Cell and Cage Volume Comparisons for Halide Sodalites

Sodalite	Unit Cell/Å	% Cell Increase	Cage Volume/Å^3	% Vol. Increase
Na[AlSi]Cl	8.8812	0	350.11	0
Na[GaSi]Cl	8.9603	0.92	359.70	2.70
Na[AlGe]Cl	9.0325	1.70	368.46	5.20
Na[GaGe]Cl	9.1159	2.64	378.76	8.20
Na[AlSi]Br	8.9304	0	356.06	0
Na[GaSi]Br	9.0000	0.78	364.50	2.37
Na[AlGe]Br	9.0915	1.59	375.72	5.52
Na[GaGe]Br	9.1725	2.71	385.86	8.37
Na[AlSi]I	9.0318	0	368.00	0
Na[GaSi]I	9.0940	0.69	374.59	2.05
Na[AlGe]I	9.1640	1.46	385.99	4.89
Na[GaGe]I	9.2669	2.60	397.9	8.13

The increase in cage volume is also of interest since this may provide more useful information relating to the possibility of entrapping large anions. The sodalite unit cell is shown in Figure 8.3, and it can be seen that the unit cell contains two complete sodalite cages - one whole beta cage at the cube centre and one-eighth of a cage at each cube vertex, making two cages in total. The volume of a single cage has thus been calculated by simply

halving the volume of the unit cell. This value gives a fair representation of the cage volume and allows valid comparison of cage volumes for different frameworks.

These data sets are represented graphically in Figure 8.4 and show linear trends when plotted against the sum of the ionic radii of the tetrahedral framework components. Although the expansion in cell and volume is linear with respect to the size of the framework cations, the increase is small compared with that which is possible: this is demonstrated by the percentage increase in cell compared with the percentage increase in (T + T') framework ionic radii. It is noteworthy that the increase of cell and volume is directly proportional to the radii of the framework components, and remains so whatever the particular halide entrapped.

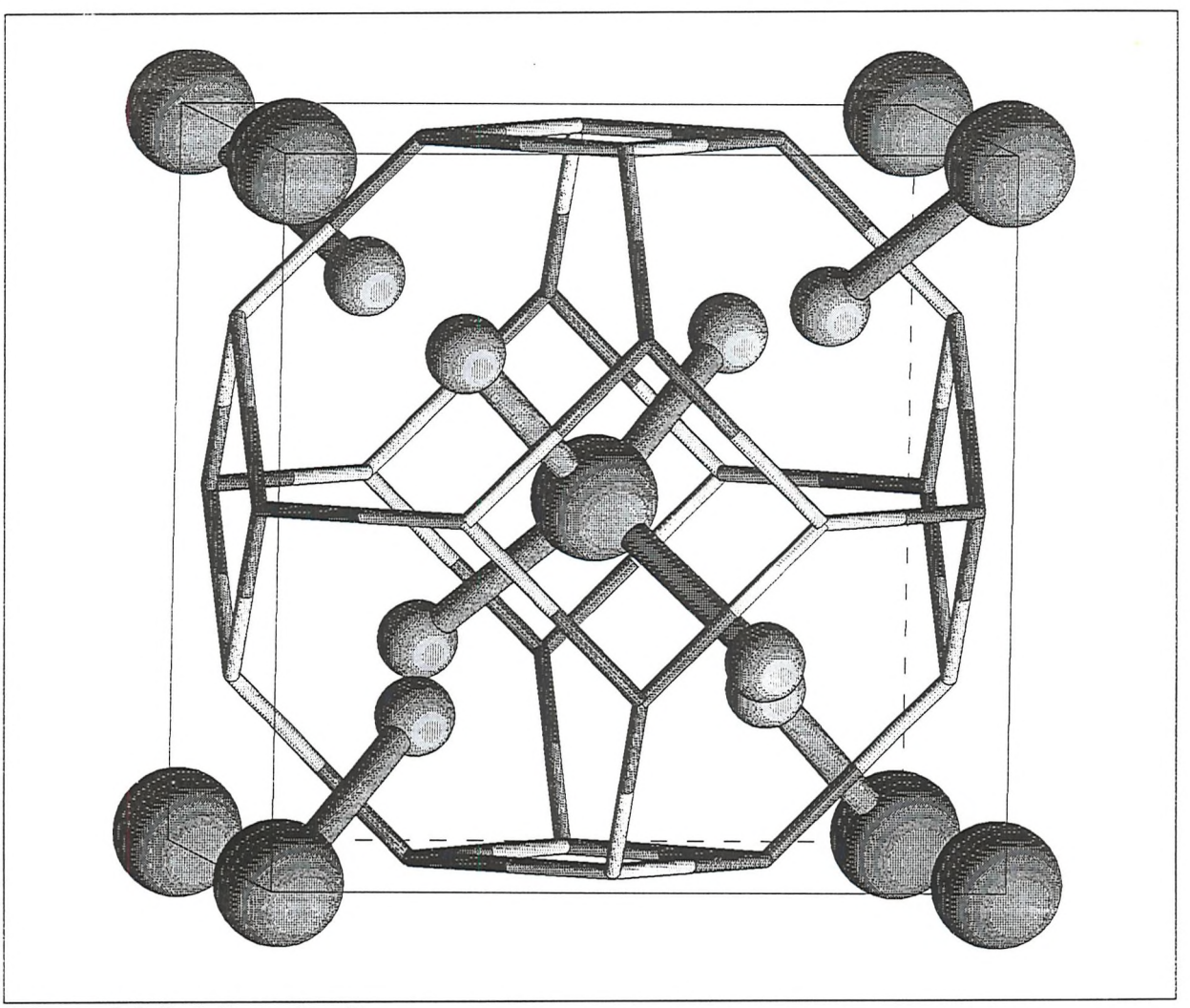

Figure 8.3 Sodalite unit cell

Figures 8.4(a) Cell parameter vs (T + T'): top left **(b)** Cage volume vs (T + T'): top right **(c)** Percentage cell parameter increase vs Percentage increase in (T + T'): bottom left **(d)** Percentage volume increase vs Percentage increase in (T + T'): bottom right.

In his study of nitrite, formate and chlorate halate substituted sodalites, Mead [13] was not able to observe linear trends relating cell expansion and introduction of gallium and germanium into the sodalite framework, and concluded that the degree of cell expansion was dependent on the particular anion in the beta cages.

Comparison of data sets reported by different authors is not always easy since the reaction conditions often vary in terms of concentration of water or salt in the starting gel or solution. This can lead to the entrapment of water molecules in addition to the required ion which affects the structural data extracted from the diffraction pattern. However, in this particular case, the synthetic procedure employed was that devised in the current work and as such the discrepancies were attributed to the rather complex orientational disorder of the entrapped anions. It was recognised that the halide anions would provide an excellent series with which to make comparisons of structural data, and this has proved to be the case. However, since the nitrite, formate and chlorate anions do not give uniform cell expansions, extrapolation of the trends observed herein must be undertaken with extreme care in order to avoid over interpretation of the data. It is recognised that the halides provide a relatively limited data series although the correlations obtained are certainly noteworthy.

In their study of the $Na_3[ABO_4]_3.4H_2O$ system, Nenoff *et al.* [14] examined the structural changes which accompany framework substitution. They found that the introduction of gallium and germanium gave rise to sodalites for which the expansion was relatively small compared with the theoretical maximum. In addition to gallium and germanium, they also examined sodalites containing zinc, phosphorous and arsenic in the framework. Their results indicate that the zincophosphate sodalite did not conform to the general trends observed for the other framework systems. A theory of diminished stability in the framework due to both a deviation from mean bond lengths and from mean O-T-O bond angles was proposed. Whilst the average T-O bond length in the Zn/P material is comparable with other sodalite frameworks, the P-O distance differs markedly from the average which is not the case for the other samples studied. It has therefore been suggested that the large difference between the Zn-O and P-O bond lengths gives rise to a more unstable, highly strained sodalite which is condensed to accommodate the alternate short and long T-O bonds. This implied that frameworks composed of T atoms with similar ionic radii would have greater stability. The deviation of the individual O-T-O and O-T'-O bond angles from the mean O-T-O value was also examined and revealed that the Zn/P analogue showed a considerable difference whereas the other framework types showed very little deviation from the mean. This causes alternating narrow and wide angles leading to a highly distorted

framework. Although their study did not reveal any significant distortions for the gallogermanate sodalite framework, it was decided to undertake an analogous study to Nenoff *et al.* [14] for the halide series. Experiments had shown that the gallogermanates were by far the most difficult series to synthesise, perhaps indicating that they have the lowest stability which may be attributable to the same kind of deviations from the ideal as observed for the Zn/P hydrosodalite. Tables 8.3(a) and (b) below summarise the results of this study.

Table 8.3(a) Bond Length Comparison (Å) for Halide Sodalites

Sodalite	Al/Ga-O	Si/Ge-O	$T\text{-}O_{av}$	Δ
Na[GaSi]Cl	1.817	1.628	1.722	0.095
Na[GaSi]Br	1.835	1.610	1.723	0.112
Na[GaSi]I	1.849	1.599	1.724	0.125
Na[AlGe]Cl	1.748	1.734	1.741	0.007
Na[AlGe]Br	1.748	1.734	1.741	0.007
Na[AlGe]I	1.752	1.728	1.740	0.012
Na[GaGe]Cl	1.806	1.763	1.785	0.021
Na[GaGe]Br	1.812	1.760	1.786	0.026
Na[GaGe]I	1.798	1.763	1.781	0.017

It is clear from the data shown that deviations of the individual T-O and O-T-O structural parameters from the average are small, and those for the gallogermanate series do not show larger deviations than the gallosilicates or aluminogermanates; indeed, it is the gallosilicates which have the largest deviations from the mean. This may point to why they are more difficult to prepare than the aluminogermanates, although it sheds no light on the synthetic problems encountered for the gallogermanates. It seems likely that another factor entirely is responsible for the relative instability of the system.

Table 8.3(b) Bond Angle Comparison (°) for Halide Sodalites

Sodalite	O-Al/Ga-O	O-Si/Ge-O	O-T-O_{av}	Δ
Na[GaSi]Cl	109.47	109.50	109.485	0.015
Na[GaSi]Br	109.48	109.53	109.505	0.025
Na[GaSi]I	109.48	109.55	109.515	0.035
Na[AlGe]Cl	109.49	109.49	109.49	0
Na[AlGe]Br	109.49	109.50	109.495	0.005
Na[AlGe]I	109.55	109.48	109.515	0.035
Na[GaGe]Cl	109.50	109.51	109.505	0.005
Na[GaGe]Br	109.51	109.51	109.51	0
Na[GaGe]I	109.49	109.55	109.52	0.03

8.3.2 Correlation of Framework Oxygen Position With Framework Expansion

It has been demonstrated above that as the central anion and the tetrahedral framework cation are varied the cell parameter, and hence the cage volume, are also altered. Since the tetrahedral framework cations are located on fixed sites in the space group $P\bar{4}3n$, their positions do not vary according to cell collapse or expansion. It is hence the framework oxygen which must move in order to accommodate the necessary change in framework geometry as cell constituents are varied. The oxygen z coordinate is seen to alter most significantly, whilst the x and y coordinated do not vary significantly with cell size. The oxygen twists about the $\bar{4}$ axis and deviation from $z = 0.5$, which corresponds to maximum cell expansion, is observed. If the oxygen z coordinate is plotted against T-O-T angle a linear correlation is obtained. One of the most important factors in framework collapse is the tetrahedral tilt angle, ϕ, which is strongly related to framework T-O-T angle, and remains largely unaffected by the T-O bond distance. The O_z coordinate has the greatest effect on the tilt angle as indicated by equations 8.2 and 8.3, and thus would be expected to be directly proportional to the T-O-T angle as is seen. The same linear relationship can be used to describe the change in O_z with T-O-T angle whatever the composition of the framework.

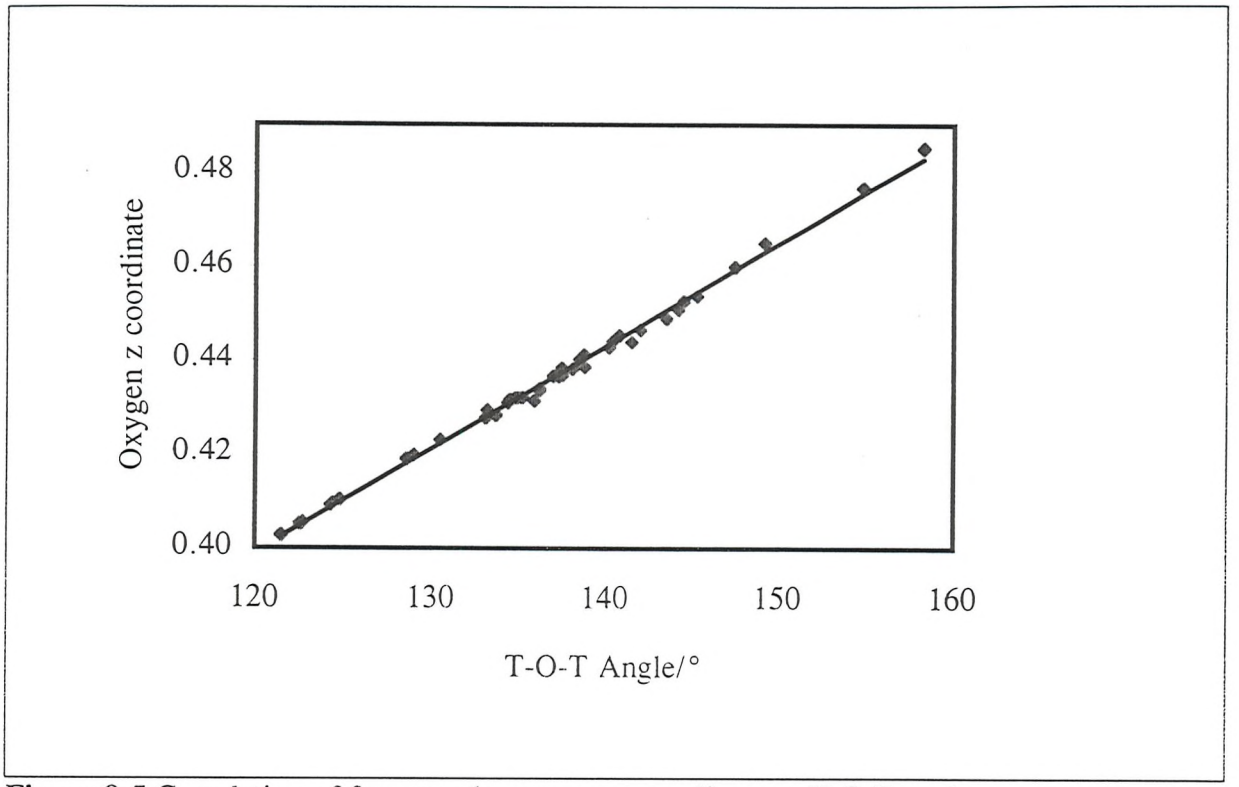

Figure 8.5 Correlation of framework oxygen z co-ordinate to T-O-T angle.

8.3.3 Mechanisms of Framework Collapse

The two main mechanisms by which cell collapse is described are tetrahedral tilting and variation of the framework T-O-T angle. These in turn fix the position of the framework oxygen which has been described in section 8.3.2 above. For a particular entrapped anion, the larger framework species are seen to undergo greater relative cell collapse with a subsequent decrease in the T-O-T angle. A plot of cell parameter versus T-O-T framework bond angle is linear for all framework types as shown in Figure 8.6(a), although different framework compositions are described by different gradients and intercepts: this is entirely in accord with the results expected, since for a certain cell parameter, T-O-T angles are dependent on framework composition due to the size variation of the tetrahedral cations. Extrapolation of these graphs to T-O-T = 109.5 ° and T-O-T = 160.5 ° provides the minimum and maximum possible cell parameter for each framework type according to the relationships derived from this study. These are shown in Table 8.4(a).

Table 8.4(a) Observed Dependence of Sodalite Size on Composition

Sodalite	a_{max}/Å	a_{min}/Å
M[AlSi]X	9.429	8.108
M[GaSi]X	9.813	8.143
M[AlGe]X	9.913	8.263
M[GaGe]X	10.185	8.467

Table 8.4(b) Theoretical Dependence of Sodalite Size on Composition

Sodalite	a_{max}/Å	a_{opt}/Å	a_{min}/Å
M[AlSi]X	9.356	9.028	7.750
M[GaSi]X	9.590	9.254	7.994
M[AlGe]X	9.696	9.356	8.032
M[ZnP]X	9.717	9.377	8.051
M[GaGe]X	9.924	9.577	8.221
M[ZnAs]X	10.180	9.824	8.434

Table 8.4(b) shows the theoretical results of Beagley and Titiloye [3], which details their optimum cell parameter relating to a T-O-T angle of approximately 144 °, which is that calculated as being the most favourable framework angle using free unstrained disiloxane $(SiH_3)_2O$ as the reference material [15]. Both the maximum and minimum cell parameters are higher for the observed than the theoretical, whilst the optimum values obtained by experiment are considerably lower than the theoretical, reflecting the relatively small increase in cell parameter seen upon introduction of larger framework cations. Using equation 8.4 a linear relationship is observed between cell parameter and sin(T-O-T/2) for all framework types, and inclusion of a framework bond length T-O term allows all the framework compositions to follow the same linear trendline, shown in Figure 8.6(b).

Figure 8.7(a) and (b) illustrate the linear variation of tetrahedral tilt angle with framework bond angle for silicon/germanium and aluminium/gallium respectively. Regression parameters reveal that these trends are very similar indeed and can be plotted on the same curve with reasonable consistency, although they are better described by separate correlations since the level of tilting does differ depending on the framework constituent. This can be seen upon examination of the values presented in Table 8.1. A linear relationship is also obtained when

the cosine of the average tilt angle is plotted against cell parameter as is expected from equation 8.1. This is represented by Figure 8.8.

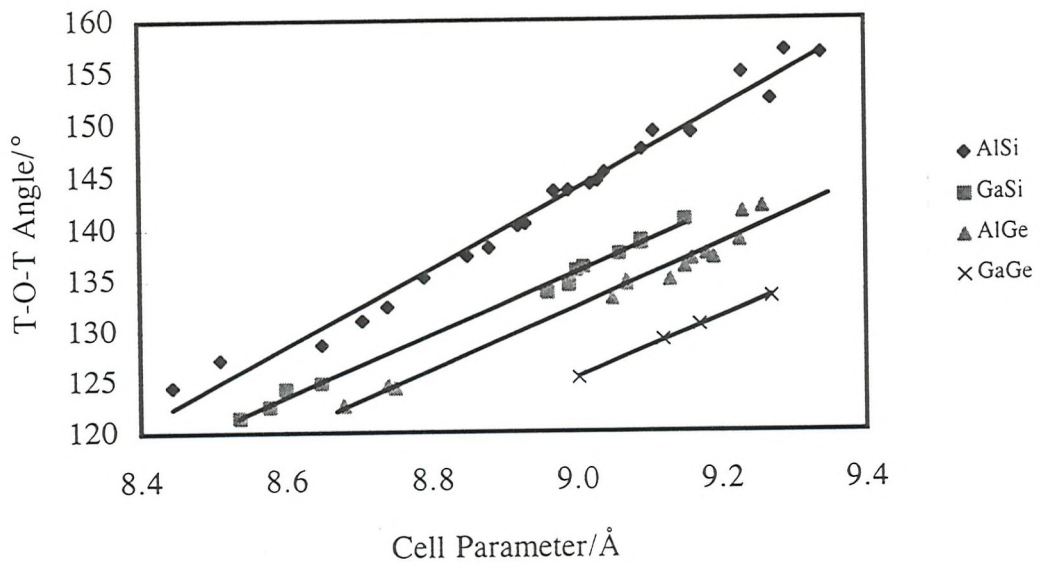

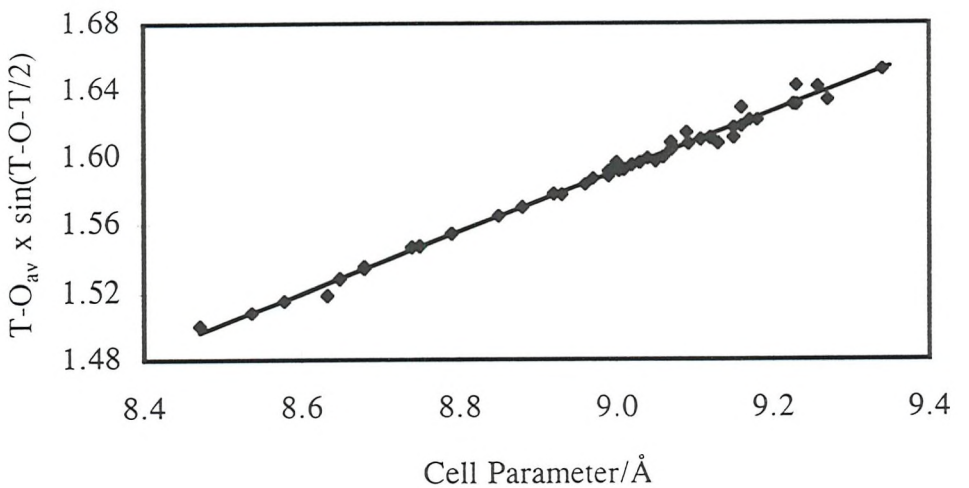

Figures 8.6(a) T-O-T angle vs Cell parameter: top **(b)** T-O_{av} x sin(T-O-T/2) vs Cell parameter: bottom

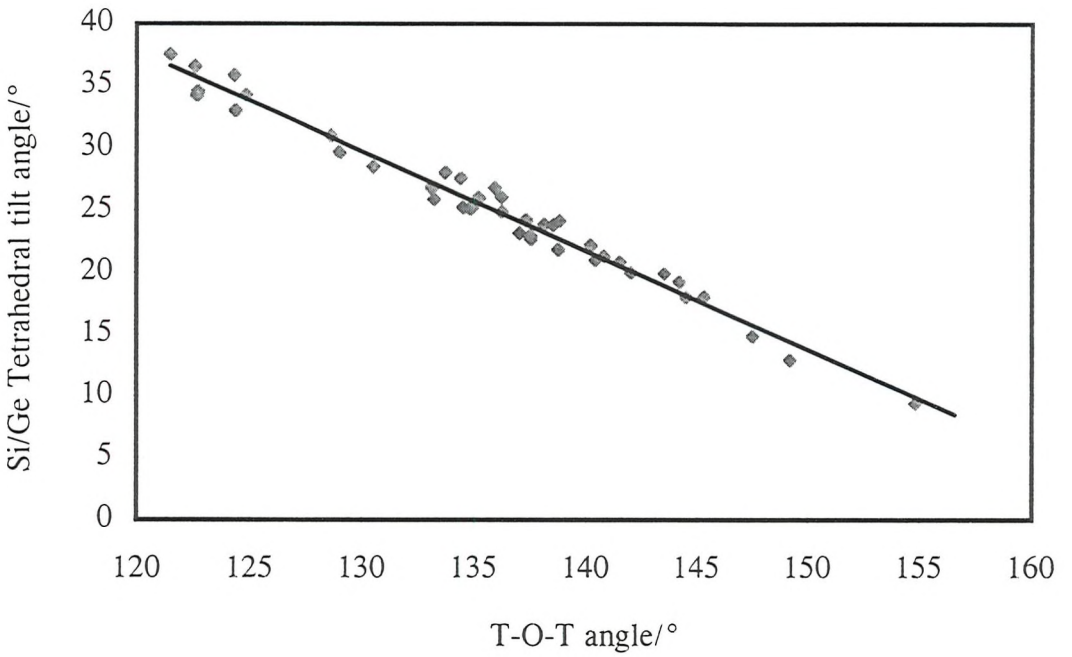

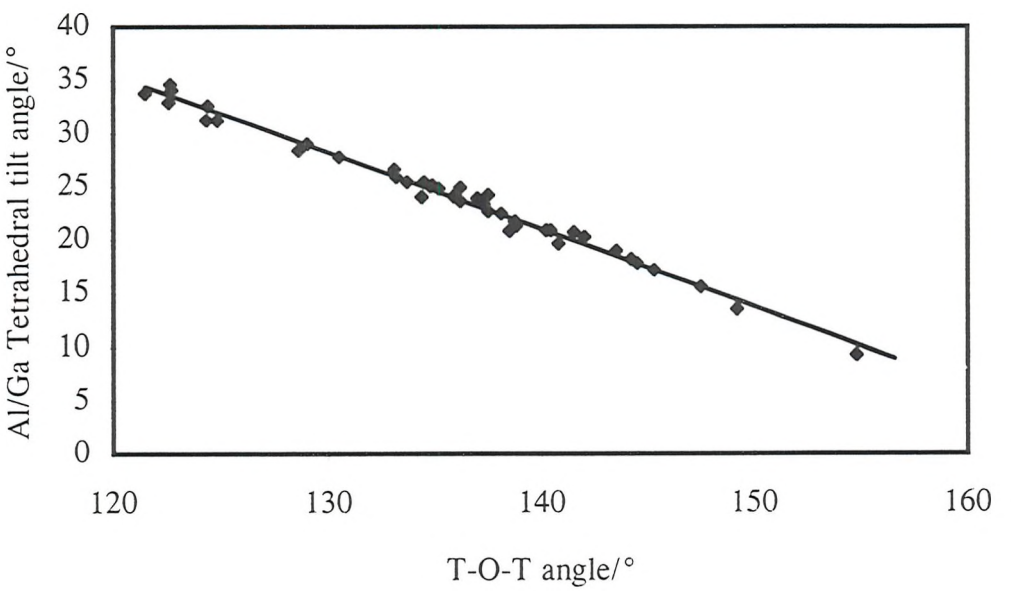

Figures 8.7(a) Silicon/Germanium tetrahedral tilt angle vs T-O-T angle: top **(b)** Aluminium/Gallium tetrahedral tilt angle vs T-O-T angle: bottom

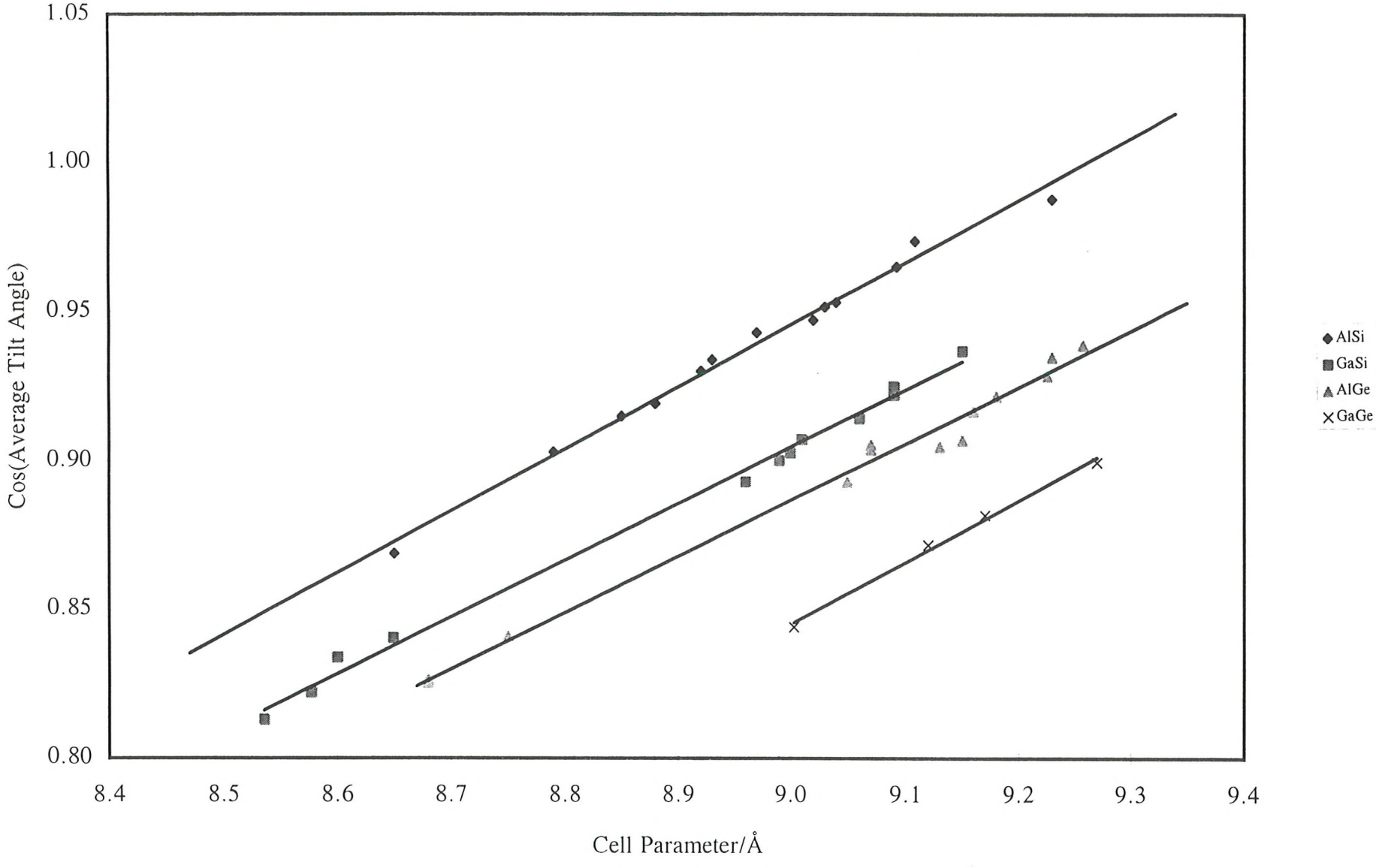

Figure 8.8 Cosine of average tetrahedral tilt angle vs Cell parameter

8.3.4 Effect of Cell Size on Framework Bond Length

It has previously been stated that there is a shortening of the T-O bond length associated with an increase in cell size or T-O-T framework bond angle. These changes in the bond length are relatively small and hence their values must be determined as accurately as possible in order to allow valid correlations to be drawn. Powder neutron diffraction data is hence preferable for investigation of framework bond length as a function of cell size. For such correlations to be valid, as large a range of data points as possible is required, and thus the results of Wong [10], Brenchley [9] and Mead [13] have been added to those obtained in this work. This changing T-O distance is directly proportional to framework T-O-T bond angle as represented by equation 8.9(a) which shows a plot of average T-O bond length against T-O-T angle, which is necessarily different as framework composition varies since the larger framework constituents clearly must give rise to longer T-O bonds due to the increased ionic radius of the tetrahedral cation.

It has been proposed that this T-O bond shortening is caused by hybridisation effects: as the cell parameter is increased the T-O-T framework bond angle also becomes higher, which alters the relative contributions of s and p bond types. At T-O-T = 109.5 ° sp^3 bonding is observed, which changes to sp^2 at 120 ° and sp at 180 °; increasing the T-O-T angle therefore results in a larger s orbital contribution to the T-O bond and shortens it accordingly. Hinze [16] proposed a mathematical expression for the relationship between degree of s hybridisation and T-O-T angle:

$$\rho \propto \cos\theta/\cos\theta\text{-}1 \qquad 8.7$$

where ρ is the degree of *s*-hybridisation and θ is the T-O-T angle. A plot of cosθ/cos θ-1 versus average T-O bond distance should therefore be linear if this relationship holds; Figure 8.9(b) shows this plot, which is indeed linear indicating that the T-O bond distance is directly proportional to the degree of hybridisation. The relationship between T-O distance and T-O-T angle can also be explained by π-bonding interactions: the degree of Si-O $d\pi$- and $p\pi$-overlap increases as the T-O-T angle becomes more linear and hence bond contraction is observed.

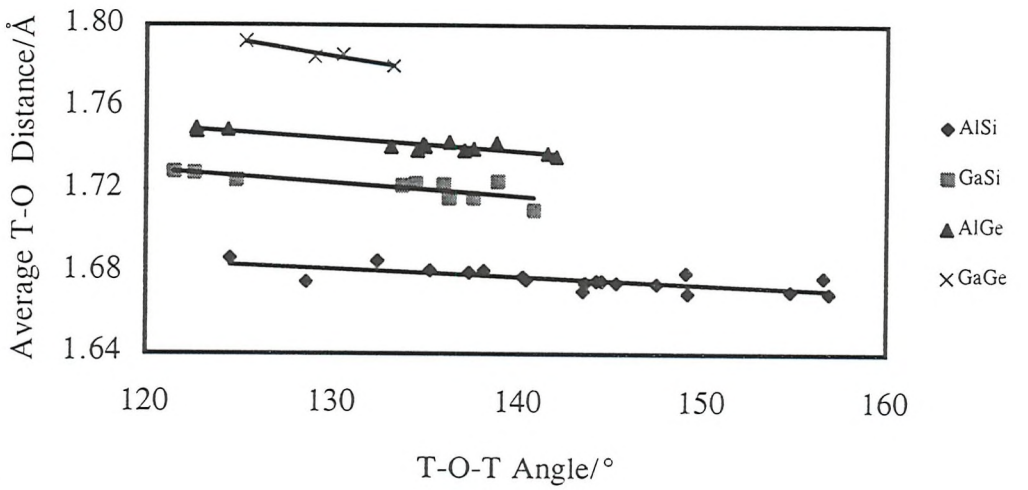

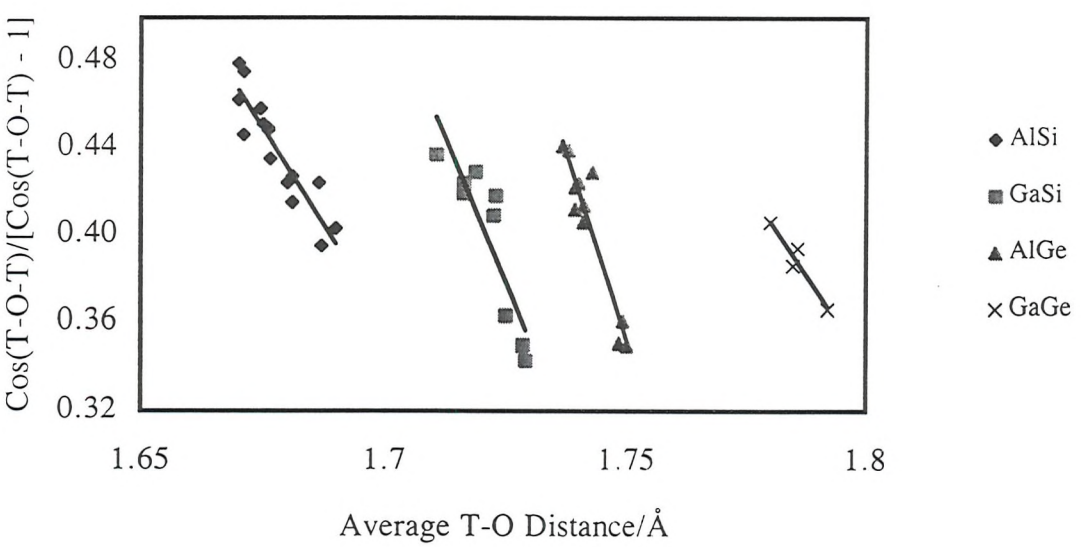

Figures 8.9(a) Average T-O distance vs T-O-T angle: top **(b)** Degree of hybridisation vs average T-O distance: bottom

8.4 CONCLUSIONS

The correlations presented here demonstrate the versatility of the sodalite structure, with respect to variation of parameters corresponding to one particular framework composition and adaptability of structure upon introduction of different framework components. The fact that trends observed for the aluminosilicates can be extended to describe materials with varying tetrahedral framework cations also shows the consistency of the sodalite structure. The limits imposed on such correlations tend to be synthetic: experimental procedures for framework modified sodalites do not as yet allow the incorporation of as wide a range of anions as the aluminosilicates, and this represents the major synthetic challenge at present. This work has furthered the synthetic methods for gallosilicates, aluminogermanates and gallogermanates although the problems encountered with the gallogermanates show that even for such a simple system as the sodalites experimental procedures are not trivial. It must surely be the eventual aim to profit from the variation in beta cage volume by enclathrating anions which are precluded from the aluminosilicate structure due to size considerations. Such materials would then allow the correlations herein to be much more fully examined and provide a wealth of information regarding sodalites with great compositional diversity.

Since sodalites are the basic building block for many important zeolites, they provide an ideal system for investigation of ionic substitution. The information gleaned from the many successful substitutions into sodalites may be able to be related to similar modification of zeolite structures. At this stage, it would certainly appear that the type of framework precursor is of crucial importance and that the use of equivalent precursor materials where appropriate in zeolite synthesis may enhance product formation.

Relationships describing variation of sodalite structure have shown that the main mechanisms for cell collapse are tetrahedral tilting and decrease in framework T-O-T bond angle. The correlations proposed for aluminosilicates have been successfully extended for gallium and germanium containing sodalites and have been presented for the first time for gallogermanates. Although the data available was limited, the gallogermanates fit in excellently with the trends followed for the other framework types. It would therefore appear that the assumptions made in deriving such relationships, such as no tetrahedral distortion and constant framework T-O distance, hold well enough for all framework components. Variation of the O-T-O angle from the ideal angle of 109.48 ° is apparent upon examination of the crystallographic data, although Table 8.3 shows that the average of this particular angle shows only marginal deviation from the perfect tetrahedron. It can therefore be stated that the

deviation from the ideal does not affect the correlations to any great degree. However, it has been clearly shown via Figure 8.9 that the T-O bond length does not remain constant with cell expansion or collapse: indeed there is a well defined contraction of the bond upon cell expansion and subsequent straightening of the framework, rationalised by the increasing level of *s* character of oxygen in the bonding [16].

One of the most difficult trends to interpret is the degree of cell collapse/expansion upon framework substitution. Section 8.3.1 has highlighted that for the halide sodalites the level of cell expansion associated with framework substitution can be linearly correlated with the combined ionic radii of the component T atoms. However, the increased cell volume obtained upon introduction of gallium and germanium is small compared with that which is available in theory. There does not appear to be highly strained bond angles as the cell expands and structural considerations have not revealed the causes of the favoured cell parameters. The maximum observed Ga-O-Ge bond angle is much smaller than the maximum Al-O-Si framework bond angle, with intermediate values for Ga-O-Si and Al-O-Ge angles. This phenomenon may have its origin in $d\pi$-$p\pi$ bonding. The preferred geometry for the oxygen would be tetrahedral, but $d\pi$- $p\pi$ interactions open the angle resulting in a more linear bond. The stronger these interactions, the more open the bond angle. The $d\pi$- $p\pi$ interactions are stronger for Al and Si, and become weaker upon introduction of gallium and germanium for which the bond overlap is reduced. Since the $d\pi$-$p\pi$ bond overlap is diminished, the consequent opening of the angle is lessened and the Ga-O-Ge framework bond angles are lower.

Computer modelling may aid the elucidation of some of these unanswered questions, and could perhaps reveal certain steric and energetic factors associated with preferred T-O-T or tetrahedral tilt angles for individual framework components which are simply not able to be observed via experiment alone. Indeed, it is important to investigate the characterisation of materials through as many means as possible, and this has been undertaken using experimental techniques for the products synthesised in this work. The very fact that certain structural features could not be rationalised solely via experiment does indicate that theoretical modelling would be a useful complementary tool, and that appropriate experimental data could be entered as starting model for computer analysis. It is important to remember however, that simply because a particular compound is theoretically feasible does not mean that it can be experimentally obtained, as illustrated by the values proposed for various framework types by Beagley and Titiloye [3]. In contrast, it should not be concluded that simply because the

theoretical structural extremities have not been observed that they are impossible to reach: this may merely be due to the fact that appropriate experimental conditions have not yet been devised. A more detailed understanding of the factors which control sodalite formation may allow the selective enclathration of a far wider range of anions than at present, and could possibly be subsequently extended to a wider variety of zeolitic species.

8.5 REFERENCES

[1] I. Hassan and H.D. Grundy, *Acta Cryst.*, B**40**, 6 (1984).

[2] W. Depmeier, *Acta Cryst.*, B**40**, 185 (1984).

[3] B. Beagley and J.O. Titiloye, *Structural Chemistry*, **3**(6), 429 (1992).

[4] D. Taylor, Contrib. *Mineral Petrol.*, **51**, 39 (1975).

[5] C.M.B. Henderson and D. Taylor, *Spectrochimica Acta*, **33**A, 283 (1977).

[6] D. Taylor and C.M.B. Henderson, *Phys. Chem. Minerals*, **2**, 325 (1978).

[7] M.J. Dempsey and D. Taylor, *Phys. Chem. Minerals*, **6**, 197 (1980).

[8] B. Beagley, C.M.B. Henderson and D. Taylor, *Mineral. Mag.*, **46**, 459 (1982).

[9] M.E. Brenchley, *Ph.D. Thesis*, University of Southampton (1994).

[10] G. Wong, *Ph.D. Thesis*, University of Southampton (1990).

[11] W.S. Fyfe, *Am. Miner.*, **39**, 991 (1954).

[12] G.V. Gibbs, M.M. Hamil, S.J. Louisnathan, L.S. Bartell and H. Yow, *Am. Miner.*, **57**, 1578 (1972).

[13] P.J. Mead, *Ph.D. Thesis*, University of Southampton (1996).

[14] T.M. Nenoff, W.T.A. Harrison, T.E. Gier, N.L. Keder, C.M. Zaremba, V.I. Srdanov, J.M. Nicol and G.D. Stucky, *Inorg. Chem.*, **33**, 2472 (1994).

[15] A. Almenningen, O. Bastiansen, V. Ewing, K. Hedberg and M. Traetteberg, *Acta Chem. Scand.*, **17**, 2455 (1963).

[16] J. Hinze, *Fortshr. Chem. Forsch.*, **9**, 448 (1968).